# SEISMIC STRENGTHENING OF MASONRY INFILLED R/C FRAMES WITH STEEL FIBER REINFORCEMENT

A THESIS SUBMITTED TO
THE GRADUATE SCHOOL OF NATURAL AND APPLIED SCIENCES
OF
MIDDLE EAST TECHNICAL UNIVERSITY

BY

TUĞÇE SEVİL

IN PARTIAL FULFILLMENT OF THE REQUIREMENTS
FOR
THE DEGREE OF DOCTOR OF PHILOSOPHY
IN
CIVIL ENGINEERING

FEBRUARY 2010

Approval of the thesis:

**SEISMIC STRENGTHENING OF MASONRY INFILLED R/C FRAMES WITH STEEL FIBER REINFORCEMENT**

submitted by **TUĞÇE SEVİL** in partial fulfillment of the requirements for the degree of **Doctor of Philosophy in Civil Engineering Department, Middle East Technical University** by,

Prof. Dr. Canan Özgen ______________________
Dean, Graduate School of **Natural and Applied Sciences**

Prof. Dr. Güney Özcebe ______________________
Head of Department, **Civil Engineering**

Assoc. Prof. Dr. Erdem Canbay ______________________
Supervisor, **Civil Engineering Dept., METU**

**Examining Committee Members:**

Prof. Dr. Tuğrul Tankut ______________________
Civil Engineering Dept., METU

Assoc. Prof. Dr. Erdem Canbay ______________________
Civil Engineering Dept., METU

Prof. Dr. Haluk Sucuoğlu ______________________
Civil Engineering Dept., METU

Assoc. Prof. Dr. Barış Binici ______________________
Civil Engineering Dept., METU

Assoc. Prof. Dr. Özgür Anıl ______________________
Civil Engineering Dept., GAZİ UNV.

**Date:** 04.02.2010

**I hereby declare that all information in this document has been obtained and presented in accordance with academic rules and ethical conduct. I also declare that, as required by these rules and conduct, I have fully cited and referenced all material and results that are not original to this work.**

Name, Last Name : Tuğçe SEVİL

Signature :

# ABSTRACT

SEISMIC STRENGTHENING OF MASONRY INFILLED R/C FRAMES WITH STEEL FIBER REINFORCEMENT

Sevil, Tuğçe
Ph.D., Department of Civil Engineering
Supervisor: Assoc. Dr. Erdem Canbay
Co-Supervisor: Prof. Dr. Güney Özcebe

February 2010, 224 pages

Seismic resistance of many buildings in Turkey is insufficient. Strengthening using R/C infills requires huge construction work. Feasible, easy strengthening techniques are being studied in Structural Mechanics Laboratory of METU.

In this project, it was aimed to develop an economical strengthening method. This method is based on addition of steel fibers and/or PP fibers in mortar and application of mortar on masonry wall. Project was sponsored by the Scientific and Technical Research Council of Turkey (TÜBİTAK).

Physical properties of cement, aggregate, and mortar used in tests were determined by material tests. After performing flexural strength and compressive strength tests, optimum mortar was obtained. R/C frames strengthened by applying the mortar to brick infilled walls were tested under reversed cyclic loads.

Before the frame tests, two series of panel tests were performed to correctly model strengthened infill walls and to gather information about behavior of walls under load. Totally 10 frame tests were done. 4 tests were done as reference tests, and other 6 were done as strengthened frame tests.

In the analytical part of study, the plastered hollow brick infill wall strengthened by FRM was modeled as two separate compression struts. First strut was used to model the plastered hollow brick infill wall. Second strut was used to model the FRM.

This technique is effective in improving seismic behavior by increasing strength, initial stiffness, energy dissipation, and ductility. Moreover, the method provides strengthening of the buildings without evacuating the structure.

Keywords: Panel, Strengthening, R/C Infill, Steel Fiber, Polypropylene Fiber.

# ÖZ

DOLGULU BETONARME ÇERÇEVELERİN ÇELİK TEL DONATI UYGULAMASI İLE DEPREME KARŞI GÜÇLENDİRİLMESİ

Sevil, Tuğçe
Doktora, İnşaat Mühendisliği Bölümü
Tez Yöneticisi: Doç. Dr. Erdem Canbay
Ortak Tez Yöneticisi: Prof. Dr. Güney Özcebe

Şubat 2010, 224 sayfa

Ülkemizdeki binaların çoğunun deprem dayanımı yetersizdir. Betonarme dolgu kullanarak güçlendirme fazlaca inşaat işi gerektirmektedir. ODTÜ Yapı Mekaniği Laboratuvarında ekonomik, kolay teknikler üzerinde çalışılmaktadır.

Bu projede, ekonomik olarak daha cazip bir güçlendirilme yönteminin geliştirilmesi amaçlanmıştır. Bu yöntem, çelik tel ve/veya polipropilen fiberlerin harç içine eklenerek tuğla duvar üzerine uygulanmasına dayanmaktadır. Proje Türkiye Bilimsel ve Teknik Araştırma Kurumu (TÜBİTAK) tarafından desteklenmiştir.

Kullanılan çimento, agrega ve deneylerde kullanılan harcın fiziksel özellikleri malzeme deneyleriyle belirlenmiştir. Eğilme dayanımı ve eğilme sonrası basınç dayanımı deneyleri sonucunda optimum harç elde edilmiştir. Harcın tuğla dolgulu

duvarlara uygulanmasıyla güçlendirilen betonarme çerçeveler tersinir tekrarlı yükler altında denenmiştir.

Çerçeve deneylerinden önce çerçevelerdeki güçlendirilmiş dolgu duvarların doğru şekilde modellenebilmesi ve bu duvarların yük altında davranışları hakkında bilgi sahibi olabilmek için iki seri halinde panel deneyleri gerçekleştirilmiştir. Toplam 10 adet çerçeve deneyi yapılmıştır. 4 adeti referans deney, diğer 6'sı ise güçlendirilmiş çerçeve deneyleri olarak yapılmıştır.

Kuramsal çalışma kısmında ise, fiber katkılı harç ile güçlendirilmiş sıvalı boşluklu tuğla dolgu duvar iki ayrı basınç çubuğu şeklinde modellenmiştir. İlk çubuk sıvalı boşluklu tuğla dolgu duvarı modellemek için kullanılmıştır. İkinci çubuk fiber katkılı harcın modellenmesi için kullanılmıştır.

Bu teknik dayanım, başlangıç rijitliği, enerji dağılımı, ve sünekliği artırarak deprem davranışını geliştirmekte etkilidir. Ayrıca, method yapının boşaltılmasını gerektirmeden binanın güçlendirilmesini sağlamaktadır.

Anahtar Kelimeler: Panel, Güçlendirme, Betonarme Dolgu, Çelik Tel, Polipropilen Fiber.

*To my family for their endless love and support*

# ACKNOWLEDGMENTS

I wish to express my sincere appreciation to my supervisor Assoc. Prof. Dr. Erdem Canbay. He behaved in a friendly, always supporting way towards me since the commencement of the research program, actually he is my real older brother since our assistantships. I would like to state my deepest gratitude to my co-supervisor Prof. Dr. Güney Özcebe, who has always had a different meaning in my life as a perfect model for me with the quality of his personality and professional life, for his guidance, support, and valuable advices since my master's education.

I would like to thank to my examining committee members, Prof. Dr. Tuğrul Tankut, Prof. Dr. Haluk Sucuoğlu, Assoc. Prof. Dr. Barış Binici, and Assoc. Prof. Dr. Özgür Anıl for their constructive criticisms, advices, and precious supports.

I would also like to thank, knowing that a thanking is nothing besides their efforts in me, to all my teachers who have trained me since the beginning of my undergraduate education and have become my second family with their warm, helpful, encouraging attitudes towards me.

I wish to express my feeling of indebtedness to Assoc. Prof. Dr. İsmail Özgür Yaman for his help, precious comments and suggestions during the materials part of my study. Also; I can never forget my friend Adel Gilani and would like to express my genuine thanking for his friendship and valuable helps in the materials section.

I want to state my heartfelt thanking to Prof. Dr. Bülent Baradan and research assistant Burak Felekoğlu, from the Dokuz Eylül University, for their help and valuable suggestions in my materials studies. Specially, I want to present my appreciation respectfully to Prof. Dr. Tuncer Toprak, from the İstanbul Technical University, for his friendly attitude and precious information on experimental stress analysis.

I also would like to send my special thanks to Asst. Prof. Dr. Mehmet Baran, who is a friend of mine since our assistantships, for his helps and suggestions throughout the analytical studies of my thesis.

I would like to especially thank Mr. Mehmet Yerlikaya for his valuable technical support and providing the steel fibers, Dramix ZP-305, used in the research.

The technical assistance of the structural laboratory staff are gratefully acknowledged. I would like to express my gratitude to our project technician Murat Demirel for his assistance in preparing experimental specimens and working along with me during numerous experiments.

A heartfelt thank you is also extended to all my friends, whose names are impossible to list here. Thank you all for your support, caring, and sharing many good times with me.

Also, I would like to present my thanks to the administrative staff of my department for being with me, as a precious part of my second family, without withholding their sincerity, support, and help.

Special thanks to the support of the Scientific and Technical Research Council of Turkey (TÜBİTAK) and also financial support provided under project, 104M566.

Finally, I wish to express my special thanks to my dear family for their profound love, support, and belief in me. They have always been with me and have never lost their trust in me. I am sending all my love and my deepest thanking to you for your support, patience, and encouragement throughout my life.

## TABLE OF CONTENTS

## LIST OF TABLES

## LIST OF FIGURES

## LIST OF SYMBOLS

| | | |
|---|---|---|
| FRCC | : | Fiber reinforced cementitious composite |
| FRC | : | Fiber reinforced concrete |
| SFRC | : | Steel fiber reinforced concrete |
| PP | : | Polypropylene |
| HFRC | : | Hybrid fiber reinforced concrete |
| R/C | : | Reinforced concrete |
| CFRP | : | Carbon fiber reinforced polymer |
| FRP | : | Fiber reinforced polymer |
| $f_m$ | : | Compressive strength in MPa |
| $P$ | : | Total maximum load in N |
| $A$ | : | Area of loaded surface in $mm^2$ |
| $R_f$ | : | Flexural strength in MPa |
| $F_f$ | : | Applied load at the center at rupture in N |
| $l$ | : | Span length in mm |
| $b$ | : | Side length of square cross-section of the prism in mm |
| REFBA | : | Bare reference frame |
| REFB | : | Non-plastered reference frame (brick infilled only) |
| REFBM | : | Plastered reference frame |
| REF2ABM | : | Plastered, anchored, 20 mm thickness of mortar not containing either steel fiber or PP fiber applied frame |
| SF1NABM | : | Plastered, non-anchored, 10 mm thickness of mortar with 2% volumetric ratio of steel fiber applied frame |
| SF2NABM | : | Plastered, non-anchored, 20 mm thickness of mortar with 2% volumetric ratio of steel fiber applied frame |
| SF1ABM | : | Plastered, anchored, 10 mm thickness of mortar with 2% volumetric ratio of steel fiber applied frame |
| SF2ABM | : | Plastered, anchored, 20 mm thickness of mortar with 2% volumetric ratio of steel fiber applied frame |
| PPF2ABM | : | Plastered, anchored, 20 mm thickness of mortar with 2% volumetric ratio of PP fiber applied frame |
| HF2ABM | : | Plastered, anchored, 20 mm thickness of mortar with 2% volumetric ratio of hybrid fiber (1% steel fiber, 1% PP fiber) applied frame |

| | | |
|---|---|---|
| $f_{sy}$ | : | Yield stress of reinforcing bar in MPa |
| $f_{su}$ | : | Ultimate stress of reinforcing bar in MPa |
| SF | : | Steel fiber |
| LVDT | : | Linear variable displacement transducer |
| TS | : | Test specimen |
| F | : | Forward loading |
| B | : | Backward loading |
| fc,frame | : | Concrete compressive strength of frame |
| fc,brick laying mortar | : | Compressive strength of brick laying mortar |
| fc,plastering mortar | : | Compressive strength of plastering mortar |
| fc,FRM | : | Compressive strength of fiber reinforced mortar |
| tfrm | : | Thickness of fiber reinforced mortar |
| PPF | : | Polypropylene fiber |
| $N/N_0$ | : | Axial load level |
| Conc. | : | Concrete |
| Str. | : | Strength |
| St. | : | Story |
| $\Delta$ | : | Relative displacement between two successive floors |
| h | : | Story height |
| S | : | Initial stiffness |
| k | : | Peak-to-peak stiffness |
| R | : | Behavior factor |
| $P_{ult}$ | : | Maximum applied load |
| $N_0$ | : | Ultimate axial load capacity |
| SFRM | : | Steel fiber reinforced mortar |
| NPP | : | Non-plastered reference wall specimens |
| PP | : | Plastered reference wall specimens |
| SF1P | : | 10 mm thickness of mortar with 2% volumetric ratio of steel fiber applied plastered wall specimens (on one side) |
| SF2P | : | 20 mm thickness of mortar with 2% volumetric ratio of steel fiber applied plastered wall specimens (on one side) |
| 2SNPP | : | Non-plastered reference wall specimens |

| | | |
|---|---|---|
| 2SPP | : | Plastered reference wall specimens |
| 2SSF1P | : | 10 mm thickness of mortar with 2% volumetric ratio of steel fiber applied wall specimens (on one side) |
| 2SSF2P | : | 20 mm thickness of mortar with 2% volumetric ratio of steel fiber applied wall specimens (on one side) |
| 2SSF1PD | : | 10 mm thickness of mortar with 2% volumetric ratio of steel fiber applied wall specimens (on double sides) |
| 2SSF2PD | : | 20 mm thickness of mortar with 2% volumetric ratio of steel fiber applied wall specimens (on double sides) |
| $\bar{\tau}$ | : | Average shear stress |
| $P_d$ | : | Applied diagonal force |
| $b$ | : | Width of the panel |
| $t$ | : | Thickness of the panel |
| R | : | Radius of Mohr Circle |
| $\sigma$ | : | Normal stress |
| $\tau$ | : | Shear stress |
| $\sigma_1$ | : | Maximum principal stress |
| $\sigma_3$ | : | Minimum principal stress |
| $a$ | : | Slope of the line in the second quadrant of the Mohr-Coulomb yield surface |
| $b$ | : | Intersection point on $\sigma_1$ axis of the Mohr-Coulomb yield surface |
| $f'_t$ | : | Tensile strength of material |
| $f'_m$ | : | Compressive strength of brick laying mortar |
| $\tau cr$ | : | Cracking shear stress |
| $f'_{plaster}$ | : | Compressive strength of plaster |
| $E_{infill}$ | : | Modulus of elasticity of the infill |
| $E$ | : | Modulus of elasticity of the column |
| $b_w$ | : | Thickness of the infill |
| $\beta_s$ | : | Angle which has a tangent of infill height to length |
| $I$ | : | Moment of inertia of the column |
| $h$ | : | Height of the infill |
| $a_{infill}$ | : | Effective width of the equivalent compression strut |
| $h_{col}$ | : | Height of column measured between beam-column joints |

$d$ : Diagonal length of the infill wall

$E_c$ : Modulus of elasticity of R/C frame

$f_c^{'}$ : Concrete compressive strength of R/C frame

$\alpha,\beta$ : Contact ratios

$f_{c,infill}$ : Average concrete compressive strength of infill

$F_{c,infill}$ : Strength of equivalent compression strut

$k_{infill}$ : Rigidity of equivalent compression strut

$\lambda h$ : Relative stiffness of infill to column

$l/h$ : Panel proportion

$a/h$ : Contact ratio

$w_{panel}$ : Width of compression strut

$F_{c,FRM}$ : Lateral load carrying capacity of equivalent compression strut

$\lambda$ : A constant dependent on FRM strength

$f_{c,FRM}$ : Compressive strength of FRM

$b_w$ : Thickness of the equivalent compression strut

$w_{FRM}$ : Width of the equivalent compression strut

$F_{strut}$ : Lateral load carrying capacity of strut

$h$ : Height of the rectangle

$w$ : Width of the rectangle

$l_1$ : Length of diagonal 1

$l_2$ : Length of diagonal 2

$l_1^{'}$ : Length of diagonal 1 after deformation

$l_2^{'}$ : Length of diagonal 2 after deformation

$\varepsilon_1$ : Strain in diagonal 1 direction

$\varepsilon_2$ : Strain in diagonal 2 direction

$\delta_1$ : Total elongation in diagonal 1 direction

$\delta_2$ : Total elongation in diagonal 2 direction

$\gamma_{xy}$ : Shear deformation

# CHAPTER 1

# INTRODUCTION

## 1.1 GENERAL

Turkey is located in a very high seismic zone. In addition to the high seismicity poor construction quality, wrong detailing, and structural mistakes have caused enormous loss of lives and properties. Therefore, seismic rehabilitation has been a major topic for civil engineers in Turkey.

Repair of damaged structures after earthquakes has been an important and care awaiting area. Turkey has gained significant experience on repair of structures. There is, however, great building stock waiting for strengthening before a major earthquake struck. Because of this huge demand to strengthening of structures, several researches have been conducted and researchers have been continuously working on strengthening of structures at Middle East Technical University. Studies have focused currently on occupant friendly strengthening techniques.

This thesis, especially, focuses on such an occupant friendly strengthening technique. The object of this research was to develop an economical, new method which will provide strengthening of buildings without evacuating the structure and to prove experimentally that this new method provides necessary strength and lateral rigidity to the structure. This method is based on addition of steel fibers in mortar and application of mortar on masonry wall.

### 1.1.1 Material Overview

The product obtained by randomly adding a small quantity of short fibers to a cementitious matrix, to improve the mechanical response, is known as fiber reinforced cementitious composite (FRCC). Commonly, FRCCs exhibit higher strength and ductility compared to unreinforced mortar or concrete, which fail in tension after the formation of a single tension crack.

Concrete is a widely used material in the construction area. The brittle behavior of concrete is one of its limitations. With the low toughness of concrete, cracks can propagate rapidly resulting in failure. In order to improve the failure behavior, fiber reinforced concrete (FRC) is made by adding discrete short fibers into the concrete matrix. These fibers act as bridges across the cracks to delay their propagation. Thus, a more ductile failure mode with a significant softening response could be obtained.

Steel fiber reinforced concrete (SFRC) is the most commonly used type of FRC. When steel fibers are added to concrete mixes, they distribute randomly through the mix at a closer spacing than conventional reinforcing steel. Depending on their aspect ratio, fibers decrease the stress at the tip of internal cracks. Steel fibers may improve the ultimate tensile strength of concrete because much energy is absorbed in de-bonding and pulling out of fibers from the matrix before the failure of concrete occurs.

Polypropylene (PP) fibers are used in concrete applications mostly due to their effectiveness in controlling plastic shrinkage cracking, and also due to their relatively low cost, alkali resistance, and high elongation. The advantages of PP fibers are high chemical resistance, high strength after stretching, high resistance to oxidation, high melting point, easy fibrillation, and the ability to use in conventional mixing of concrete. Disadvantages are poor fire resistance, sensitivity to sunlight and oxygen, low modulus of elasticity, and weak bond with the matrix.

Hybrid fiber reinforced concrete (HFRC) is a FRC obtained by adding two or more different types of fibers as reinforcement in the concrete mix. A combination of two or more types or sizes of fibers can improve the composite performance by taking advantage of benefits of each fiber. A high modulus fiber with a strong fiber-matrix bond can be combined with a low modulus fiber with a weaker fiber-matrix bond to produce a composite that is both strong and ductile. Shorter fibers that increase composite strength by preventing micro-cracks can be combined with longer fibers that enhance composite ductility by bridging macro-cracks.

### 1.1.2 Structural Overview

Strengthening of existing R/C-framed buildings to improve the seismic resistance is an important problem. Many of the existing buildings have inadequate strength and/or ductility and/or stiffness. The aim of intervention is to upgrade the insufficient properties of the structure. Different intervention techniques are being used in practice. These techniques range from conventional techniques, which use braces, jacketing, or infills, to more recent practices such as base isolation, supplemental damping devices or advanced materials [1].

Masonry has been a common construction material all over the world for centuries. Masonry infill panels can be frequently found as interior and exterior partitions in R/C structures. Since they are generally considered as nonstructural components, they are ignored in structural analysis. However, they interact with the surrounding frame when the structure is subjected to earthquake loads.

R/C frames without infill have low lateral stiffness and may show excessive lateral drifts during earthquakes. Masonry being a stiff but brittle material is weak in shear, but can carry great in-plane compression if properly confined. The two materials acting together have much greater strength and stiffness than either of the two acting independently. The masonry infill provides significant lateral stiffness, thus reducing lateral drift, while the frame provides confinement and ductility to the frame-infill system. The infill actually acts as a stiff bracing element and reduces the deformation of the framed structure when subjected to lateral loads.

However, the masonry infill contributes additional mass and stiffness to the system, which causes it to attract large seismic forces and reduces the period of the system. This considerably changes the dynamic response of the structure from that of the bare frame structure without the infill. Therefore, it is important that the interaction of the masonry infills with the bounding frames be taken into account while analyzing or designing buildings.

Based on the relative stiffness of the confining frame and infill, and the nature of frame-infill interface, the behavior of the composite may vary widely. The lateral stiffness and load carrying capacity of the infilled frame acting as a unit is much greater than that of the corresponding bare frame. For seismic design of infilled frames, either of the following two approaches may be followed.

The frame-infill system may be considered to act as a unit, taking frame-infill interaction into account. This is true in cases where a positive bond between the frame and infill elements is provided.

On the other hand, in case of unreinforced masonry infills, where the elements act separately, the response of the infill may be separated from that of the frame and modeled accordingly. The behavior of an infilled frame may differ significantly from that of a bare frame. After the infill panel isolates from the bounding frame, it may impact against the column causing high moments and shears which leads to brittle shear failure. The overall frame system may then behave in a brittle manner, contrary to the design assumption of ductile behavior of framed structures.

## 1.2 OBJECTIVE AND SCOPE

The main objective of this research is to develop a new, effective, and economical technique which will provide strengthening of buildings that do not have adequate seismic resistance without evacuating the structure and to prove experimentally that the new proposed method provides necessary strength and lateral rigidity to the structure.

Many studies on more feasible, rapid and easy techniques that do not require evacuating the structure, have been successfully implemented in Structural Mechanics Laboratory of METU. Studies on strengthening of masonry infilled walls with CFRP (Carbon Fiber Reinforced Polymer) or prefabricated panel infills may be cited in the context of these studies. Those studies have been almost completed and offer different alternatives for seismic strengthening. Still, it has to be mentioned that CFRP is an import material and prefabricated panel has to be attached by means of costly epoxy materials which leads strengthening costs to take a significant portion among the overall costs.

The scope of this study was to develop a method that gives importance to domestic materials while using the knowledge acquired from the strengthening methods being developed. When the number of buildings that have to be strengthened is concerned, this approach becomes significantly important in terms of country’s economy.

Steel fiber reinforcements are being widely used in the construction sector. In this study, possibilities of using steel fiber reinforcements also in the field of strengthening of structures were investigated. This new proposed method is based on application of a ‘high strength mortar’, containing ‘steel fibers’ having proper volumetric ratio, on masonry wall. The aim of this study was to convert masonry infill wall to a load carrying wall by applying steel fiber reinforced high strength mortar on the masonry wall.

Physical properties of the cement and aggregate used in the tests and physical properties of the mortar used in the main tests were determined by the preliminary material tests. The optimum mortar giving the required strength was selected after performing flexural strength and compressive strength tests. R/C frames strengthened by the application of the mortar to masonry walls were tested under reversed cyclic loads simulating earthquake loads.

Prior to the frame tests, two series of panel tests were performed with the object of modeling the strengthened masonry walls of the frames truly and gathering knowledge about the behavior of the walls under load.

Totally 10 frame tests were conducted in the scope of the project. Among the performed tests, 4 were done as reference tests, and the other 6 were done as strengthened frame tests.

The main variables were the ratio of fiber (0% and 2%), fiber reinforced mortar thickness (0 mm, 10 mm, and 20 mm), anchorage (non-anchored or anchored), type of fibers (steel fiber, polypropylene fiber, and hybrid fiber).

# CHAPTER 2

# LITERATURE SURVEY

This Chapter briefly summarizes experimental researches conducted on masonry infilled R/C frames. The main objective is not to give all the researches on this area but pick up the most relevant ones to this study. Studies performed in the Structural Mechanics Laboratory of the Middle East Technical University constitute the main body of this chapter. Studies are given in a chronological order.

**Altın (1990) [2] and Altın, Ersoy, and Tankut (1992) [3]** investigated the behavior of infilled frames under seismic loads. For that purpose, fourteen two-story, one-bay infilled frames were tested under reversed cyclic loading simulating seismic action. The main variables investigated were, the effect of the type of infill reinforcement and the connection between the frame and the infill. Four different types of infill reinforcement and connection details were used in the test specimens. The effect of column axial loads and flexural capacity of columns on strength and behavior were the other two variables studied. Test results were evaluated to understand the effect of infills on stiffness, strength, energy dissipation, lateral drift, and ductility.

Feasibility of different analytical methods was alsoinvestigated in this study. In the analytical work, models developed for monotonic loading were adopted to the case of cyclic reversed loading. Strength and stiffness of the infilled frame specimens were calculated using the emprical equations proposed by the researchers and code recommendations. The results obtained using the analytical methods were compared with the experimental observations. A simple dynamic analysis was made using the dynamic characteristics observed in tests to predict the behavior of infilled frames under seismic action. Recommendations were made for the design and detailing of infilled frames to be used for strengthening purpose.

**Haider (1995) [4]** studied the in-plane cyclic response of R/C frames with unreinforced masonry infill. Four full-scale R/C frame assemblies with masonry infills were designed and tested under reversed cyclic loading. The effect of panel aspect ratio and the stiffness of the infill relative to the frame were studied in terms of stiffness, strength, energy dissipation, and failure mode. Based on the test results, an equivalent diagonal compression strut model was developed to represent the behavior of masonry infill bounded by an R/C frame and a simplified method for the linear-elastic analysis of R/C frames with masonry infills was proposed. Using the experimental load-deformation plots, the hysteretic parameters relating to stiffness degradation, strength deterioration, and pinching of the hysteretic loops were identified.

**Crisafulli (1997) [5]** focused on the seismic behavior of R/C structures with masonry infills. The properties of masonry and its constitutive materials were reviewed. Theoretical procedures were developed for the rational evaluation of the strength of masonry subjected to compressive and shear stresses. Two theoretical procedures, with different degree of refinement, were proposed in the study for the analysis of infilled frames.

A test program was implemented to investigate the seismic response of infilled frames. The main criterion followed for the design was that the R/C columns should yield in tension in order to obtain a reasonable ductile response under lateral loading.

A new design approach was proposed for infilled frames, in which two cases were considered: cantilever and squat infilled frames. In the first case, the ductile behavior was achieved by yielding of the longitudinal reinforcement, which was limited to occur only at the base of the columns, and by avoiding large elongations of the remaining parts of the surrounding frame. In the second case, ductility was conferred to the structure by allowing controlled sliding of the infilled frame over the foundation.

The effect of pinching of the hysteresis loops in the response of infilled frames subjected to earthquakes was investigated. A parametric study was conducted using a one degree of freedom oscillator subjected to ground accelerations recorded in five different earthquakes.

**Marjani (1997) [6]** investigated the behavior of infilled frames under seismic loads. For that purpose, six two-story, one-bay brick infilled frames were tested under reversed cyclic loading simulating seismic action. Furthermore, six infill panels were tested to get primitive information on infill characteristics. Effect of plaster and concrete quality were the parameters. The behaviors of the frames were compared with the frames' behaviors without infills. Analytical works were performed to determine stiffness, strength, and behavior of the frames. Analytical calculations were compared with the experimental results.

**Dymiotis, Kappos, and Chryssanthopoulos (2001) [7]** focused on the probabilistic assessment of R/C frames infilled with clay brick walls and subjected to earthquake loading. The adopted methodology extended that was previously developed by the writers for bare R/C frames by introducing additional random variables to account for the uncertainty in the masonry properties. Quantification of the latter was achieved through the use of experimental data describing the difference in force-displacement behavior between bare and infilled frames. The vulnerability and seismic reliability of two ten-story, three-bay infilled frames (a fully infilled one and one with a soft ground story) were derived and subsequently compared with values corresponding to the bare frame counterpart. It was found that failure probabilities, especially at the ultimate limit state, were highly sensitive to the structural stiffness; hence, bare frames benefited from lower spectral ordinates than infilled ones. Nevertheless, all structural systems studied appeared to be exposed to a reasonably low seismic risk.

**Calvi and Bolognini (2001) [8]** presented a research work related to the seismic response of R/C frames infilled with weak masonry panels. More specifically, the benefits derived from the insertion of a light reinforcement, in the mortar layers or in the external plaster, were studied in some detail. Tests were performed on different types of single-bay, single-story, infilled frames to investigate the in-plane response at different earthquake intensity levels and the out-of-plane strength as a function of the in-plane damage. A series of parametric simulations were performed to evaluate the effects of the different panels characteristics on the response of whole buildings, with different infill patterns. Both in-plane and the out-of-plane response were considered. The results were described in terms of peak ground acceleration required to induce given limit states of serviceability or damage relatively far from the collapse of the structure, which was governed by the R/C frame design more than by the infill panels properties.

**Sonuvar (2001) [9]** constructed five two-story, one-bay, 1/3 scale R/C frames having the deficiencies observed in common practice in Turkey. The frames were tested under the reversed cyclic loading until considerable damage was observed, and then they were rehabilitated by means of cast-in-place R/C infill walls and local strengthening techniques. Later, the rehabilitated frames were tested under reversed cyclic loading in order to observe the performance of the specimens. Strength, stiffness, energy, and story drift characteristics of the specimens were examined by evaluating the test results. In the analytical part of the study, the simulation of R/C infills by means of equivalent diagonal struts was studied; and the analytical results were compared with experimental results and with the results of a well-known analytical model as well.

**Canbay (2001) [10]** investigated the behavior and strength of R/C infill frames (cast-in-place R/C panels) that are commonly used in Turkey for seismic strengthening. A test set-up for a multi-bay, multi-story specimen was developed in which only one bay was infilled. This specimen was tested in a vertical position under reversed cyclic lateral loads. The test specimen was a three-bay, two-story frame. The frame was detailed and built to have the deficiencies common to the buildings in Turkey (low concrete strength, inadequate lateral stiffness, inadequate confinement, lapped splices at floor levels, etc.). The test frame was 1/3 scale of a prototype building.

The R/C infill was introduced to the middle bay, after damaging the bare frame under reversed cyclic lateral loads. The specimen with the infill was tested to failure under reversed cyclic lateral loads. Since the main objective of the test program was to observe the contribution of the frame columns to the lateral load resistance, two special transducers were designed and manufactured to measure the axial force, shear and moment at the base of frame columns. Analytical tools were used to predict the behavior of the test specimen.

Strength, stiffness, energy dissipation, and story drifts of the test specimens were examined by evaluating the test results. In the analytical part of the study, the simulation of R/C infills by means of limit analysis and computer programs were done; and the calculated values were compared with the experimental results.

**Mertol (2002) [11]** used carbon fiber reinforced polymer strengthening in his tests. The combination of carbon fiber sheets and the masonry infill walls were used. A behavior like a shear wall behavior was aimed with this combination. For this purpose, two two-story, one-bay, 1/3 scale R/C frames infilled with plastered brick masonry were constructed. The frames had poor concrete quality. They did not have confining of the stirrups at the column and beam ends. The frames were tested under reversed cyclic loading. One frame was used as a reference frame (tested with no strengthening) and only infill walls of the other frames were strengthened over the plaster. At the end of the tests, strength, stiffness, energy dissipation and story drift characteristics of the specimens were examined.

**Keskin (2002) [12]** studied the behavior of brick infilled R/C frames strengthened by carbon fiber reinforced polymer (CFRP) reinforcement. In the research program, two one-third scale, one-bay, two-story R/C frames were infilled with hollow clay tiles and strengthened with CFRP. The main test variable was detailing of CFRP reinforcement. Test specimens were tested under reversed cyclic loading. Axial loads were kept constant throughout the tests. One of the test specimens failed prematurely, whereas the other one performed well. Test results were evaluated in terms of strength, stiffness, energy dissipation, and interstory drift characteristics.

In addition to experimental study, an analytical study was performed on DBI Building in Dinar. The building was moderately damaged after the Dinar earthquake in 1995, and, then, rehabilitated with R/C infill walls. Analyses on four different arrangements of CFRP reinforcement were performed and compared with the analysis of the building rehabilitated with R/C infill walls. As a result, a re-design criterion was suggested for pre-earthquake rehabilitation of structures.

**Erduran (2002) [13]** applied CPRP on mainly the existing plastered brick infill walls of brick infilled R/C frames. For this, two one-bay, two-story, one to third scale specimens were constructed and tested under reversed cyclic loading. The specimens were constructed with the most common deficiencies observed in practice. The test results were evaluated in terms of strength, stiffness, interstory drift, and energy dissipation capacity characteristics. A model for composite material was derived using the test results. This model was used to develop design criteria for strengthening of structures using CFRP.

**Shing and Mehrabi (2002) [14]** summarized some of the recent findings and developments on the behavior and modeling of infilled structures, and provided thoughts for future research. Discussed subjects by the authors included the following: Masonry infills are frequently used as interior partitions and exterior walls in buildings. They are usually treated as non-structural elements. The performance of such structures during an earthquake has attracted major attention. A number of different analytical models have been developed to evaluate infilled structures. Nevertheless, most of the models proposed have been validated with limited experimental data. Limit analysis methods seem to be the most promising approach. However, these methods need to be further refined. Sophisticated finite element models have also been developed. While these models are widely applicable to different types of infilled frames, they should be used with caution because they could be easily misused.

**Anıl (2002) [15]** investigated the behavior of R/C infilled frames under earthquake loading. Nine one-bay, one-story R/C infilled frames were tested under reversed cyclic lateral loads that simulated earthquake loading. Size and place of the openings in infills were the main variables. The effect of the size and place of the openings in infills on rigidity, strength, ductility, and energy dissipation capacity of R/C infilled frames were evaluated. By examining the test results, different analytical approaches were investigated. The strength's of specimens were calculated by using regulations and empirical equations that were suggested by researchers. Analytical results were compared with experimental results. Suggestions were constituted for design of R/C infilled frames with openings that were used for the purpose of strengthening.

**Hanoğlu (2002) [16]** tested 1/3 scale specimens under quasi-static reversed cyclic seismic loads. Four ductile and four non-ductile framed single-bay, single-story specimens with and without infill panels were tested simulating the seismic actions on lowest interior spans of typical of low-rise infilled frame structures. During the tests on masonry infill material, the testing procedures originally developed for solid brick masonry were shown unsuitable for the hollow clay tile masonry testing. A new method for tensile strength testing of the hollow clay tile units was proposed and used coupling with finite element models to establish a tile tensile strength estimate.

Infilled frames with plain hollow clay tile infill were shown to have failure loads well in excess of the bare frames. Glass fiber woven sheet and CFRP laminates were used to confine and brace the hollow clay tile infill. Addition of glass-fiber overlays and carbon fiber laminates increased the strength of the infilled frames above the conventionally infilled frames. However, the maximum displacement capacity of the new system reduced due to low compressive strength of the tile infill, which confined the failures and deformations to infill corners and column mid-height.

A new finite element modeling approach was developed based on the use of plane framework analysis methods for plane stress analysis. Two different model scales were considered to show the capabilities of the proposed approach and the possibilities of simplification for engineering office use. The results showed a good agreement with the test results for the detailed model.

**Colangelo (2003) [17]** dealt with the inelastic analysis of infilled frames. The author aimed to appraise the effectiveness of existing member-by-member models and damage indices in representing seismic response and sustained damage. Results from pseudo-dynamic and cyclic tests on one-story, one-bay, half-size-scale specimens were the basis for this evaluation. The frame was modelled with linear beam elements and hysteretic end springs, and the infill with diagonal struts for which two inelastic behavioral laws were compared. Provided parameters were carefully calibrated, time-histories of the global response could be traced with an accuracy that depended on model refinement. Certain indices reflected the visible damage of structure and infill. Nevertheless, if the structure index was derived from the calculated local response, even the major damage of the weak beam was not captured.

**Duvarcı (2003) [18]** aimed to strengthen the buildings by using precast concrete panels. This is an easy method which results in a rapid construction and least disturbance is given to the occupants. In the study, two preliminary test were conducted to verify the proper functioning of the newly developed test setup and then three hollow clay tile infilled, one-third scale, one-bay, two-story R/C frames which reflect the common deficiencies of the buildings in Turkey were constructed as test specimens. First, a reference specimen was tested and the other two specimens were strengthened by using precast concrete panels. Test results were evaluated in terms of strength, stiffness, energy dissipation, and interstory drift characteristics.

**Öktem (2003) [19]** examined non-linear behavior of structures. Non-linear static procedure (Pushover Analysis) was applied in the analysis of R/C frame systems. The infill influence on the behavior of the system subjected to external loads was examined and base shear-top displacement relations obtained from the bare frame and masonry infilled frame results were compared.

The second chapter covered the detailed investigation of non-linear behavior of R/C members. Moment-curvature relationships and yield surface of R/C sections were obtained by a computer program. Axial force-bending moment interaction diagrams were also presented in the study.

**Erdem (2003) [20] and Erdem, Akyüz, Ersoy, and Özcebe (2006) [21]** prepared two-story, three-bay, 1/3 scaled two test frames. The details of the bare frame were similar to the most of the residential buildings in Turkey. The system improvement of the R/C frame was investigated. Only the middle bay of the specimens was infilled. Two strengthening methods were evaluated and compared. The first frame was strengthened with R/C infill wall. The second specimen was strengthened with CFRP applied on the hollow clay tile infill. Reversed cyclic quasi-static load was applied at the second story level of the specimens. Two force transducers were used at the base of the exterior columns to measure the internal forces. Strength, stiffness, and energy dissipation characteristics of the specimens were investigated. Analytical models were made to simulate the behavior. Test results were compared with analytical study results.

**Özcebe, Ersoy, Tankut, Erduran, Keskin, and Mertol (2003) [22]** discussed retrofitting of undamaged R/C frames using CFRP. The main objective of the experimental program was to reinforce the hollow clay tile infill walls. The scope of the study included testing of seven one-bay, two-story, 1/3 scale specimens which were constructed and tested under reversed cyclic loading. The specimens were constructed with the most common deficiencies observed in practice. The test results were evaluated in terms of strength, stiffness, interstory drift, and energy dissipation capacity characteristics. A model for composite material was derived using the test results. This model was used to develop design criteria for strengthening of structures using CFRP.

**Süsoy (2004) [23]** aimed to observe the seismic behavior of R/C frames strengthened by precast concrete panel infills by testing different types of panel and connection designs in eight single-story, single-bay R/C frame specimens.

**Gün (2005) [24]** investigated improving shear strength of nonductile R/C frames by means of infill walls. In strengthening of R/C frames by means of infill walls, effects of the connection between infill walls and bare frame and additional boundary column, adjacent to existing column, on behavior and strength were investigated. Consequently, four R/C frame specimens which consist of two-story, one-bay were constructed and tested under reversed-cyclic lateral loads simulating earthquake loads. By evaluating the test results, strength, ductility, rigidity, and energy consumption capacity of the specimens were examined. Experimental results were compared with the results of the equations proposed by researchers and the Turkish Earthquake Code.

**Baran (2005) [25]** proposed a strengthening technique in his thesis on the basis of the principle of strengthening the existing hollow brick infill walls by using high strength precast concrete panels. The technique would not require evacuation of the building and would be applicable without causing too much disturbance to the occupant. For that purpose, after two preliminary tests to verify the proper functioning of the newly developed test set-up, a total of fourteen one-bay, two-story R/C frames with hollow brick infill wall, two being unstrengthened reference frames, were tested under reversed cyclic lateral loading simulating earthquake loading. The specimens were strengthened by using six different types of precast concrete panels. Strength, stiffness, energy dissipation, and story drift characteristics of the specimens were examined by evaluating the test results. Test results indicated that the proposed seismic strengthening technique could be very effective in improving the seismic performance of the R/C framed building structures commonly used in Turkey.

In the analytical part of the study, hollow brick infill walls strengthened by using high strength precast concrete panels were modeled once by means of equivalent diagonal struts and once as monolithic walls having an equivalent thickness. The experimental results were compared with the analytical results of the two approaches mentioned. On the basis of the analytical work, practical recommendations were made for the design of such strengthening intervention to be executed in actual practice.

**Güney (2005) [26]** presented a mathematical model for frame elements based on a 3D Hermitian beam/column finite element and an equivalent strut model for the infill walls. The spread-of-plasticity approach was employed to model the material nonlinearity of the frame elements. The cross-section of the frame element was divided into triangular sub regions to evaluate the stiffness properties and the response of the element cross-section. By the help of the triangles spread over the actual area of the section, the biaxial bending and the axial deformations were coupled in the inelastic range. A frame super-element was also formed by combining a number of frame finite elements.

Two identical compression-only diagonal struts were used for modeling the infill. A computer code was developed using the object-oriented design paradigm and the models were implemented into that code. Efficiency and the effectiveness of the models were investigated for various cases by comparing the numerical response predictions produced by the program with those obtained from experimental studies.

**Öztürk (2005) [27]** investigated the contribution of the hollow masonry infill walls to the lateral behavior of R/C buildings. Two different buildings were chosen as case studies. Three- and six-story symmetric buildings were modeled as bare and infilled frames. The parameters investigated were column area, infill wall area, distribution of masonry infill walls throughout the story. To determine the effect of each parameter, global drift ratios were computed and compared for each case.

**Malekkianie (2006) [28]** aimed to find out the effects of infill walls and retrofitted infill walls with carbon fiber on the response of R/C frames. The non-linear analysis of R/C frames were performed by means of a computer program. The results of the experimental study which consisted of bare frame, infilled frame, and retrofitted infilled frame with carbon fiber were compared with the results of the theoretical analysis.

**Dönmez (2006) [29]** defined modeling of infill walls and the influence of infill walls during the earthquake. For that purpose, the R/C building structure which had been damaged during August 17, 1999 Kocaeli earthquake, was analyzed for four situations. The program SAP 2000 was utilized in the analysis. The infilled frames were investigated under different acceleration-time histories recorded during the Kocaeli and Düzce earthquakes.

**Kara (2006) [30]** investigated the strengthening of non ductile concrete frames by introducing partial infills into existing frames. Nine specimens were tested under reversed cyclic lateral loads. Parameters of the study were the infill length to height ratio, the arrangements of infills into frame openings, and the existence of edge member at the free end of infill. One-bay, two-story reinforced infilled frames were designed with the common deficiencies seen in our country. Test results showed that partial infills significantly improved the lateral load carrying capacity, stiffness and energy dissipation capacity of the bare frame. The more infill length to height ratio of partial infill was utilized, the more lateral load capacity, stiffness was observed. The most successful results were obtained when the partial infill wall was connected to both columns and beams of the frame. In addition, the existence of edge members affected the specimen's lateral load carrying capacity, stiffness and energy dissipation capacity.

**Akın (2006) [31]** created a model to provide a simple method to analyze the behavior of R/C frames with infills in earthquakes. The model was tested using experimental work done by Benjamin and Fiorato. It was then applied to four buildings surveyed in Bingöl, Turkey, following the May 1, 2003 earthquake. From these four buildings, three distinct damage states were observed. Using a database compiled from research done to date on R/C frames with masonry infills, and on masonry panels, the damage states corresponded to a specific drift range, which was used to compare the damage found in the buildings, and the drift level calculated when using the model. From the results, it was apparent that in earthquake zones where masonry infilled R/C frames were common, it was possible to accurately model the response of structures to a given ground motion by including the masonry infills with and without openings, creating a simple check of the deflection, and damage state expected in a building.

**Binici and Özcebe (2006) [32]** proposed analysis guidelines for FRP strengthened infill walls for use in seismic evaluation methods. For that purpose, a diagonal compression-strut and tension-tie model was presented to model the strengthened infill wall that was integrated to the boundary frame members. The comparisons of test results with estimated load-deformation curves showed that model was capable of estimating stiffness, strength and deformation capacity of FRP strengthened R/C frames with sufficient accuracy. The outcome of this research was believed to enable the structural engineers to perform retrofit design of deficient infilled R/C frames with FRPs.

**Shaingchin, Lukkunaprasit, and Wood (2007) [33]** subjected five R/C structural wall specimens to cyclic loading in order to study the influence of diagonal web reinforcement. The experimental parameters included the amount and configuration of reinforcing bars in the web. The conventionally reinforced wall failed due to web crushing with an abrupt drop in load capacity, whereas the walls reinforced with diagonal web reinforcement failed in a more ductile mode. Test results indicated that the diagonal web reinforcement reduced the shear and sliding displacement components. The specimens with diagonal web reinforcement exhibited less pinching in the hysteresis loops than the conventional one. Consequently, the energy dissipation capacity of the former was superior to the latter. An alternative web reinforcement configuration which combined the superior performance of the diagonal reinforcement and the simplicity of placement of the conventional type was also proposed. Test results revealed that the wall with mixed web reinforcement exhibited performance comparable with the wall with diagonal reinforcement.

**El-Sokkary (2007) [34]** analytically investigated the effectiveness of different rehabilitation patterns in upgrading the seismic performance of existing non-ductile R/C frame structures. The study investigated the performance of three R/C frames (with different heights) with or without masonry infill when rehabilitated and subjected to three types of ground motion records. The heights of the R/C frames represented low, medium, and high-rise buildings. The ground motion records represented earthquakes with low, medium, and high frequency contents. Three models were considered for the R/C frames; bare frame, masonry-infilled frame with soft infill, and masonry-infilled frame with stiff infill. The studied rehabilitation patterns included (1) introducing a R/C shear wall, (2) using steel bracing, (3) using diagonal FRP strips (FRP bracings) in case of masonry-infilled frames, and (4) wrapping or partially wrapping the frame members (columns and beams) using FRP confinement.

The seismic performance enhancement of the studied frames was evaluated in terms of the maximum applied peak ground acceleration or velocity resisted by the frames, maximum interstory drift ratio, maximum story shear to weight ratio and energy dissipation capacity.

**Erduran and Yakut (2007) [35]** developed displacement-based damage functions for the components of R/C moment resisting frames. R/C columns, beams and brick infills were considered in the study as the structural elements contributing to the seismic behavior of R/C moment resisting frames. Finite element analyses were carried out on R/C columns and beams to investigate the effects of their material and geometrical properties on the behavior of these elements, and also to develop the damage functions. The independent parameter used in the damage functions developed for R/C columns was the interstory drift ratio, while rotation was used as the main parameter to evaluate damage in R/C beams. The equivalent strut models available in the literature were used to determine the parameters affecting the damageability of brick infills and to develop drift-based damage functions. Additional damage functions for shear critical R/C columns and beams were also developed. The damage functions proposed were validated via comparison to the test results available in the literature.

**Tucker (2007) [36]** intended in his research to: (1) translate existing experimental data into analytical methods for predicting the in-plane stiffness, capacity, and structural behavior of various types of infill materials and (2) formulate and verify possible code approaches which might be used by practicing engineers for the design of new and the analysis of existing infilled frame structures.

Linear and nonlinear finite element models were developed to analyze the behavior of masonry infilled frames. The linear model focused on the behavior of the infilled frame at the first crack load. The nonlinear model focused on the behavior of the infilled frame at the first crack load and then at the ultimate load.

A new equation was presented for predicting the width of the equivalent diagonal strut and thus the stiffness of the masonry infilled frame system. Six new equations were presented for determining the strength of the masonry infilled frame system. These strength equations were specific to the masonry infill material.

**Altın, Anıl, Kara, and Kaya (2008) [37]** investigated experimentally the behavior of strengthened masonry infilled R/C frames using diagonal CFRP strips under cyclic loads. Ten test specimens were constructed and tested under cyclic lateral loading. Specimens were constructed as 1/3 scale, one-bay, one-story perforated clay brick-infilled nonductile R/C frames. The aspect ratio ($l_w/h_w$, where $l_w$ is the infill length and $h_w$ is the infill height) of masonry-infilled wall was 1.73.

CFRP strips were applied with different widths and with three different arrangements such as on both sides (i.e. symmetrically) and on the interior side or the exterior side of the masonry walls. The experimental study investigated the effects of CFRP strips' width and arrangement type on specimens' behavior. Strength, stiffness and story drifts of the test specimens were measured. Test results indicated that, CFRP strips significantly increased the lateral strength and stiffness of perforated clay brick infilled nonductile R/C frames. Specimens receiving symmetrical strengthening showed higher lateral strength and stiffness. Specimens at which CFRP strips of the same width were applied to one of the interior or exterior surface of the infill wall showed similar lateral strength and stiffness.

**Puglisi, Uzcategui, and Florez-Lopez (2009) [38]** proposed a model of the behavior of the masonry in infilled frames. The model was based on the theory of plasticity and the concept of an equivalent strut. It was first shown that the equivalent strut model, in its conventional form, introduced artificial effects that did not correspond to the observed behavior. The real infill was a unique element while the conventional model represented it as two independent bars. The conventional strut model was modified by the inclusion of a new concept: The plastic concentrator. It was assumed that all inelastic effects could be lumped at the concentrator. The idea was that plastic concentrators could be compared with the plastic hinges in the theory of frames. The plastic concentrator linked the two bars of the strut model and allowed for a transfer of effects between the bars. It was shown that the use of plastic concentrators lead to a more realistic representation of the behavior than the conventional models. The new concept could be used to model in a simplified way the behavior of any infilled frame (i.e. R/C or steel frame). Finally, it was shown how models with arbitrary force-displacement envelopes could be modified by the inclusion of plastic concentrators.

**Puglisi, Uzcategui, and Florez-Lopez (2009) [39]** proposed a model of the behavior of infill panels in framed structures. The model was based on the equivalent strut model, the concept of a plastic concentrator, and damage mechanics. First some fundamental concepts of damage mechanics were briefly presented. Then, an experimental study for the behavior of masonry specimens under compressive forces was described. The results were used for the development of the constitutive law for the equivalent strut bars. The model was analyzed, first in the case of monotonic loads, and then for cyclic loads. Finally, the model was validated by numerical simulation of a test carried out on infilled frames subjected to monotonic and cyclic loads.

# CHAPTER 3

# FRAME TESTS

## 3.1 INTRODUCTION

Physical properties of the cement, aggregate, and mortar used in the tests were determined by the preliminary material tests. Using two series of mortar, flexural strength tests and compressive strength tests using portions of prisms broken in flexure were performed at 7 and 28 days of age. The mortar containing cement, fine aggregate, water, and plasticizer, which gave the required strength, was selected as the optimum mortar to be used in the main tests.

In the main scope of this research, R/C frames were strengthened by the application of the mortar to masonry walls. The R/C infilled frames were tested under reversed cyclic lateral loads simulating earthquake loads.

The main test specimens used included 1/3 scale, two-story, single-bay R/C frames with hollow brick masonry infills. The frames were prepared to reflect typical characteristics and common deficiencies observed in the frames of R/C buildings in Turkey. The weaknesses were low concrete strength, poor confinement, inadequate transverse reinforcement, insufficient lateral stiffness, and non-ductile members. The frames were infilled with hollow bricks and plastering was applied on both faces. Continuous reinforcement was used in all of the specimens.

## 3.2 MATERIAL TESTS

### 3.2.1 Introduction

Tests aiming to determine the physical properties of aggregate included sieve analysis of fine aggregate, determination of lightweight pieces, determination of unit weight, and specific gravity and absorption of fine aggregate. Tests on cement to determine the physical properties included normal consistency, setting time, soundness, density, fineness, and compressive strength. Compressive strength tests were performed at 7 and 28 days of age.

The mortar used in the tests contained cement, fine aggregate, water, and plasticizer. Compressive strength tests of mortar were done at 7 and 28 days. To determine mechanical properties of mortar, flexural strength tests and compressive strength tests using portions of prisms broken in flexure were conducted. $70 \times 70 \times 320$ mm prisms were used for the flexural strength tests.

Prior to frame tests, 20 mm thick mortar with 0%, 1%, 2%, and 4% volumetric steel fiber contents were applied on a wall. In the 4% volume content case, the mortar did not stick to the wall at all. Consequently, 4% volume content of steel fiber reinforced specimens were excluded from the test series.

Flexural strength tests and compressive strength tests using portions of prisms broken in flexure were performed with reference mortar and mortars having 1% and 2% volume contents of steel fibers. These tests were performed at $7^{th}$ and $28^{th}$ days. Moreover, adherence tests on the mortar were carried out in order to determine the adhesion strength of the mortar. The adherence tests were done for the reference mortar and mortars having 1% and 2% volume contents of steel fibers. These tests were performed at $28^{th}$ day.

At the end, a new series of flexural strength tests and compressive strength tests using portions of prisms broken in flexure were carried out with the same mortar which also included a bonding agent for mortar. The tests were performed for the reference mortar and mortars having 1% and 2% volume contents of steel fibers.

### 3.2.2 Material Properties

Chemical and physical properties of all ingredients used in the study are provided in this section.

#### a) Cement

Ordinary Turkish Portland Cement, CEM I 42.5 R, was used throughout the preliminary tests. This type of cement corresponds to ASTM Type I cement.

#### b) Fine Aggregate

Natural river sand was used as the fine aggregate in the tests. The specific gravity and absorption capacity of the aggregate, and its gradation are shown in **Table 3.1** and **Table 3.2**, respectively.

**Table 3.1** Properties of Fine Aggregate

| **Property** | **Determined as** |
|---|---|
| Specific Gravity | |
| Dry | 2.46 |
| Saturated Surface Dry | 2.55 |
| Absorption, (%) | 3.60 |

**Table 3.2** Sieve Analysis of Fine Aggregate

| Sieve No | Cumulative Passing (%) | |
|---|---|---|
| | **Fine Aggregate** | **ASTM C 33 Requirements** |
| 3/8" (9.5 mm) | 100 | 100 |
| No.4 (4.75 mm) | 95.90 | 95-100 |
| No.8 (2.36 mm) | 70.90 | 80-100 |
| No.16 (1.18 mm) | 47.70 | 50-85 |
| No.30 (600 µm) | 28.43 | 25-60 |
| No.50 (300 µm) | 12.33 | 10-30 |
| No.100 (150 µm) | 5.77 | 2-10 |

### c) Steel Fiber

Dramix ZP-305 steel fiber that conforms to ASTM A 820 and TS 10513 was used in the tests. Steel fiber was procured from the BEKSA Steel Cord Manufacturing and Training Inc. It is a cold drawn wire fiber, with hooked ends, and glued in bundles. The fibers are filaments of wire, deformed and cut to lengths, for reinforcement of concrete, mortar and other composite materials. There is no coating on the fiber. The applications of the fiber are shotcrete, screeds, and compression layers. The fiber has a length of 30 mm and diameter of 0.55 mm, thus the aspect ratio is 55. Minimum tensile strength of the fiber is 1100 MPa.

### d) Plasticizer

A commercial normal setting plasticizer was used in all mortar mixes. It is a liquid, ready to use plasticizer that increases the cohesion and workability of cement-sand masonry mortars, and renders. It has a specific density of $1.10 \pm 0.02$ kg/l.

Application dosage of the plasticizer is 0.1%-0.2% by weight of cement. It is added to the mixing water prior to its addition to the cement-sand mix to provide high quality mortar.

**e) Bonding Agent**

A commercial water resistant bonding agent was used in the mortar mixes of the second series of flexural strength tests and compressive strength tests using portions of prisms broken in flexure. It is a synthetic rubber emulsion for adding to cement mortars where good adhesion and water resistance are required. It has a specific density of $1.02 \pm 0.02$ kg/l. The bonding agent is added to the mixing water within the range 1:1 – 1:4 depending on application.

**f) Water**

Tap water from the city water network of Ankara was used as mixing water in all mortar mixes.

### 3.2.3 Experimental Program

**a) Applications on Wall**

Mortar having 20 mm thickness was applied on a wall with no steel fibers as reference and mortars having 1%, 2%, and 4% volume contents of steel fibers (**Figure 3.1**). The mortar should stick to the wall when it is thrown to the wall by using a trowel. The reference mortar stuck to the wall easily. However, in the 4% volume content case the mortar did not stick to the wall, and in the 1% and 2% volume contents cases the mortar could hardly be fixed to the wall. Consequently; reference, 1%, and 2% steel fiber contents were selected to be used for the tests.


**Figure 3.1** Applications of Mortars on Wall

**b) Compressive Strength**

Specimens were taken out from steel forms the next day and were put in saturated lime water at $23.0 \pm 2.0$ oC. Compressive strength of the cubical mortars were measured at 7 and 28 days. Tests were conducted in accordance with ASTM C 109. A universal testing machine shown in **Figure 3.2** is used for tests.

Total maximum load indicated by the testing machine was recorded and by dividing the total maximum load to loaded surface area, compressive strength values were calculated, **Equation 3.1**.

$$f_m = \frac{P}{A} \qquad \textbf{(3.1)}$$

where $f_m$ is the compressive strength in MPa, $P$ is the total maximum load in N, $A$ is the area of loaded surface in mm$^2$.


**Figure 3.2** Views of Compressive Strength Testing

Two different mixes for mortar were prepared. The first mix included plasticizer whereas bonding agent was used in the second mix. First series' compressive strength of the mortars, obtained from $50 \times 50 \times 50$ mm cubic specimens in accordance with ASTM C 109, at 28 days is presented in **Table 3.3**.

**Table 3.3** First Series' Compressive Strength of Cubic Mortars (MPa)

| **Average Compressive Strength (MPa)** |
|---|
| 39.02 |

### c) Flexural Tensile Strength

Flexural tensile strength of prismatic specimens having dimensions of $70 \times 70 \times 320$ mm was measured using a simple beam test with center-point loading at 7 and 28 days. The distance between supports was 260 mm. Although cross-sectional dimensions of the prism should be 70 mm, actually it was measured as 75 mm. Tests were performed according to TS EN 196-1. Views of flexural tensile strength testing are shown in **Figure 3.3**.

**Figure 3.3** Views of Flexural Tensile Strength Testing

Flexural tensile strengths of prism specimens were calculated according to following equation, **Equation 3.2**:

$$R_f = \frac{M \cdot y}{I} = \frac{\dfrac{F_f \cdot l}{4} \cdot \dfrac{b}{2}}{\dfrac{b \cdot b^3}{12}} = \frac{1.5 \times F_f \times l}{b^3} \qquad \textbf{(3.2)}$$

where $R_f$ is the flexural tensile strength in MPa, $F_f$ is the applied load at the center at rupture in N, $l$ is the span length in mm, and $b$ is the side length of square cross-section of the prism in mm.

Flexural strength of prism specimens, reference mortar and mortars having 1% and 2% volume contents of steel fibers, at 28 days are provided in **Table 3.4**. There are two different test results given in the table. In the first series, the mix includes plasticizer whereas the second series uses bonding agent instead of plasticizer.

**Table 3.4** Flexural Tensile Strength of Prism Specimens (MPa)

| | **Average Flexural Tensile Strength (MPa)** | |
|---|---|---|
| | **First Series** | **Second Series** |
| Reference Mortar | 7.40 | 6.53 |
| Mortar with 1% Volumetric Ratio of Steel Fiber | 6.93 | 6.81 |
| Mortar with 2 % Volumetric Ratio of Steel Fiber | 8.57 | 8.47 |

Comparison of the flexural tensile strength tests of mortar shows that adding 1% volumetric ratio of steel fiber does not change the flexural capacity considerably. However, 2% steel fiber addition has a noticeable effect which is approximately 20% increase in flexural capacity of unreinforced concrete prisms.

### d) Compressive Strength using Portions of Prisms Broken in Flexure

Cube specimens of 75 mm were obtained by cutting ends of each portion of the prisms. Compressive strengths of the cubic mortars were determined at 7 and 28 days. Tests were conducted in accordance with TS EN 196-1. A universal testing machine is used for tests.

Compressive strength, for reference mortar and mortars having 1% and 2% volume contents of steel fibers, at 28 days are shown in **Table 3.5**. Plasticizer and bonding agent are added to the mixes in the first and second series, respectively.

**Table 3.5** Compressive Strength using Portions of Prisms Broken in Flexure (MPa)

| | **Average Compressive Strength (MPa)** | |
|---|---|---|
| | **First Series** | **Second Series** |
| Reference Mortar | 41.99 | 26.51 |
| Mortar with 1% Volumetric Ratio of Steel Fiber | 39.73 | 28.53 |
| Mortar with 2% Volumetric Ratio of Steel Fiber | 39.06 | 31.01 |

For the first series, addition of steel fiber has no effect on the compressive strength of mortar. Yet it even decreases the strength approximately 7%. Mortar with bonding agent (2$^{nd}$ series) shows different compressive strength trend with the addition of steel fiber. 2% steel fiber enhances the compressive strength of mortar approximately 17%. Since the first series prepared with plasticizer has larger compressive strength, it was selected as the strengthening agent of masonry infill wall.

**e) Adhesion Strength**

Adhesion strength of the mortars were determined at 28 days. Tests were conducted according to TS EN 1015-12. Views of testing are shown in **Figure 3.4**.

**Figure 3.4** Views of Adhesion Strength Testing

Adhesion strength was calculated by dividing the maximum tensile load to the corresponding loading area. Average adhesion strength is calculated by taking average of adhesion strengths of five specimens for each mortar and rounding this number to the closest 0.1 MPa.

Adhesion strength of the mortars, reference mortar and mortars having 1% and 2% volume contents of steel fibers, at 28 days are presented in **Table 3.6**.

**Table 3.6** Adhesion Strength of the Mortars (MPa)

| | **Ave. Adhesion Strength (MPa) (28 Days)** |
|---|---|
| Reference Mortar | 1.02 |
| Mortar with 1% Volumetric Ratio of Steel Fiber | 1.73 |
| Mortar with 2% Volumetric Ratio of Steel Fiber | 1.92 |

As can be seen from the table, addition of steel fiber to the mortar increased the adhesion strength considerably.

## 3.3 PREPARATION OF THE MAIN SPECIMENS

Preparation of the test specimens includes following steps: Preparation, making cage, and placing of reinforcement in formwork, concrete casting, brick laying, plastering, anchoring, strengthening using mortar containing steel fiber, placing the test specimen in the set-up, mounting measurement instruments, performing the test, taking down the test specimen after the test and taking it to the place that it will be stored temporarily until the end of the project.

### 3.3.1 Details of the Test Specimens

The frame specimens had a clear span of 1300 mm, and a net story height of 750 mm. The columns were 100 $\times$ 150 mm and the beams were 150 $\times$ 150 mm. The rigid foundation beam was 400 $\times$ 450 $\times$ 1900 mm [25]. First Duvarcı [18] used this size of specimen in his tests. Dimensions of specimens are given in **Figure 3.5**.

Details of the test specimens were selected by Duvarcı [18] to present the lack of satisfactory qualifications seen in most of the structures in Turkey. For beams, 6$\phi$8 plain bars were used as longitudinal reinforcement. Top reinforcements of the beams were extended into the columns, bent 90º downwards, and hooked. The beams' bottom reinforcement was extended into the columns and their ends were bent 90º upwards. For columns, 4$\phi$8 plain bars were used as longitudinal reinforcements. Outer longitudinal reinforcements of columns were bent 90º inwards and hooked 135º. Columns' inner longitudinal reinforcements were bent 90º outwards and hooked 135º. For both the columns and beams, $\phi$4 plain bars were used as stirrups at 100 mm intervals. Ends of the stirrups were bent only

90º. Straight portions of the hooks were extended fifteen bar diameters (60 mm) [25]. Reinforcement patterns of the test specimens are illustrated in **Figure 3.6**.

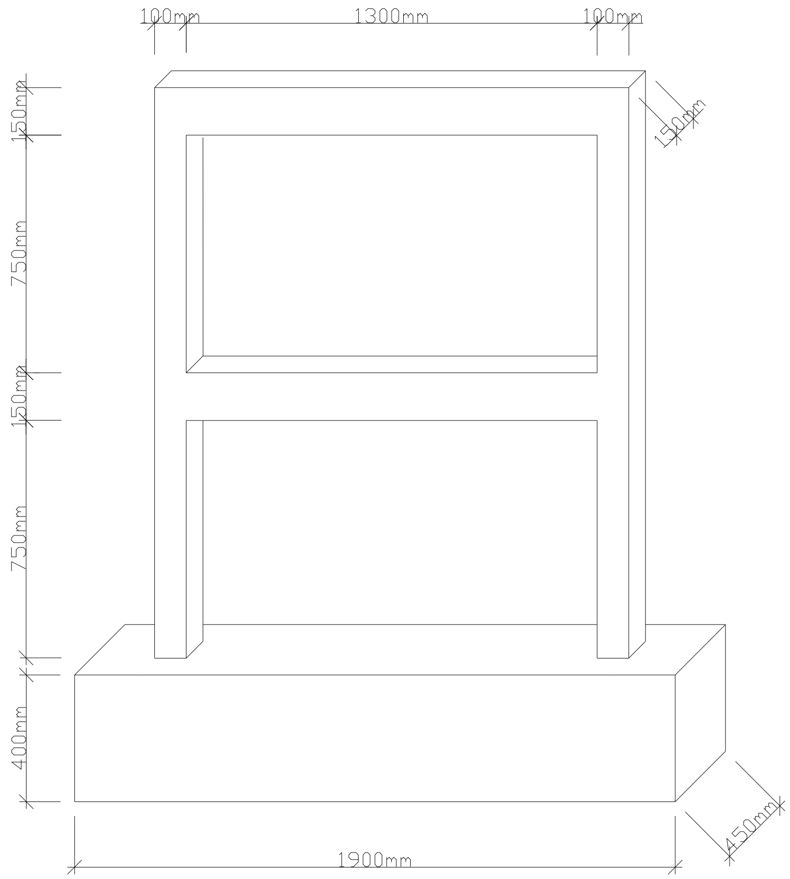


**Figure 3.5** Dimensions of the Test Specimens

Reinforcement details of the columns and beams are given in **Figure 3.7**. Same reinforcement details were used for all of the test specimens. Reinforcement views of columns and beams are shown in **Figure 3.8**.

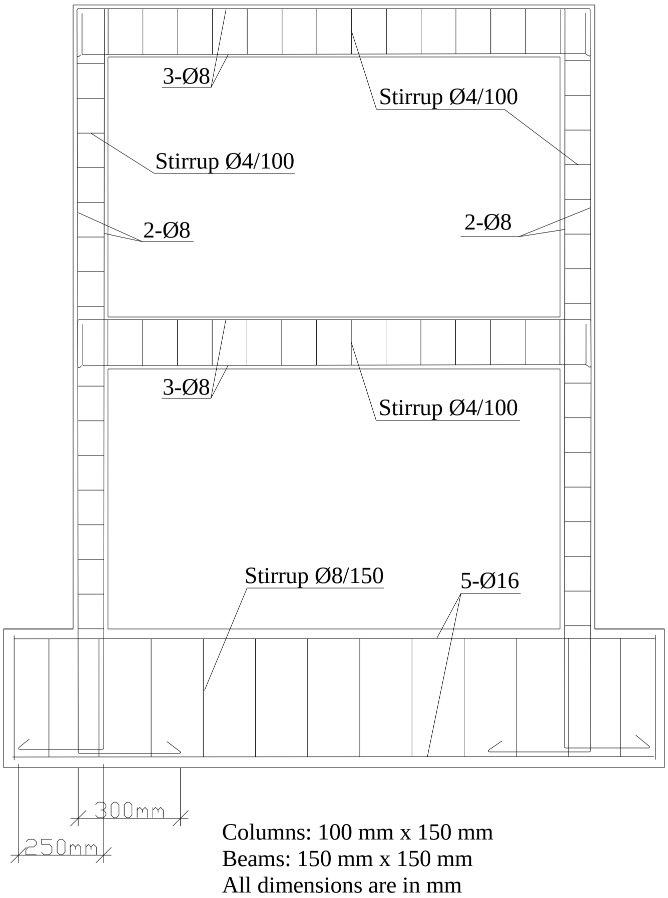


**Figure 3.6** Reinforcement Patterns of the Test Specimens

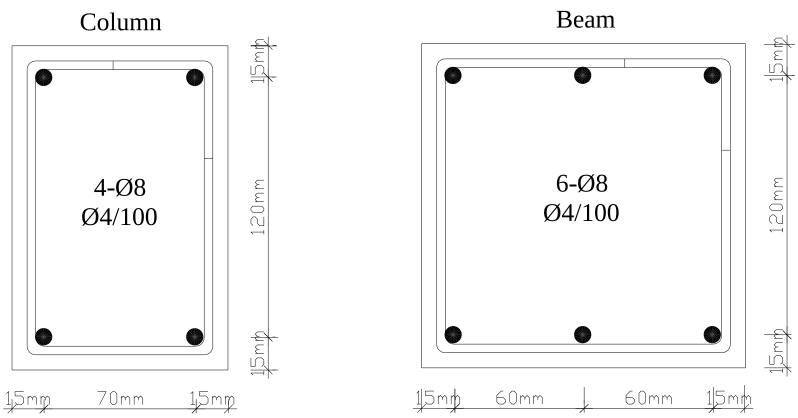


**Figure 3.7** Reinforcement Details of the Columns and Beams

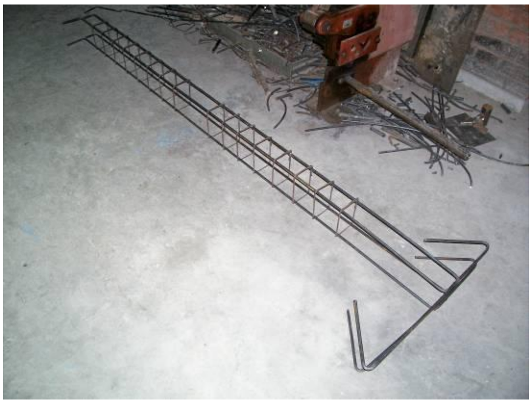

View of Column Reinforcement View of Beam Reinforcement

**Figure 3.8** Reinforcement Views of the Columns and Beams

### 3.3.2 Formwork

All of the frame specimens were cast horizontally using steel formwork already available in the laboratory. The formwork was produced by Duvarcı [18] from 2 mm thick steel plates, which were connected with bolts. The formwork was strong enough to prevent any deformations during concrete casting. The stiffness was obtained by bending the edge of forms. The width and length of the bent edges were 20 mm and 50 mm, respectively [25].

### 3.3.3 Foundation

Rigid foundation beams were prepared and cast with each frame. Foundations had dimensions of 1900 mm length, 450 mm width, and 400 mm height. For the foundation beam, 10$\phi$16 deformed bars, being 5 at the top and 5 at the bottom, were used as longitudinal reinforcement. Deformed bars having 8 mm diameter were used as stirrups at a spacing of 150 mm. Ends of the stirrups were 135º hooked. Straight portion of the hook was extended fifteen bar diameters (120 mm). Bottom and top longitudinal reinforcements of the foundation beams were welded to each other using deformed bars of 16 mm diameter [25]. Plan drawing of the foundation beam is presented in **Figure 3.9**. Reinforcement views of specimen foundation are given in **Figure 3.10**.

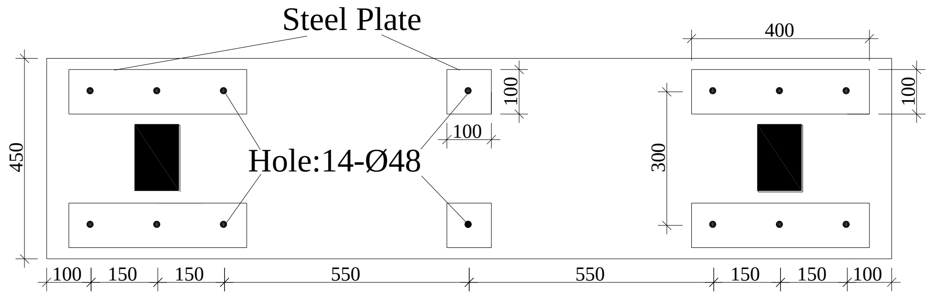


All dimensions are in mm

**Figure 3.9** Plan View of the Foundation Beam

General View of Reinforcements View of Foundation Beam Reinforcement

**Figure 3.10** Reinforcement Views of the Foundation Beams

### 3.3.4 Universal Base

A universal base, already available in the laboratory, was used to fix the frame specimens. The specimens were mounted on the universal base which was fixed with steel bolts to the strong floor of the laboratory. The purpose of the universal base was to prevent movement of the specimens in any direction during the test.

The universal base is an R/C mat having dimensions of 400 $\times$ 1500 $\times$ 2950 mm. Dimensions and details of the universal base is shown in **Figure 3.11**. Ready mixed self-compacting concrete having strength of 30 MPa was used by previous researchers for the base.

In order to fix the foundation to the strong floor, six 60 mm diameter holes were left in the foundation, matching the holes in the strong floor. The foundation was pre-stressed to the strong floor by 50 mm diameter steel bolts passing through the holes.

The universal base was designed, previously, to be able to fix different specimens. For this purpose, M38 nuts were used corresponding to the holes of specimens. In order to fix specimen on the universal base, each specimen had 14 holes. On the foundation, 34 fastener bolt holes were arranged [18].

### 3.3.5 Casting of Concrete

Concrete of the frames was produced in the Structural Mechanics Laboratory of the Middle East Technical University. Concrete of one frame specimen was cast in 3 batches. Formworks of frame and cylinders were oiled; afterwards reinforcement was placed in the formwork. Then, concrete was cast. To determine the concrete strength, 3 standard cylinder specimens were taken from each batch. Totally 10 cylinders, including 1 reserve, were taken for one frame specimen. Test cylinders were 150 mm in diameter and 300 mm in height. Cylinders were kept under same conditions as the test specimens. Curing was done by covering the specimens

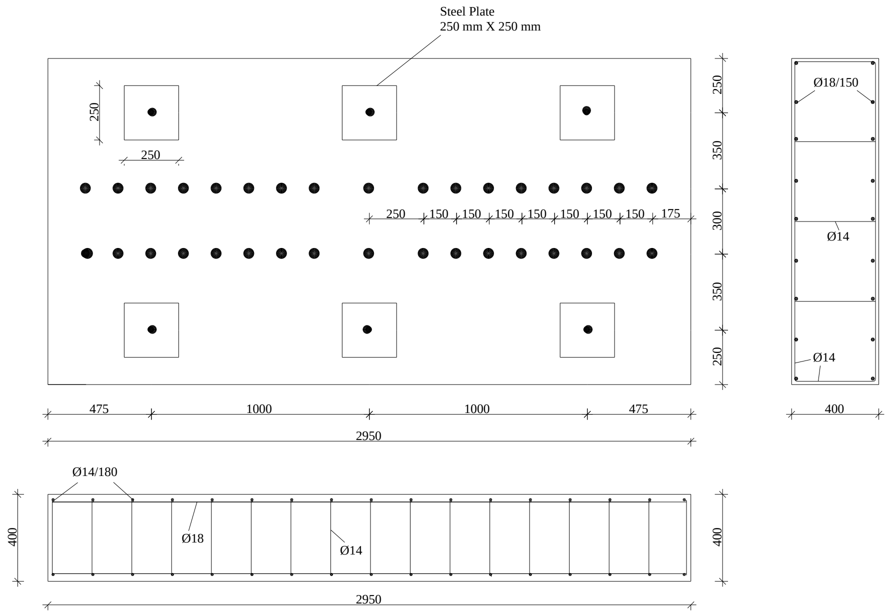


**Figure 3.11** Dimensions and Details of the Universal Base (all dimensions in mm)

with wet burlap in order to maintain moisture [25]. View after concrete casting is presented in **Figure 3.12**.

**Figure 3.12** View of Frame Specimen after Concrete Casting

### 3.3.6 Brick Laying and Plastering

After minimum 7 days of curing, forms were removed and specimens were hold up in vertical position. After preparation of the frame specimens, brick laying operations were completed. On the brick walls, plaster having 6 mm thickness was applied. Brick laying and plastering applications are illustrated in **Figures 3.13** and **3.14**, respectively.

### 3.3.7 Anchoring and Strengthening

After completing plastering operations, mortar with 2% volumetric ratio of steel fibers was applied on original plaster. For comparison purposes, one specimen was strengthening with 2% polypropylene (PP), another specimen with 2% hybrid fiber (1% steel fiber + 1% PP), and one more specimen with mortar lacking of any fiber.

To ensure force transfer between frame and strengthened masonry infill wall, anchorage bars were fixed to the surrounding frame. As anchorage, deformed bars having 180 mm length and 8 mm diameter were used. Bars were placed at 200 mm intervals with 60 mm embedded in to the frame and 120 mm remained outside. Totally 80 anchorage bars were used for one frame.

Anchoring of a frame specimen is shown in **Figure 3.15**. Strengthening using mortar with or without fibers is presented in **Figure 3.16**.

**Figure 3.13** View of Brick Laying Application

**Figure 3.14** View of Plastering Application

**Figure 3.15** View of Anchoring Operation

**Figure 3.16** View of Strengthening Operation

## 3.4 PROPERTIES OF THE MAIN TEST SPECIMENS

Totally 10 frame tests were performed in the scope of the project. Among the conducted tests, 4 were done as reference tests. Reference specimens were produced as one bare frame, one non-plastered frame with infill walls, one plastered frame with infill walls, and one plastered, anchored, 2 cm thickness of mortar without fibers applied frame.

The other 6 tests were strengthened frame tests. One of the frames was a plastered, non-anchored, 10 mm thickness of mortar with 2% volumetric ratio of steel fiber applied frame. Also, one of the frames was a plastered, non-anchored, 20 mm thickness of mortar with 2% volumetric ratio of steel fibers applied frame. Two of the frames were produced as plastered, anchored, one of the frames as 10 mm and the other one as 20 mm thickness of mortar with 2% volumetric ratio of steel fibers applied frames. Another frame was a plastered, anchored, 20 mm thickness of mortar with 2% volumetric ratio of PP fiber applied frame. The last frame was produced as a plastered, anchored, 20 mm thickness of mortar with 2% volumetric ratio of hybrid fiber, obtained by mixing 1% of steel fibers and 1% of PP fibers, applied frame.

Properties of the frame tests' specimens are summarized in **Table 3.7**.

**Table 3.7** Properties of the Test Specimens

| Specimen | Brick | Plaster (mm) | Anchorage | Steel Fiber Ratio | Polypropylene Fiber Ratio | Thickness of Fiber Reinforced Mortar (mm) |
|---|---|---|---|---|---|---|
| REFBA | - | - | - | - | - | - |
| REFB | + | - | - | - | - | - |
| REFBM | + | 6 | - | - | - | - |
| REF2ABM | + | 6 | + | - | - | 20 |
| SF1NABM | + | 6 | - | 2% | - | 10 |
| SF2NABM | + | 6 | - | 2% | - | 20 |
| SF1ABM | + | 6 | + | 2% | - | 10 |
| SF2ABM | + | 6 | + | 2% | - | 20 |
| PPF2ABM | + | 6 | + | - | 2% | 20 |
| HF2ABM | + | 6 | + | 1% | 1% | 20 |

## 3.5 MATERIALS

### 3.5.1 Concrete

Concrete mix design of frames is given in **Table 3.8**. Materials used are given by weight for 1 $m^3$ of concrete. Target compressive strength of the frame concrete was determined as 10 MPa. For each frame specimen 10 standard cylinders were taken in order to determine concrete strength [18]. Concrete strengths of the frame specimens are shown in **Table 3.9**. As can be seen in **Table 3.9**, concrete strength of frames varied considerably. This variation can be attributed to curing condition, curing time, temperature difference, and water content difference in sand.

**Table 3.8** Concrete Mixture Design of the Frames

| | Weight (kN) | Ratio by Weight (%) |
|---|---|---|
| Cement | 1.54 | 12 |
| 0-3 mm Aggregate | 2.43 | 19 |
| 3-7 mm Aggregate | 4.86 | 38 |
| 7-15 mm Aggregate | 2.56 | 20 |
| Water | 1.40 | 11 |
| Total | 12.79 | 100 |

**Table 3.9** Concrete Strengths of the Frame Specimens (MPa)

| Specimen | Average Concrete Strength (MPa) |
|---|---|
| REFBA | 12.7 |
| REFB | 13.3 |
| REFBM | 12.7 |
| REF2ABM | 8.6 |
| SF1NABM | 9.9 |
| SF2NABM | 14.8 |
| SF1ABM | 17.0 |
| SF2ABM | 13.6 |
| PPF2ABM | 10.0 |
| HF2ABM | 11.6 |

### 3.5.2 Steel

In specimens $\phi 4$, $\phi 8$ plain bars and $\phi 8$, $\phi 16$ deformed bars were used. In columns 4 and in beams 6 $\phi 8$ plain bars were used as longitudinal reinforcement. In columns and beams, $\phi 4$ plain bars, which had 90º hooks at the ends, were used as stirrups. In foundation beams, $\phi 16$ deformed bars were used as longitudinal reinforcement and $\phi 8$ deformed bars were used as stirrups. They were 135º hooked at the ends. Longitudinal and transverse reinforcements were produced from the same steel batch. For the anchoring operations, $\phi 8$ deformed bars were used [25]. For each steel 3 test coupons were taken randomly from the batch. Coupons were tested in tension. Typical properties of steel bars are provided in **Table 3.10**.

**Table 3.10** Properties of Reinforcing Bars

| **Bar Type** | **Property** | **Location** | **Yield Stress, $f_{sy}$ (MPa)** | **Ultimate Stress, $f_{su}$ (MPa)** |
|---|---|---|---|---|
| $\phi 4$ | Plain | Column and Beam Stirrup | 271 | 398 |
| $\phi 8$ | Plain | Column and Beam Longitudinal Bars | 365 | 511 |
| $\phi 8$ | Deformed | Anchorage Bar, Foundation Beam Stirrup | 557 | 782 |
| $\phi 16$ | Deformed | Foundation Beam Longitudinal Bar | 453 | 682 |

### 3.5.3 Infill

In all of the specimens, hollow brick was used as infill material. Special production was done and bricks were scaled down (1/3 scale) to simulate real brick. Totally 10 bricks were tested by loading in the direction parallel to holes and average result of compression tests on tiles are presented in **Table 3.11**. The dimensions of the hollow brick used as infill material are shown in **Figure 3.17**. As can be seen from **Table 3.11**, compressive strength of bricks are relatively high. The outer dimensions of bricks were scaled down by 1/3. But, the thickness of the brick walls could not be scaled in the same manner. Therefore, their net area is high, which results in higher gross compressive strength.

**Table 3.11** Results of Compression Tests on Tiles

| | **Failure Load (kN)** | **Gross Area ($mm^2$)** | **Gross Compressive Strength (MPa)** | **Net Area ($mm^2$)** | **Net Compressive Strength (MPa)** |
|---|---|---|---|---|---|
| Ave. | 73.8 | 5865 | 13.1 | 2815 | 27.3 |

### 3.5.4 Mortars

Mix proportions of the mortars used are presented in **Table 3.12**. Compressive strength of the mortars were determined by testing 3 cylinders having 75 mm diameter and 150 mm height for each test individually. Test results of cylinders taken from the mortars of the frame specimens are given in **Table 3.13**.

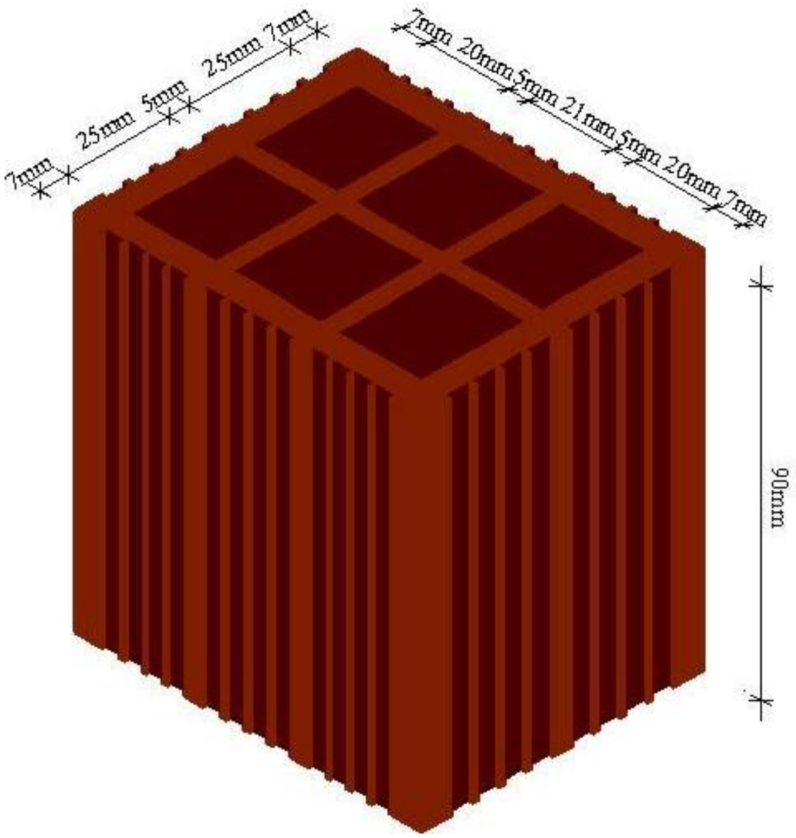


**Figure 3.17** Dimensions of the Hollow Brick

**Table 3.12** Mix Proportions of the Frame Specimens' Mortars

| | **Weight (kg)** | | | | | |
|---|---|---|---|---|---|---|
| | **Brick Laying Mortar** | **Plastering Mortar** | **Strength Mortar with 2% SF** | **Strength Mortar with 2% PP Fiber** | **Strength Mortar without Fiber** | **Strength Mortar Hybrid** |
| Cement (CEM I 32.5 R) | 13.8 | 11.9 | 22 | 23.3 | 23.4 | 22.6 |
| 0-3 mm Aggregate | 66.0 | 67.9 | 60 | 63.4 | 63.8 | 61.6 |
| Lime | 6.4 | 5.5 | - | - | - | - |
| Water | 13.8 | 14.7 | 12 | 12.7 | 12.8 | 12.3 |
| Plasticizer | - | - | 0.04 | 0.042 | 0.043 | 0.041 |
| Steel Fiber | - | - | 6 | - | - | 3.1 |
| PP Fiber | - | - | - | 0.63 | - | 0.41 |
| Total | 100 | 100 | 100 | 100 | 100 | 100 |

**Table 3.13** Strengths of Mortars of the Frame Specimens (MPa)

| | Compressive Strength at test day (MPa) | | | | | |
|---|---|---|---|---|---|---|
| | **Brick Laying Mortar** | **Plastering Mortar** | **Strength Mortar with 2% SF** | **Strength Mortar with 2% PP Fiber** | **Strength Mortar without Fiber** | **Strength Mortar Hybrid** |
| REFBA | - | - | - | - | - | - |
| REFB | 3.4 | - | - | - | - | - |
| REFBM | 8.4 | 8.2 | - | - | - | - |
| REF2ABM | 8.7 | 6.0 | - | - | 40.8 | - |
| SF1NABM | 7.5 | 6.4 | 17.0 | - | - | - |
| SF2NABM | 7.4 | 7.2 | 20.8 | - | - | - |
| SF1ABM | 6.0 | 7.2 | 22.0 | - | - | - |
| SF2ABM | 12.9 | 7.6 | 20.9 | - | - | - |
| PPF2ABM | 10.8 | 6.6 | - | 29.3 | - | - |
| HF2ABM | 9.9 | 6.2 | - | - | - | 24.8 |

While performing plastering operation of the frames, only the face of the brick wall was plastered at the interior side whereas at the exterior side brick wall together with the columns and beams were plastered. Plaster thickness was 6 mm on each face.

Mortars with 2% volumetric ratio of steel fibers, without steel fiber and/or PP fiber, with 2% volumetric ratio of PP fibers, and with 2% volumetric ratio of hybrid fibers, 1% steel fiber and 1% polypropylene fiber were applied on the plaster of the frame specimens.

## 3.6 TEST SET-UP AND LOADING SYSTEM

One-bay, two-story specimens, have been tested in the METU Structural Mechanics Laboratory for years. This test set-up was first used by Duvarcı [18]. In this research, specimens have been tested vertically in their original position. The set-up and testing system consisted of strong floor, reaction wall, loading equipment, instrumentation, and the data acquisition system.

In order to apply and measure the lateral force, a load cell was attached to the hydraulic jack, which was bearing against the reaction wall. The reaction wall was also fixed to the strong floor using bolts. Height of the reaction wall is 4.5 m. There are fourteen holes on the wall that are spaced as two columns and seven rows. The distance between the columns is 1 m and the distance between the rows is 700 mm.

The lateral loading system was attached to the strong wall and in line with the beams of the test specimen. The loading system consisted of a hydraulic jack, a load cell, and adaptors for connecting the load cell and the hydraulic jack and hinges at both ends. The loading system had to move freely on the strong wall allowing accurate positioning. For this reason, a rail system was designed using steel sections. The sliding mechanism was fixed to the reaction wall by means of 4 steel pipes.

Reversed cyclic lateral loading was applied by using a double acting hydraulic jack. A load cell was connected between the hydraulic jack and the test frame to measure the applied lateral load. The load cell was calibrated in the laboratory prior testing. An adapter made from steel was used to connect the hydraulic jack and load cell. The lateral loading system had pin connections at both ends to eliminate any accidental eccentricity [25]. A general view of the sliding mechanism between the reaction wall and lateral loading system is shown in **Figure 3.18**.

A steel guide frame was constructed around the test specimen in order to prevent out-of-plane deformations. The columns in the long direction were connected to each other by steel box sections. In the short direction the columns were connected by L steel section. The connection of the steel frame with the test specimen was done at second story level by means of roller supports in order to permit in

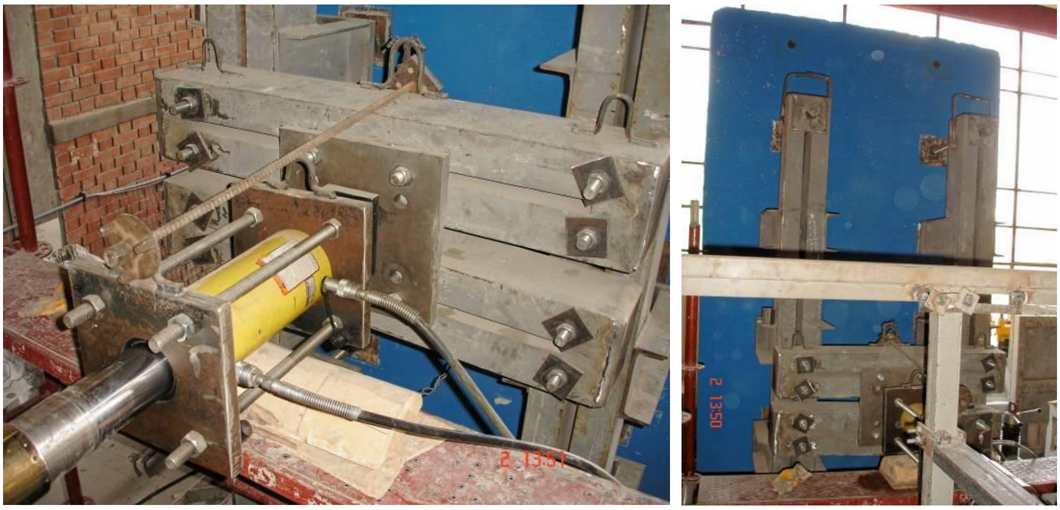

**Figure 3.18** A General View of the Sliding Mechanism

plane movement of the specimen. Four rollers were attached to the box sections, and they touched the test frame beam. For rollers, ball bearings were used since the test frame had to make vertical as well as horizontal displacement [18]. Guide frame and ball bearings are shown in **Figures 3.19** and **3.20**, respectively.

**Figure 3.19** Appearance of Guide Frame

**Figure 3.20** Ball Bearings

Lateral load was applied on both stories in triangular manner simulating earthquake. The lateral load was applied to the stories through a spreader beam which transfers the load coming from the hydraulic jack in 2:1 ratio to the stories as illustrated in **Figure 3.21**. At floor levels, clamps made of four steel bars were loosely attached to the test frame. At the spreader beam side, loading plates at both floor levels were welded to the spreader beam. Before every test, the clamps were carefully controlled to be loose enough without any external stressing on the beams.

The axial load on columns, 53.38 kN, was provided by steel cables post-tensioned by hydraulic jacks. This axial load corresponds between 9.2% and 14.6% of axial load capacity depending on frame concrete strength. Two hydraulic jacks were used for this purpose. To apply the axial load, built up box sections were attached to the bolts fixing the foundation beam to the main foundation. On both sides of the test specimen, built up steel sections were fixed by using the bolts on the universal base and bolts on the foundation of the test frame. The steel cables were threaded through the holes provided in the box sections and fixed at the hydraulic

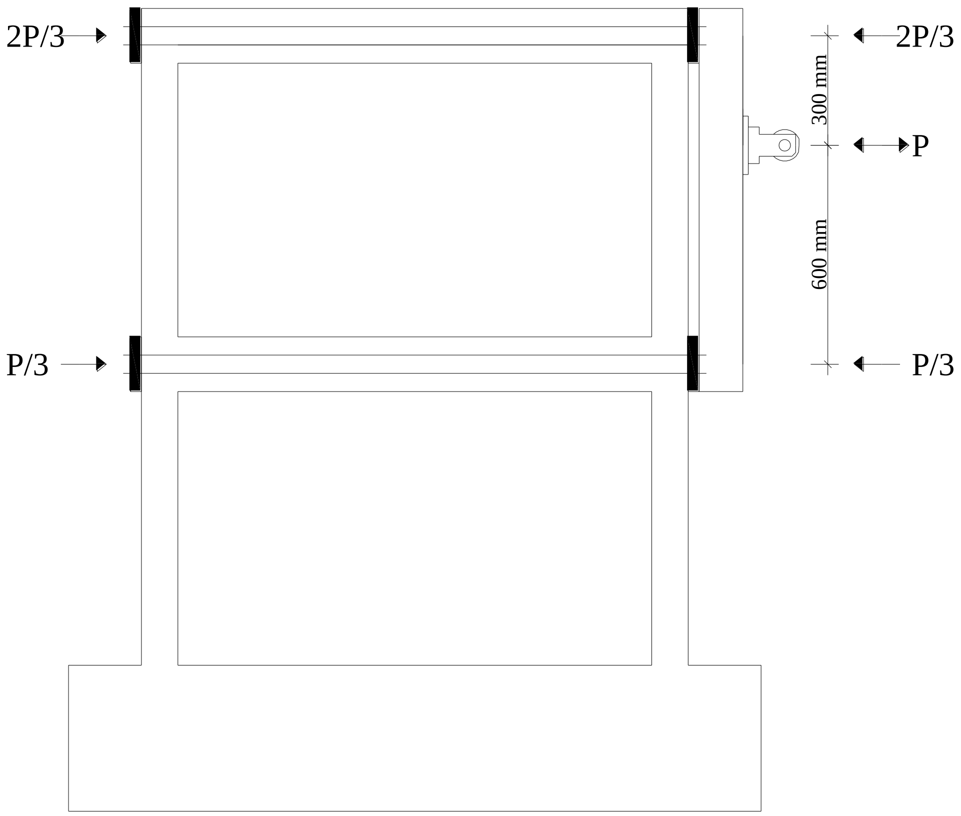


**Figure 3.21** Load Distribution between the Floor Levels

jacks which were placed under the box sections. The other ends of the steel cables were connected to a cross beam which was welded to another spreader steel beam simply supported at the top story columns of the specimens. When the load was applied, the spreader beam divided the load developing in the hydraulic jacks and the steel cables into two equal components and transferred it to the two columns. The load was continuously monitored and readjusted during the test [25].

Application of axial load is shown in **Figure 3.22**. General view of the test set-up is given in **Figures 3.23** and **3.24**.

**Figure 3.22** Application of Axial Load

## 3.7 INSTRUMENTATION

Displacement transducers, either LVDTs (Linear Variable Differential Transformer) or electrical dial gages were used for deformation measurements and load cells were used for load measurement. Also, strain gages having a length of 120 mm were used in the first test, REFBM for strain measurements. The capacity of the load cell was 266.89 kN in the first test and the capacity of the load cell used in all of the remaining tests was 444.82 kN.

Deformations were measured by LVDTs with 200 mm, 100 mm, and 50 mm strokes and dial gages with 50 mm, in the first test, and 30 mm strokes, in the other tests. A general view of the instrumentation is shown in **Figure 3.25**. In each test voltage signals coming from the transducers were recorded by a data acquisition system named System 6000 Vishay and the results were send to a personal

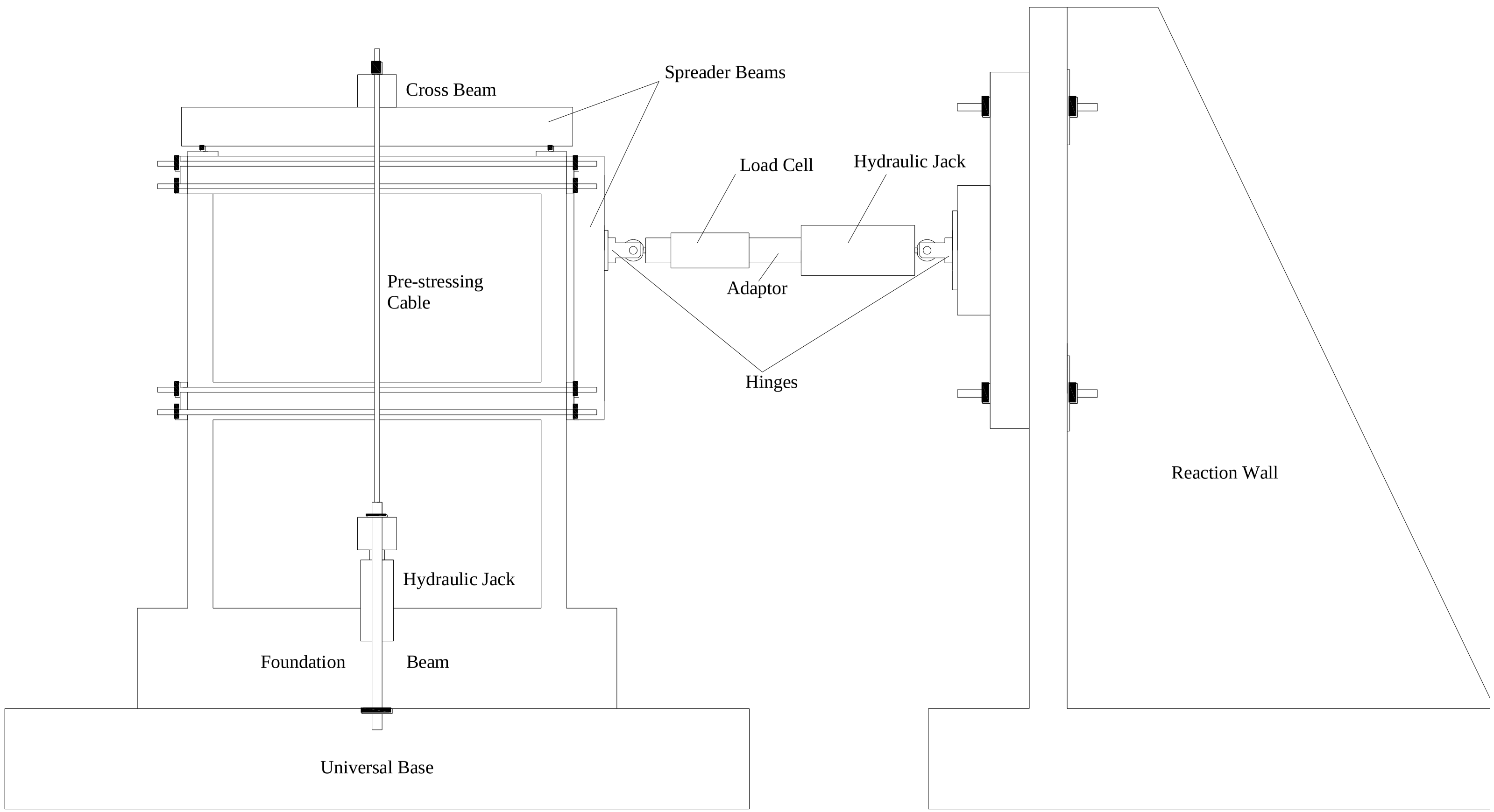


**Figure 3.23** General View of the Test Set-up

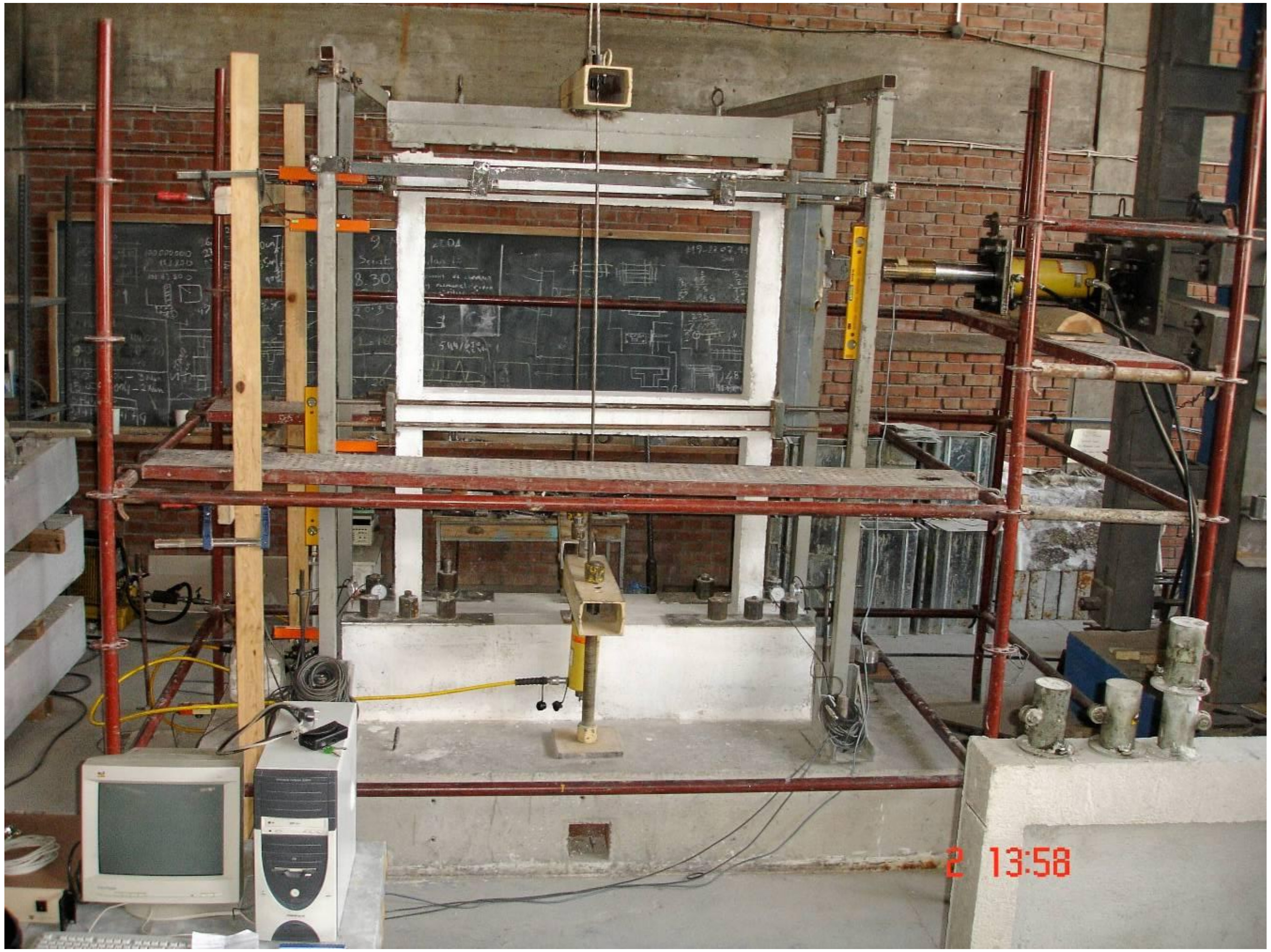


**Figure 3.24** Appearance of the Test Set-up

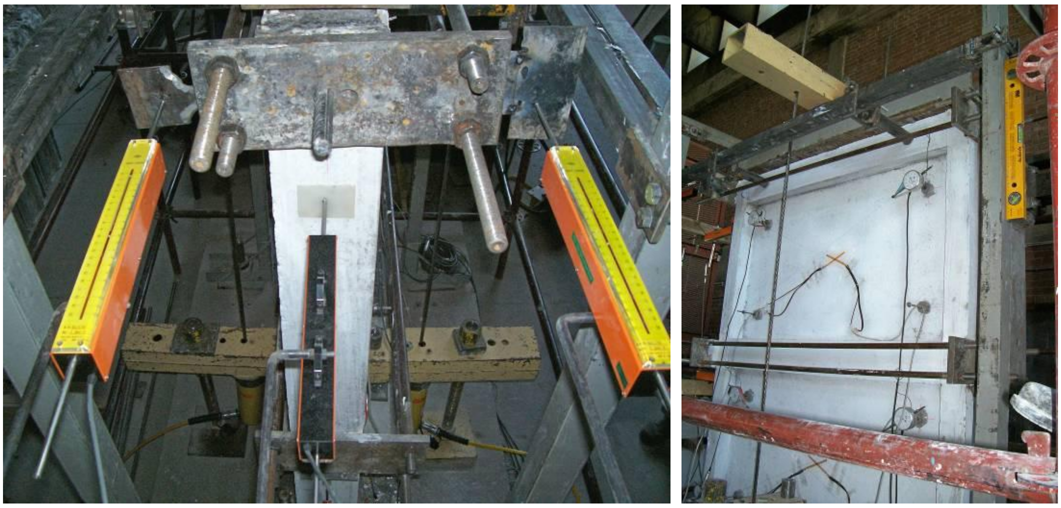

**Figure 3.25** A General View of the Instrumentation

computer. The results were converted to displacements and load values. They were monitored from the software named StrainSmart 4.0.

Lateral displacement of each story was measured with respect to the universal base. Three LVDTs, two at the 2$^{nd}$ story level and one at the bottom of the column-beam connection, were mounted at the 2$^{nd}$ story level whereas one LVDT was mounted at the 1$^{st}$ story level for this purpose. These transducers measured the second and first story displacements. The readings from the LVDTs were used to construct load-displacement and load-story drift curves. Details of the instrumentation are presented in **Figure 3.26**.

Shear deformations were measured on both first and second story infill walls by means of two diagonally placed dial gages mounted on infill. Transducers were located 130 mm away from the corner of the infill walls. The reason for choosing this location was to avoid localized effects like crushing of concrete during experiment.

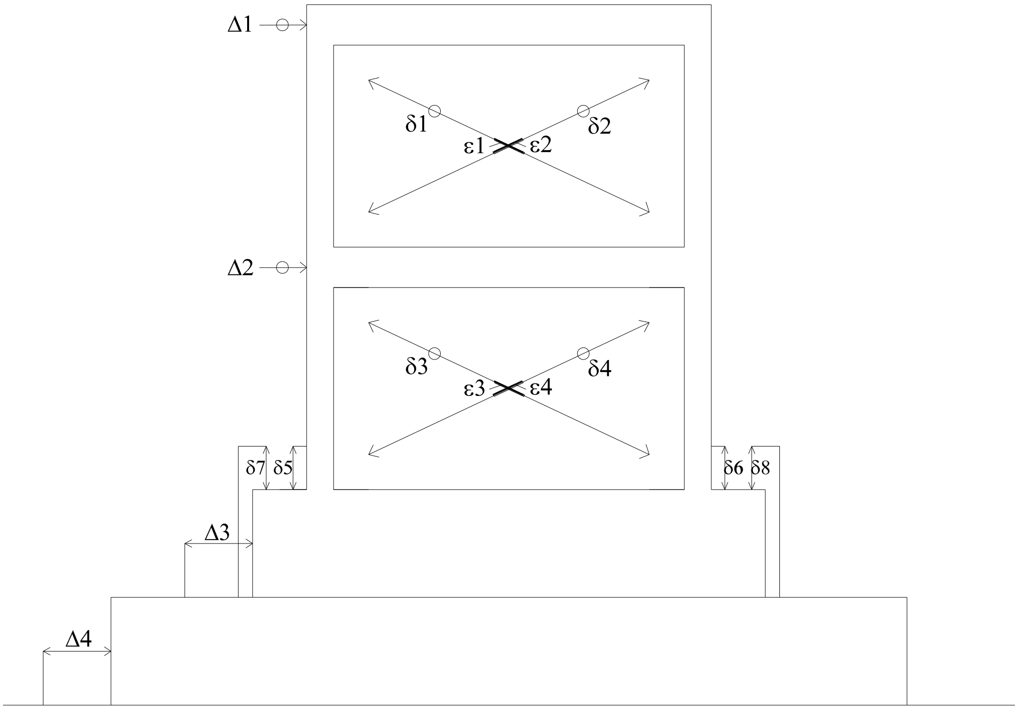


$\varepsilon 1, \varepsilon 2, \varepsilon 3, \varepsilon 4$ : Strain gages of 120 mm length (used in REFBM test only)
$\delta 1, \delta 2, \delta 3, \delta 4$ : Dial gages with 30 mm strokes (50 mm in REFBM test)
$\delta 5, \delta 6$ : Dial gages with 20 mm strokes
$\delta 7, \delta 8$ : Dial gages with 10 mm strokes
$\Delta 1$: LVDTs with 200 mm strokes
$\Delta 2, \Delta 3$ : LVDTs with 100 mm strokes
$\Delta 4$ : LVDT with 50 mm stroke

**Figure 3.26** Details of the Instrumentation

In order to measure the strain values at the bottom of the columns dial gages were mounted in vertical position at the bottom of north and south columns. These readings would be used to have an idea about the crack widths at the column-foundation connections.

The rigid body displacements of the frame and universal base were measured by means of LVDTs. An LVDT was mounted on the universal base in order to measure the displacement with respect to the ground and another was mounted on the frame foundation in order to measure the displacements with respect to the universal base. Also, dial gages at both sides were mounted on the frame foundation to measure the displacements with respect to the universal base.

## 3.8 TEST PROCEDURE

After fixing the main foundation to the strong floor, the specimen was carried and positioned so that it was perpendicular to the reaction wall. They were fixed to the universal base by post-tensioning of the bolts. Each test specimen was whitewashed before the test to be able to observe the cracks better during the test. After the axial load apparatus were mounted, the clamps were loosely attached, the load cell and the hydraulic jack for applying lateral load was mounted. Then, displacement transducers (LVDTs and dial gages) were mounted onto the test specimens and their connections to the data acquisition system were established. The calibration of the transducers was re-checked. As a safety precaution, the spreader beam was suspended by a chain attached to the crane. After all, concrete cylinders were tested to get the compressive strength of the test specimen and plaster. Eventually, a constant axial load of 53.38 kN (9.2% $N_0$ – 14.6% $N_0$) was applied on the columns and tried to be kept constant throughout the testing of all of the specimens.

Loading a specimen to a pre-determined lateral load level and then unloading it to zero level constitutes a half cycle loading. Addition of a backward half cycle to a forward half cycle represents a full cycle. All specimens were tested under reversed cyclic lateral loading simulating earthquake loading. During the tests, second story level displacement versus lateral load diagrams were monitored. At each half cycle’s peak, cracks were marked on the specimens and notes were taken describing the observations. Up to the yielding of specimen load controlled loading scheme was applied. After yielding displacement controlled (5 mm steps) were used. The lateral loading histories and top displacement histories are provided in Chapter 4.

# CHAPTER 4

# TEST RESULTS AND OBSERVED BEHAVIOR

## 4.1 GENERAL

Test results and observations are presented in detail in this chapter. In the scope of the project, totally 10 R/C frames were tested. 4 of the tests were performed as reference tests and the remaining 6 tests were done as strengthened frame tests. For each specimen; load history, second story displacement history, load vs. second story displacement, load vs. first story displacement, load-second story shear displacement, and load-first story shear displacement graphs are provided in this chapter. The calculation of shear displacement is given in **Appendix A**. While drawing charts about the second story displacements, only 2/3 of the total applied load is shown on the lateral load axis. For the first story displacements, however, the total load (base shear) is taken into consideration in the graphs. This is due to the fact that second story is displaced under only 2/3 of the total applied lateral load.

## 4.2 REFERENCE SPECIMEN, REFBA

The first test performed was the reference test REFBA which was the bare frame TS5. The test results of this specimen would be used as a reference for the behavior of the strengthened frame specimens. The specimen was subjected to the lateral loading history presented in **Figure 4.1**. The maximum forward load was 14.53 kN and the displacement at this load level at the second story was measured as 20.04 mm.

After this test, due to a problem in the load cell, the load cell was recalibrated and all of the load data was modified. Therefore, load cycles in **Figure 4.1** in the load controlled part is not symmetrical.

This frame displaced 20.52 mm at the top at a maximum backward loading of 12.03 kN. Second story displacement history is given in **Figure 4.2**.

In the observations, north column term is used for right column and south column term is used for left column when viewed from the front side of the specimen. Main observations are presented below verbally and also as figures in **Figure 4.3**.

- In the second forward cycle: At the front side, a crack at the bottom of the north column at the outer side. Also, a shear crack at the first story beam-north column joint. At the south column, a flexural crack at the inner part near to the bottom. At the back side, a shear crack at the first story beam-north column joint.
- In the third forward cycle: At the back side, a flexural crack at the bottom of the north column. Also, a flexural crack above this crack and three shear cracks at the first story beam-north column joint.
- In the fourth forward cycle: displacement controlled loading was started by loading to 20 mm displacement.
- In the fourth backward cycle: At the front side, two shear cracks at the south column-first story beam joint which turned also to the inside of the joint.
- In the fifth forward cycle: At the front side, crushing at the south column bottom. A new vertical crack to the lower part of the previous shear crack formed in the fourth backward cycle, at the joint of the first story beam-south column. At the back side, progress in the shear cracks in the third forward cycle at the first story beam-north column.
- In the fifth backward cycle: At the front side, at the north column bottom inner side cracking between the column and the foundation.

- In the sixth backward cycle: At the front side, below the first story beam-column at the south column a vertical shear cracking and cover crushing. Also, at the north column a flexural crack at the inner side of the first story beam- second story column joint up to the back side of the frame.
- In the seventh forward cycle: At the front side, cover crushing at the bottom of the south column. No reading could be taken from the dial gage at the north column anymore. At the back side, a flexural crack at the outer side of the south column and cover crushing.
- In the seventh backward cycle: The eleventh channel was off-scale.
- In the eighth forward cycle: At the front side, near to the bottom of the south column an opening and the stirrup could be seen. At the north column outer side close to the bottom an opening. An opening at the bottom of the north column at the inner side.
- In the eighth backward cycle: The dial gage at the south column could not take any measurement anymore. At the front side, at the south column opening in the first story beam-column joint.
- In the ninth forward cycle: The specimen could not displace 60 mm and the displacement was stopped at 48 mm. It was unloaded, reloaded on the other side to 50 mm, and zeroed. Then, the test was finalized.

As can be seen from Figure 4.3, failure occurred mainly due to hinges formed at the first story column ends.

Load-second story displacement/drift and load-first story displacement/drift graphs are presented in **Figures 4.4** and **4.5**, respectively. Views of TS5 (REFBA) specimen during the test are shown in **Figure 4.6**. Figure 4.4 shows that second story columns remained in the elastic range within 1% drift limits. The reason for this limited drift is that the damage concentrated on the first story members. Lateral load decreased to 85% of its maximum value at approximately 2.2% first story drift ratio level.

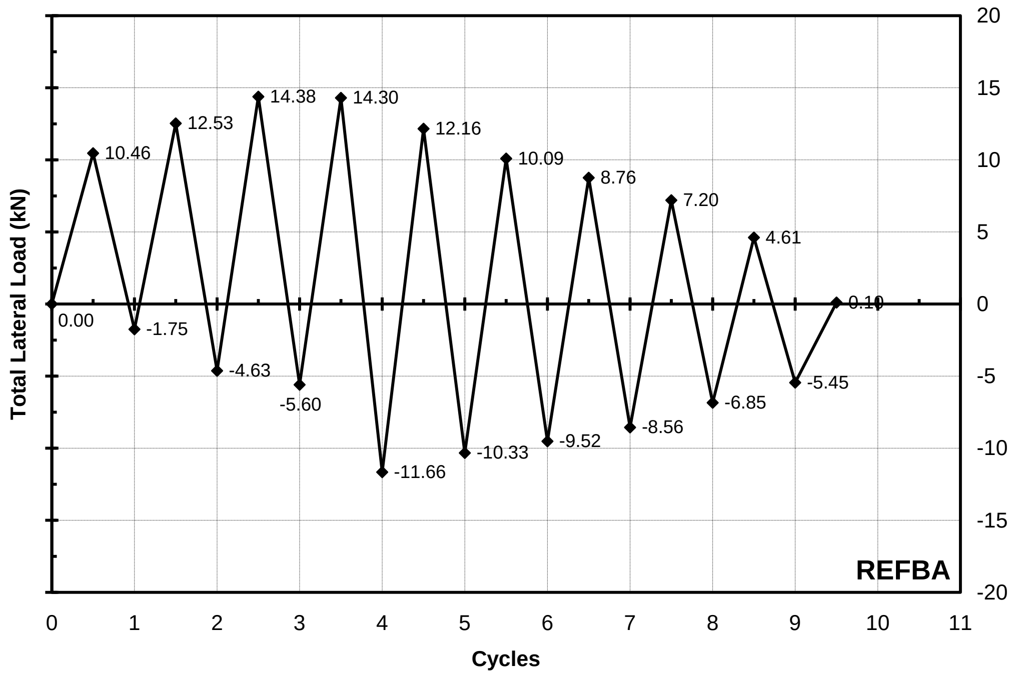


**Figure 4.1** Lateral Load History Graph of TS5 (REFBA) Specimen

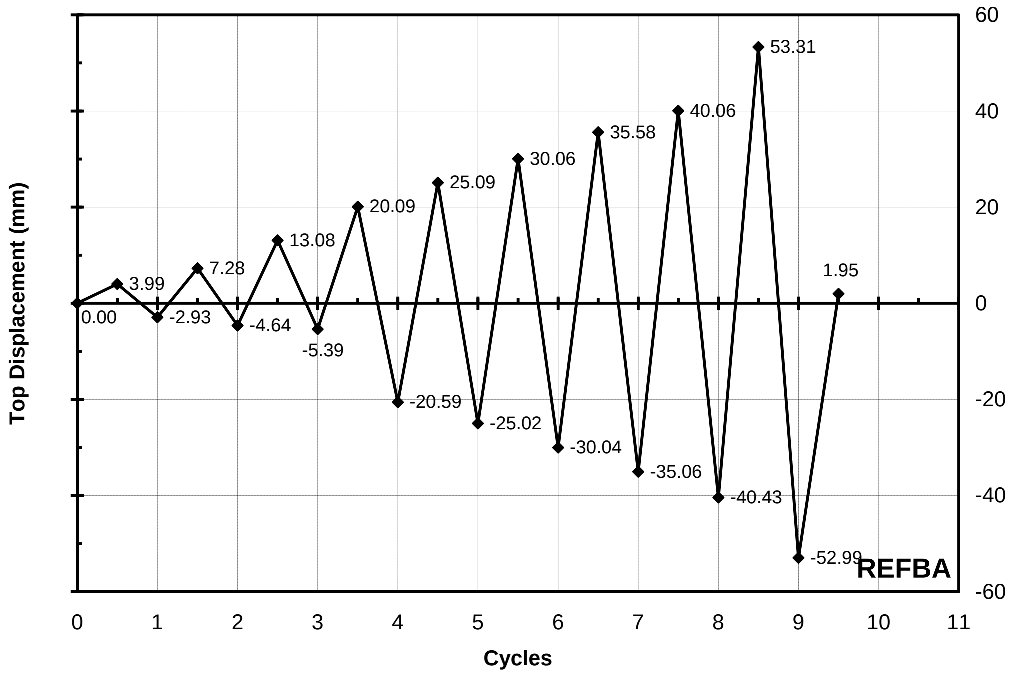


**Figure 4.2** Top Displacement History Graph of TS5 (REFBA) Specimen

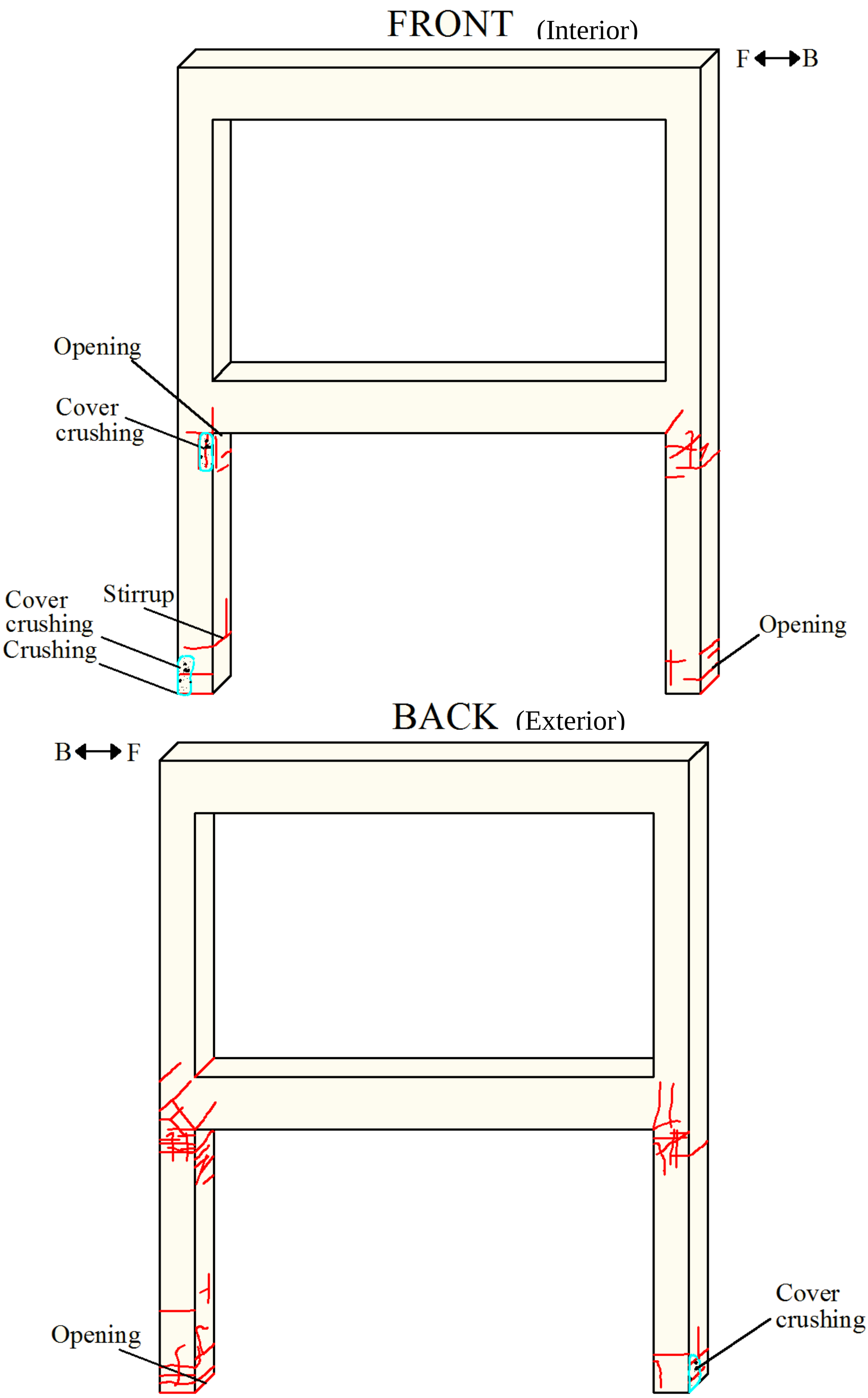


**Figure 4.3** Main Observations during the Reference Test REFBA

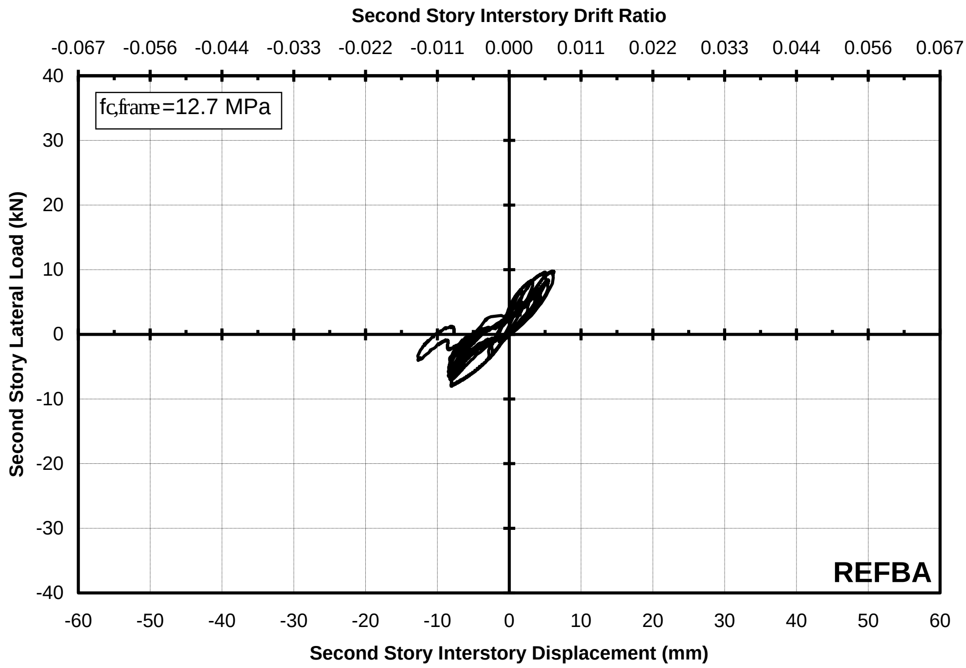


**Figure 4.4** Second Story Lateral Load-Second Story Displacement/Drift Ratio Graph of TS5 (REFBA) Specimen

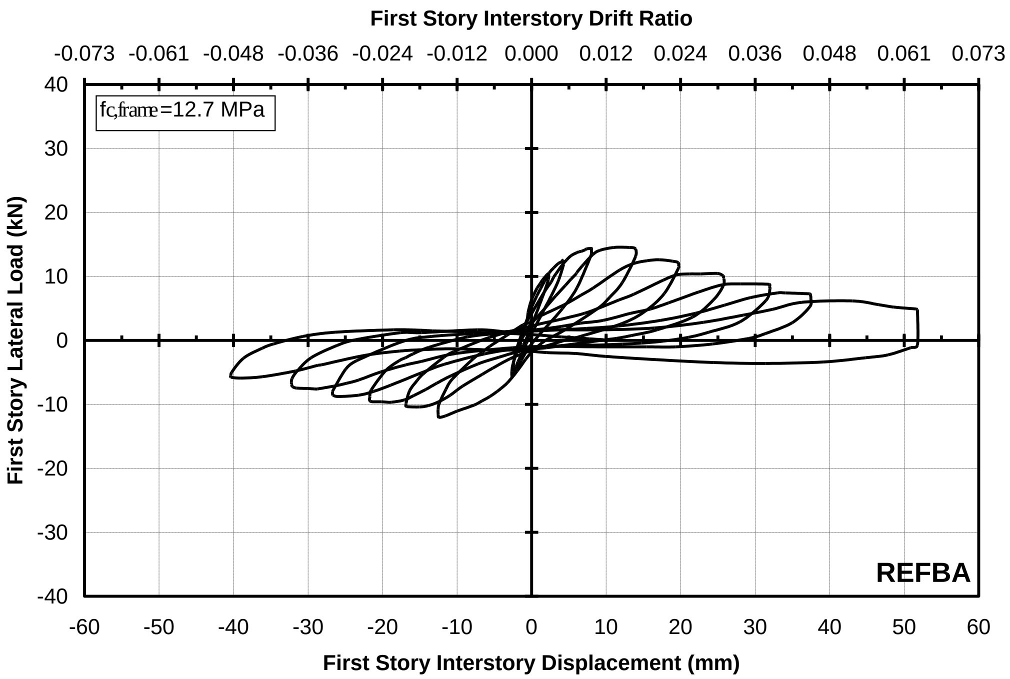


**Figure 4.5** First Story Lateral Load-First Story Displacement/Drift Ratio Graph of TS5 (REFBA) Specimen


**Figure 4.6** Views of TS5 (REFBA) Specimen during the Test

## 4.3 REFERENCE SPECIMEN, REFB

The second frame test REFB, another reference test, was the test of non-plastered, only brick infilled frame TS6. The specimen was subjected to the lateral loading history presented in **Figure 4.7**. For this test, the maximum forward load was measured as 50.23 kN and the corresponding top displacement was 14.94 mm. The maximum backward load of 50.29 kN caused a top displacement of 14.30 mm. Second story displacement history is given in **Figure 4.8**. Main observations of the test are given below verbally and also as figures in **Figure 4.9**.

- In the second forward cycle: At the front side, two shear cracks at the first story infill wall.
- In the second backward cycle: At the front side, two shear cracks at the first story infill wall perpendicular to the shear cracks formed in the second forward cycle.
- In the third backward cycle: A crack just above the first story beam-south column joint at the second story infill wall.
- In the fourth forward cycle: Displacement controlled loading up to 8 mm displacement was applied. At the front side, a crack at the outside of the north column and foundation connection.
- In the fourth backward cycle: At the front side, a horizontal crack between the first story beam and second story infill wall near to the south column. At the back side, two vertical cracks, one near to the south column and one near to the middle of the beam. A shear crack at the second story beam-south column joint.
- In the fifth forward cycle: At the front side, shear cracks in the hollow bricks below the first story beam-north column joint. A horizontal crack at the outside of the bottom of the north column. At the back side, shear cracks in the first row hollow bricks below the first story beam near to the north column. Two vertical cracks in the first story beam. In addition, shear cracks at the joints of the hollow bricks at the second story infill wall.
- In the fifth backward cycle: At the front side, openings in the hollow bricks. At the back side, a vertical crack at the first story beam between the middle and the south column.

- In the sixth forward cycle: At the front side, crushing in the hollow brick below the middle of the first story beam at the top row.
- In the sixth backward cycle: At the front side, separation between the infill wall and the first story beam-north column joint.
- In the seventh forward cycle: At the front side, shear cracks and opening in the joints of all of the hollow bricks of the first story infill wall. Also, crushing in the hollow bricks in the top row near to the north column and falling of the dial gage at that location. In the second story infill wall, also shear cracks in the joints of the hollow bricks.
- In the ninth backward cycle: At the front side, cover crushing at the first story beam-south column joint.

Load-second story displacement/drift, load-first story displacement/drift, load-second story shear displacement, and load-first story shear displacement graphs are shown in **Figures 4.10-4.13**, respectively. Views of TS6 (REFB) specimen during the test are shown in **Figure 4.14.**

Flexural cracks were observed along the first story columns in this specimen whereas in REFBA cracks accumulated at the first story column ends. Because of the infill, flexural cracks occurred also on the first story beam. On the second story beam-column joint, diagonal cracks were observed. Cracks initiated first in the first story infill wall. Both on the first and second story brick infill wall, zigzag pattern cracks were observed along the mortar between bricks. Cracks were much denser in the first story wall.

The second story drift ratio remained within 1% limits. For this un-plastered brick wall specimen, load sustained up to 1.2% first story drift ratio. Crushing of brick was first observed approximately at 1.5% first story drift ratio. The strength of specimen decreased rapidly after crushing of bricks and even out of plane fall down of wall was observed.

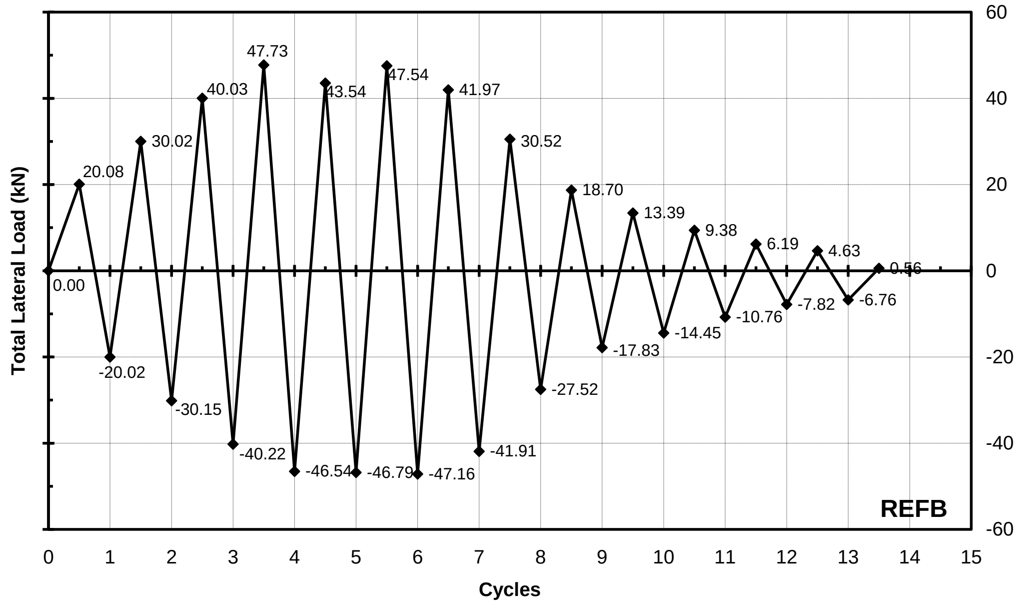


**Figure 4.7** Lateral Load History Graph of TS6 (REFB) Specimen

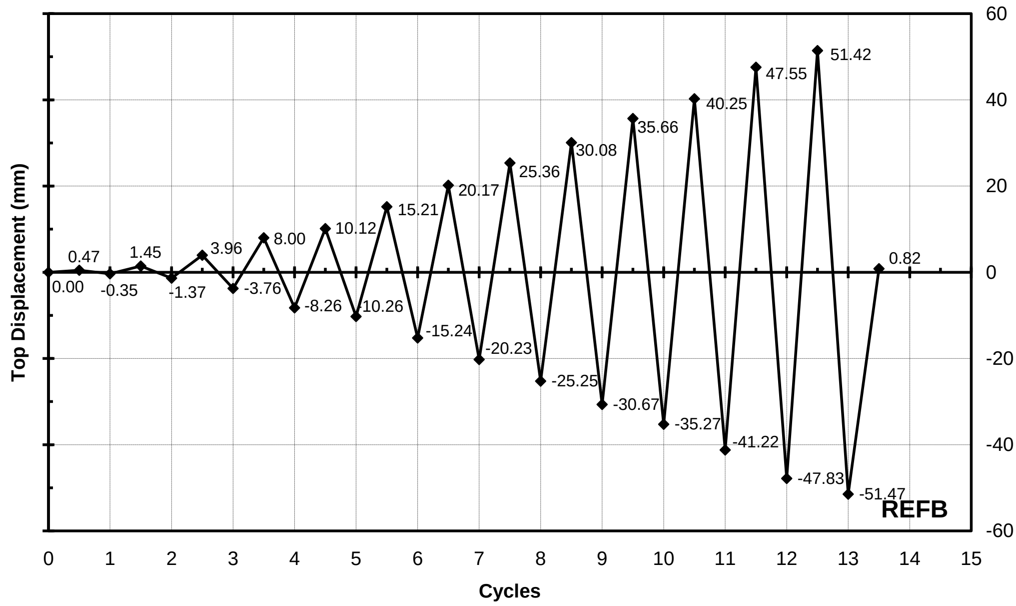


**Figure 4.8** Top Displacement History Graph of TS6 (REFB) Specimen

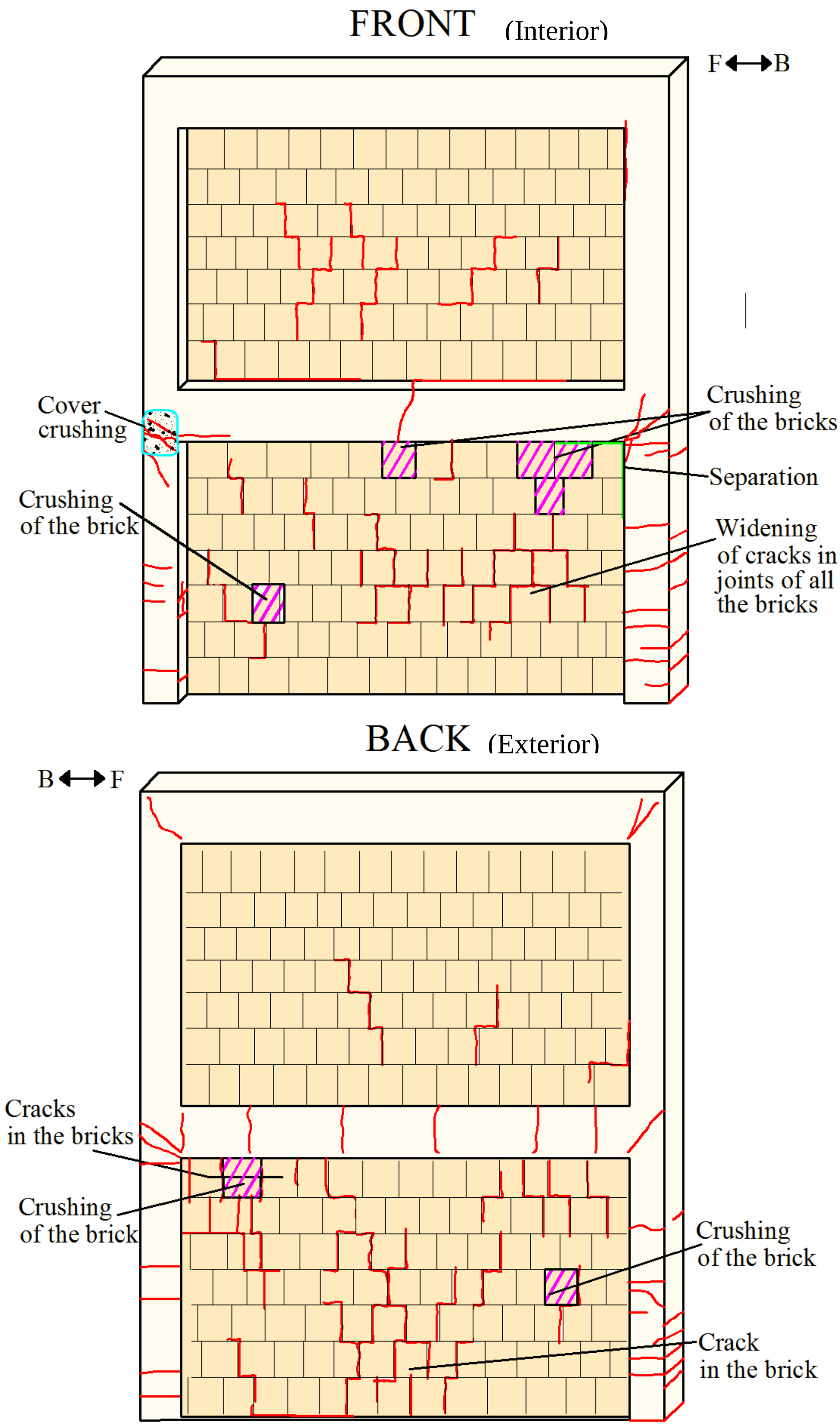


**Figure 4.9** Main Observations during the Reference Test REFB

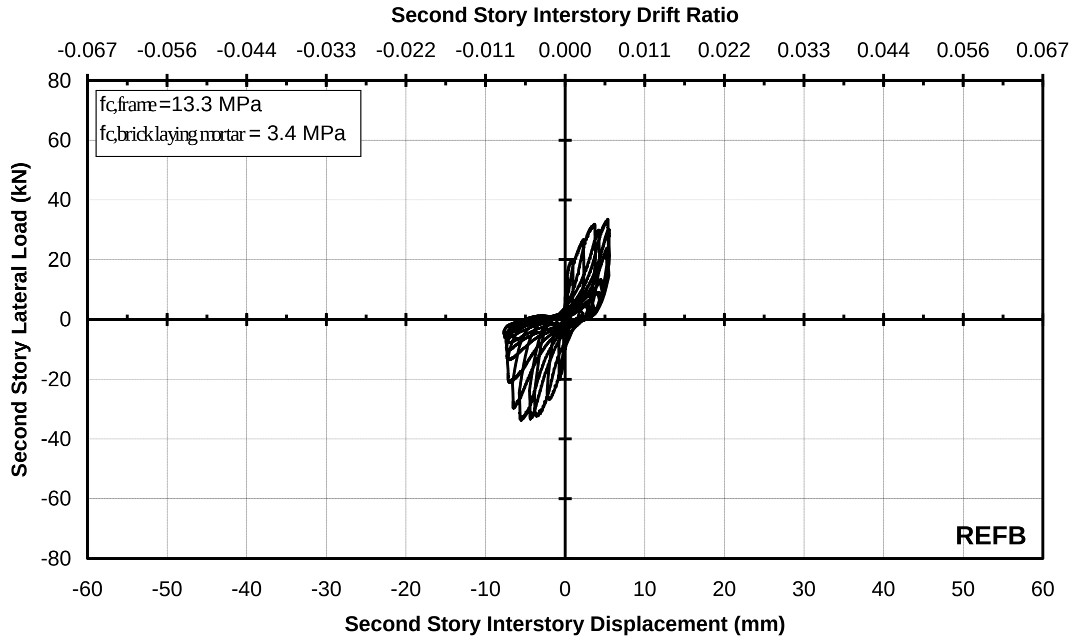


**Figure 4.10** Second Story Lateral Load-Second Story Displacement/Drift Ratio Graph of TS6 (REFB) Specimen

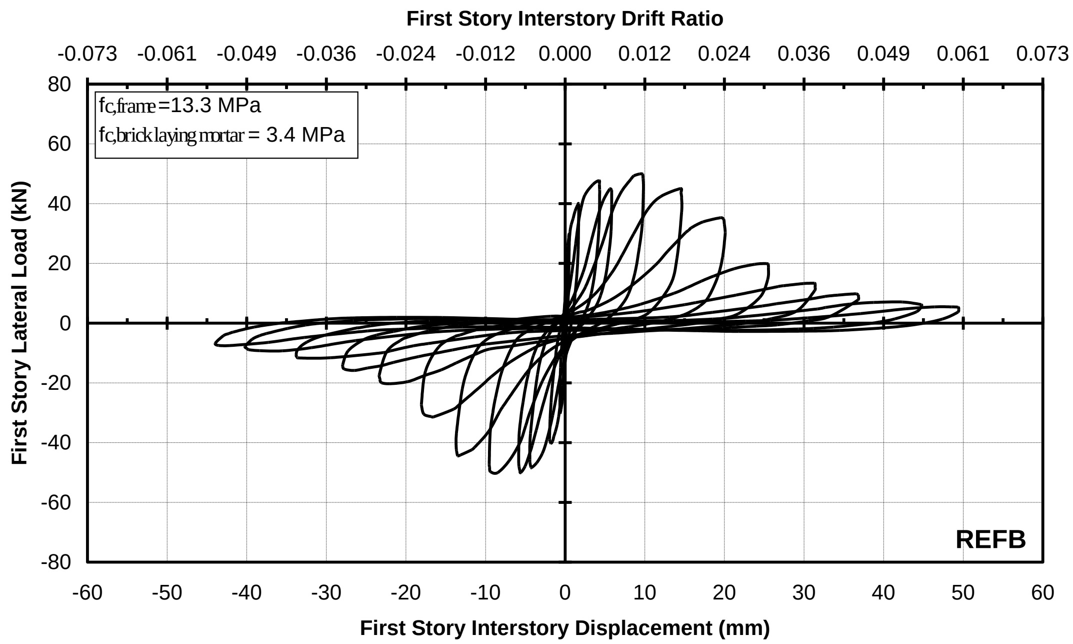


**Figure 4.11** First Story Lateral Load-First Story Displacement/Drift Ratio Graph of TS6 (REFB) Specimen

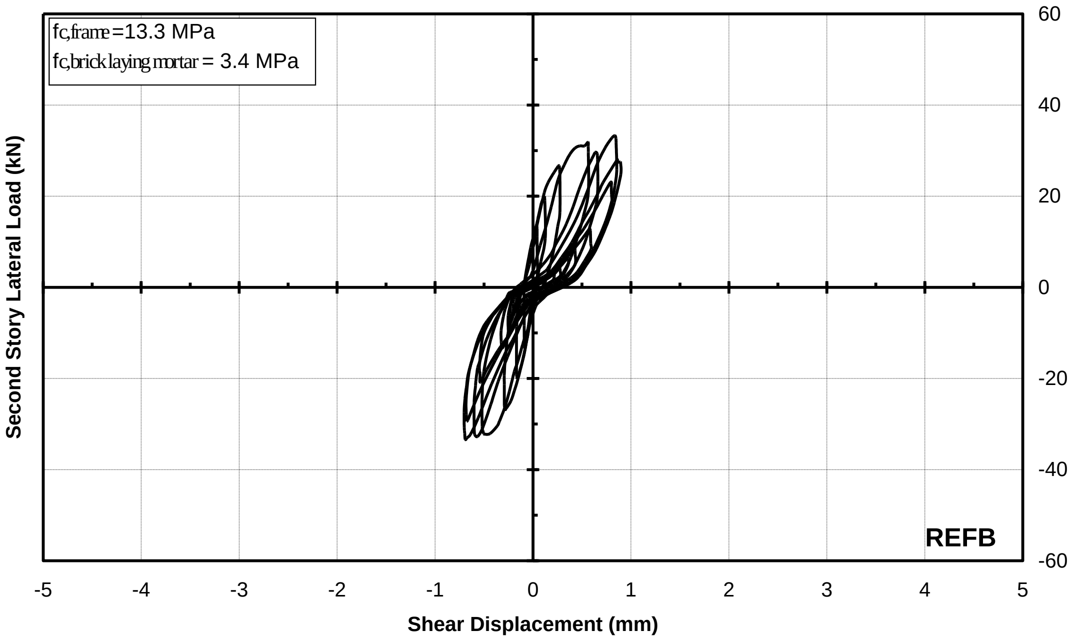


**Figure 4.12** Load-Second Story Shear Displacement Graph of TS6 (REFB) Specimen

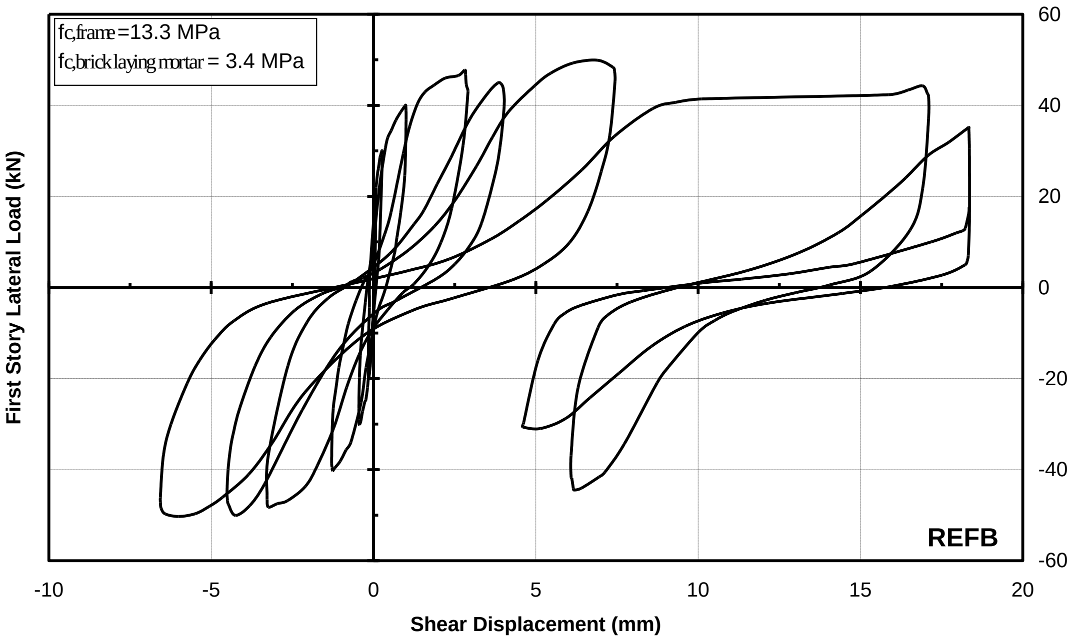


**Figure 4.13** Load-First Story Shear Displacement Graph of TS6 (REFB) Specimen

**Figure 4.14** Views of TS6 (REFB) Specimen during the Test

## 4.4 REFERENCE SPECIMEN, REFBM

The third reference frame test REFBM (TS1) with plastered brick infill was subjected to the lateral loading history given in **Figure 4.15**. In this frame test, the maximum forward load value was recorded as 66.59 kN and the top displacement corresponding to this load was measured as 6.43 mm. In the same frame test, the maximum backward loading was 66.59 kN with a displacement value of 6.37 mm at the second story level. Second story displacement history is given in

**Figure 4.16**. Main observations are presented below verbally and also as figures in **Figure 4.17**.

- In the second forward cycle: At the front side, a shear crack at the second story infill wall. At the back side, a shear crack on the plaster of the second story infill wall. Also, two shear cracks on the plaster of the first story infill wall at a place near to the north column.
- In the second backward cycle: At the front side, a shear crack at the first story infill wall, continuing up to the middle of the infill wall by dividing into two branches. Widening of the previously formed cracks. At the back side, a shear crack continuing up to the middle of the plaster of the first story infill wall. Also, a shear crack up to the middle part of the plaster of the second story infill wall.
- In the third forward cycle: At the front side, extending of the shear crack formed in the second forward cycle at the second story infill wall up to the first story beam and second story beam. A flexural crack at the mid-height of the first story north column turning to the outside of the column.
- In the fourth forward cycle: At the front side, a crack between the first story infill wall and the north column. Moreover, an opening at the bottom of the specimen.
- In the fourth backward cycle: At the back side, shear cracks and openings in the plaster and falling down of it.
- In the fifth forward cycle: At the front side, at the bottom of the specimen, cracking. Extending and widening of the previously formed cracks. At the back side, falling down of the plaster.
- In the fifth backward cycle: At the front side, falling down of the plaster of the first story infill wall from two parts.
- In the cycles starting from the sixth forward cycle, since the cracks progressed no notes were taken. Extending of the previously formed cracks. Falling down of the plaster. Shear cracks in the hollow bricks. Also,

crushing in the hollow bricks, especially in the corner and the connection between the infill wall and the beam. The test was continued up to the ninth cycle, and then it was terminated.

Load-second story displacement/drift, load-first story displacement/drift, load-second story shear displacement, and load-first story shear displacement graphs are given in **Figures 4.18-4.21**, respectively. Views of TS1 (REFBM) specimen during the test are shown in **Figure 4.22.**

First cracking was observed on the plaster of the brick. At approximately 0.8% of first story drift ratio, the infill wall separated from the surrounding frame. With widening and increasing of cracks, plaster initiated to fall down. In the large displacement cycles, mortar between bricks cracked and opened in the tension region and bricks crushed in the compression region.

As can be observed from Fig. 4.18 and 4.19, load-displacement (drift) cycles are not symmetrical. Since the first structural cracking occurred in the forward cycle in the first story, damage was observed mainly in the first story and consequently second story drift ratio remained almost elastic during entire testing. In the backward cycles, drift ratios of first and second stories were similar to each other.

Corner crushing was observed at top of the infill wall in the first story. Crushing of brick was followed by falling down of the infill at this region. Accordingly short columns were created at the top half of the first story columns and hinging at the mid column height and shear cracking were observed.

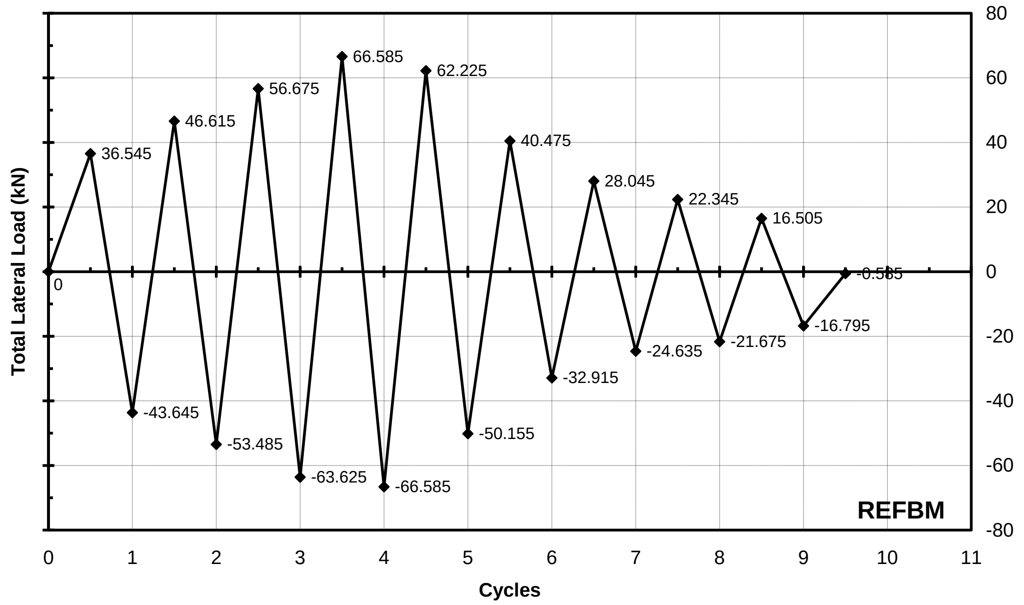


**Figure 4.15** Lateral Load History Graph of TS1 (REFBM) Specimen

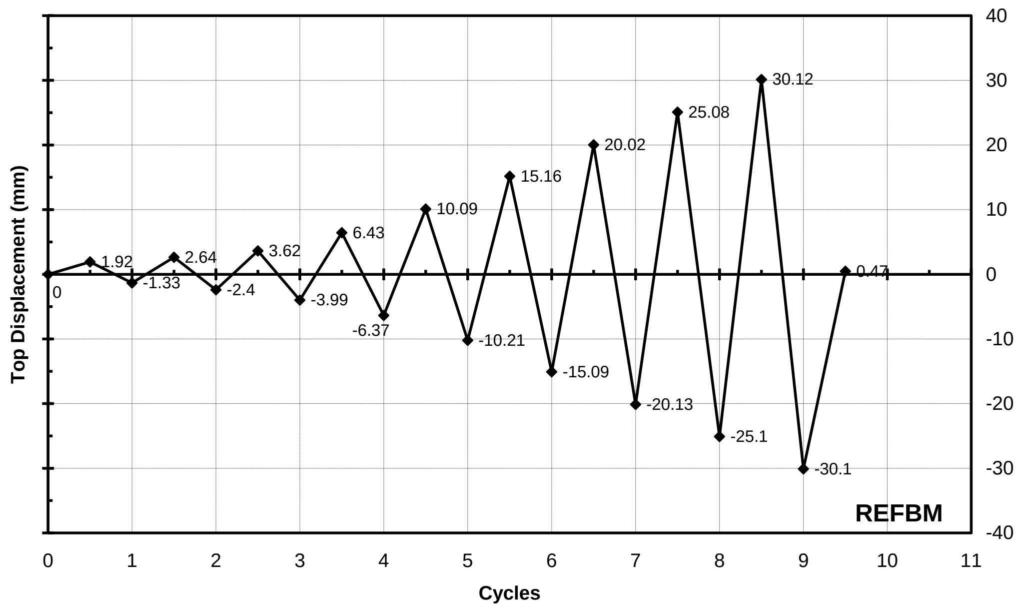


**Figure 4.16** Top Displacement History Graph of TS1 (REFBM) Specimen

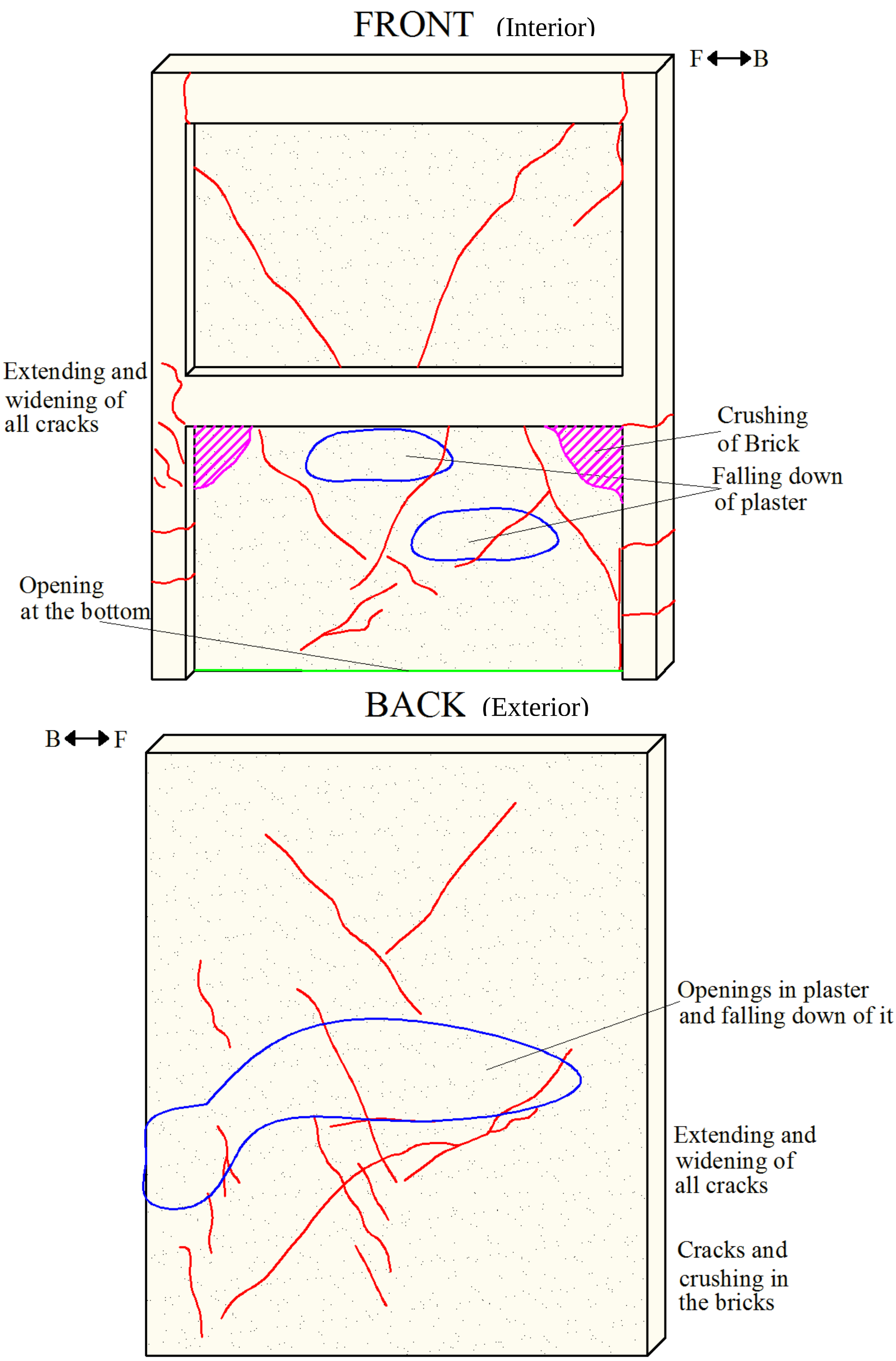


**Figure 4.17** Main Observations during the Reference Test REFBM

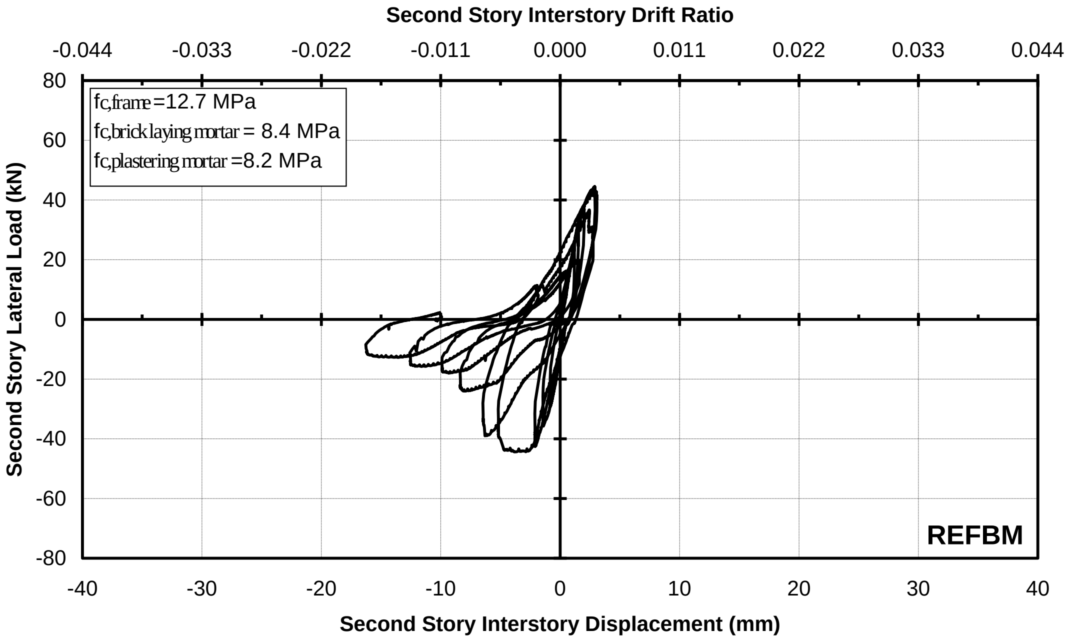


**Figure 4.18** Second Story Lateral Load-Second Story Displacement/Drift Ratio Graph of TS1 (REFBM) Specimen

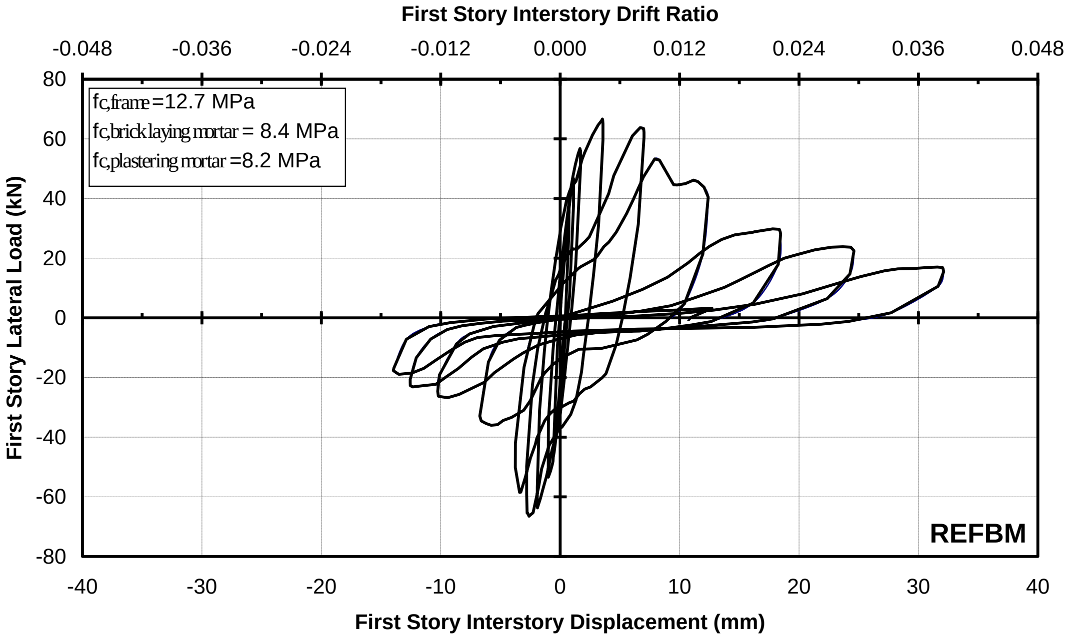


**Figure 4.19** First Story Lateral Load-First Story Displacement/Drift Ratio Graph of TS1 (REFBM) Specimen

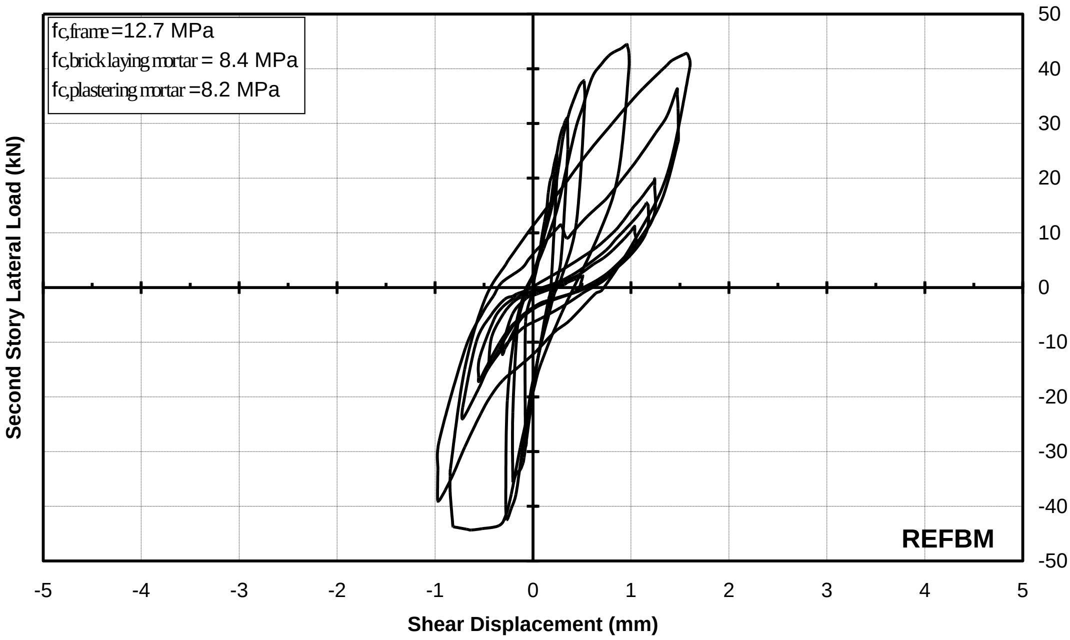


**Figure 4.20** Load-Second Story Shear Displacement Graph of TS1 (REFBM) Specimen

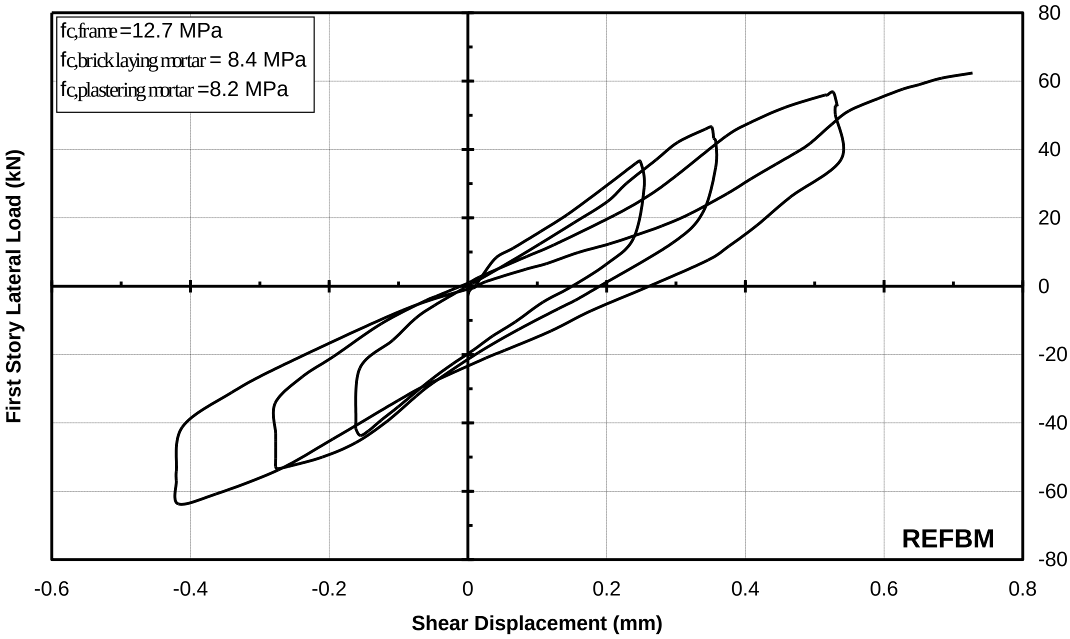


**Figure 4.21** Load-First Story Shear Displacement Graph of TS1 (REFBM) Specimen


**Figure 4.22** Views of TS1 (REFBM) Specimen during the Test

## 4.5 REFERENCE SPECIMEN, REF2ABM

The fourth reference test REF2ABM was the test of frame specimen TS7 which was a plastered, anchored, 20 mm thickness of plain mortar (containing neither steel fiber nor PP fiber) applied frame. The specimen was subjected to the lateral loading history given in **Figure 4.23**. For this test, the maximum forward and backward loads were 104.52 kN and 101.52 kN. The top displacements were 15.24 mm and 15.03 mm, respectively. Top displacement history is given in **Figure 4.24**. Main observations are presented below verbally and also as figures in **Figure 4.25**.

- In the first forward cycle: At the front side, a small flexural crack at the bottom of the outside of the north column.
- In the first backward cycle: Similar symmetrical cracks at the south column.
- In the fourth forward cycle: At the front side, a shear crack at the first story infill wall nearby south joint. At the back side, on the plaster of the first story infill wall two vertical shear cracks next to the south column and also one shear crack on the plaster below the first story beam-north column joint.
- In the fourth backward cycle: At the front side, a shear crack at the first story beam-south column joint.
- In the fifth forward cycle: At the front side, a shear crack just above the bottom of the first story infill wall next to the north column.
- In the sixth forward cycle: At the front side, a diagonal crack at the first story infill wall. Shear crack at the first story beam-north column joint. A flexural crack at the first story north column near to the mid-height. At the back side, diagonal cracks on the plaster of the first story infill wall.
- In the sixth backward cycle: At the front side, at the first story beam-south column joint two shear cracks. A diagonal crack at the first story infill wall. Moreover, a flexural crack just above the bottom of the south column on the front side. At the back side: falling down of the plaster at the middle of the first story beam.

- In the seventh forward cycle: At the front side, extending and widening of previous cracks. A separation between the first story infill wall and the foundation.
- In the seventh backward cycle: At the back side, shear cracks at the plaster of the first story infill wall. Also, a separation parallel to the first story beam at the plaster of the first story infill wall.
- In the eighth forward cycle: At the front side, a diagonal crack of approximately 5 mm width at the first story infill wall.
- In the eighth backward cycle: At the front side, crack width nearly 3-4 mm. At the back side, a shear crack at the plaster of the first story infill wall at a location near to the bottom of the infill wall.
- In the ninth forward cycle: At the front side, widening of the previous shear cracks at the first story infill wall. Opening in the previous flexural cracks at the first story north column.
- In the tenth forward cycle: At the front side, a serious opening at the first story beam-south column joint. Falling down of two dial gages on the first story infill wall. The width of the diagonal crack at the first story infill wall reached 20 mm.
- In the tenth backward cycle: At the front side, crushing of the concrete cover and the reinforcement was seen at the first story beam-south column connection.
- In the eleventh forward cycle: At the front and the back side, crushing of the plaster of the first story infill wall, crushing of the hollow bricks also. The anchorage reinforcements were visible.
- In the eleventh backward cycle: Beginning to crush of the first story infill wall.
- In the twelfth forward cycle: Crushing of the first story infill wall. The test was terminated after doing the twelfth backward cycle also.

Load-second story displacement/drift, load-first story displacement/drift, load-second story shear displacement, and load- first story shear displacement graphs are presented in **Figures 4.26-4.29**, respectively. Views of TS7 (REF2ABM) specimen during the test are shown in **Figure 4.30.**

First cracking was observed on columns as flexural crack. Afterwards, shear cracks occurred in the first story joints. Plaster on the back side also cracked at the first story column and beam interfaces. Later on, cracks were observed on the strengthening mortar as well.

At approximately 0.4% first story drift ratio, plaster at the back side initiated to fall down. However, the strengthening plaster on the front side which is inside the frame and supported by the surrounding frame did not fall down until large displacements.

At approximately 1% first story drift ratio, strengthening wall lifted up and separated from the foundation. Maximum load was reached at nearly 1.2% first story drift ratio.

The added wall was able to carry applied load with serious cracks but without fall down until the end of testing. Therefore, the applied lateral load was kept without any considerable decrease until 3% first story drift ratio for the forward cycles.

There was no significant damage observed on the second story. Shear-displacement graphs also verify this observation. Excluding the last three cycles, the second story shear displacements are very small as compared to first story shear displacements.

At the end of the test, infill wall and bricks crushed and fell down at nearly 4% first story drift ratio. It should be noted that the strengthening mortar gained compressive strength of almost 41 MPa.

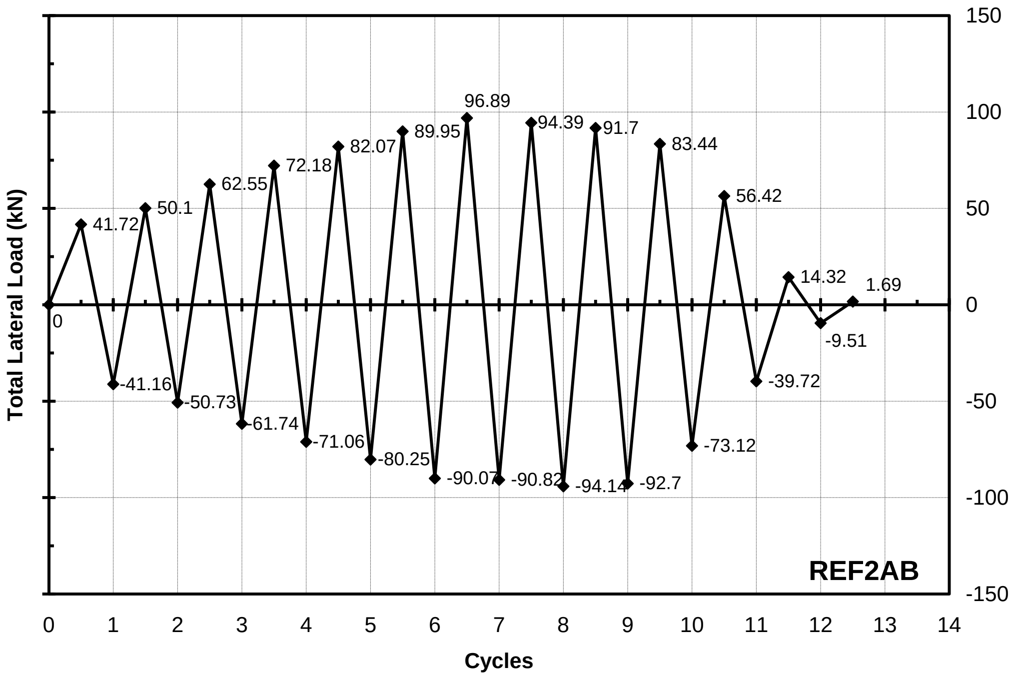


**Figure 4.23** Lateral Load History Graph of TS7 (REF2ABM) Specimen

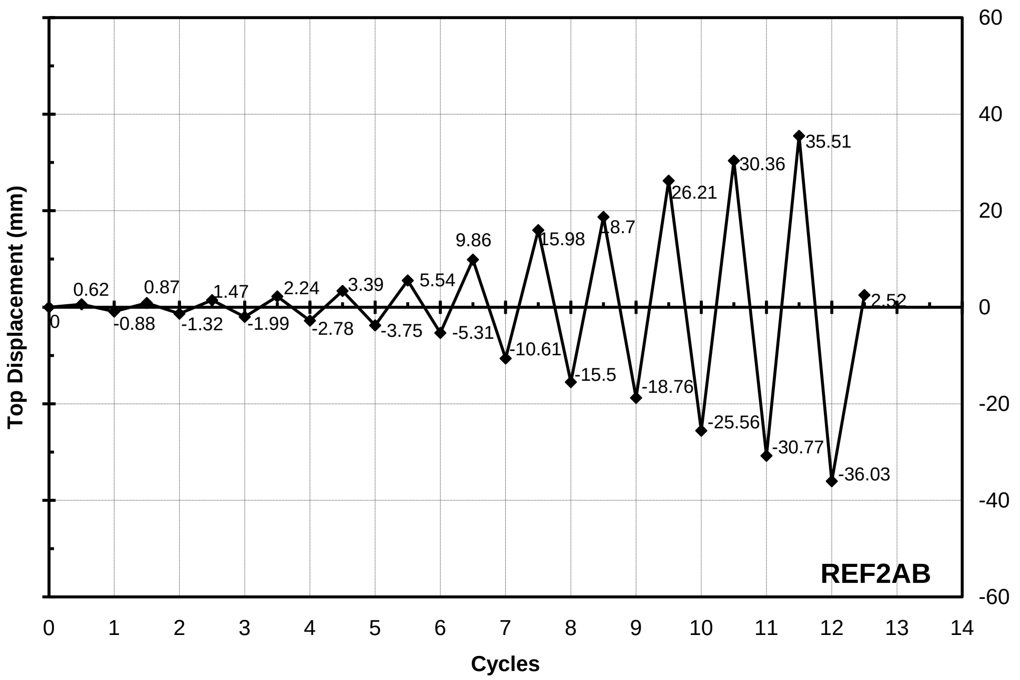


**Figure 4.24** Top Displacement History Graph of TS7 (REF2ABM) Specimen

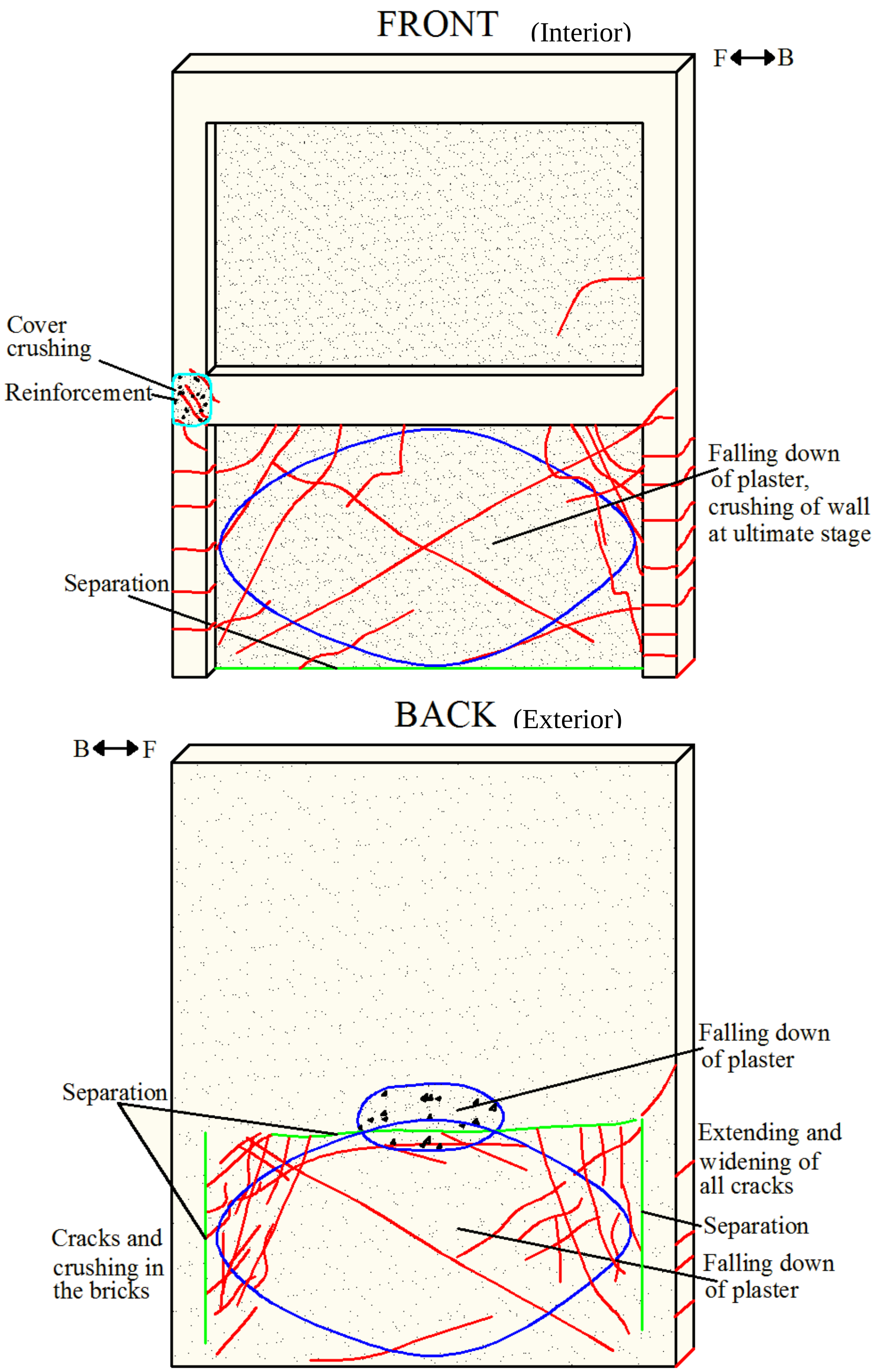


**Figure 4.25** Main Observations during the Reference Test REF2ABM

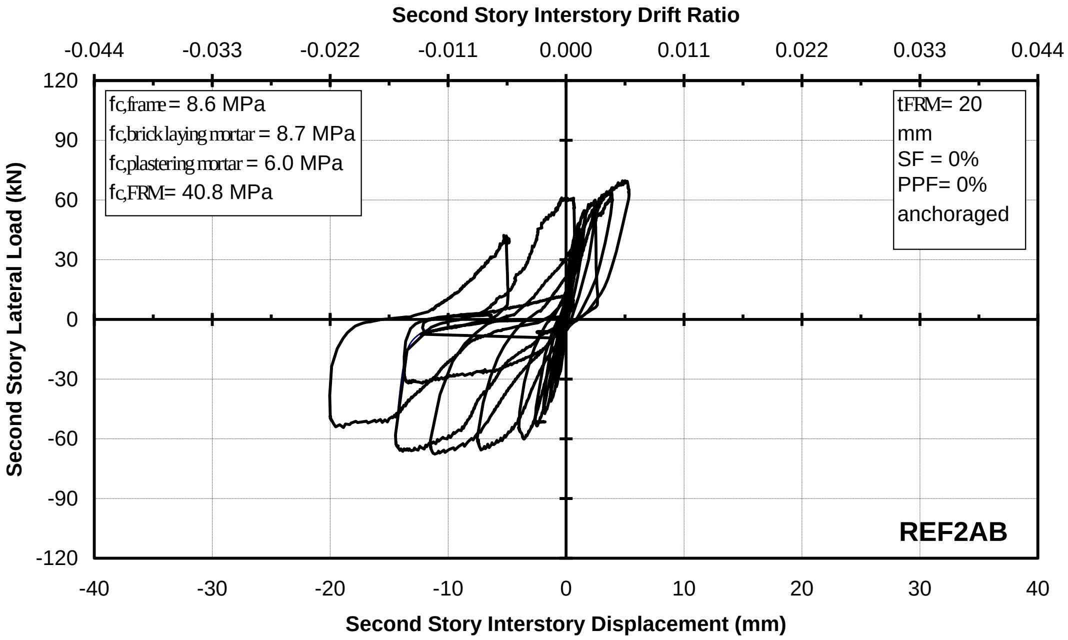


**Figure 4.26** Second Story Lateral Load-Second Story Displacement/Drift Ratio Graph of TS7 (REF2ABM) Specimen

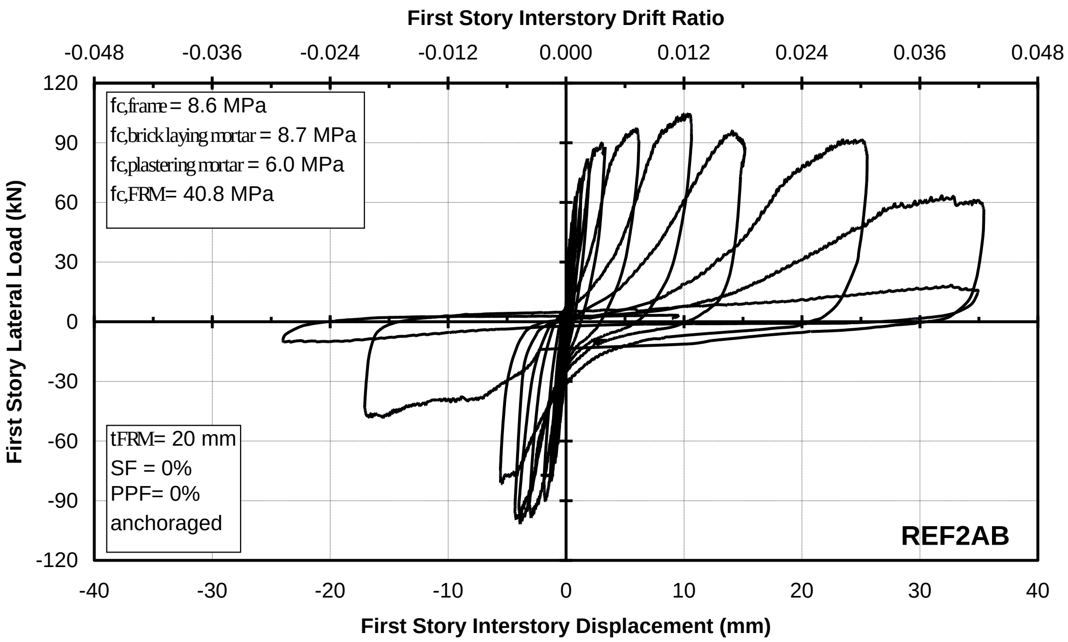


**Figure 4.27** First Story Lateral Load-First Story Displacement/Drift Ratio Graph of TS7 (REF2ABM) Specimen

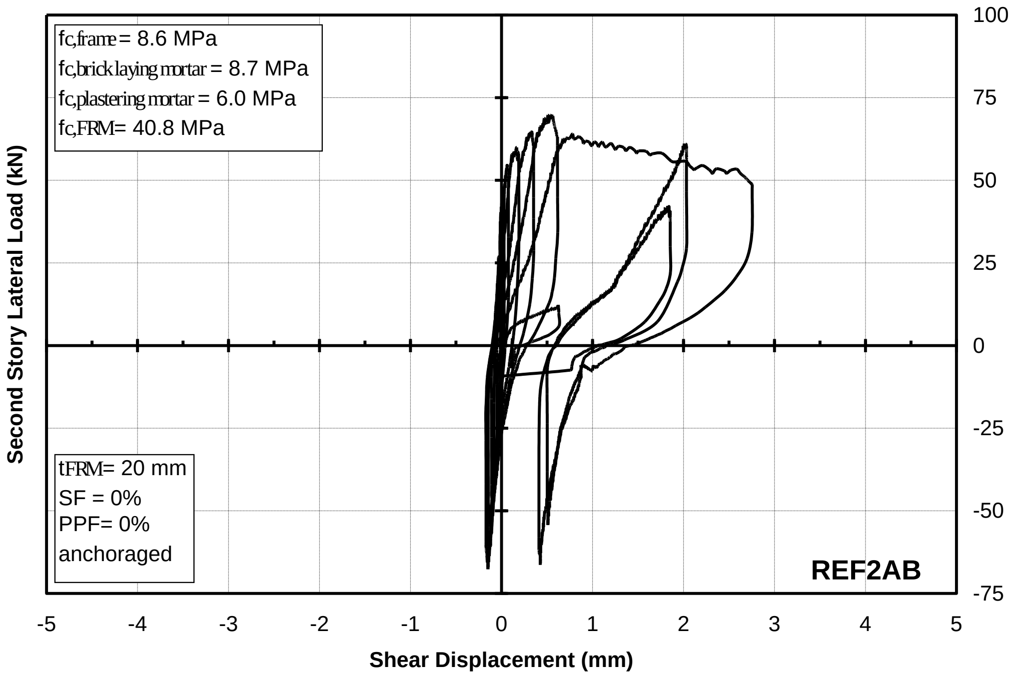


**Figure 4.28** Load-Second Story Shear Displacement Graph of TS7 (REF2ABM) Specimen

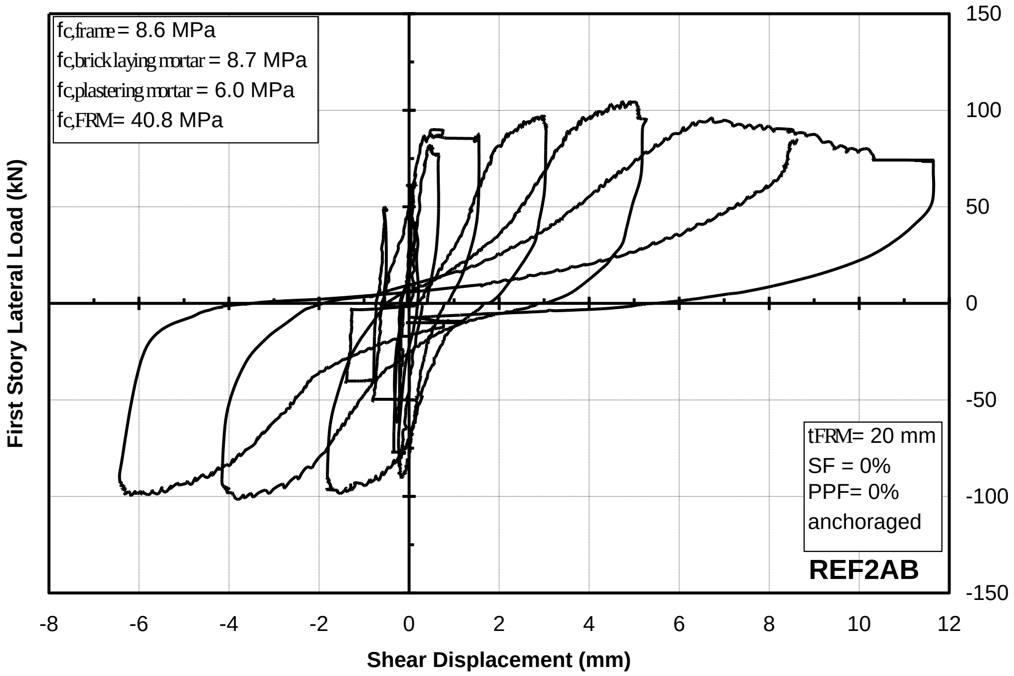


**Figure 4.29** Load-First Story Shear Displacement Graph of TS7 (REF2ABM) Specimen


**Figure 4.30** Views of TS7 (REF2ABM) Specimen during the Test

## 4.6 STRENGTHENED SPECIMEN, SF1NABM

The fifth test performed was the first strengthened frame test SF1NABM, TS9, which was a plastered, non-anchored, 10 mm thickness of mortar with 2% volumetric ratio of steel fiber applied frame. The specimen was subjected to the lateral loading history given in **Figure 4.31**. The maximum applied forward load to this specimen was 80.56 kN with top displacement of 5.15 mm. The maximum backward load was 80.69 kN with corresponding top displacement of 4.18 mm. Second story displacement history is given in **Figure 4.32**.

Main observations are given below verbally and also as figures in **Figure 4.33**.

- In the third forward cycle: At the front side, a flexural crack at the mid-height of the first story north column and at the outside of the north column. At the back side, shear cracks at the plaster of the first story infill wall at a location of bottom of the north column.
- In the third backward cycle: At the front side, a shear crack below the first story beam-south column connection.
- In the fourth forward cycle: At the front side, a shear crack at the first story beam-north column joint. At the back side, three shear cracks at the plaster of the first story infill wall.
- In the fourth backward cycle: At the back side, almost vertical three shear cracks at the plaster of the first story infill wall next to south column.
- In the sixth forward cycle: At the back side, a big shear crack at the plaster parallel to the second story north column, continuing parallel to the first story beam and parallel to the first story south column.
- In the sixth backward cycle: At the front side, separation between the first story south column and the first story infill wall. At the back side, separation at the plaster between the first story infill wall and both of the first story columns and first story beam. Falling down of the plaster at two corners.
- In the eighth forward cycle: At the back side, falling down of the plaster of the first story infill wall at first story north column. Also, falling down of the plaster at a location of the middle of the first story beam. Moreover, separation between the plaster of the first story infill wall and south column. Also, separation between the plaster of the first story infill wall and the first story beam.
- In the eighth backward cycle: At the front side, separation between the first story infill wall and the two first story column. In addition, separation between the first story infill wall and the first story beam. At the back side, crushing of the hollow brick just below the first story beam-north column joint.

- In the ninth forward cycle: At the front side, widening of the separation between the first story infill and the two first story columns and the first story beam. At the back side, crushing of the hollow brick below the first story beam-south column joint, at the top row.
- Starting from the tenth forward cycle, no notes were taken since the cracks widened and extended so much. The test was terminated at the twelfth cycle.

Load-second story displacement/drift, load-first story displacement/drift, load-second story shear displacement, and load-first story shear displacement graphs are given in **Figures 4.34-4.37**, respectively. Views of TS9 (SF1NABM) specimen during and after the test are shown in **Figure 4.38**.

Specimen SF1NABM had a relatively thin strengthening wall which was not anchored to the surrounding frame. Cracks were first observed on the first story column in a flexural manner. Cracks were both at mid height and base level. At this level of load cracks were also observed on the original backside plaster at column-brick interface.

At approximately 0.4% first story forward drift ratio, specimen reached to its maximum load carrying capacity. Separation of infill wall initiated at this load level. Separation took place at infill wall and first story column interface. With increasing displacement, separation was also observed at infill-first story beam border. At 0.7% first story drift ratio, load capacity decreased 15% in forward direction.

Separation was excessive at large displacement cycles. Therefore, infill wall touched the surrounding frame at certain regions and damaged those zones extremely. Therefore, column damage was not uniformly distributed but accumulated at certain regions. Corner crushing of brick caused also excessive deformation of frames at this region.

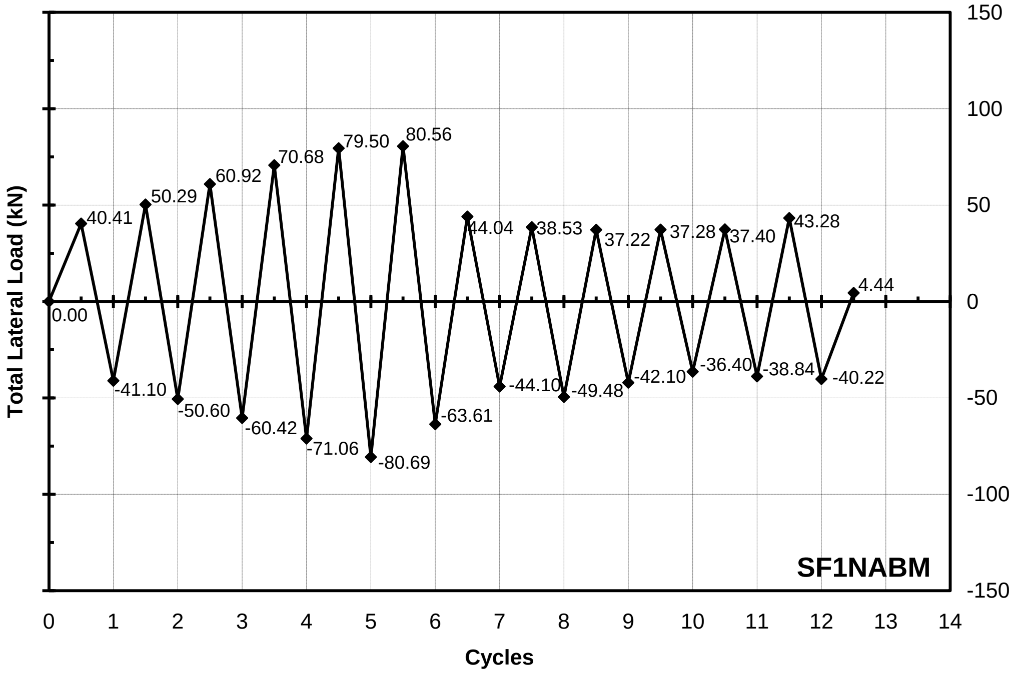


**Figure 4.31** Lateral Load History Graph of TS9 (SF1NABM) Specimen

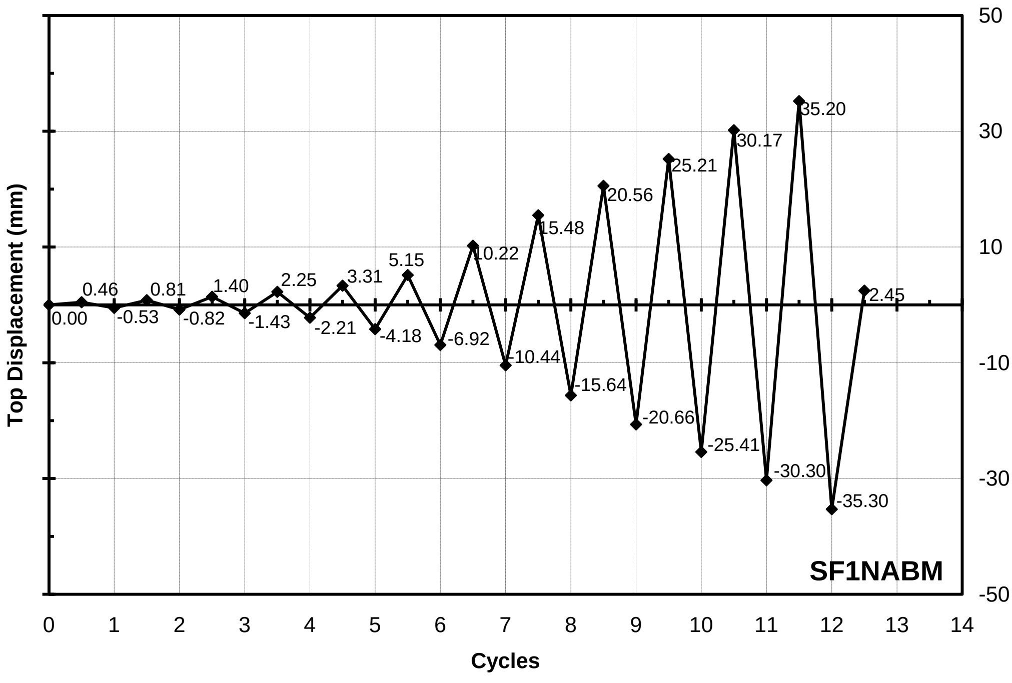


**Figure 4.32** Top Displacement History Graph of TS9 (SF1NABM) Specimen

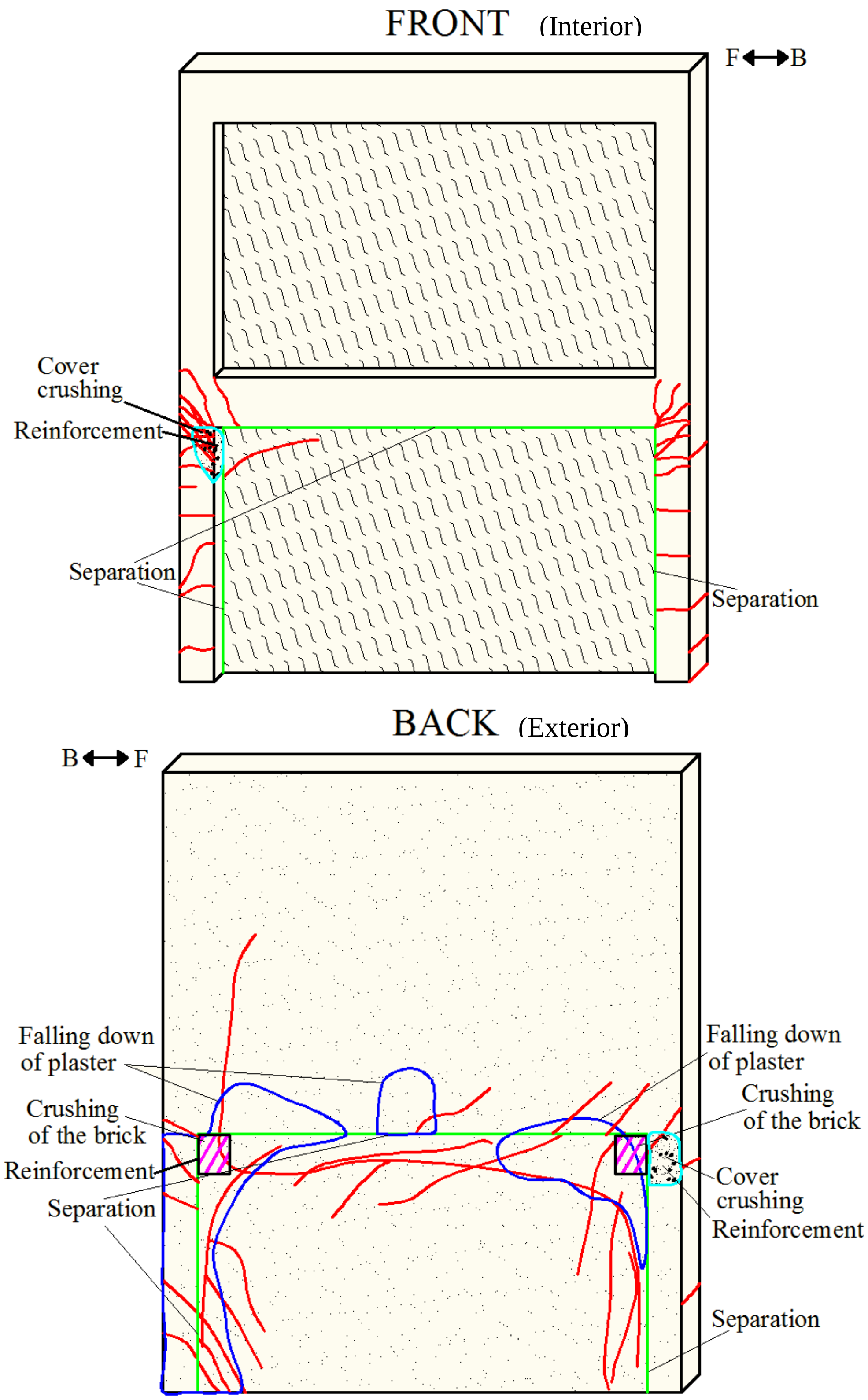


**Figure 4.33** Main Observations during the Strengthened Test SF1NABM

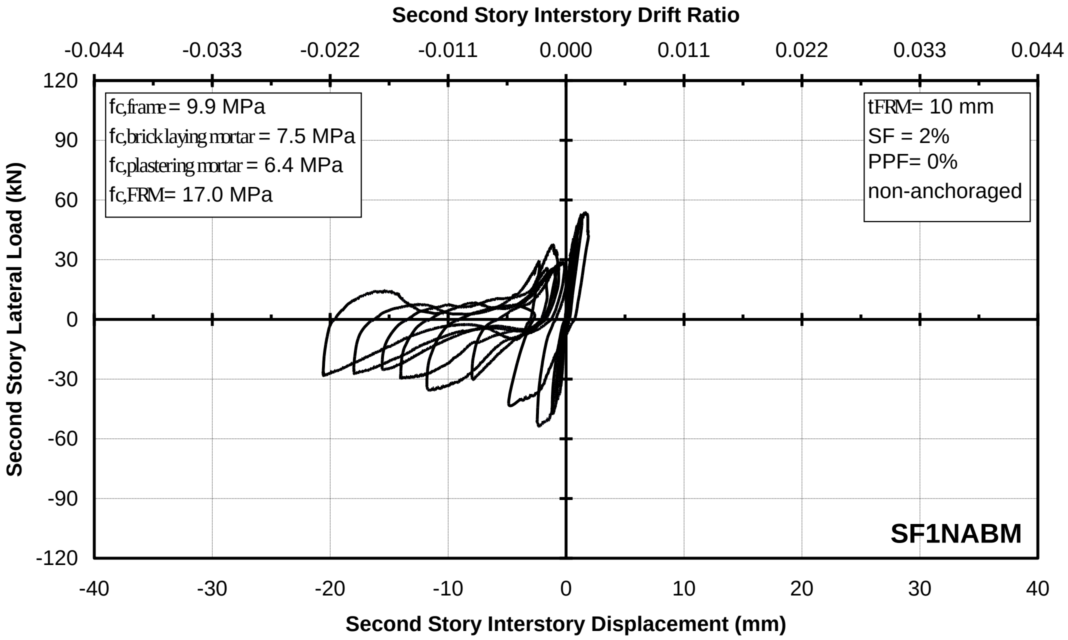


**Figure 4.34** Second Story Lateral Load-Second Story Displacement/Drift Ratio Graph of TS9 (SF1NABM) Specimen

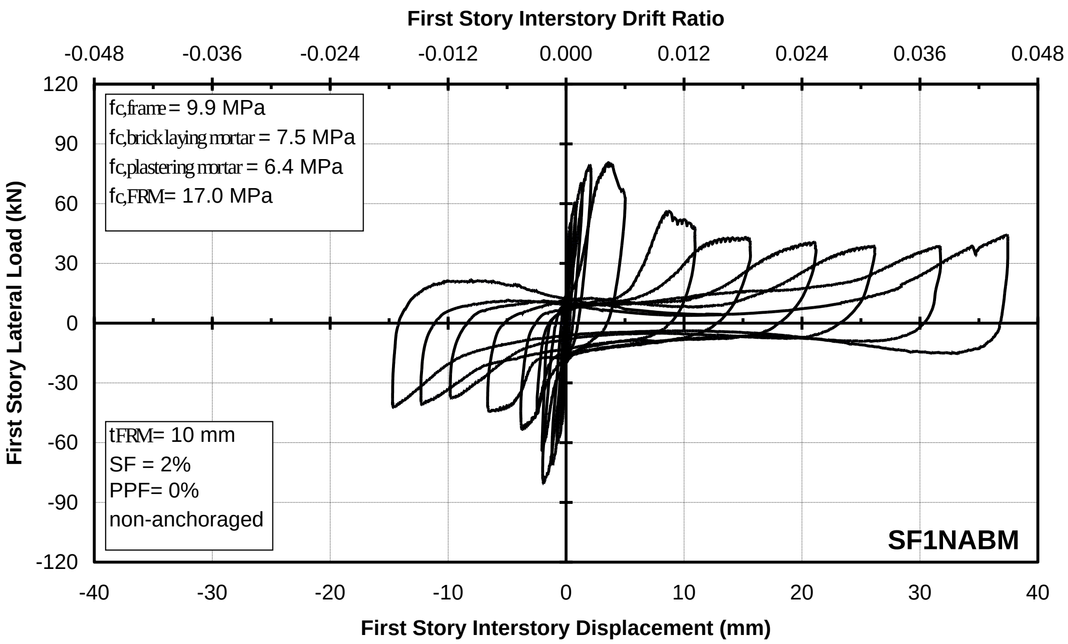


**Figure 4.35** First Story Lateral Load-First Story Displacement/Drift Ratio Graph of TS9 (SF1NABM) Specimen

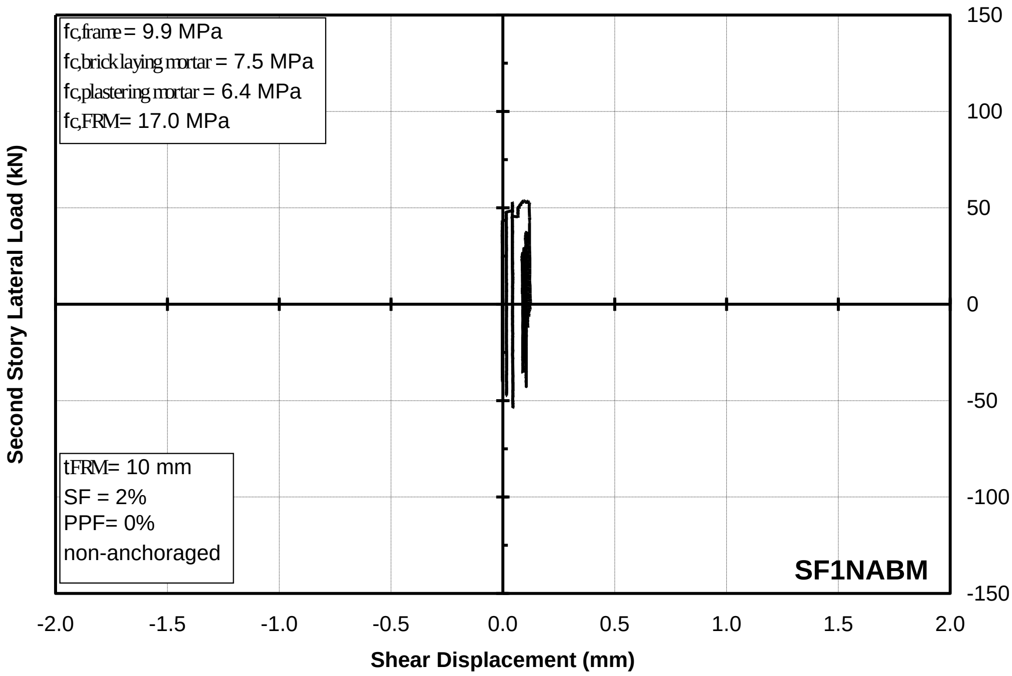


**Figure 4.36** Load-Second Story Shear Displacement Graph of TS9 (SF1NABM) Specimen

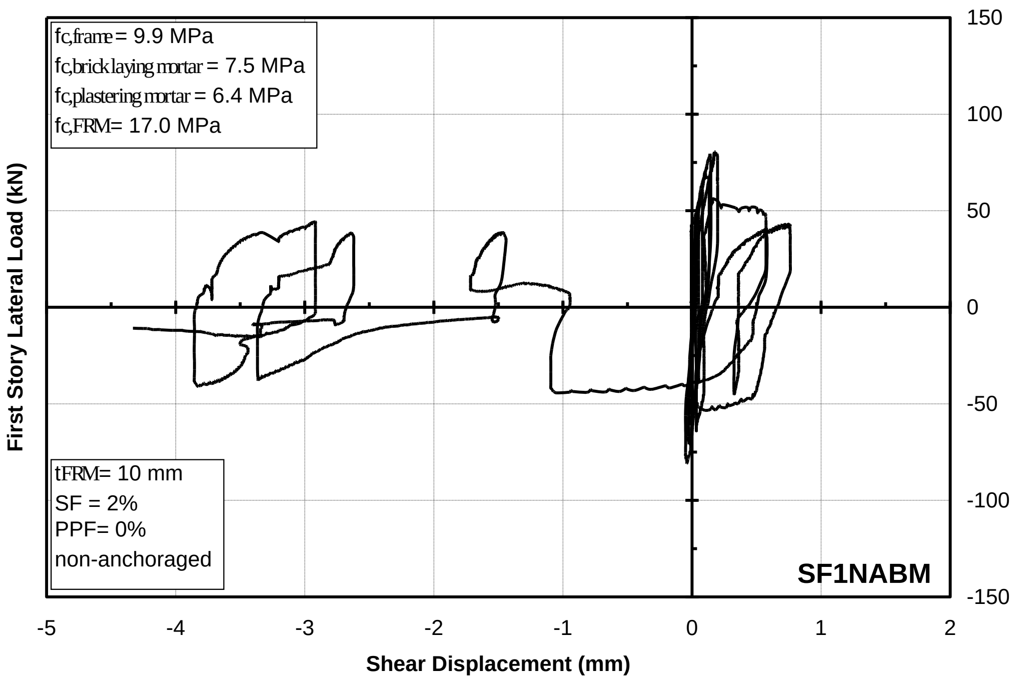


**Figure 4.37** Load-First Story Shear Displacement Graph of TS9 (SF1NABM) Specimen

**Figure 4.38** Views of TS9 (SF1NABM) Specimen during the Test

## 4.7 STRENGTHENED SPECIMEN, SF2NABM

The sixth test in the series SF2NABM was the second strengthened test of the frame specimen TS2, which was plastered, non-anchored, 20 mm thickness of mortar with 2% volumetric ratio of steel fiber applied frame. The specimen was subjected to the lateral loading history given in **Figure 4.39**. The maximum applied forward load of this specimen was 96.58 kN. The top displacement at this load value was recorded as 5.15 mm. The maximum backward loading was 90.51 kN showing a top displacement of 3.70 mm. Top displacement history is presented in **Figure 4.40**. Main observations are presented below verbally and also as figures in **Figure 4.41**.

- In the second forward cycle: At the back side, vertical crack on plaster at first story north column boundary which is extending to second story. A flexural crack at outside of the north column mid-height.
- In the second backward cycle: At the back side, three almost vertical shear cracks at the plaster of the first story infill wall.
- In the fourth forward cycle: At the front side, separation with the first story infill wall and the bottom of the south column because of the non-existence of anchorages in this frame. Moreover, a crack at the outside of the first story north column at a place between the column and the foundation. At the back side, two shear cracks at the plaster of the second story infill wall parallel to the first story beam and a crack at first story north column and the infill.
- In the fourth backward cycle: Separation of infill at bottom surface and at outside of the south column base.
- In the fifth forward cycle: At the back side, debonding of plaster parallel to the first story beam.
- In the fifth backward cycle: At the back side, a vertical crack at the plaster spanning from the mid-height of the second story infill wall to the mid-height of the first story infill wall near to the north column.

- In the sixth forward cycle: At the front side, a shear crack at the first story infill wall starting from the mid-height of the first story south column, continuing upwards by passing the dial gage, and then finishing at approximately 1/3rd of the first story beam. Two shear cracks initiated at the opposite compression corner frame joint, causing crushing of concrete.
- In the sixth backward cycle: At the front side, separation between the first story infill wall and the first story north column.
- In the seventh forward cycle: At the front side, widening of former cracks. Also, separation of infill at the corner of the first story beam-north column joint.
- In the eighth forward cycle: At the front side, the reinforcement was seen at a location just below the first story beam-north column joint.
- In the ninth forward cycle: At the back side, buckling of the reinforcement below the first story beam-north column connection.
- Starting from the tenth forward cycle, no notes were taken. The cracks widened and extended very much. After tenth full cycle, test was terminated.

Load-second story displacement/drift, load-first story displacement/drift, load-second story shear displacement, and load-first story shear displacement graphs are presented in **Figures 4.42-4.45**, respectively. Views of TS2 (SF2NABM) specimen during and after the test are shown in **Figure 4.46.**

The non-anchoraged strengthening wall separated from column interface at approximately 0.23% first story drift ratio. The original plaster at the backside showed excessive cracking parallel to the frame boundaries. In this test, separation at column base was also observed. At 0.35% first story drift ratio, the original plaster at the backside initiated to debond. The strengthening mortar cracked nearby the first story top corner at 0.8% drift ratio. At 1.8% drift ratio, lateral load decreased 15%. At 2% drift ratio the load was at 78% of the maximum value. At 3.3% drift ratio, column longitudinal reinforcement buckled. No widespread cracking was observed on the infill.

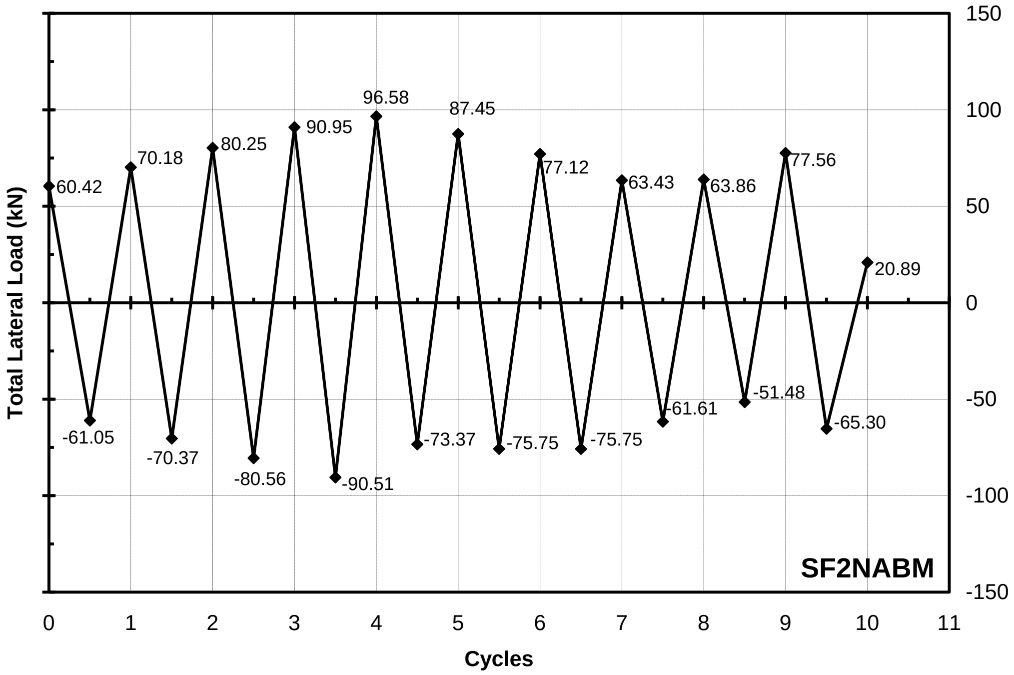


**Figure 4.39** Lateral Load History Graph of TS2 (SF2NABM) Specimen

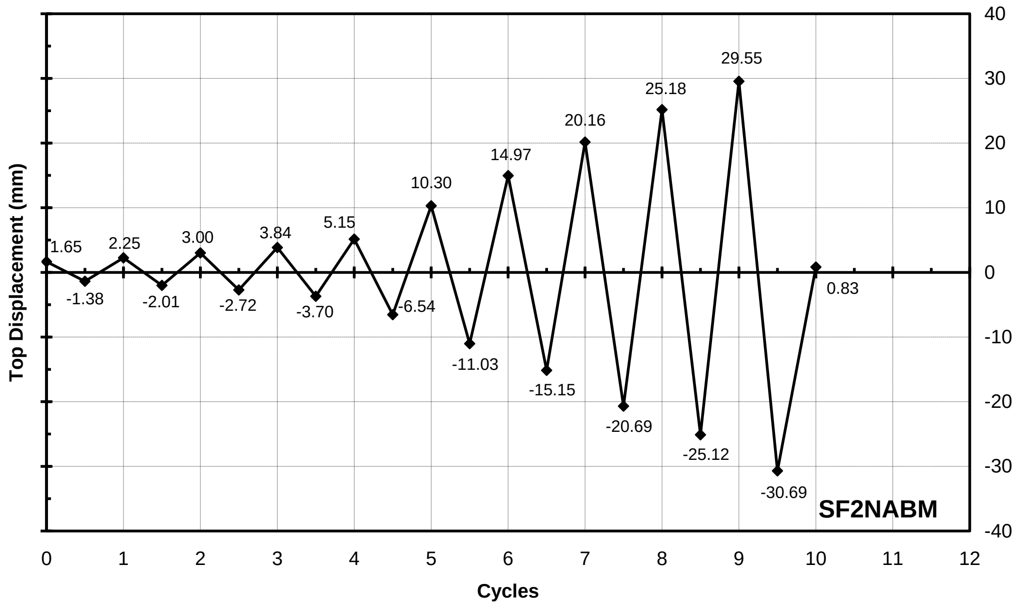


**Figure 4.40** Top Displacement History Graph of TS2 (SF2NABM) Specimen

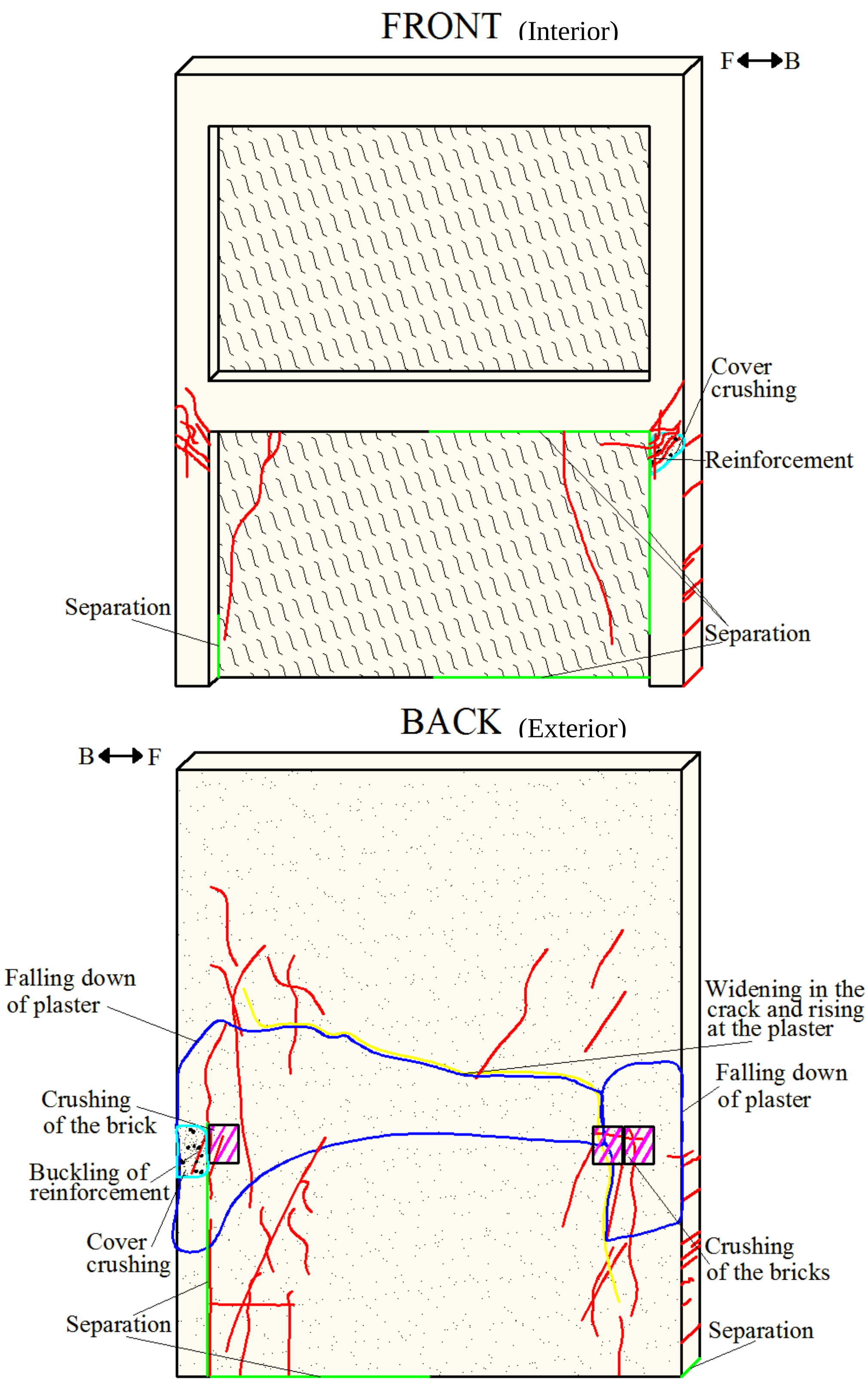


**Figure 4.41** Main Observations during the Strengthened Test SF2NABM

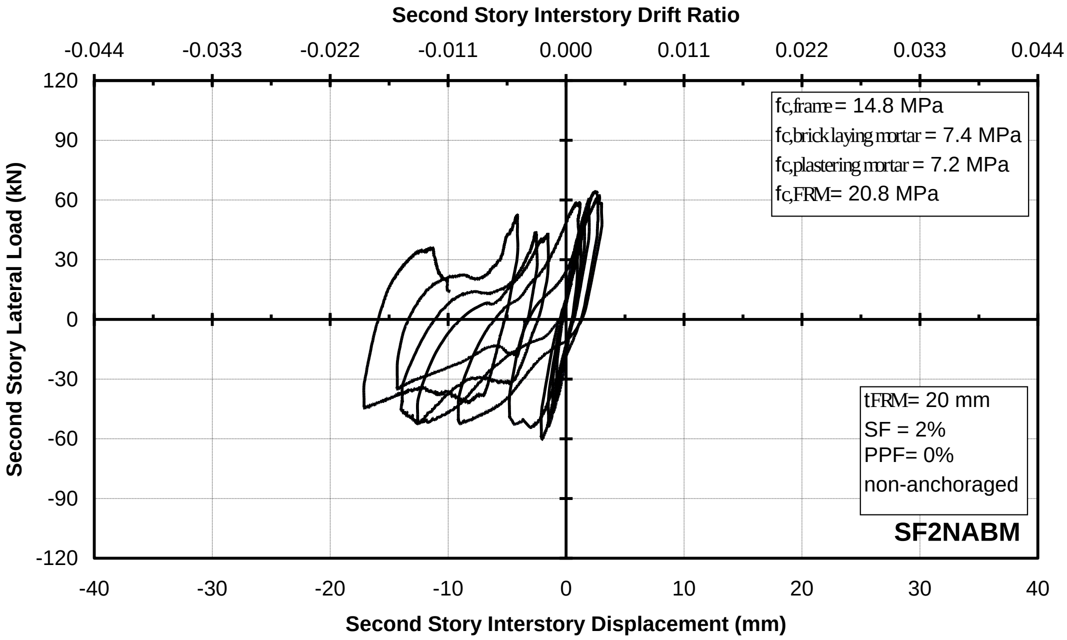


**Figure 4.42** Second Story Lateral Load-Second Story Displacement/Drift Ratio Graph of TS2 (SF2NABM) Specimen

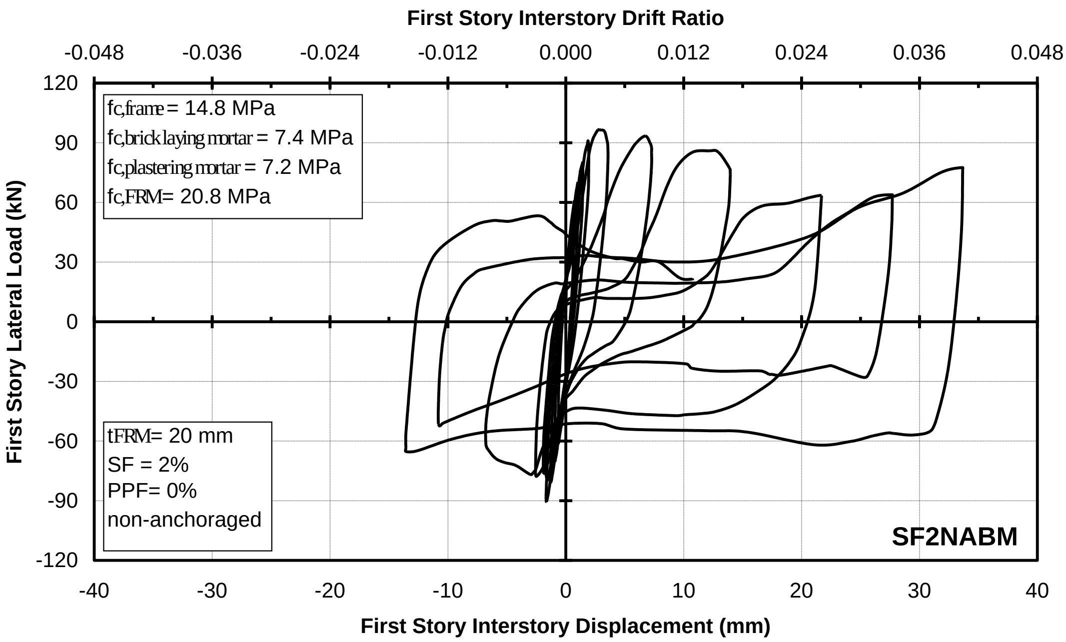


**Figure 4.43** First Story Lateral Load-First Story Displacement/Drift Ratio Graph of TS2 (SF2NABM) Specimen

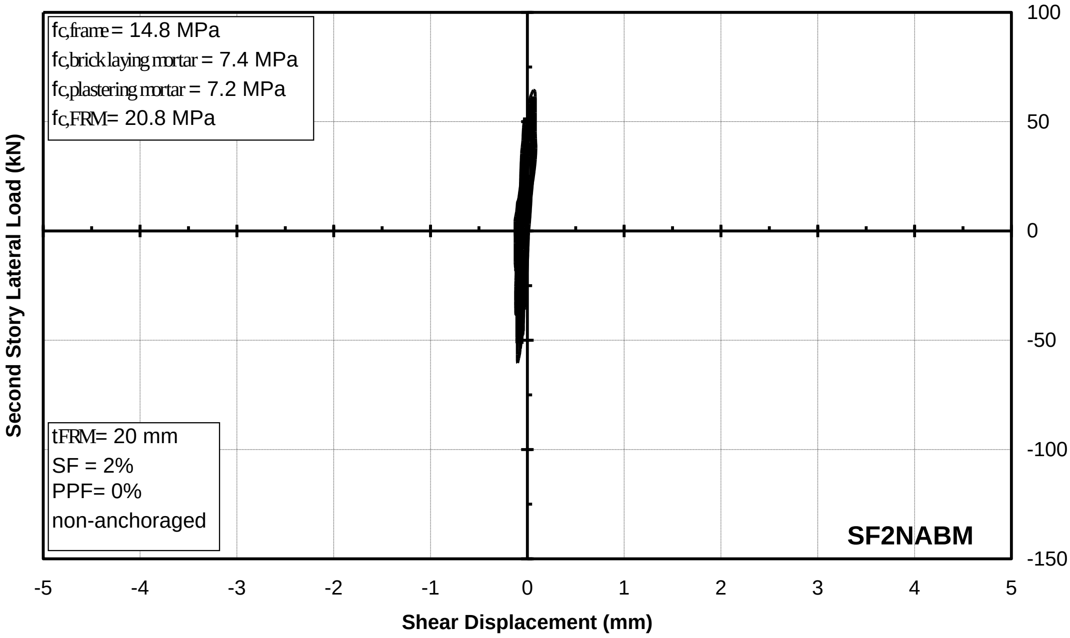


**Figure 4.44** Load-Second Story Shear Displacement Graph of TS2 (SF2NABM) Specimen

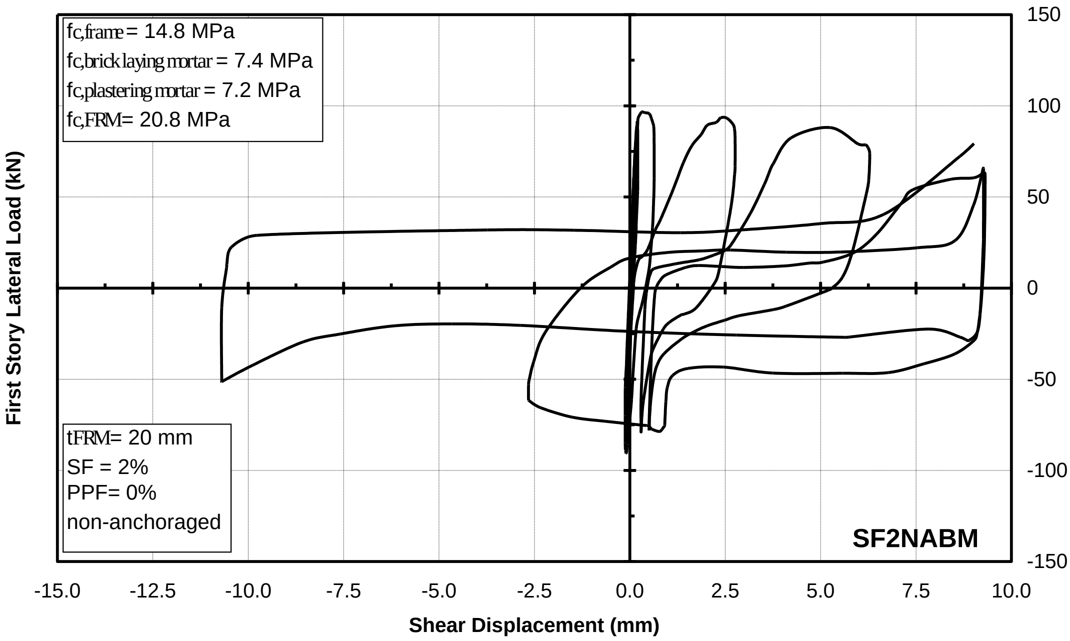


**Figure 4.45** Load-First Story Shear Displacement Graph of TS2 (SF2NABM) Specimen

**Figure 4.46** Views of TS2 (SF2NABM) Specimen during the Test

## 4.8 STRENGTHENED SPECIMEN, SF1ABM

The seventh test was the frame test SF1ABM. This third strengthened frame test (TS3) was a plastered, anchored, 10 mm thickness of mortar with 2% volumetric ratio of steel fiber applied frame. The specimen was subjected to the lateral loading history given in **Figure 4.47**. Lateral maximum forward loading and the top displacement were recorded as 125.66 kN and 8.47 mm. The same frame exhibited top displacement of 7.29 mm at a maximum backward loading of 116.84 kN. Top displacement history is presented in **Figure 4.48**. Main observations are presented below verbally and also as figures in **Figure 4.49**.

- In the third forward cycle: At the front side, a crack at the outside of the north column base. At the back side, a crack at the second story infill wall above and parallel to the first story beam.
- In the third backward cycle: At the back side, a crack at the outside of the south column base. Also, two shear cracks at the first story infill wall.
- In the fourth forward cycle: At the front side, shear cracks at the first story north bottom corner infill wall. At the back side, diagonal cracking of plaster from center of base to the mid-height of the first story north column.
- In the fifth forward cycle: At the front side, separation of the first story infill wall at base.
- In the fifth backward cycle: At the back side, two shear cracks on plaster of the first story infill wall near south column. Two flexural cracks on the first story south column.
- In the sixth forward cycle: At the front side, a shear crack at the first story infill wall corner. At the back side, diagonal cracks on plaster of the first story infill wall.
- In the sixth backward cycle: At the back side, a big diagonal crack on plaster from the second story infill wall to first story infill wall.

- In the seventh forward cycle: At the front side, two big shear cracks at the first story infill wall parallel to each other.
- In the seventh backward cycle: At the front side, one shear crack at the second story infill from mid-height of south column to the first story beam. A short vertical shear crack at the second story infill wall at the middle of the first story beam. At the back side, a crack at the plaster of the second story infill wall near the south column.
- Starting from the ninth forward cycle, no notes were taken. The cracks widened and extended. The test was stopped after the fourteenth full cycle.

Load-second story displacement/drift, load-first story displacement/drift, load-second story shear displacement, and load-first story shear displacement graphs are shown in **Figures 4.50-4.53**, respectively. Views of TS3 (SF1ABM) specimen during the test are shown in **Figure 4.54.**

Since the strengthening infill wall was anchored to the surrounding frame, the load transfer between wall and frame could be achieved along the frame members without assembled at certain regions.

First crack occurred at the column base followed by plaster cracking at backside. With the increasing lateral load, the strengthening mortar cracked at its bottom corners. At 0.3% first story drift ratio, the added infill initiated to separate at base level. Specimen reached to its maximum lateral load value at 0.67% drift ratio. At this stage, there was not a single diagonal crack but two diagonal cracks from opposite diagonal corners with approximately 45 degree and parallel to each other.

After ultimate load reached, cracks were also observed on the second story strengthening mortar. At approximately 1.2% first story drift ratio, maximum load decreased 15%. The frame damage was not concentrated at corners but dispersed to the column height as flexural cracks. There was no distinctive joint shear crack.

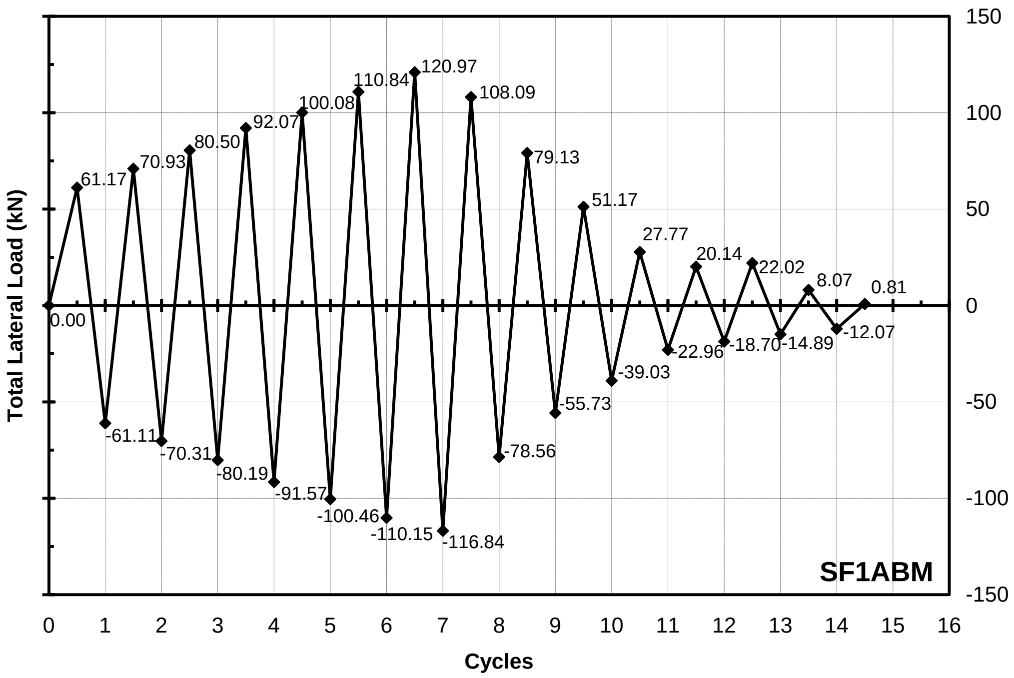


**Figure 4.47** Lateral Load History Graph of TS3 (SF1ABM) Specimen

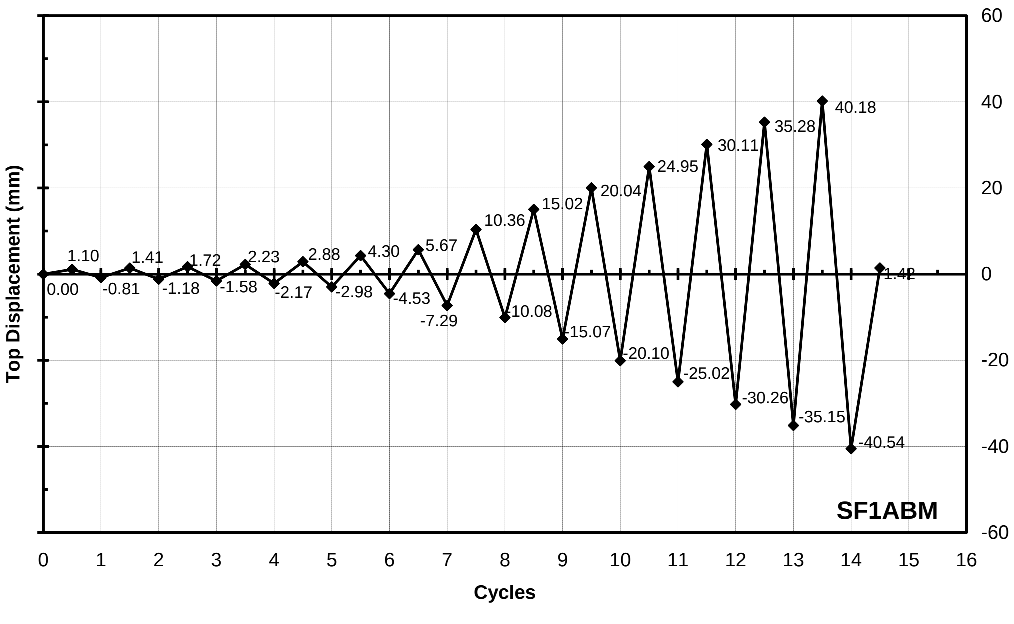


**Figure 4.48** Top Displacement History Graph of TS3 (SF1ABM) Specimen

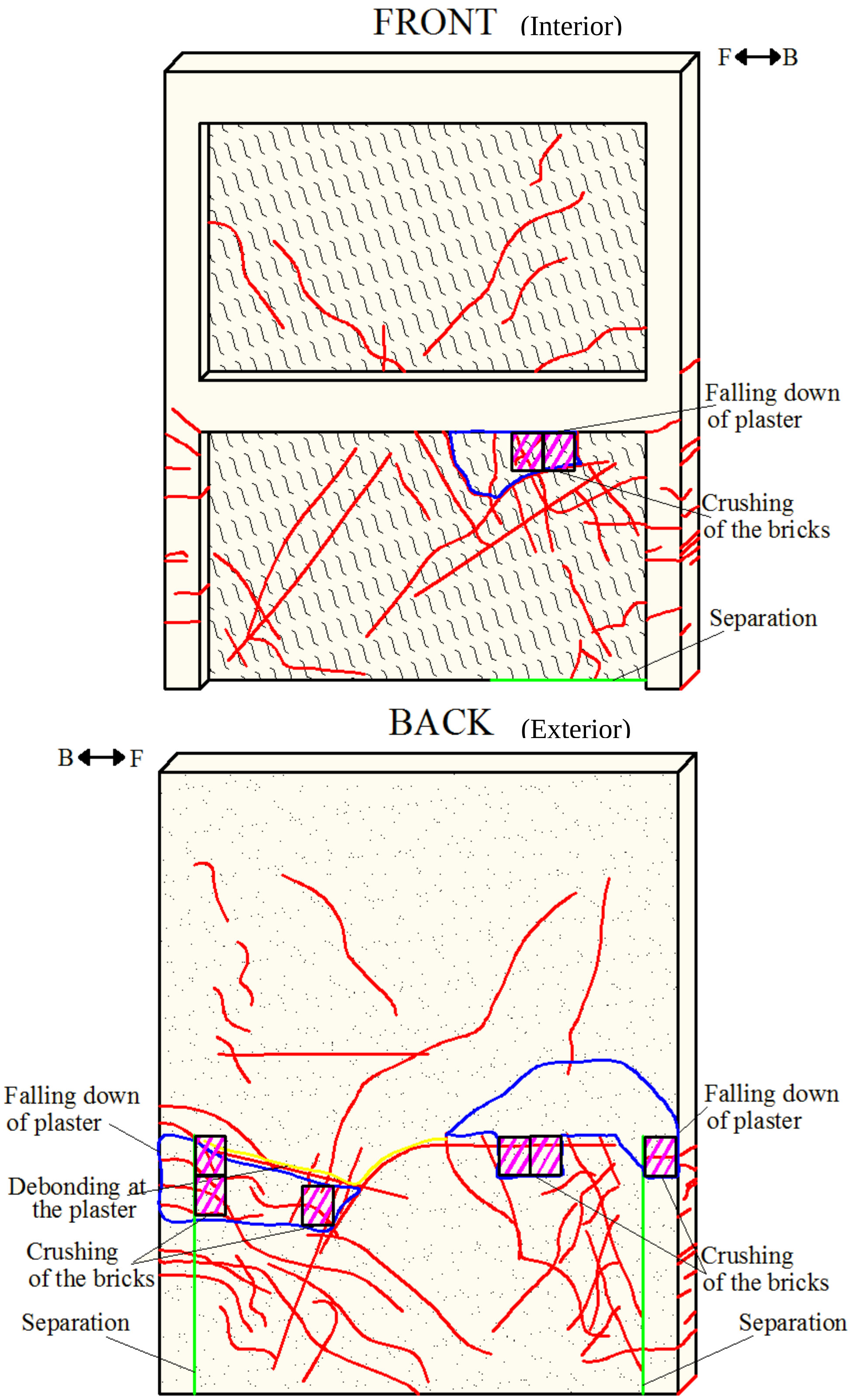


**Figure 4.49** Main Observations during the Strengthened Test SF1ABM

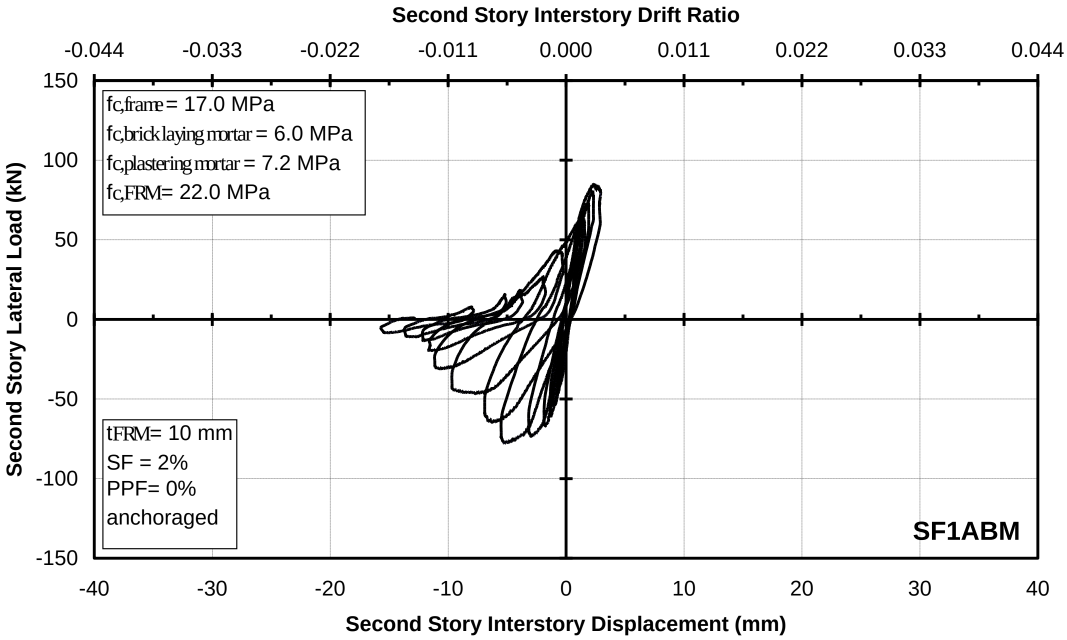


**Figure 4.50** Second Story Lateral Load-Second Story Displacement/Drift Ratio Graph of TS3 (SF1ABM) Specimen

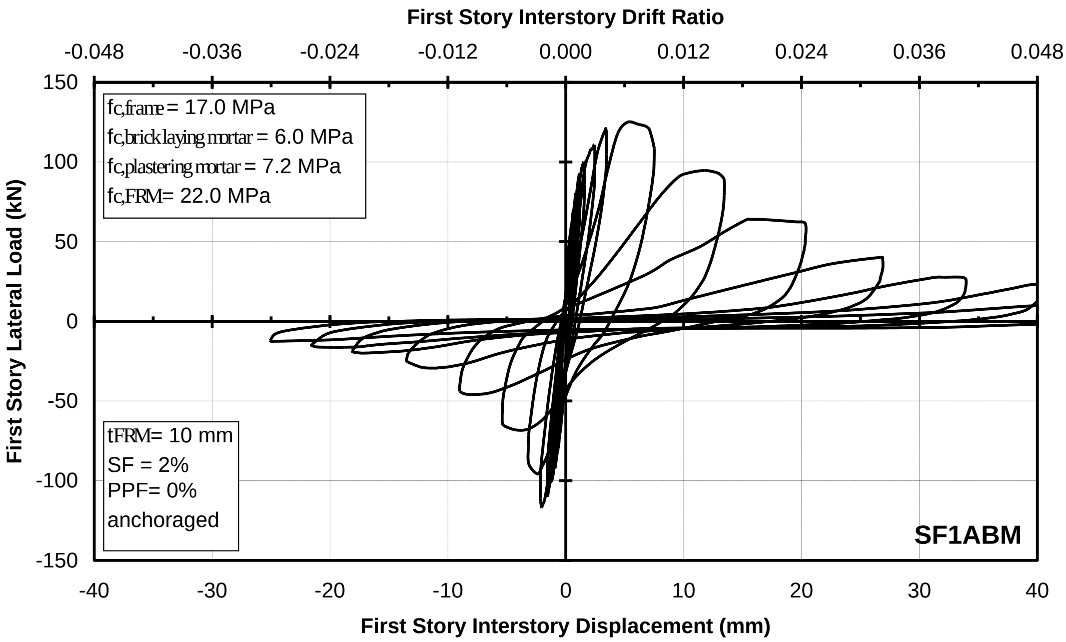


**Figure 4.51** First Story Load-First Story Displacement/Drift Ratio Graph of TS3 (SF1ABM) Specimen

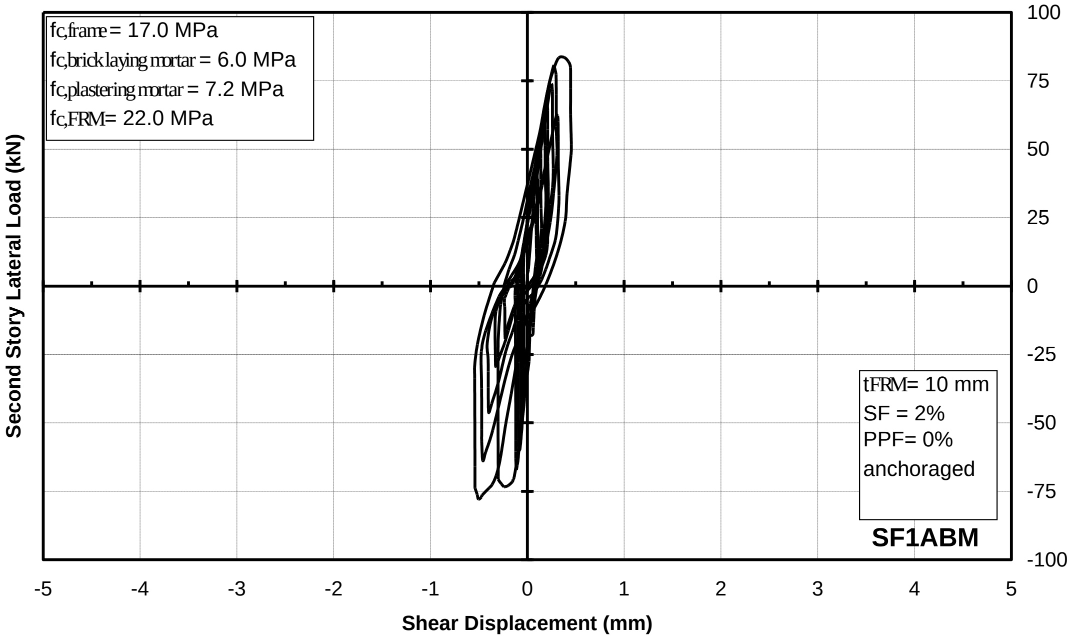


**Figure 4.52** Load-Second Story Shear Displacement Graph of TS3 (SF1ABM) Specimen

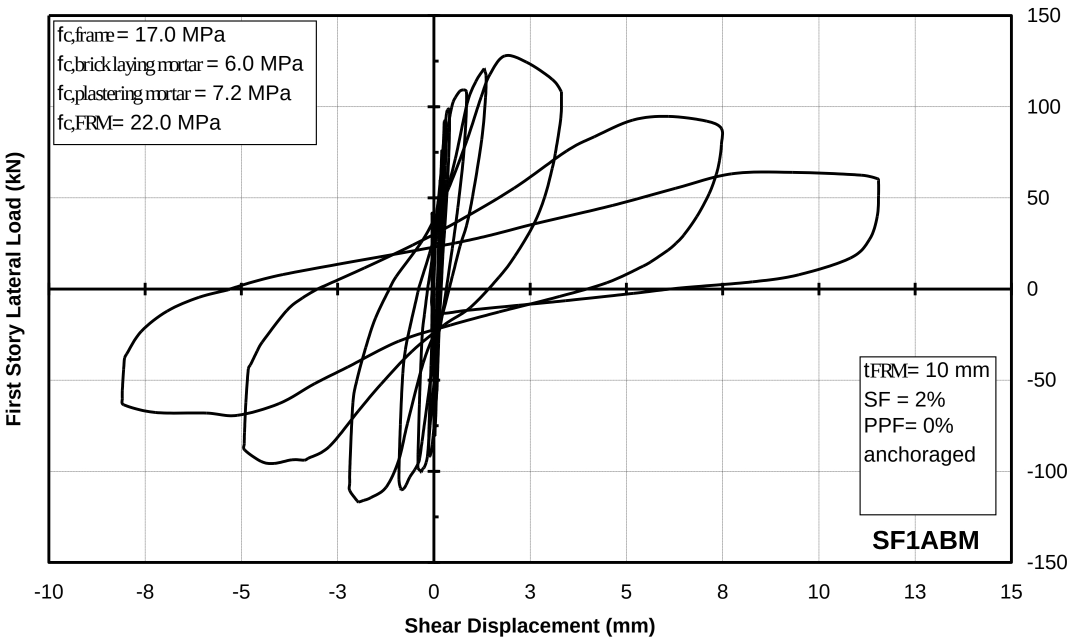


**Figure 4.53** Load-First Story Shear Displacement Graph of TS3 (SF1ABM) Specimen


**Figure 4.54** Views of TS3 (SF1ABM) Specimen during the Test

## 4.9 STRENGTHENED SPECIMEN, SF2ABM

The eighth test performed was SF2ABM, fourth strengthened frame test, of the frame specimen TS4 which was a plastered, anchored, 20 mm thickness of mortar with 2% volumetric ratio of steel fiber applied frame. The specimen was subjected to the lateral loading history given in **Figure 4.55**. The maximum forward load was measured as 140.42 kN and the top displacement at this load was 6.71 mm. The maximum backward loading and the corresponding top displacement was 134.17 kN and 8.91 mm. Top displacement history is shown in **Figure 4.56**.

Main observations are presented below verbally and also as figures in **Figure 4.57**.

- In the third forward cycle: At the front side, two shear cracks at the first story beam-north column joint. Also, a flexural crack at the outside of the bottom of the north column.
- In the fifth forward cycle: At the front side, a crack at outside of the bottom of the north column.
- In the fifth backward cycle: At the back side, a crack at the outside of the bottom of the south column.
- In the sixth backward cycle: At the back side, two minor shear cracks at the plaster of the first story infill wall at a location near to the south column.
- In the seventh forward cycle: At the front side, a shear crack starting from a place near to the bottom of the south column continuing upwards up to the middle of the first story beam. In addition, several shear cracks at the first story beam-north column connection and column base cracking.
- In the eighth forward cycle: At the back side, crack on plaster between the first story infill wall and the first story beam.
- In the eighth backward cycle: A vertical crack on mortar from the middle of the first story beam down to mid height.
- In the ninth forward cycle: At the front side, separation between the first story infill wall and the first story beam. Flexural cracks at the middle of the first story beam. Also, two shear cracks at the second story infill wall near to the second story north column.
- In the ninth backward cycle: At the front side, two flexural cracks at the mid-height of the first story south column. Three cracks at the first story beam. At the back side, at the plaster of the second story infill wall a horizontal crack at the top of the wall and diagonal crack near the top of the second story south column spanning up to the middle of the first story beam. A vertical crack at the outside of the first story south column.

- Starting from the tenth cycle, no notes were taken. The cracks progressed very much. The test was completed with the twelfth full cycle.

Load-second story displacement/drift, load-first story displacement/drift, load-second story shear displacement, and load-first story shear displacement graphs are presented in **Figures 4.58-4.61**, respectively. Views of TS4 (SF2ABM) specimen during the test are shown in **Figure 4.62.**

The first cracking was observed at the first story beam-column joint followed by flexural column cracks. With increasing load, cracks occurred on the backside plaster. A diagonal crack initiated on the strengthening mortar at 0.2% first story drift ratio. This crack extended from base corner up to beam mid span. This crack caused an increase in the shear deformation and caused several additional shear cracks at beam-column joint and column base cracking.

At 0.56% first story drift ratio, specimen reached to its maximum lateral load capacity. At this stage, a separation between the strengthening mortar and first story beam was observed and flexural cracks occurred on this beam. Additionally, cracks occurred on the second story strengthening wall.

At approximately 1.3% first story drift, lateral load decreased 15%. At 2% drift ratio, load decreased to 55% of its maximum value.

After the maximum load cycle, the surrounding frame members damaged excessively. Cover concrete of columns crushed and longitudinal bars buckled.

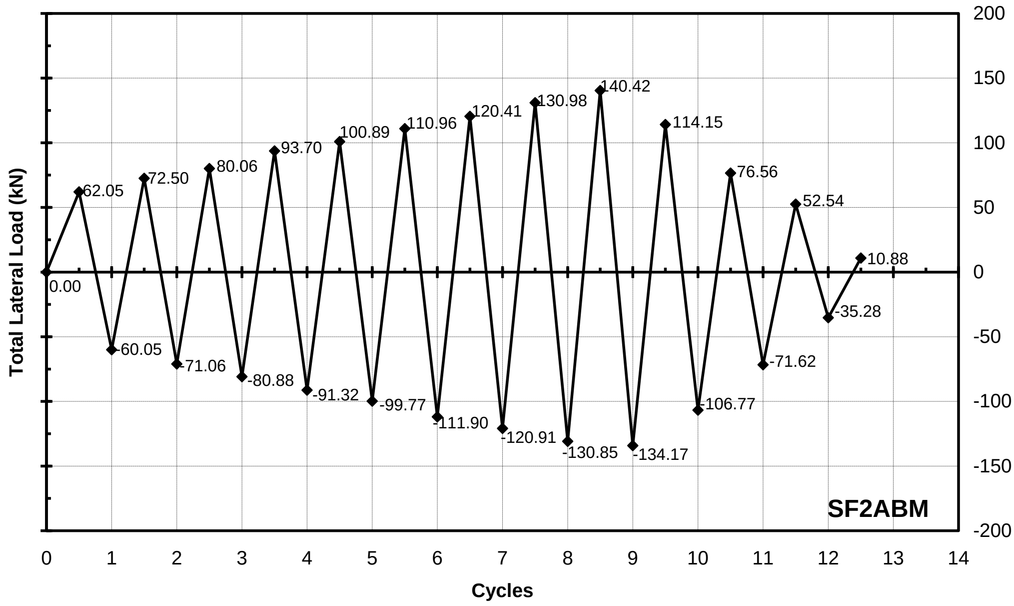


**Figure 4.55** Lateral Load History Graph of TS4 (SF2ABM) Specimen

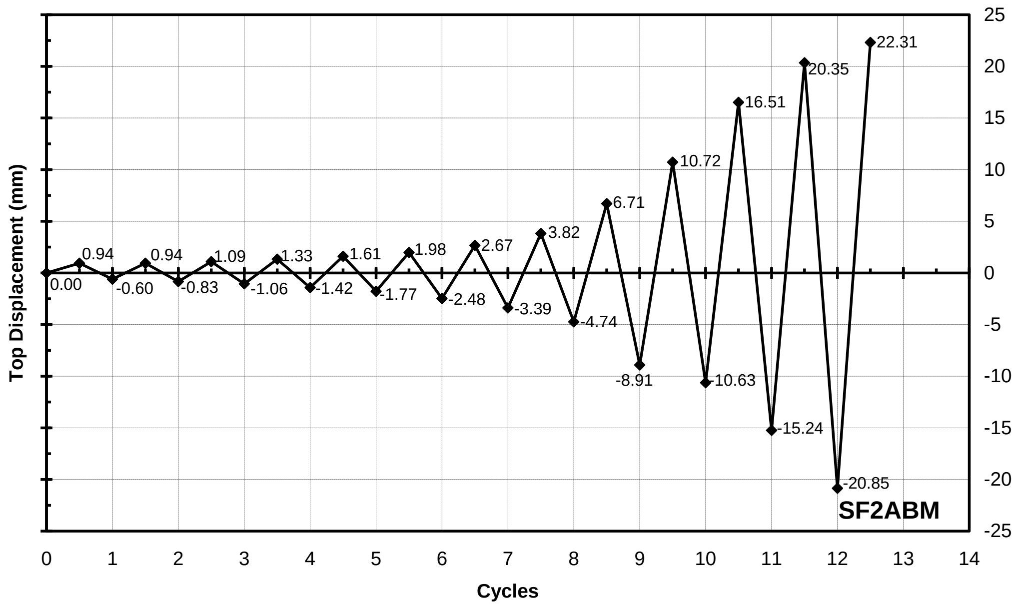


**Figure 4.56** Top Displacement History Graph of TS4 (SF2ABM) Specimen

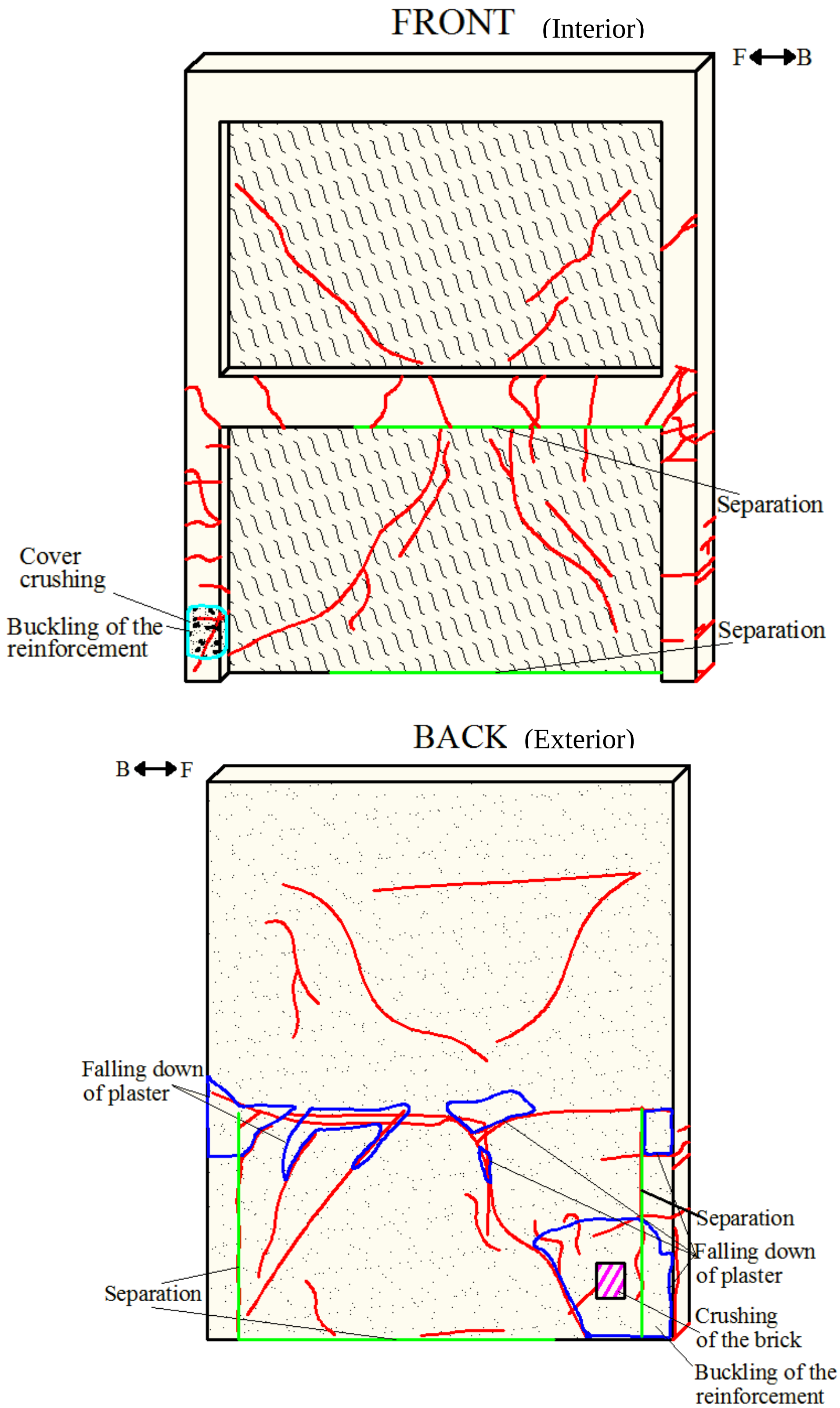


**Figure 4.57** Main Observations during the Strengthened Test SF2ABM

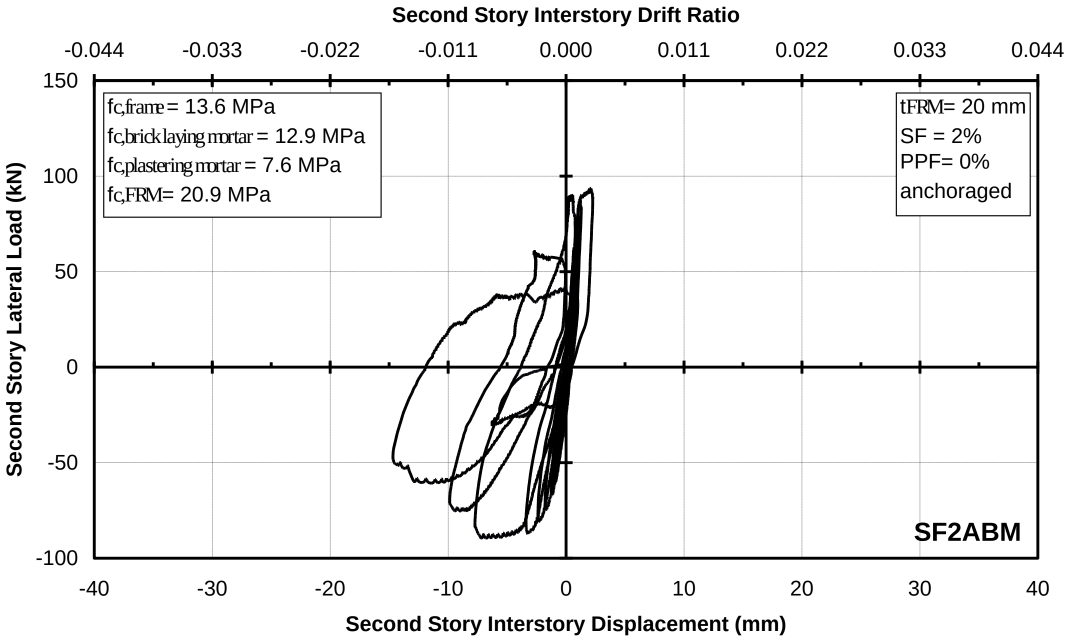


**Figure 4.58** Second Story Lateral Load-Second Story Displacement/Drift Ratio Graph of TS4 (SF2ABM) Specimen

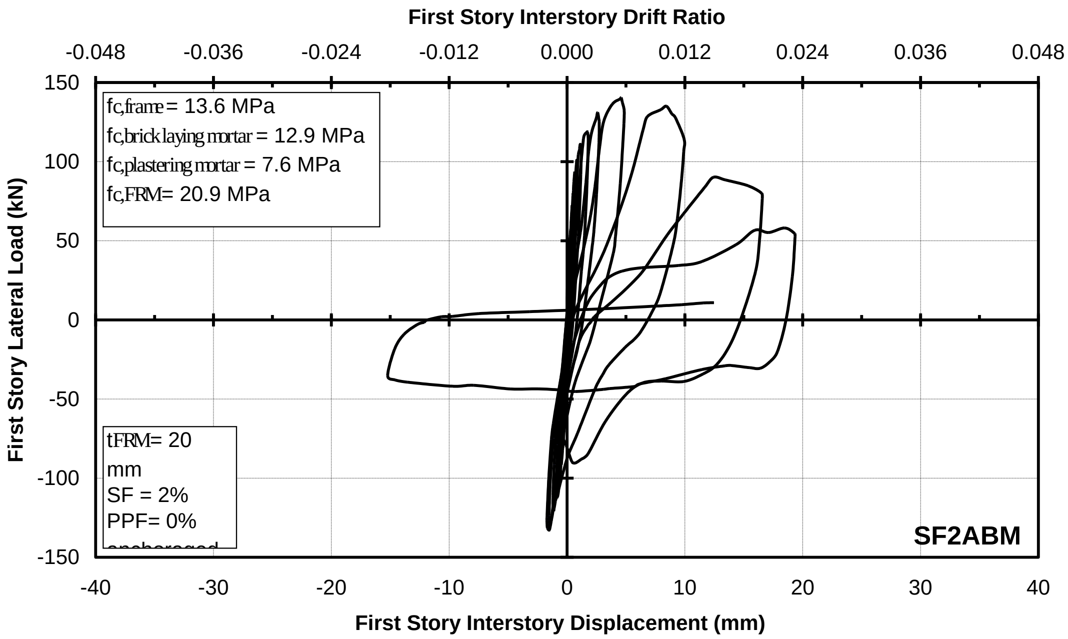


**Figure 4.59** First Story Lateral Load-First Story Displacement/Drift Ratio Graph of TS4 (SF2ABM) Specimen

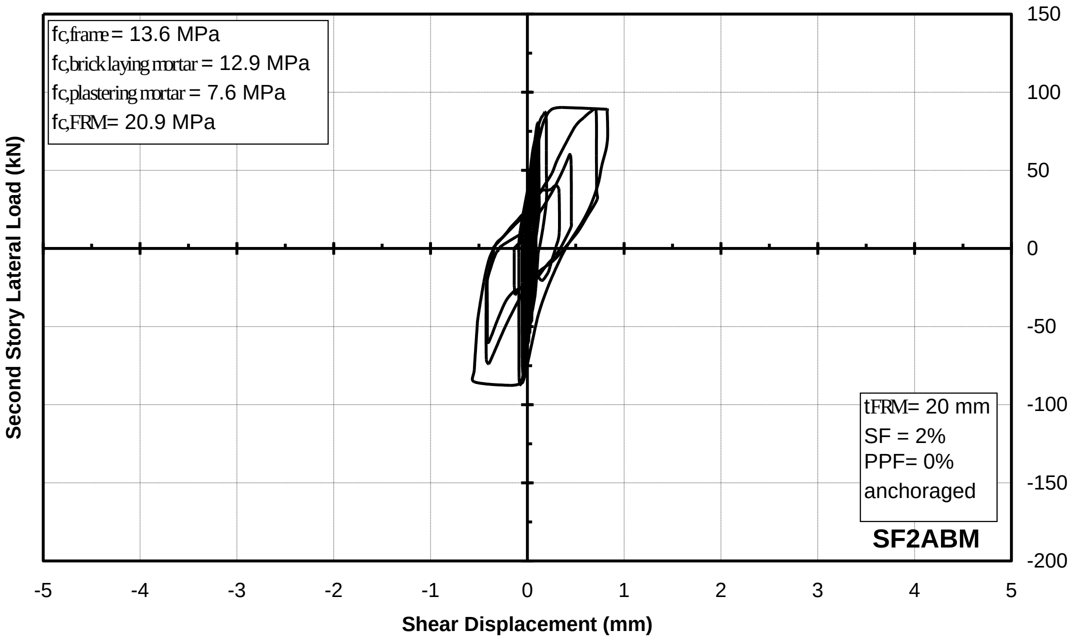


**Figure 4.60** Load-Second Story Shear Displacement Graph of TS4 (SF2ABM) Specimen

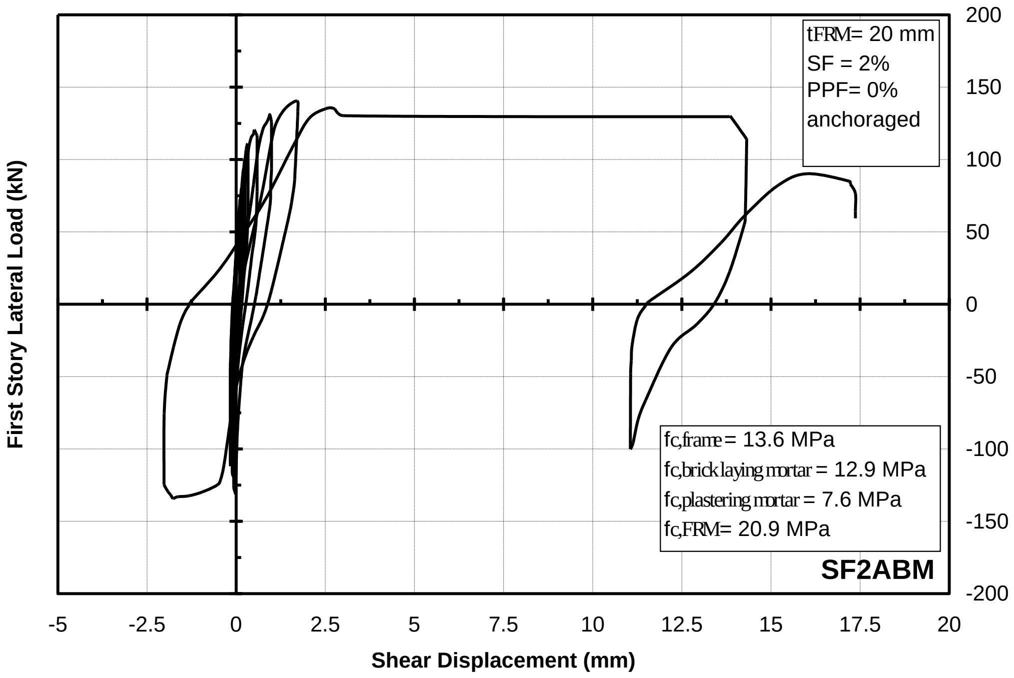


**Figure 4.61** Load-First Story Shear Displacement Graph of TS4 (SF2ABM) Specimen

**Figure 4.62** Views of TS4 (SF2ABM) Specimen during the Test

## 4.10 STRENGTHENED SPECIMEN, PPF2ABM

The ninth frame test PPF2ABM, fifth strengthened frame test was the test of the frame specimen TS8 which was a plastered, anchored, 20 mm thickness of mortar with 2% volumetric ratio of PP fiber applied frame. The specimen was subjected to the lateral loading history given in **Figure 4.63**. The maximum lateral forward load applied to this frame was 123.85 kN. The top displacement at this load was recorded as 14.19 mm. The maximum backward loading of the frame was 113.34 kN which resulted in a top displacement of 10.10 mm. Second story displacement history is shown in **Figure 4.64**. Main observations are presented below verbally and also as figures in **Figure 4.65**.

- In the third forward cycle: At the front side, a flexural crack at the bottom of the outside of the north column.
- In the third backward cycle: At the front side, a flexural crack at the bottom of the outside of the south column.
- In the fifth forward cycle: At the front side, a flexural crack at the first story north column.
- In the fifth backward cycle: At the front side, a flexural crack near to the middle of the first story south column.
- In the sixth forward cycle: At the front side, a shear crack at the first story infill wall near first story south column. At the back side, shear cracks on the plaster of the first story infill wall.
- In the sixth backward cycle: At the front side, a shear crack at the first story beam-south column connection.
- In the seventh forward cycle: At the back side, three shear cracks at the plaster of the first story infill wall, parallel to each other.
- In the eighth backward cycle: At the back side, a large shear crack at the plaster of the second story infill wall at first story beam boundary and

second story south column boundary.

- In the ninth forward cycle: At the front side, widening of the shear crack at the first story infill wall. At the back side, rising of the plaster at the first story infill wall.
- In the tenth forward cycle: At the front side, shear cracks at the second story beam-north column connection. Two flexural cracks at the second story north column.
- In the tenth backward cycle: At the front side, width of the strengthening mortar crack reached to 20 mm. At the back side, falling down of the plaster of the first story infill wall.
- In the twelfth forward cycle: At the back side, crushing of the hollow bricks.
- In the following cycles no notes were taken. The test was stopped after doing the fifteenth cycle, and then terminated.

Load-second story displacement/drift, load-first story displacement/drift, load-second story shear displacement, and load-first story shear displacement graphs are presented in **Figures 4.66-4.69**, respectively. Views of TS8 (PPF2ABM) specimen during the test are shown in **Figure 4.70.**

First cracking initiated at the column base. Later, flexural cracks were observed on first story columns. At 0.15% first story drift ratio, the strengthening wall initiated to crack. Simultaneously, cracks were observed on backside plaster followed by first story beam-column joint cracking. With increasing load, plaster cracking was observed also at second story wall. Specimen reached its maximum lateral load carrying capacity at almost 0.6% drift and kept it up to 1.8% drift. At this interval, plaster at backside debonded and lifted up, cracks were observed at second story joint and columns. The width of the crack of strengthening mortar reached up to 20 mm without fall down. However, the original plaster fell down at this level of displacement. The decrease on strength was insignificant at 2% drift. At 2.5% drift, 15% decrease was observed. At this displacement levels excessive shear damage was observed on top of the first story columns.

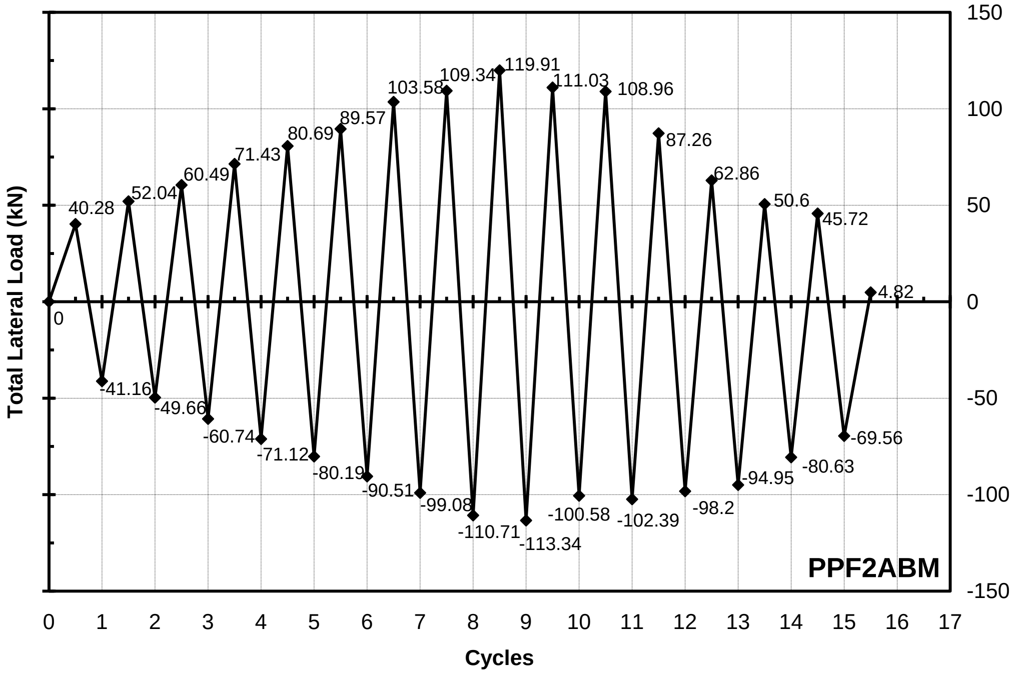


**Figure 4.63** Lateral Load History Graph of TS8 (PPF2ABM) Specimen

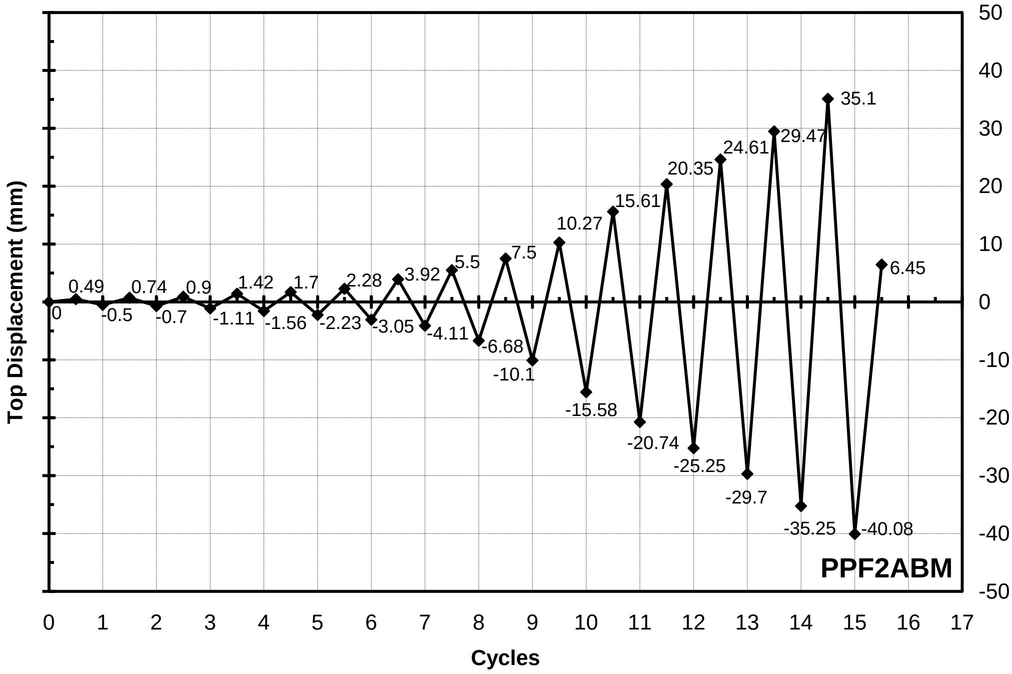


**Figure 4.64** Top Displacement History Graph of TS8 (PPF2ABM) Specimen

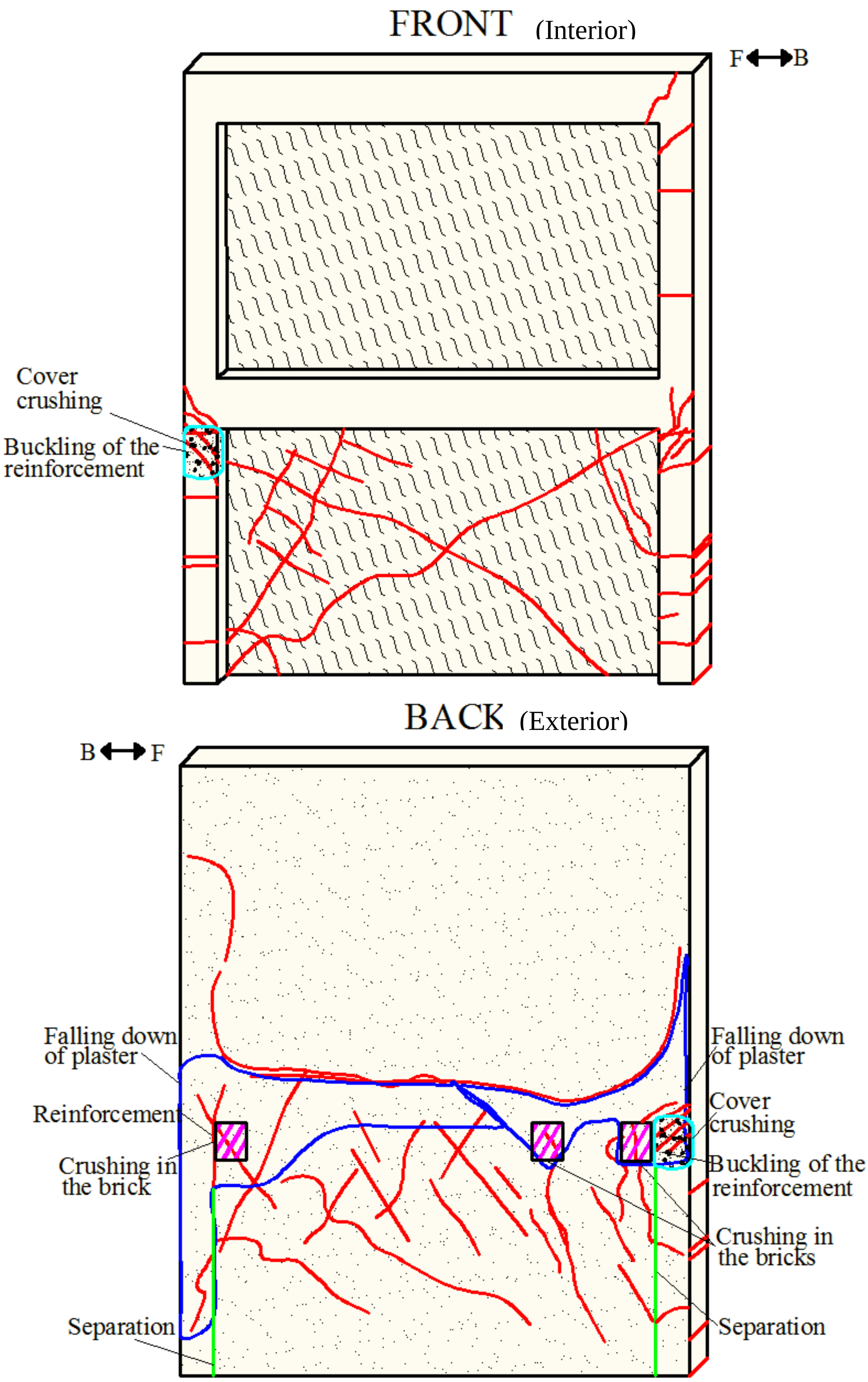


**Figure 4.65** Main Observations during the Strengthened Test PPF2ABM

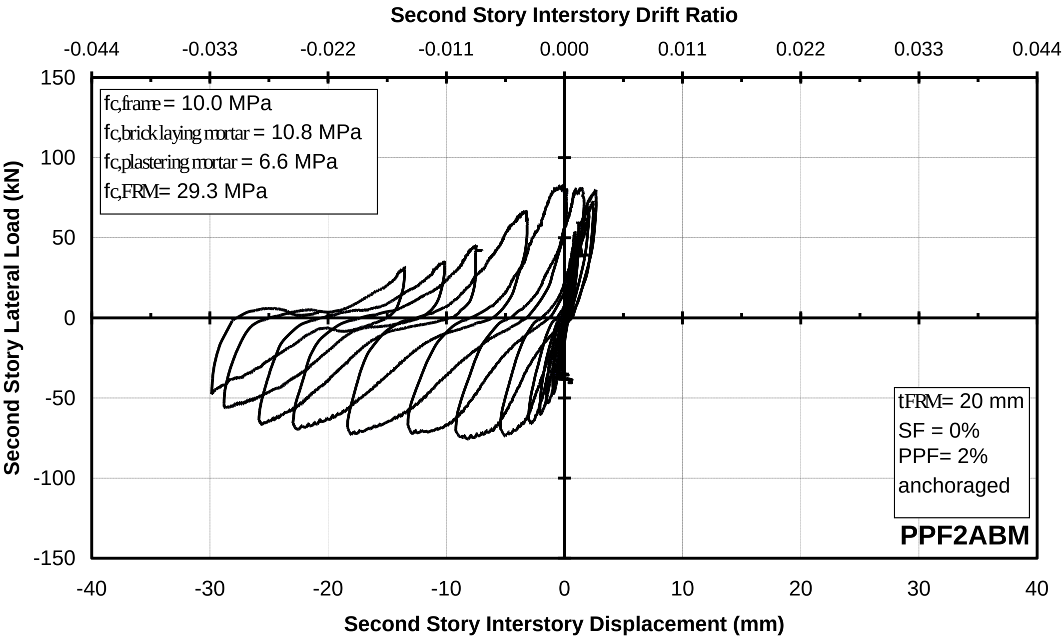


**Figure 4.66** Second Story Lateral Load-Second Story Displacement/Drift Ratio Graph of TS8 (PPF2ABM) Specimen

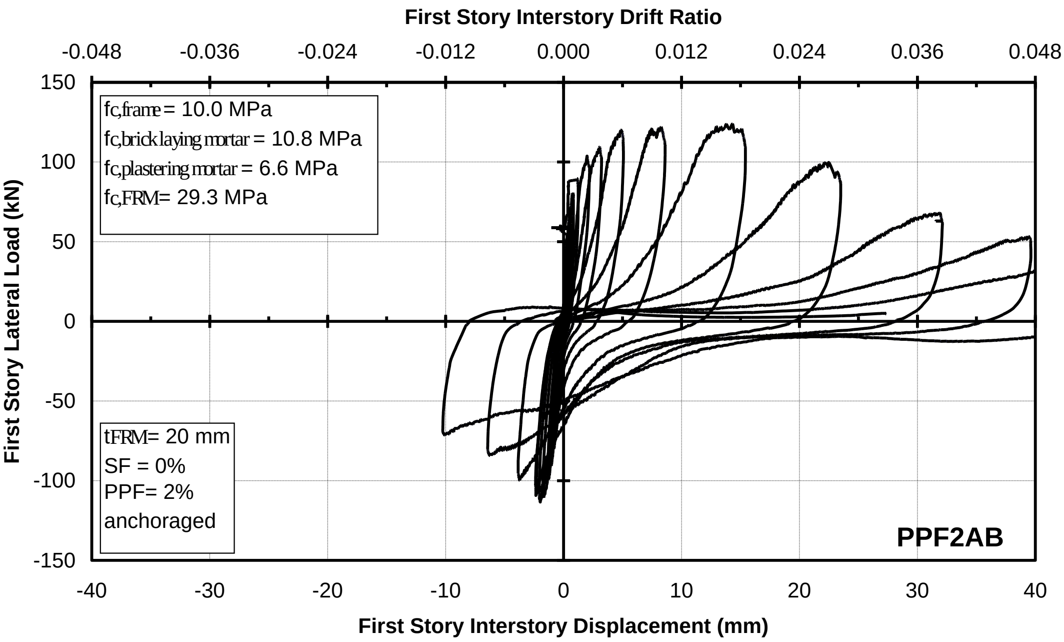


**Figure 4.67** First Story Lateral Load-First Story Displacement/Drift Ratio Graph of TS8 (PPF2ABM) Specimen

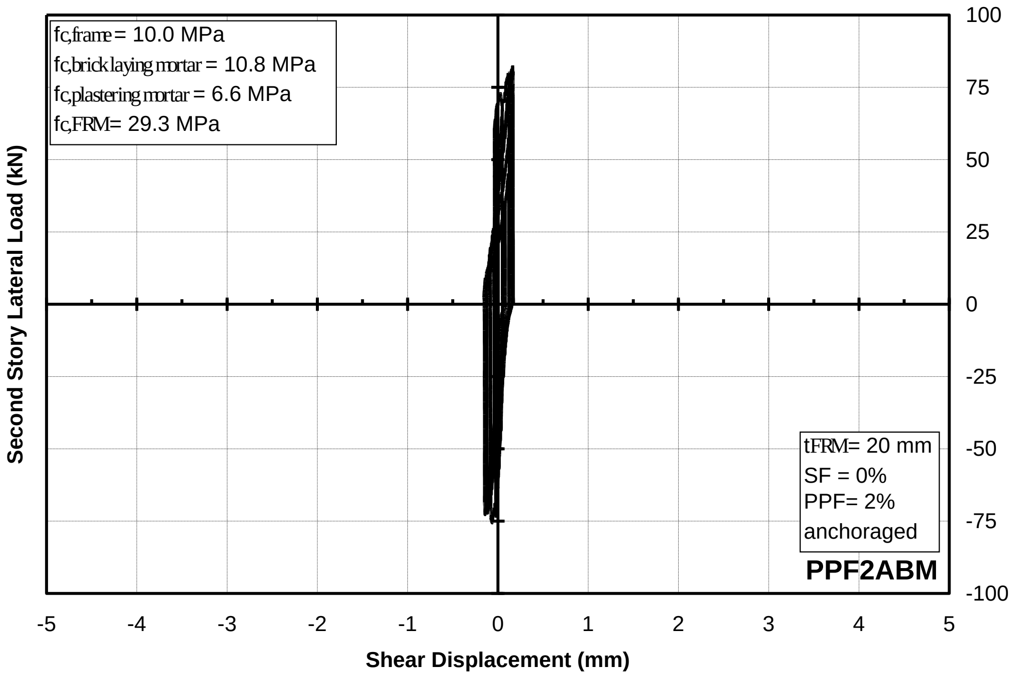


**Figure 4.68** Load-Second Story Shear Displacement Graph of TS8 (PPF2ABM) Specimen

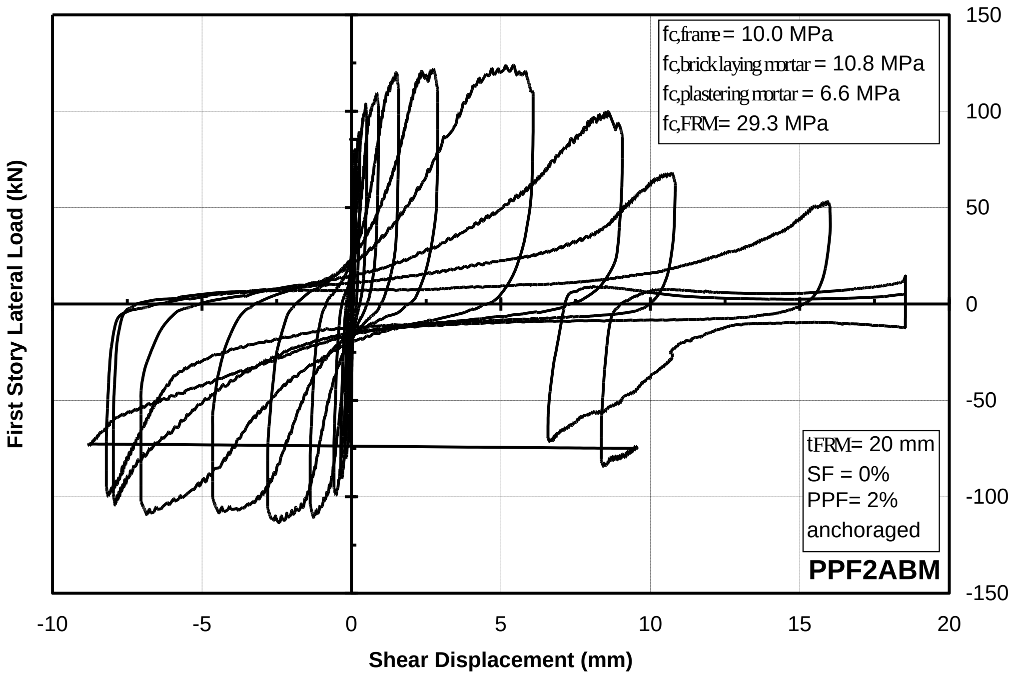


**Figure 4.69** Load-First Story Shear Displacement Graph of TS8 (PPF2ABM) Specimen


**Figure 4.70** Views of TS8 (PPF2ABM) Specimen during the Test

## 4.11 STRENGTHENED SPECIMEN, HF2ABM

The tenth frame test HF2ABM, sixth strengthened frame test, was the test of the specimen TS10 which was a plastered, anchored, 20 mm thickness of mortar with 2% volumetric ratio of hybrid fiber (1% steel fiber, 1% PP fiber) applied frame. The specimen was subjected to the lateral loading history given in **Figure 4.71**. The maximum forward load was recorded as 122.04 kN and the top displacement at this load was 10.01 mm. The maximum backward loading was 119.03 kN and the corresponding top displacement was observed as 7.56 mm. Second story displacement history is shown in **Figure 4.72**. Main observations are given below verbally and also as figures in **Figure 4.73**.

- In the second forward cycle: At the front side, a flexural crack at the bottom of the outside of the north column.
- In the second backward cycle: At the front side, a flexural crack at the bottom of the outside of the south column.
- In the third forward cycle: At the front side, opening between the right side of the first story infill wall and the foundation.
- In the third backward cycle: At the front side, opening this time between the left side of the first story infill wall and the foundation.
- In the fifth forward cycle: At the front side, a flexural crack at the first story north column just below the first story beam-north column joint.
- In the sixth backward cycle: At the front side, a flexural crack at the first story south column below the first story beam-south column joint. At the back side, shear cracks at the plaster of the first story infill wall.
- In the seventh forward cycle: At the front side, a flexural crack at the second story bottom of north column. At the back side, shear cracks at the plaster of the first story infill wall at a location near to the first story north column.
- In the eighth forward cycle: At the back side, two parallel shear cracks at the

plaster at a location of the intersection of the north column and first story beam.

- In the eighth backward cycle: At the front side, the first shear crack at the first story infill wall starting from the mid-height of the first story north column and ending near to the middle of the first story beam. At the back side, crack from bottom corner of the north column up to middle of the infill wall.
- In the ninth forward cycle: At the front side, a shear crack at the first story infill wall at a location below the first story beam-south column joint. At the back side, several parallel shear cracks at the plaster of the first story infill wall starting from the first story beam-south column joint up to the middle of the first story infill wall.
- In the ninth backward cycle: In this cycle, the load was given as displacement controlled.
- In the tenth backward cycle: Increasing to approximately 3-4 mm of the width of the shear crack at the first story infill wall at a location below the first story beam-north column joint.
- In the eleventh forward cycle: At the front side, width of crack at first story beam-south column joint approximately 10 mm. At the back side, falling down of the plaster in line with the beam of the first story.
- In the eleventh backward cycle: At the front side, width of the shear crack, at the first story infill wall nearly 15-20 mm. At the back side, falling down of the plaster. The hollow bricks became visible.
- In the twelfth backward cycle: At the back side, falling down of the plaster at the first story beam and below the beam and crushing of the hollow bricks.
- Starting from the thirteenth forward cycle, no notes were taken. The test was terminated after completing the fourteenth full cycle.

Load-second story displacement/drift, load-first story displacement/drift, load-second story shear displacement, and load- first story shear displacement graphs are presented in **Figures 4.74-4.77**, respectively. Views of TS10 (HF2ABM) during and after the test are shown in **Figure 4.78**.

First cracking was observed at column base. At early stages, cracking occurred at the base of strengthening wall. Later, top of the first story columns cracked followed by plaster cracking at backside.

At 0.4% first story drift ratio, the strengthening mortar cracked from mid-span of beam to mid-height of first story column. The maximum lateral load was reached at approximately 0.8% first story drift ratio. 15% decrease at the lateral load capacity was observed at 1.5% drift ratio. At 2% drift ratio, strength decreased about 30%.

Beyond the ultimate, with increasing displacement (after 1.4% drift ratio), joint cracks opened excessively. Also width of cracks on strengthening mortar reached almost to 20 mm. Bricks crushed at this level of displacement.

The strengthening infill in this specimen cracked at top corner of first story and opened excessively. Therefore, the behavior was much similar to non-anchored specimens in which damage was concentrated at joints.

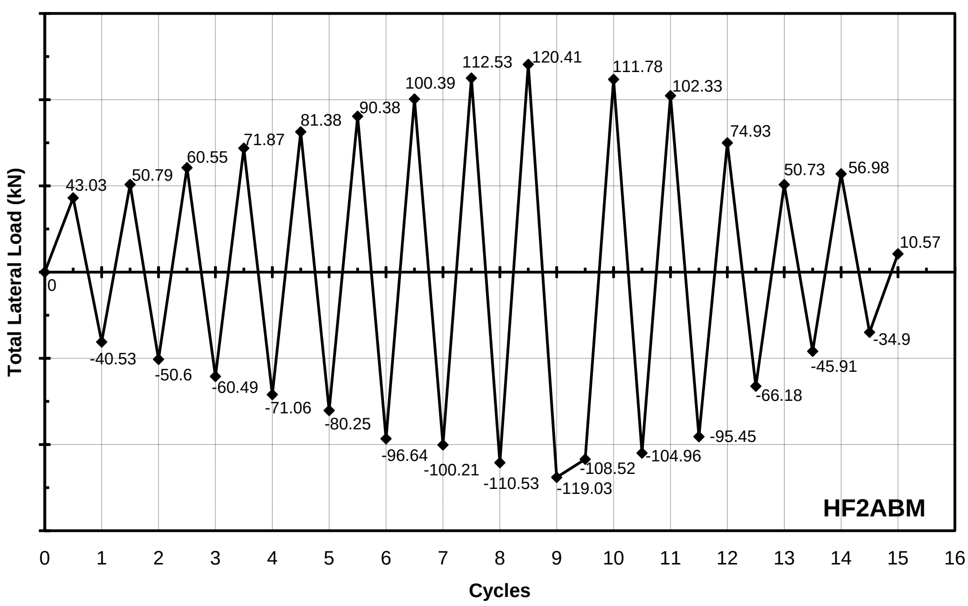


**Figure 4.71** Lateral Load History Graph of TS10 (HF2ABM) Specimen

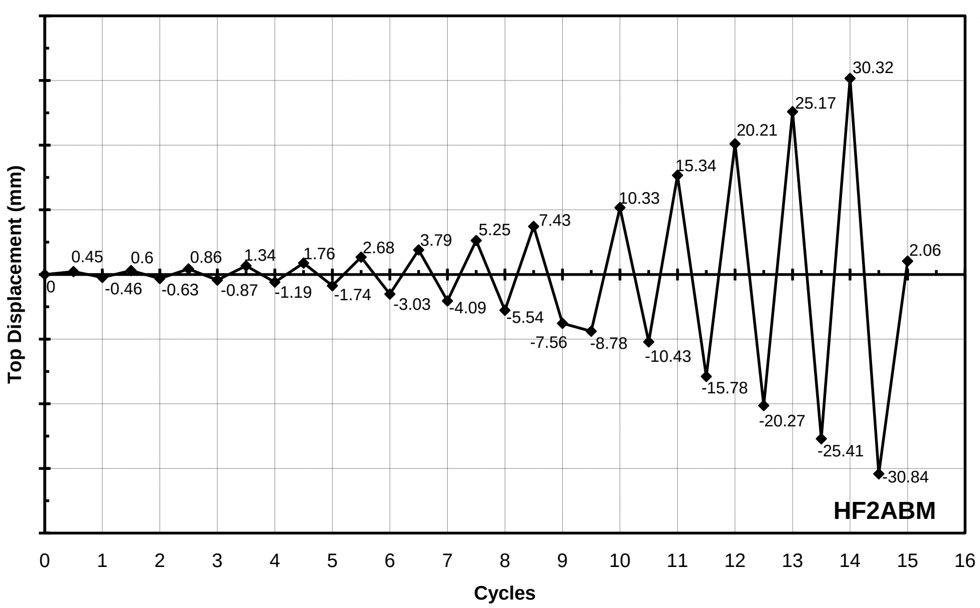


**Figure 4.72** Top Displacement History Graph of TS10 (HF2ABM) Specimen

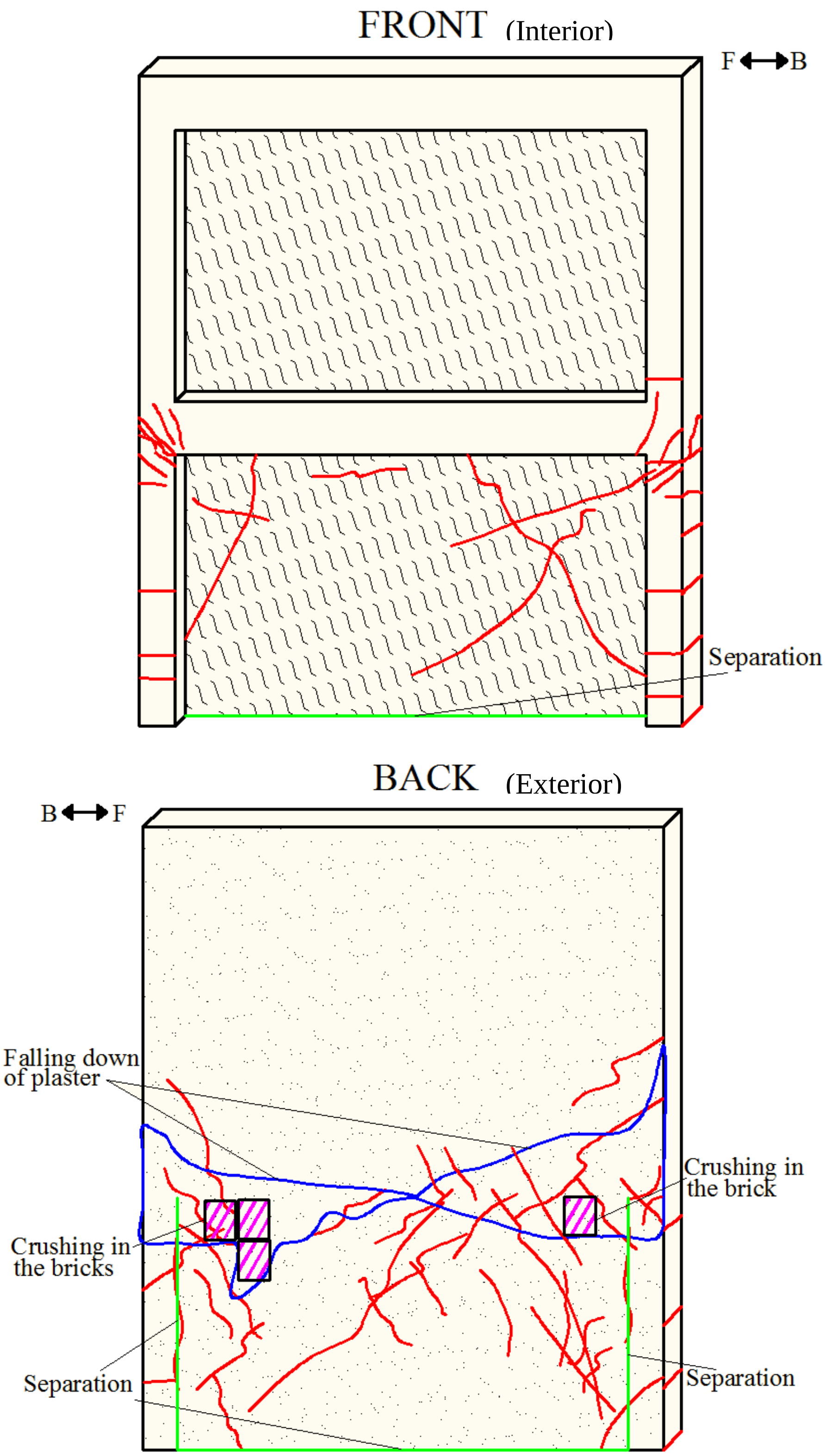


**Figure 4.73** Main Observations during the Strengthened Test HF2ABM

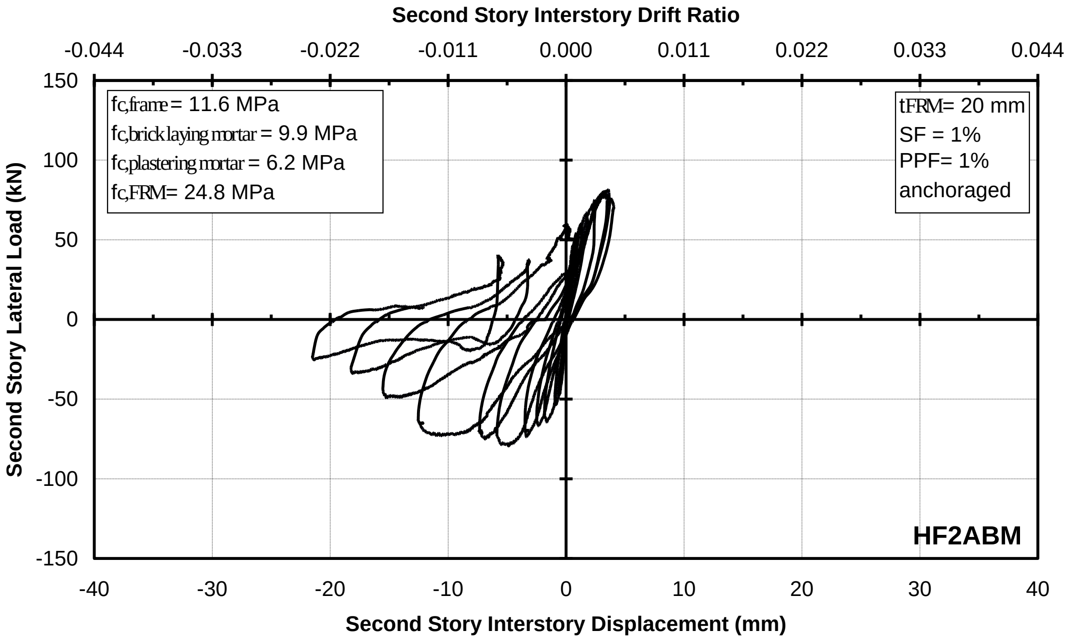


**Figure 4.74** Second Story Lateral Load-Second Story Displacement/Drift Ratio Graph of TS10 (HF2ABM) Specimen

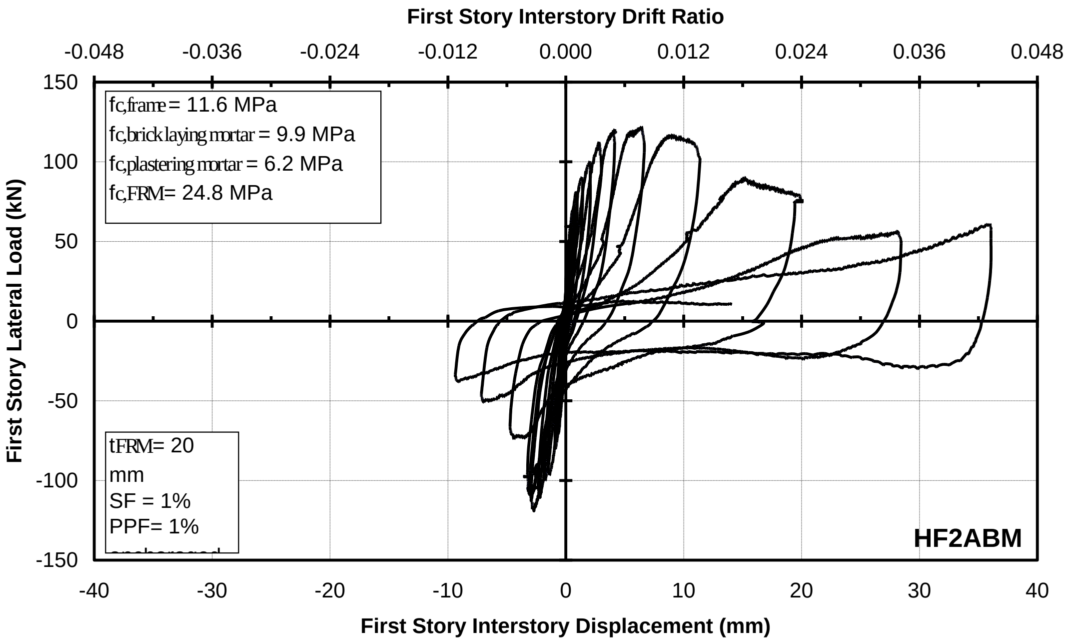


**Figure 4.75** First Story Lateral Load-First Story Displacement/Drift Ratio Graph of TS10 (HF2ABM) Specimen

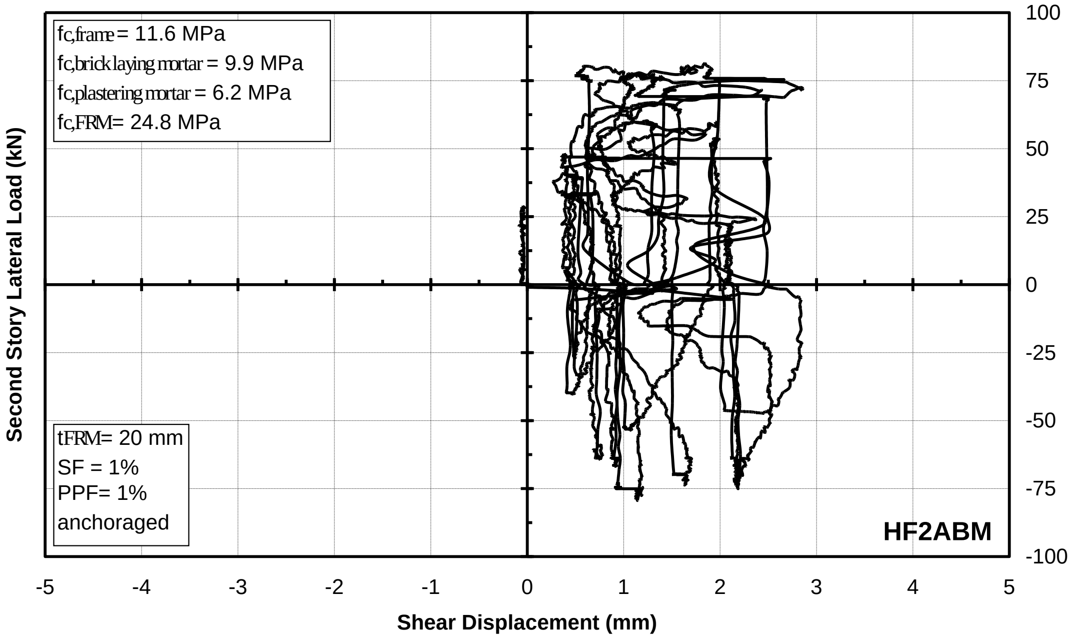


**Figure 4.76** Load-Second Story Shear Displacement Graph of TS10 (HF2ABM) Specimen

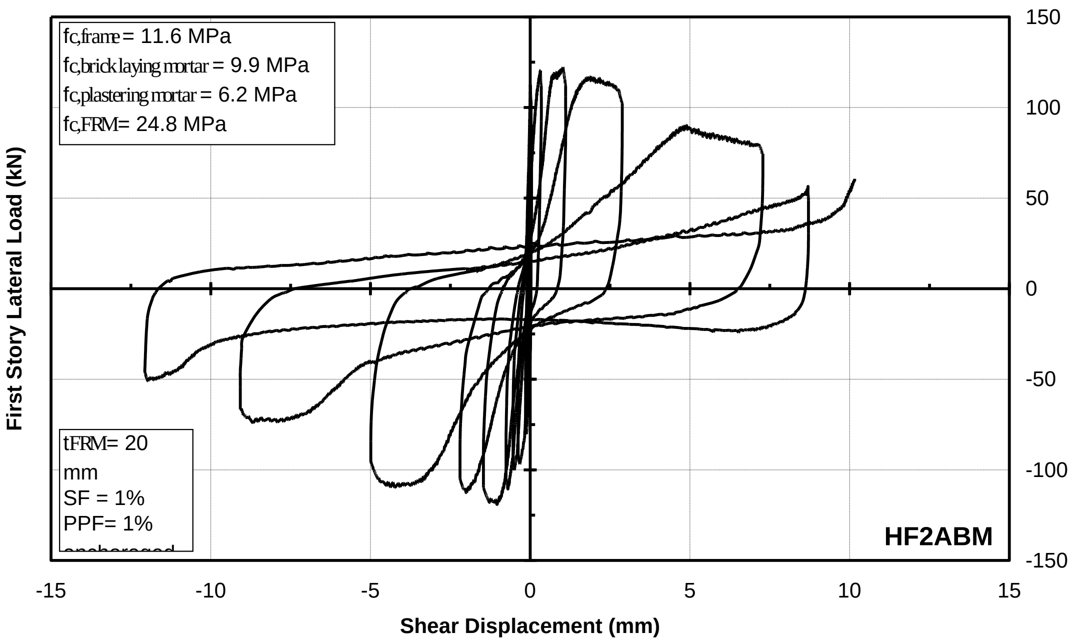


**Figure 4.77** Load-First Story Shear Displacement Graph of TS10 (HF2ABM) Specimen

**Figure 4.78** Views of TS10 (HF2ABM) Specimen during the Test

# CHAPTER 5

# EVALUATION OF TEST RESULTS

## 5.1 GENERAL

In this chapter, test results are evaluated in terms of strength, stiffness, energy dissipation and inter-story drift ratios. Summary of the test results are presented in **Table 5.1**. First story lateral load-first story interstory displacement/drift graphs drawn to a common scale are shown in **Figure 5.1**. All the hysteresis loops show a pronounced pinching effect. The differences in the hysteretic behavior of bare and infilled frame are obvious. The loops in the case of bare frame are wider, due to the inelastic behavior of flexural plastic hinges. The envelope of the hysteresis loops obtained from cyclic tests is similar to the force-displacement relationship measured under monotonic loading. The loops indicate a significant pinching effect and strength degradation. Moreover, the stiffness is low in the initial part of each half-cycle which corresponds to the closing of the cracks due to the applied force in the opposite direction. With the increase of lateral force, stiffness also increases.

As can be seen in **Figure 5.1**, first story interstory displacements in backwards cycles are smaller than that of forward cycles in all specimens except REFBA and REFB. Since the tests are displacement controlled after yielding of specimens, the backward displacements have to be taken as second story interstory displacement. As can be observed from the second story interstory displacement graphs given in Chapter 4, in all of the aforementioned specimens the backward second story displacements are excessive to that of the forward ones. This permanent odd behavior is attributed to the test setup. The load is applied by a very stiff spreader beam in forward cycles. The touch points of the spreader beam to the frame are not pinned in this setup. Consequently, the second and first story levels are forced to displace the same amount. In the backward cycles, however, there is no spreader beam, story lateral loads are applied separately as shown in **Figure 3.21**. Therefore, in the backwards direction the load application boundaries can be considered as pins. In this case, the second story level can displace independently from the first story level.

As observed in **Figure 5.1**, specimen SF2NABM does not show pinching effect unlike other specimens. It is hard to explain this unexpected behavior. The reason of very sharp (almost vertical) decrease of lateral load at unloading points (similar to other specimens) is either separation of infill wall from surrounding frame or excessive opening of particular cracks on the infill wall. Main cracks on infill were not diagonal in this specimen. The cracks moved from column base to 1/3$^{th}$ of beam with approximately 75$^{o}$. Therefore, compression strut did not created diagonally, but with steeper inclination inside the V-cracks. At the unloading point, a compression strut created in the opposite direction simultaneously as explained above. When the capacity is reached in the opposite direction, the infill slips inside the frame due to the lack of anchorages. In this non-anchored frame the beam-column joints are directly sheared by the infill and consequently damaged excessively. Excessive damage and displacement at certain points cause strain hardening of longitudinal bars at this point. The capacity increase on the graph at high drift level can be explained by this strain hardening of rebars.

## 5.2 RESPONSE ENVELOPES

In order to evaluate the strength characteristics of the frame specimens, response envelope curves were used. Response envelope curves were constructed by connecting the maximum points of the hysteretic load-displacement curves of the specimens. First story response envelope graphs of reference specimens and performances of the strengthened frame specimens are compared with the reference frame specimens, it can be seen that strengthened specimens performed better than the reference specimens. Both strength and stiffness increased significantly after strengthening operations.

Comparing the behavior of the reference specimens according to **Figure 5.2**, it can be said that REF2ABM, which is the test of the plastered, anchored, 20 mm thickness of mortar not containing either steel fiber or PP fiber applied frame, exhibited the best behavior among the reference specimens. It had the largest lateral load carrying capacity. Although, it is counted as a reference specimen for this study, 20 mm anchored mortar application itself is a strengthening technique. In the former chapter it was stated that since this specimen had no anchorages on the surrounding frame the damage was localized at the corner regions. The load transfer between the strengthening mortar and frame could not be established properly. The wall separated excessively from the surrounding frame. The main advantage of this strengthening technique was keeping the brick masonry in place. It should be also noted that the strength of the mortar was 40 MPa which is almost twice the other mortar strengths. Therefore, this specimen carried approximately 100 kN lateral load. REFBM, the test of the plastered reference frame, showed the 2$^{nd}$ best behavior. REFB, the test of the non-plastered reference frame, showed better behavior than the test of the bare reference frame, REFBA. All of the reference specimens behaved almost same in the forward and backward cycles. Specimen of the REFBM test lost its lateral load carrying capacity earlier than the other reference specimens. The differences in lateral load of REFBA, REFB and REFBM clearly indicate that there may be significant reserve capacity due to nonstructural infill brick walls. This reserve capacity should be carefully handled because of early out of plane failure of the wall.

According to **Figure 5.3**, it is observed that the test of plastered, anchored, 20 mm thickness of mortar with 2% volumetric ratio of steel fiber applied frame, SF2ABM had the largest lateral load carrying capacity. But, this specimen lost its lateral load carrying capacity earlier with respect to the other specimens. Therefore, in the design of such strengthening technique the drift limits should be carefully checked and the design should be remained inside certain limits. Strengthened frame specimen tests SF1ABM, PPF2ABM, and HF2ABM showed very similar behavior and their lateral load carrying capacities were approximately the same. The frame specimen used in the test SF2NABM showed less lateral loading capacity than these frame specimens. The least performance was exhibited by the frame specimen of the test SF1NABM. This frame was plastered, non-anchored, 10 mm thickness of mortar with 2% volumetric ratio of steel fiber applied frame. It was observed that anchored specimens behaved better than the non-anchored ones.

**Table 5.1** Summary of the Test Results

| Specimen | Axial Load Level $N/N_0$ | Frame Conc. Str. (MPa) | Brick Laying Mortar Str. (MPa) | Plaster Mortar Str. (MPa) | Mortar wt. Steel F. Str. (MPa) | Mortar wo. Steel and/or PP F. Str. (MPa) | Mortar wt. PP F. Str. (MPa) | Mortar wt. Hybrid F. Str. (MPa) | Forward Loading | | | Backward Loading | | | Initial Stiffness (kN/mm) | Cumulative Energy Dissipation (kN.m) |
|---|---|---|---|---|---|---|---|---|---|---|---|---|---|---|---|---|
| | | | | | | | | | Max. Load (kN) | 1[st] St. Drift Ratio* $\Delta_1/h_1$ | 2[nd] St. Drift Ratio* $(\Delta_2-\Delta_1)/h_2$ | Max. Load (kN) | 1[st] St. Drift Ratio** $\Delta_1/h_1$ | 2[nd] St. Drift Ratio** $(\Delta_2-\Delta_1)/h_2$ | | |
| REFBA | 0.11 | 12.7 | | | | | | | 14.53 | 0.0160 | 0.0076 | 12.03 | 0.0151 | 0.0090 | 1.74 | 2.06 |
| REFB | 0.11 | 13.3 | 3.4 | | | | | | 50.23 | 0.0113 | 0.0062 | 50.29 | 0.0103 | 0.0065 | 24.44 | 5.88 |
| REFBM | 0.11 | 12.7 | 8.4 | 8.2 | | | | | 66.59 | 0.0043 | 0.0032 | 66.59 | 0.0032 | 0.0042 | 21.39 | 4.49 |
| REF2ABM | 0.15 | 8.6 | 8.7 | 6.0 | | 40.8 | | | 104.52 | 0.0124 | 0.0055 | 101.52 | 0.0047 | 0.0124 | 61.08 | 10.78 |
| SF1NABM | 0.13 | 9.9 | 7.5 | 6.4 | 17.0 | | | | 80.56 | 0.0043 | 0.0018 | 80.69 | 0.0023 | 0.0025 | 101.31 | 8.40 |
| SF2NABM | 0.10 | 14.8 | 7.4 | 7.2 | 20.8 | | | | 96.58 | 0.0033 | 0.0027 | 90.51 | 0.0020 | 0.0023 | 34.25 | 15.56 |
| SF1ABM | 0.09 | 17.0 | 6.0 | 7.2 | 22.0 | | | | 125.66 | 0.0084 | 0.0017 | 116.84 | 0.0025 | 0.0058 | 53.91 | 9.52 |
| SF2ABM | 0.11 | 13.6 | 12.9 | 7.6 | 20.9 | | | | 140.42 | 0.0056 | 0.0024 | 134.17 | 0.0021 | 0.0080 | 67.12 | 9.43 |
| PPF2ABM | 0.13 | 10.0 | 10.8 | 6.6 | | | 29.3 | | 123.85 | 0.0174 | 0.0 | 113.34 | 0.0024 | 0.0090 | 93.82 | 15.74 |
| HF2ABM | 0.12 | 11.6 | 9.9 | 6.2 | | | | 24.8 | 122.04 | 0.0078 | 0.0040 | 119.03 | 0.0033 | 0.0054 | 93.70 | 12.27 |

* values at the maximum forward load

** values at the maximum backward load

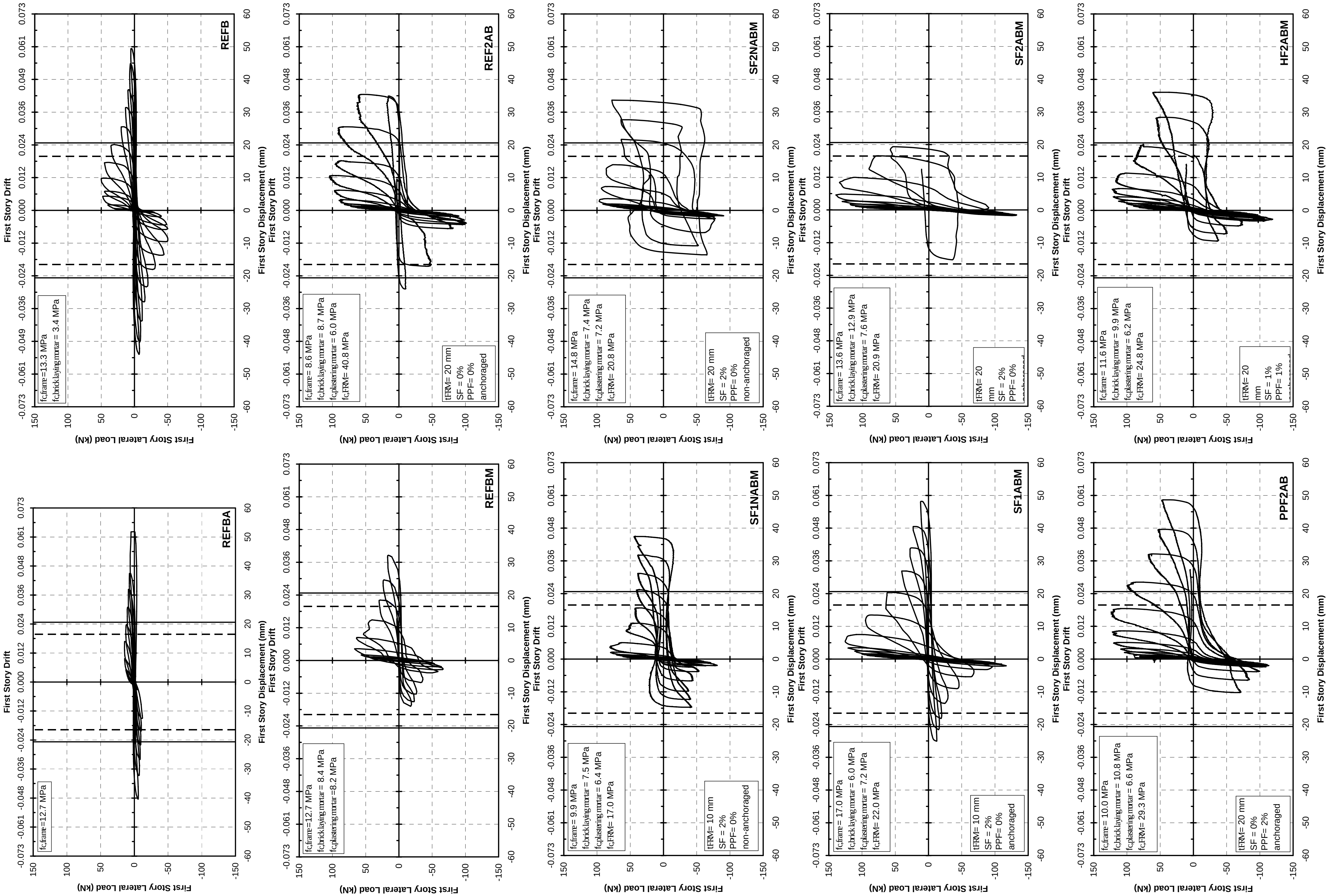
REFB
REFBA
REF2AB
REFBM
SF2NABM
SF1NABM
SF2ABM
SF1ABM
HF2ABM
PPF2AB
First Story Drift
First Story Displacement (mm)
First Story Lateral Load (kN)

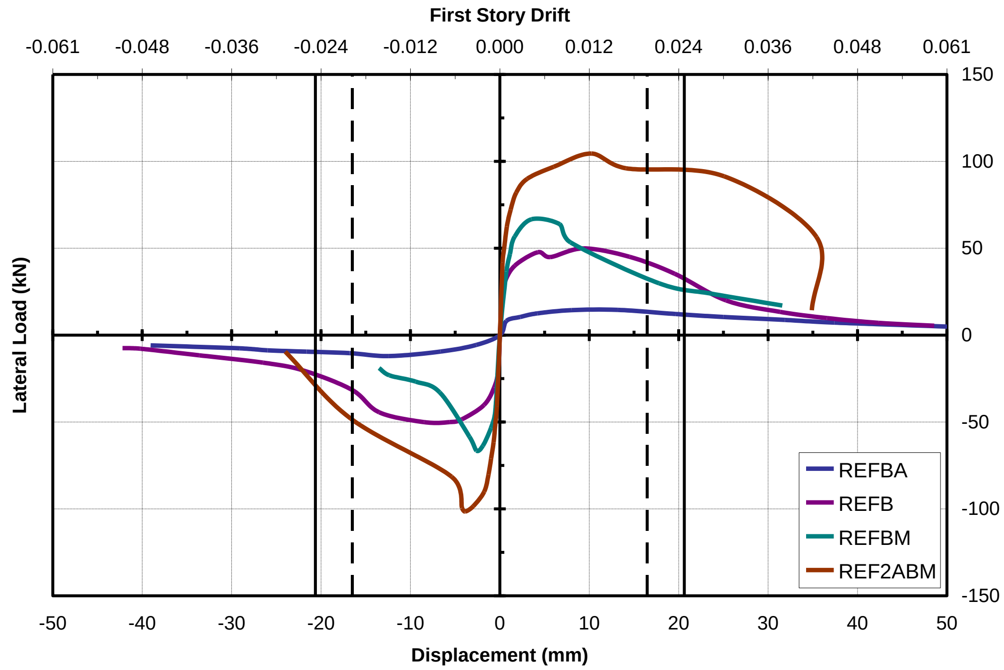


**Figure 5.2** First Story Envelope Graph of Reference Specimens

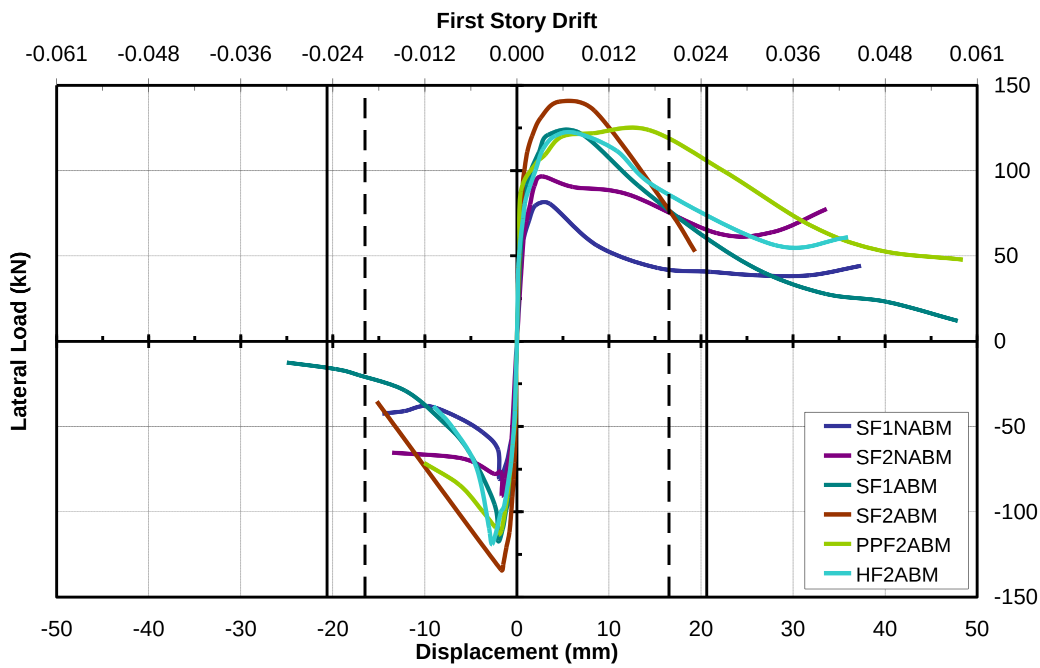


**Figure 5.3** First Story Envelope Graph of Strengthened Specimens

## 5.3 STRENGTH

In seismic strengthening, providing adequate lateral strength is very important. Strength is one of the most important parameters to be considered in order that a strengthening method is said to be effective. To evaluate the strength characteristics of the frame specimens, the lateral load carrying capacities of the specimens were investigated. Comparison of the lateral load carrying capacities of the specimens are shown in **Table 5.2**.

**Table 5.2** Comparison of the Lateral Load Carrying Capacities of the Specimens

| **Specimen** | **Maximum Forward Load (kN)** | **Ratio of Max. Forward Load to That of Reference Specimen** | **Maximum Backward Load (kN)** | **Ratio of Max. Backward Load to That of Reference Specimen** |
|---|---|---|---|---|
| REFBA | 14.53 | *0.22* | 12.03 | *0.18* |
| REFB | 50.23 | *0.75* | 50.29 | *0.76* |
| **REFBM** | **66.59** | ***1.00*** | **66.59** | ***1.00*** |
| REF2ABM | 104.52 | *1.57* | 101.52 | *1.53* |
| SF1NABM | 80.56 | *1.21* | 80.69 | *1.21* |
| SF2NABM | 96.58 | *1.45* | 90.51 | *1.36* |
| SF1ABM | 125.66 | *1.89* | 116.84 | *1.76* |
| SF2ABM | 140.42 | *2.11* | 134.17 | *2.02* |
| PPF2ABM | 123.85 | *1.86* | 113.34 | *1.70* |
| HF2ABM | 122.04 | *1.83* | 119.03 | *1.79* |

After evaluating the load-displacement graphs of the specimens, it can be said that there was a significant increase in the lateral load carrying capacities of the specimens after the strengthening operations were done. The increase in the load carrying capacities of the frame specimens can be seen from **Table 5.2**. When the load-first story displacement graphs drawn to a common scale in **Figure 5.1** are examined, it can be said that after performing the strengthening operations by the application of the mortar with 2% volumetric ratio of steel fibers and/or PP fibers for strengthening purpose the behaviors and the capacities of the frame specimens were improved greatly.

There was significant increase in the energy dissipation capacities of the strengthened specimens as compared to reference specimens. The width of the loops is a sign of the improvement in the energy dissipation capacity. In **Figure 5.1** it can be observed that strengthened specimens have wider loops. Moreover, from the lateral rigidity point of view, when the strengthened specimens are compared with the reference specimens it is observed that the lateral rigidities of the strengthened specimens were improved. The lateral load carrying capacities of the strengthened specimens were much more and their displacements were smaller than the reference specimens.

***<u>Shear Deformation</u>:*** Lateral load-first story shear displacement graphs of the frame specimens are given in **Figure 5.4**. The strengthening method which is applied by the usage of the steel and/or PP fibers also improved the shear behavior of the strengthened specimens. In the shear deformation graphs of the reference specimens there was an apparent shear deformation. After the application of the fiber reinforced mortar on the frames for strengthening purpose, the shear deformation reduced not in all of the strengthened specimens but most of them. Mainly the reduction in shear deformations was evident in the steel fiber reinforced mortar applied frames. In the PP or hybrid fiber reinforced mortar applied frames no reduction in shear deformations was observed.

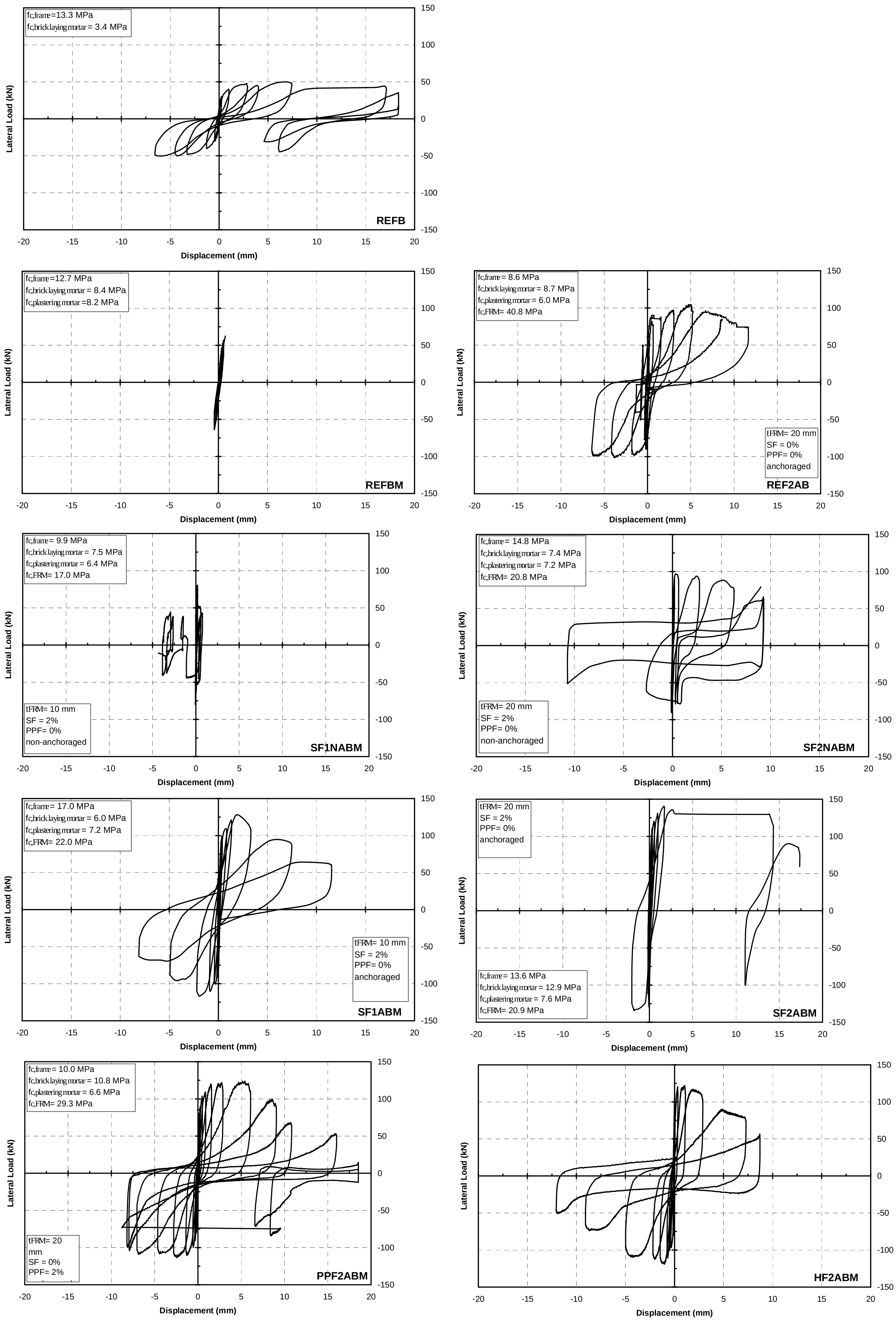


**Figure 5.4** Load-First Story Shear Displacement Graphs of the Specimens

The proposed strengthening method was observed to be effective in that the strengthened frame specimens behaved as monolithic cantilevers rather than a frame. The frame behavior was seen in the reference specimens. In these specimens the frame lost its lateral rigidity after the separation of the infill wall from the frame. But, the non-anchored strengthened specimens did not behave as monolithic cantilevers, they showed classical frame behavior.

## 5.4 STIFFNESS

Stiffness of a structure can be defined as its resistance against imposed displacements. When the stiffness of a structure is high, the deformation that it will experience is small. Lack of sufficient lateral stiffness is an important cause of the failure of structures. Stiffness can be calculated as the slopes of the load-deformation curves obtained from the frame tests as shown in **Figure 5.5**.

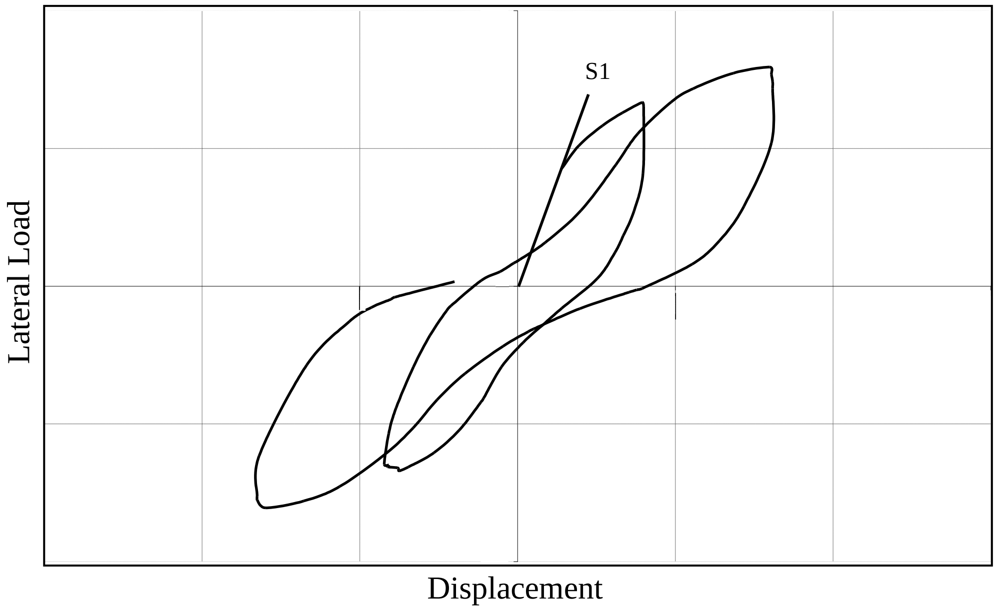


**Figure 5.5** Representative Cycle Slopes

The initial stiffness of the specimen was calculated as the initial slope of the load-deformation curve in the first forward half cycle and it was used for comparing the behavior of the test specimens. The initial stiffnesses of the specimens are presented in **Table 5.3**.

**Table 5.3** Initial Stiffnesses of the Specimens

| **Specimen** | **Initial Stiffness (kN/mm)** | **Ratio of Initial Stiffness to That of Reference Specimen** |
|---|---|---|
| REFBA | 1.74 | *0.08* |
| REFB | 24.44 | *1.14* |
| **REFBM** | **21.39** | ***1.00*** |
| REF2ABM | 61.08 | *2.86* |
| SF1NABM | 101.31 | *4.74* |
| SF2NABM | 34.25 | *1.60* |
| SF1ABM | 53.91 | *2.52* |
| SF2ABM | 67.12 | *3.14* |
| PPF2ABM | 93.82 | *4.39* |
| HF2ABM | 93.70 | *4.38* |

As a consequence of the damage in the infilled frame and the deterioration of the panel-frame interfaces, the stiffness significantly decreases when the lateral displacement increases.

As it can be observed from **Table 5.3**, the ratio of the initial stiffness of the strengthened specimens to that of the reference specimen varied in between 1.60 and 4.74. The ratio for SF2NABM is low, i.e. 1.60. But, when the ratio of the

SF1NABM is considered, a significant increase is observed, the ratio is 4.74 times that of the reference specimen. This difference cannot be explained on theoretical basis. Therefore, the difference attributed to workmanship and possible testing variations. The huge difference of initial stiffness between bare frame and infilled frames demonstrates again the importance of computer modeling of structures. Without nonstructural infills, surely the natural period could not be calculated accurately.

The effectiveness of the strengthening process can be seen evidently in **Table 5.3**. Addition of strengthening mortar increased initial stiffness and consequently decreased lateral displacements and drifts.

Another method used to obtain stiffness degradation curves of the specimens given in **Figures 5.7** and **5.8** is calculating peak-to-peak stiffnesses. The peak-to-peak stiffness of a specimen is calculated as the average slope of the load-deformation curve in the cycles. Stiffness can be calculated by the peak-to-peak method as shown in **Figure 5.6**.

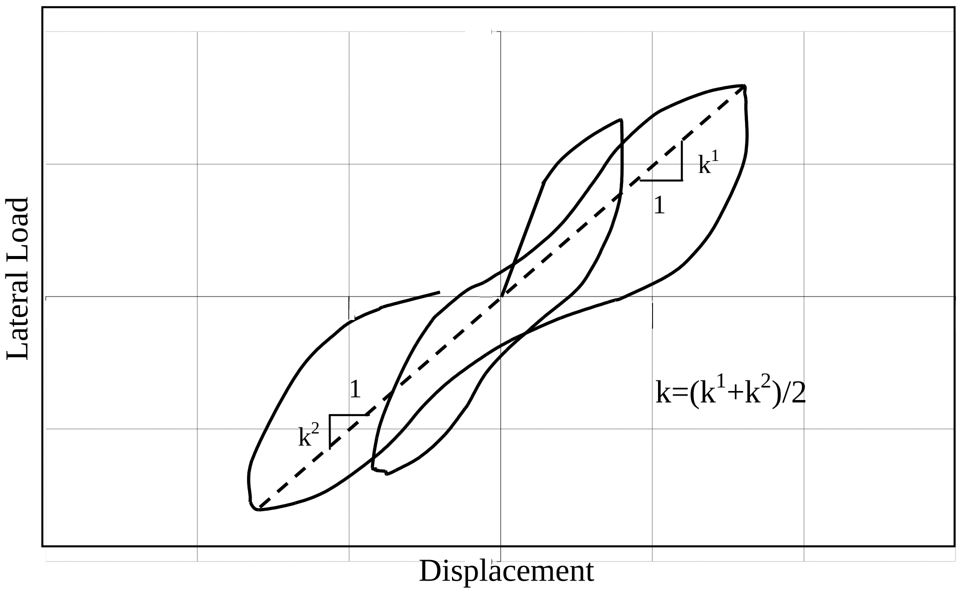


**Figure 5.6** Definition of Peak-to-Peak Stiffness

Stiffness degradation curves for the reference and strengthened specimens are shown in **Figures 5.7** and **5.8**, respectively.

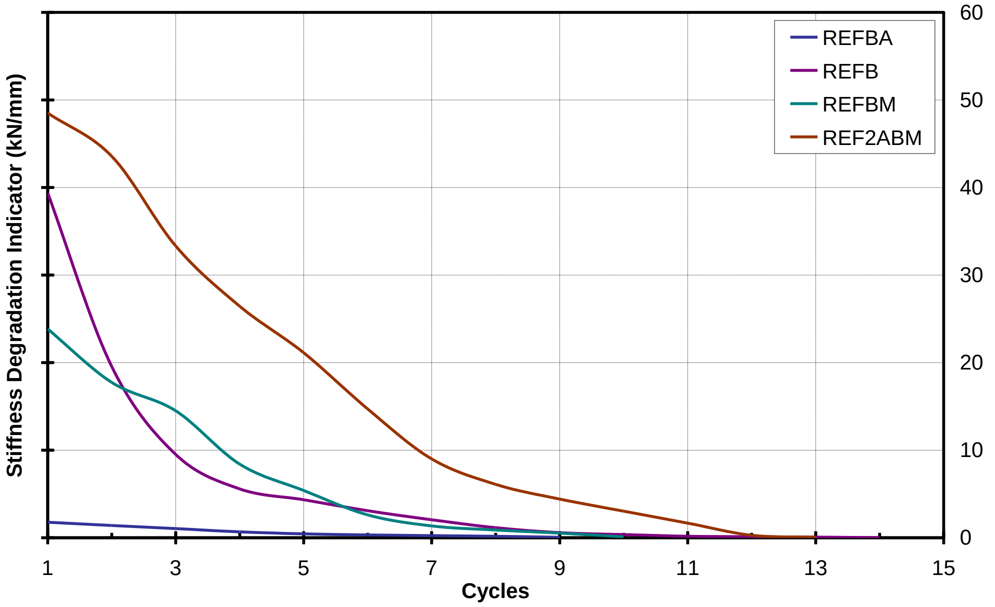


**Figure 5.7** Stiffness Degradation Curves for Reference Specimens

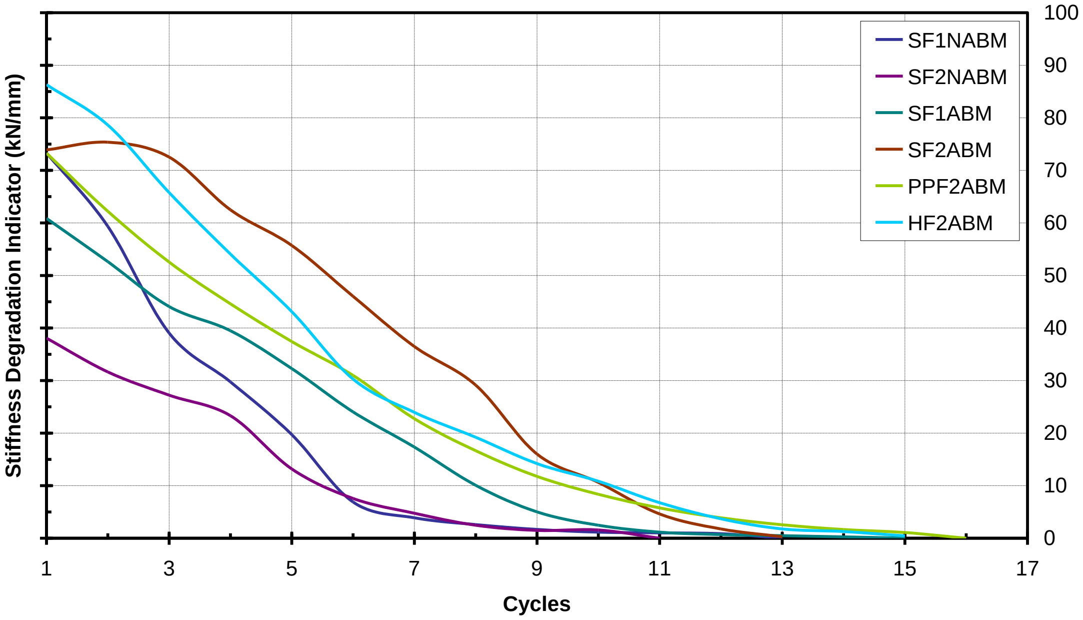


**Figure 5.8** Stiffness Degradation Curves for Strengthened Specimens

## 5.5 ENERGY DISSIPATION

When a structural system deforms, the work done is stored as strain energy. Part of this energy is released in the unloading process, whereas the remaining energy is dissipated through different mechanisms.

Energy dissipation capacity is an important indicator of the structure's ability to withstand severe ground motions. It can be determined from the area enclosed by the hysteretic loops of the load deformation relationship. First, the area under each half cycle was calculated. Then, the values of each forward and backward cycle were added to determine the dissipated energy of the full cycle. Cumulative dissipated energy of a specimen was calculated by the addition of dissipated energies in all of the cycles.

The energy dissipation characteristics of the specimens strongly depend on the loading history. It is better to compare the energy dissipation characteristics of specimens with the same loading history. The loading histories were aimed to be same, but when the response became non-linear, the loadings were controlled by the second story displacements. The same displacements were obtained for the forward and backward half cycles.

The cumulative energy dissipation curves of the specimens are presented in **Figure 5.9**.

The cumulative dissipated energy values of the specimens are given in **Table 5.4**. When the values in the table are examined, it can be said that the ratio of the cumulative dissipated energy of the strengthened specimens to that of the reference specimen varied in between 1.87 and 3.51. This indicates that the strengthening method used improves the energy dissipation characteristics of the specimens.

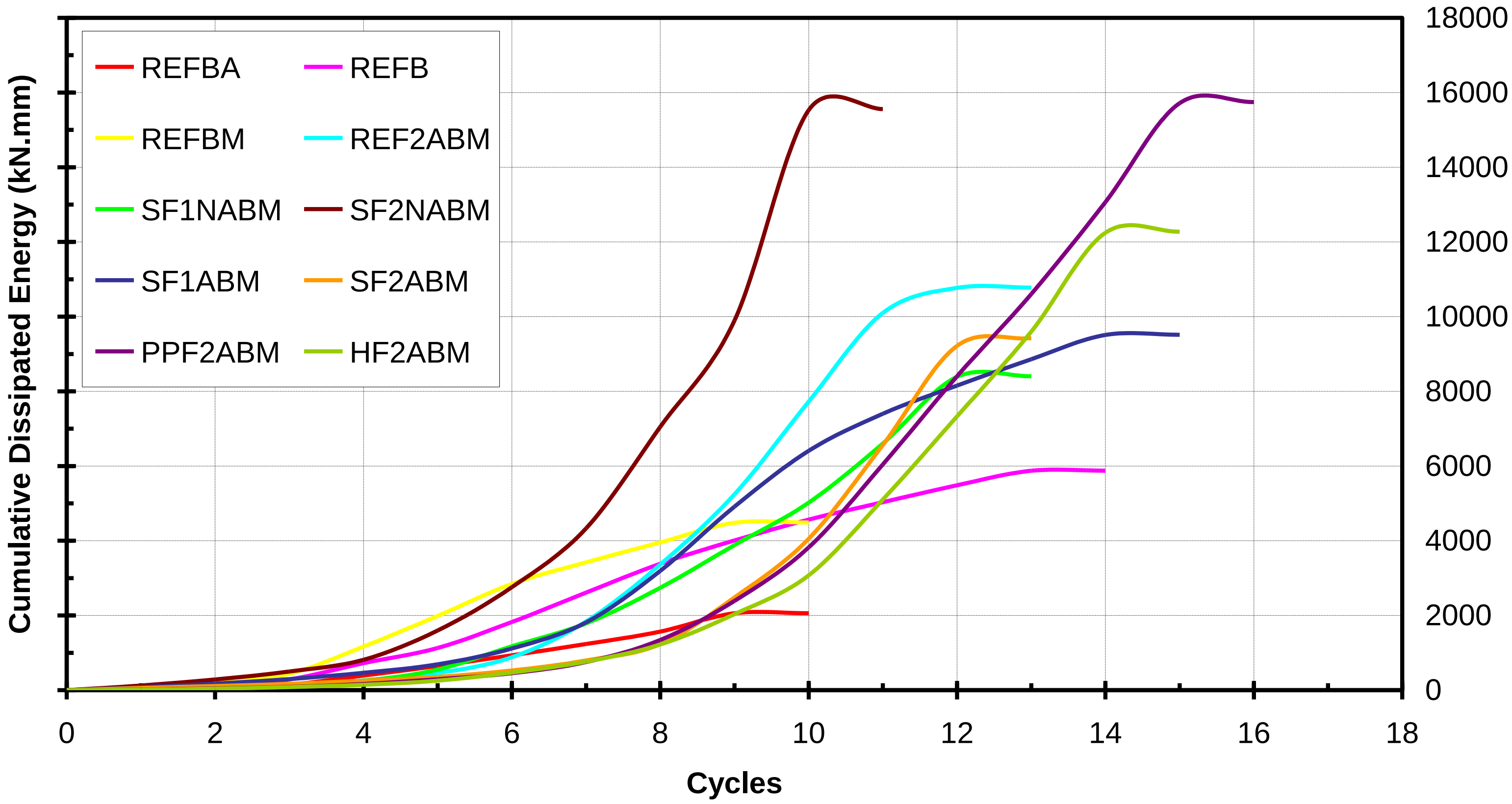


**Figure 5.9** Cumulative Energy Dissipation Curves of the Specimens

It should be noted that the main purpose of the strengthening technique was not to convert nonstructural brick walls in to high ductile shear walls which can absorb high energy during an earthquake. It is also impossible to behave the strengthened walls as shear walls. Because they do not have end confined columns. The original columns represent typical columns with common deficiencies. The main objective was keeping the brick walls in place, increasing the lateral load capacity and decreasing the lateral displacements.

**Table 5.4** Cumulative Dissipated Energy Values of the Specimens

| **Specimen** | **Cumulative Dissipated Energy (Joule)** | **Ratio of Cumulative Dissipated Energy to That of Reference Specimen** |
|---|---|---|
| REFBA | 2,059 | *0.46* |
| REFB | 5,875 | *1.31* |
| **REFBM** | **4,486** | ***1.00*** |
| REF2ABM | 10,780 | *2.40* |
| SF1NABM | 8,401 | *1.87* |
| SF2NABM | 15,558 | *3.47* |
| SF1ABM | 9,516 | *2.12* |
| SF2ABM | 9,426 | *2.10* |
| PPF2ABM | 15,744 | *3.51* |
| HF2ABM | 12,273 | *2.74* |

## 5.6 STORY DRIFT INDEX

Story drift index can be defined as the relative displacement between two successive floors divided by the story height. It is a term frequently used  in earthquake engineering. Maximum inter-story drift is a reliable damage parameter which can be used to judge the performance of strengthened structures.

In order to prevent structural and non-structural damage story drift index is generally not allowed to exceed a certain limit. According to the Turkish Seismic Code [40], the maximum story drift index is limited to 0.0035 and 0.02/R based on the elastic analysis of the structure. R is defined as the behavior factor.  For frames with normal ductility level, R=4.0. Also, according to UBC, the maximum story drift index for inelastic analysis is limited to 0.025 for the structures with a fundamental period less than 0.7 seconds and 0.020 for the structures with a fundamental period greater than 0.7 seconds [41]. When the numbers are compared, it can be said that the Turkish Seismic Code is more conservative about the story drift index.

According to **Figure 5.1**, it can be concluded that the maximum interstory drift should be limited to 1% according to forward cycles and anchored specimens. Backward cycles were not considered as explained in Section 5.1.

Load-first story displacement/drift graphs drawn to a common scale were shown in **Figure 5.1**. According to the figure, it can be said that strengthening the frames resulted in a reduced inter-story drift. This can be attributed to the fact that the strengthening operation increased the stiffness of the structure.

It is not simple to conclude about effectiveness of strengthening techniques just comparing story drift ratios. Addition of strengthening wall definitely decreased story drift ratios. At the same time stiffness and lateral load carrying capacities increased. Therefore, under the same earthquake excitation, the structure would most probably not require the same ductility. However, it should be noted that due to the increase in stiffness and decrease in building natural period, design acceleration spectrum will also increase which may end up with an increase in seismic load.

## 5.7 DUCTILITY

Displacement ductility is defined by the ratio of the ultimate displacement to yield displacement. The ultimate displacement is defined as the displacement at which the lateral load dropped to 85% of the maximum applied load. The yield displacement was described with a secant drawn between origin and 70% of the maximum applied load. This line was extended up to the horizontal line drawn from the maximum load [42]. The definition of ductility is given in **Figure 5.10**. The calculated ductility values are listed in **Table 5.5**.

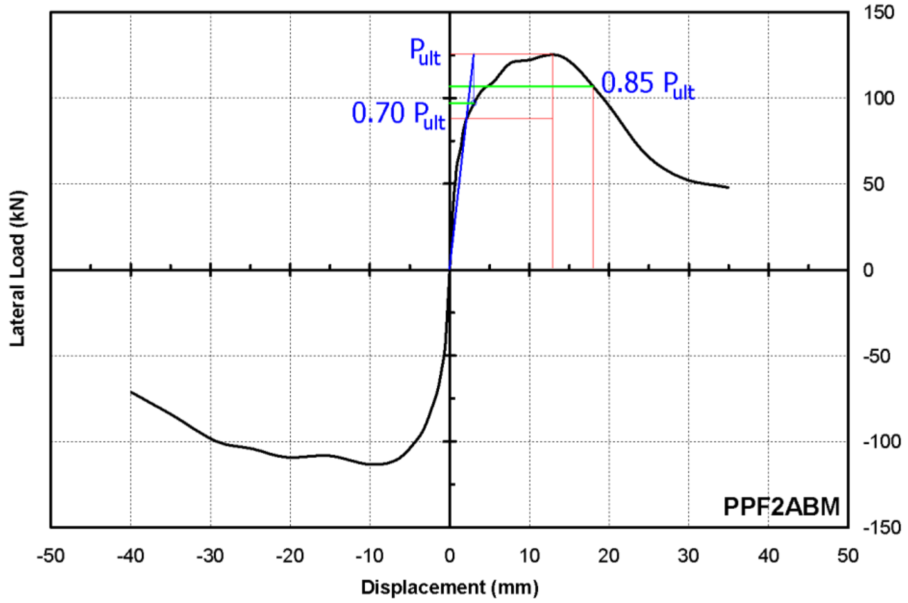


**Figure 5.10** Displacement Ductility Definition

**Table 5.5** shows that the maximum ductility was achieved by REF2ABM. This specimen, however, suffered greatly during the test. The beam-column joints of the first story had shear cracks, concrete at this region crushed and reinforcement buckled. Moreover, the strengthened brick infill separated excessively from the surrounding frame. Strengthened specimens show almost similar displacement ductility values close to approximately five.

**Table 5.5** was calculated considering forward cycles only as shown in **Figure 5.10**. The reason is that in the first story interstory displacement, the drifts in backwards directions are extremely small which was attributed to a drawback in the test setup already mentioned in Section 5.1. Moreover, the evaluation of ductility should be carefully handled. Because, strengthened brick infill walls have limited displacement ability. Therefore, it is believed that instead of ductility evaluation, drift examination is much worthy.

**Table 5.5** Displacement Ductility

| Specimen | Displacement Ductility | Ratio to REFBM |
|---|---|---|
| REFBA | 4.74 | 1.68 |
| REFB | 5.88 | 2.09 |
| REFBM | 2.82 | 1.00 |
| REF2ABM | 7.70 | 2.73 |
| SF1NABM | 4.07 | 1.44 |
| SF2NABM | 4.89 | 1.73 |
| SF1ABM | 4.09 | 1.45 |
| SF2ABM | 5.64 | 2.00 |
| PPF2ABM | 5.94 | 2.11 |
| HF2ABM | 5.16 | 1.83 |

## 5.8 EFFECT OF TEST VARIABLES

***Effect of Anchorage:*** In order to evaluate the effect of anchorages between the frame and infill; specimen SF1NABM is compared with its companion specimen SF1ABM. Similarly, SF2NABM is compared with SF2ABM. Comparisons have shown that, lateral load capacities increases 45% and 49% for 10 mm and

20 mm thick plaster specimens, respectively. It can be concluded that, using anchorages increases lateral load carrying capacity approximately %45.

***Effect of Thickness:*** The effect of the thickness of the strengthening mortar can be observed comparing either SF1NABM with SF2NABM or SF1ABM with SF2ABM. The lateral load carrying capacities increased approximately 12% and 15% in either cases respectively. Doubling the strengthening mortar thickness increases lateral strength approximately 12% only.

***Effect of Steel Fibers in Strengthening Mortar:*** This effect can be studied via the comparison of REF2ABM and SF2ABM. It should be paid attention, however, to the difference in mortar strengths. Specimen without steel fiber in mortar (REF2ABM) had a mortar strength of 40.8 MPa whereas the companion specimen with 2% steel fiber 20.9 MPa only. Despite the disadvantage in mortar strength of the specimen SF2ABM, lateral strength was 34% higher than the REF2ABM.

## 5.9 SUMMARY

After all of the evaluations of the test results made, the proposed method of strengthening the infill panels of the R/C frames by the application of steel and/or PP fiber reinforced mortar is seen to improve the seismic behavior of the frame specimens. The behavior improvement in the strengthened specimens is presented in **Table 5.6**.

As can be observed from **Table 5.6**, lateral load carrying capacity increased two fold for Specimen SF2ABM. For this specimen lateral rigidity improved two fold and cumulative energy dissipation doubled as compared to REFBM. In view of the former Chapter and evaluation of the test results, it can be concluded that strengthening nonstructural infill walls by means of steel fiber high strength mortar may offer a way of upgrading buildings. Anchorages ensure proper load transfer between wall and frame, and prevent damage concentration by spreading the damage. Hybrid fiber mortar (HF2ABM) also put on similar strengthening results to that of steel fiber mortar (SF2ABM).

**Table 5.6** Behavior Improvement in the Strengthened Specimens

| | **Specimen** | **Ratio to that of REFBM** |
|---|---|---|
| **Lateral Load Carrying Capacity** | SF1NABM | 1.21 |
| | SF2NABM | 1.36 |
| | SF1ABM | 1.76 |
| | SF2ABM | 2.02 |
| | PPF2ABM | 1.70 |
| | HF2ABM | 1.79 |
| **Lateral Rigidity** | SF1NABM | 4.74 |
| | SF2NABM | 1.60 |
| | SF1ABM | 2.52 |
| | SF2ABM | 3.14 |
| | PPF2ABM | 4.39 |
| | HF2ABM | 4.38 |
| **Cumulative Energy Dissipation** | SF1NABM | 1.87 |
| | SF2NABM | 3.47 |
| | SF1ABM | 2.12 |
| | SF2ABM | 2.10 |
| | PPF2ABM | 3.51 |
| | HF2ABM | 2.74 |
| **Ductility** | SF1NABM | 1.44 |
| | SF2NABM | 1.73 |
| | SF1ABM | 1.45 |
| | SF2ABM | 2.00 |
| | PPF2ABM | 2.11 |
| | HF2ABM | 1.83 |

## 5.10 COMPARISON WITH OTHER STRENGTHENING TECHNIQUES

There have been many attempts in the Structural Mechanics Laboratory of the Middle East Technical University to invent occupant friendly, effective and yet economical strengthening techniques. With this motivation, the nonstructural brick walls have been strengthening by many methods to move the task to structural member. The proposed techniques are applying diagonal FRP, precast concrete panels, and wire mesh reinforced mortar on the brick walls. In order to observe the effectiveness of the proposed strengthening techniques better, the results of the tests conducted on the proposed strengthening techniques will be compared. To condense the comparison, only the applied load vs. top drift curves will be compared and only one recommended, comprehensible curve will be chosen. All the tests were conducted on the same scale and even dimensions with one bay and two stories. The dimension and reinforcement detail are the same for all. In **Table 5.7**, properties of the materials used in the proposed strengthening techniques are given.

In the first strengthening technique, 25 mm, 4.6 MPa mortar together with one layer of welded wire mesh reinforcement was applied on the single wall surface (specimen MRIF#2) [43]. The frame concrete compressive strength was 16.9 MPa, and yield strength of longitudinal bars was 340 MPa. Dowel anchorages were used on the surrounding frame. The bed mortar and plaster strength was 5.6 MPa. 60 kN axial force (19% of $N_0$) was applied on each columns.

In the second strengthening technique, 200 mm wide, one layer FRP sheets were applied on both faces of the wall in diagonal direction (cross bracing) (specimen SP-5) [44]. The frame concrete compressive strength and longitudinal reinforcement yield strengths were 12 MPa and 388 MPa, respectively. The mortar and plaster strength was 4.2 MPa. FRP sheets were attached to the surrounding frame by specially produces FRP anchorages and stick with epoxy on the wall surface. The tensile strength of FRP was 3430 MPa. The applied axial load on each column was 60 kN (23.5% of $N_0$).

The third strengthening technique is application of high strength precast concrete panels on the wall by means of epoxy-based resin [45]. In this technique, 20 mm thick precast rectangular panels with 45.6 MPa compressive strength was utilized (specimen CIC4). Only in the first story anchorages were used on the surrounding frame. The frame concrete compressive strength and longitudinal reinforcement yield strength were 19.4 MPa and 330 MPa, respectively. The mortar and plaster strength of the wall was 3.3 MPa. Axial load applied on the columns was 60 kN (17% of $N_0$).

For the proposed model with steel fibers, specimen with 20 mm thick mortar and 2% of steel fiber ratio was selected (SF2ABM). The strengthening mortar was anchoraged to the frame with dowels. The original plaster thickness was 6 mm. The bed mortar, plaster, and strengthening mortar strength were 12.9 MPa, 7.6 MPa, and 20.9 MPa, respectively. Frame concrete compressive strength was 13.6 MPa, and yield strength of longitudinal bars was 365 MPa. Axial load applied on the columns was 53.38 kN (19.4% of $N_0$).

The applied lateral load (Base Shear) vs. top drift ratio curves are given in **Figure 5.11**. The reason of the higher capacity of the specimen strengthened with precast concrete panels was mainly due to high frame concrete strength and very high panel strength. Specimen strengthened with FRP showed the least initial stiffness. All strengthening techniques ended up with similar lateral load carrying capacities and top drift ratios. Consequently, the proposed technique in this study along with the other techniques can be used with the same reliability and effectiveness level.

**Table 5.7** Properties of Materials Used in the Strengthening Techniques

| | Frame Concrete Strength (MPa) | Rebar Yield Strength (MPa) | Plaster Strength (MPa) | Strengthening Mortar Strength (MPa) |
|---|---|---|---|---|
| **Mesh** | 16.9 | 340 | 5.6 | 4.6 |
| **FRP** | 12.0 | 388 | 4.2 | 3430 * |
| **Panel** | 19.4 | 330 | 3.3 | 45.6 |
| **Steel Fiber** | 13.6 | 365 | 7.6 | 20.9 |

* Carbon fiber strength

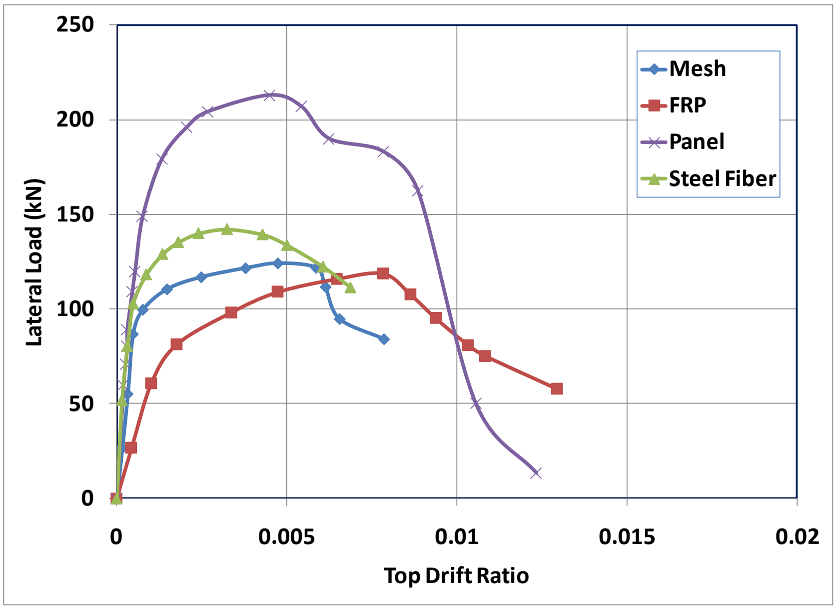


**Figure 5.11** Comparison of Different Strengthening Techniques

# CHAPTER 6

# PANEL TESTS

## 6.1 GENERAL

Before the frame tests, two series of panel tests were conducted to obtain information about the behavior of the strengthened masonry walls. The information gathered in panel tests were used to model the frame tests in analytical evaluation. In these tests, square masonry walls having dimensions of $700 \times 700$ mm and width of 69 mm were loaded in diagonal direction.

Test set-up was prepared between two heavy concrete support blocks. Test specimen was placed on thin metal plates parallel to floor. Steel plate was oiled and sat on ball roller supports to ensure friction free movement of panel specimens. Steel heads were placed to corners of the wall specimen in the diagonal direction and were attached with gypsum. Dial gages were placed in six directions to measure displacements on the wall. Test set-up is illustrated in **Figures 6.1** and **6.2**.

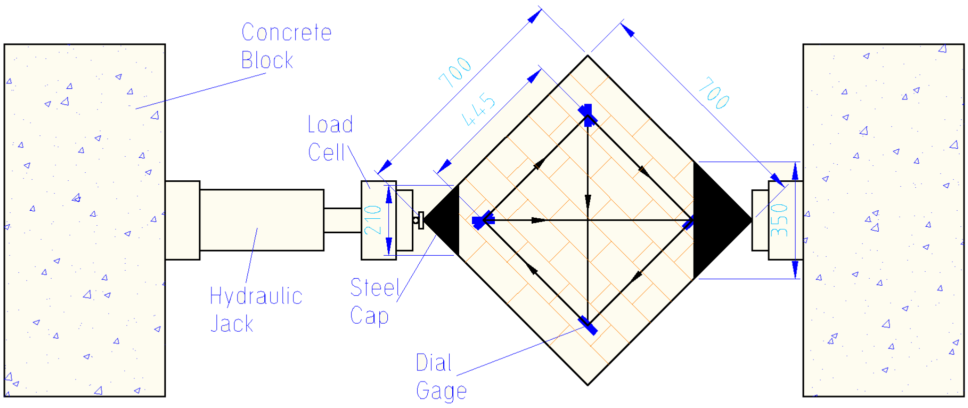


**Figure 6.1** Test Set-up of Panel Tests

**Figure 6.2** General View of Panel Tests

## 6.2 PANEL TESTS

### 6.2.1 First Series Panel Tests

In the scope of the first series, 12 tests were conducted. First, 6 reference wall specimens, composed of 3 non-plastered and 3 plastered, were tested. Then, 6 plastered wall specimens strengthened in different ways were tested. Plastered wall specimens were produced of 10 mm plaster thickness on both sides. 10 mm thickness of mortar with 2% volumetric ratio of steel fibers was applied on one side of 3 specimens. To the remaining 3 specimens, 20 mm thickness of mortar with 2% volumetric ratio of steel fibers was applied again on one side. Specimen properties are given in **Table 6.1**.

Mix proportions of the mortar used for the first series brick laying are presented in **Table 6.2** and mix proportions of the mortar used for plastering are given in **Table 6.3**. Mix proportions for 1 $m^3$ of the mortar with steel fibers applied on the plaster of the first series panel specimens are shown in **Table 6.4**.

**Table 6.1** Properties of the First Series Panel Specimens

| Test Specimen | Plaster (mm) | Steel Fiber (%) | Thickness of SFRM (mm) | # of SFRM Applied Sides |
|---|---|---|---|---|
| NPP-1 | - | - | - | - |
| NPP-2 | - | - | - | - |
| NPP-3 | - | - | - | - |
| PP-1 | 10 | - | - | - |
| PP-2 | 10 | - | - | - |
| PP-3 | 10 | - | - | - |
| SF1P-1 | 10 | 2 | 10 | 1 |
| SF1P-2 | 10 | 2 | 10 | 1 |
| SF1P-3 | 10 | 2 | 10 | 1 |
| SF2P-1 | 10 | 2 | 20 | 1 |
| SF2P-2 | 10 | 2 | 20 | 1 |
| SF2P-3 | 10 | 2 | 20 | 1 |

**Table 6.2** Mix Proportion of the First Series Brick Laying Mortar

| | Weight (kN) | Ratio by Weight (%) |
|---|---|---|
| Cement (CEM I 32.5 R) | 0.34 | 9 |
| 0-3 mm Aggregate | 2.94 | 76 |
| Lime | 0.20 | 5 |
| Water | 0.38 | 10 |
| Total | 3.86 | 100 |
| Strength at test day (MPa) | **3.5** | |

**Table 6.3** Mix Proportion of the First Series Plastering Mortar

| | Weight (kN) | Ratio by Weight (%) |
|---|---|---|
| Cement (CEM I 32.5 R) | 0.29 | 8 |
| 0-3 mm Aggregate | 2.45 | 71 |
| Lime | 0.25 | 7 |
| Water | 0.48 | 14 |
| Total | 3.47 | 100 |

**Table 6.4** Mix Proportion of the First Series Mortar with Steel Fiber

| | **Weight (kN)** | **Ratio by Weight (%)** |
|---|---|---|
| Cement (CEM I 42.5 R) | 5.68 | 21.79 |
| 0-3 mm Aggregate | 15.61 | 59.88 |
| Water | 3.24 | 12.43 |
| Plasticizer | 0.009 | 0.04 |
| Steel Fiber | 1.53 | 5.87 |
| Total | 26.07 | 100.0 |
| Strength at test day (MPa) | **21.2** | |

Load carrying capacities of the wall specimens are shown in **Table 6.5**. General view of first series panel specimens is shown in **Figure 6.3**.

**Table 6.5** Load Carrying Capacities of the First Series Panel Specimens

| **Panel** | **Brick Laying Mortar Strength (MPa)** | **Steel Fiber Reinforced Mortar (SFRM) Strength (MPa)** | **Load Carrying Capacity (kN)** | **Average Load Carrying Capacity (kN)** |
|---|---|---|---|---|
| NPP-1 | 3.5 | - | * | 10.30 |
| NPP-2 | 3.5 | - | 9.35 | |
| NPP-3 | 3.5 | - | 11.24 | |
| PP-1 | 3.5 | - | 29.55 | 31.83 |
| PP-2 | 3.5 | - | 40.72 | |
| PP-3 | 3.5 | - | 25.23 | |
| SF1P-1 | 3.5 | 21.2 | 69.92 | 68.69 |
| SF1P-2 | 3.5 | 21.2 | 68.67 | |
| SF1P-3 | 3.5 | 21.2 | 67.49 | |
| SF2P-1 | 3.5 | 21.2 | 110.20 | 103.04 |
| SF2P-2 | 3.5 | 21.2 | 95.62 | |
| SF2P-3 | 3.5 | 21.2 | 103.30 | |

* reliable data could not be taken due to improper set-up.

**Figure 6.3** General View of First Series Panel Specimens

### 6.2.2 Second Series Panel Tests

For the second series, 20 panel specimens were produced. 8 reference wall specimens (5 non-plastered and 3 plastered) and 12 strengthened plastered wall specimens were tested. The main difference of this second series was plaster thickness of the specimens, which was 6 mm on both sides. For 3 specimens, 10 mm thick mortar with 2% volumetric ratio of steel fibers was used on one side. To the other 3 specimens, 20 mm thickness of mortar with 2% volumetric ratio of steel fibers was applied on one side. To remaining 3 specimens, 10 mm thick mortar with 2% volumetric ratio of steel fibers was applied on both sides. To last 3 specimens, 20 mm thick mortar with 2% volumetric ratio of steel fibers was applied on both sides. Specimen properties are given in **Table 6.6**.

**Table 6.6** Properties and Titles of the Second Series Panel Specimens

| Test Specimen | Plaster (mm) | Steel Fiber (%) | Thickness of SFRM (mm) | # of SFRM Applied Sides |
|---|---|---|---|---|
| 2SNPP-1 | - | - | - | - |
| 2SNPP-2 | - | - | - | - |
| 2SNPP-3 | - | - | - | - |
| 2SNPP-4 | - | - | - | - |
| 2SNPP-5 | - | - | - | - |
| 2SPP-1 | 6 | - | - | - |
| 2SPP-2 | 6 | - | - | - |
| 2SPP-3 | 6 | - | - | - |
| 2SSF1P-1 | 6 | 2 | 10 | 1 |
| 2SSF1P-2 | 6 | 2 | 10 | 1 |
| 2SSF1P-3 | 6 | 2 | 10 | 1 |
| 2SSF2P-1 | 6 | 2 | 20 | 1 |
| 2SSF2P-2 | 6 | 2 | 20 | 1 |
| 2SSF2P-3 | 6 | 2 | 20 | 1 |
| 2SSF1PD-1 | 6 | 2 | 10 | 2 |
| 2SSF1PD-2 | 6 | 2 | 10 | 2 |
| 2SSF1PD-3 | 6 | 2 | 10 | 2 |
| 2SSF2PD-1 | 6 | 2 | 20 | 2 |
| 2SSF2PD-2 | 6 | 2 | 20 | 2 |
| 2SSF2PD-3 | 6 | 2 | 20 | 2 |

In the second series, strain gages were applied on some specimens. Strain gages with grid lengths of 60, 80, and 120 mm were used in the tests. Strain gage details are given in **Table 6.7**. Mix proportions of the mortar used for the second series panel specimens' brick laying are presented in **Table 6.8** and mix proportions of the mortar used for plastering are given in **Table 6.9**. Mix proportion for 1 $m^3$ of the mortar with steel fibers applied on the plaster of the second series panel specimens are the same as first series' mix proportions. The compressive strength at test day was **29.2 MPa** in this series.

**Table 6.7** Strain Gage Applications of the Second Series Panel Specimens

| Test Specimen | Applied Strain Gage |
|---|---|
| 2SPP-1 | One, 60 mm length, in compression direction |
| 2SPP-2 | One, 80 mm length, in compression direction |
| 2SPP-3 | One, 120 mm length, in compression direction |
| 2SSF1P-1<br>2SSF1P-1(2) | Two, perpendicular, 60 mm length, in compression and tension directions |
| 2SSF1P-2 | Two, perpendicular, 80 mm length, in compression and tension directions |
| 2SSF1PD-2 | Two, perpendicular, 120 mm length, in compression and tension directions |
| 2SSF2PD-3 | Two, perpendicular, 60 mm length, in compression and tension directions |

**Table 6.8** Mix Proportion of the Second Series Brick Laying Mortar

| | **Weight (kN)** | **Ratio by Weight (%)** |
|---|---|---|
| Cement (CEM I 32.5 R) | 0.49 | 13 |
| 0-3 mm Aggregate | 2.45 | 67 |
| Lime | 0.25 | 7 |
| Water | 0.49 | 13 |
| Total | 3.68 | 100 |
| Strength at test day (MPa) | **10.0** | |

**Table 6.9** Mix Proportion of the Second Series Plastering Mortar

| | **Weight (kN)** | **Ratio by Weight (%)** |
|---|---|---|
| Cement (CEM I 32.5 R) | 0.25 | 9 |
| 0-3 mm Aggregate | 0.96 | 33 |
| Sieved 0-3 mm Aggregate | 0.96 | 33 |
| Lime | 0.25 | 9 |
| Water | 0.44 | 16 |
| Total | 2.86 | 100 |
| Strength at test day (MPa) | **4.0** | |

Load carrying capacities of the wall specimens after the second series panel tests are shown in **Table 6.10**. General view of second series panel specimens is shown in **Figure 6.4**.

**Table 6.10** Load Carrying Capacities of the Second Series Panel Specimens

| Panel | Brick Laying Mortar Strength (MPa) | Plastering Mortar Strength (MPa) | SFRM Strength (MPa) | Load Carrying Capacity (kN) | Average Load Carrying Capacity (kN) |
|---|---|---|---|---|---|
| 2SNPP-1 | 10.0 | - | - | 45.26 | 44.11 |
| 2SNPP-2 | 10.0 | - | - | 39.00 | |
| 2SNPP-3 | 10.0 | - | - | 49.04 | |
| 2SNPP-4 | 10.0 | - | - | 46.88 | |
| 2SNPP-5 | 10.0 | - | - | 40.37 | |
| 2SPP-1 | 10.0 | 4.0 | - | 54.34 | 57.64 |
| 2SPP-2 | 10.0 | 4.0 | - | 62.44 | |
| 2SPP-3 | 10.0 | 4.0 | - | 56.13 | |
| 2SSF1P-1, 2SSF1P-1(2) | 10.0 | 4.0 | 29.2 | 61.21 65.51 * | 85.33 |
| 2SSF1P-2 | 10.0 | 4.0 | 29.2 | 77.78 | |
| 2SSF1P-3 | 10.0 | 4.0 | 29.2 | 112.70 | |
| 2SSF2P-1 | 10.0 | 4.0 | 29.2 | 131.87 | 119.55 |
| 2SSF2P-2 | 10.0 | 4.0 | 29.2 | 107.23 | |
| 2SSF2P-3 | 10.0 | 4.0 | 29.2 | ** | |
| 2SSF1PD-1 | 10.0 | 4.0 | 29.2 | 103.89 | 132.06 |
| 2SSF1PD-2 | 10.0 | 4.0 | 29.2 | 163.98 | |
| 2SSF1PD-3 | 10.0 | 4.0 | 29.2 | 128.31 | |
| 2SSF2PD-1 | 10.0 | 4.0 | 29.2 | 101.86 | 128.53 |
| 2SSF2PD-2 | 10.0 | 4.0 | 29.2 | 123.18 | |
| 2SSF2PD-3 | 10.0 | 4.0 | 29.2 | 160.56 | |

* Test was repeated by placing the specimen in the set-up again because of a problem caused by the set-up during the test.

** Test could not be performed because specimen was broken during preparation to the test while placing in the set-up.

**Figure 6.4** General View of Second Series Panel Specimens

### 6.2.3 Test Results & Observed Behavior

Load vs. tensile/compressive displacement/strain graphs of first series and second series panel tests are presented in **Figures 6.5-6.22**. Views of first series panel specimens after the tests are shown in **Figures 6.23-6.33**. Views of second series panel specimens after the tests are illustrated in **Figures 6.34-6.52**. Summary about the observed damage of the first series and second series panel specimens after the tests are presented in **Tables 6.11** and **6.12**, respectively.

**1$^{st}$ Series:**

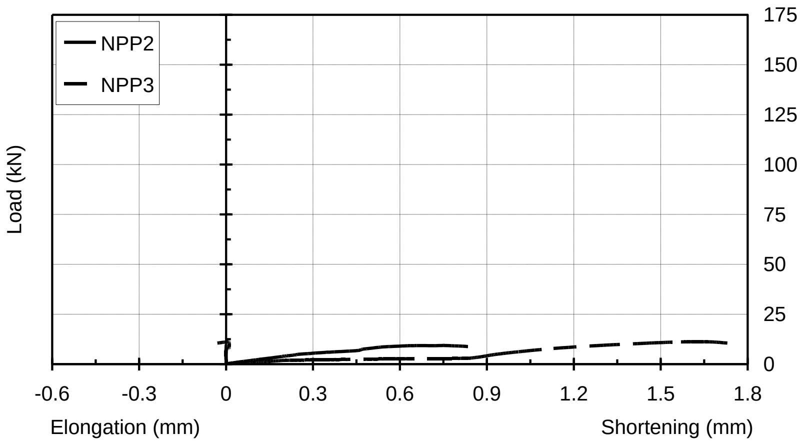


**Figure 6.5** Load vs. Elongation/Shortening Graph of NPP Specimens

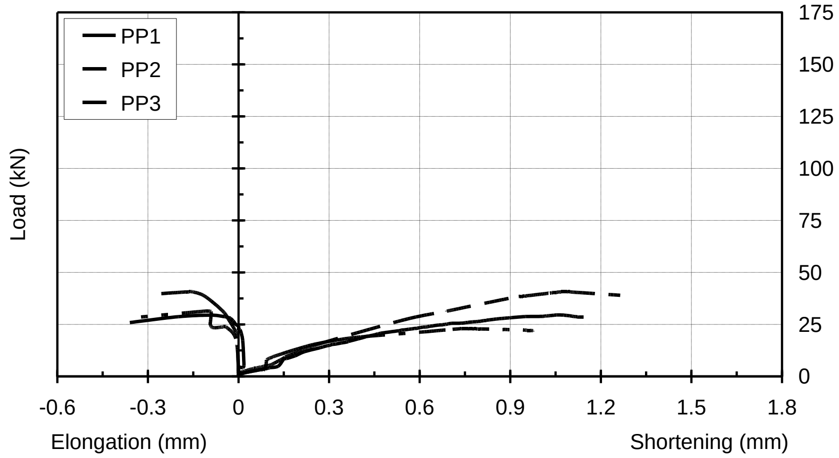


**Figure 6.6** Load  vs. Elongation/Shortening Graph of PP Specimens

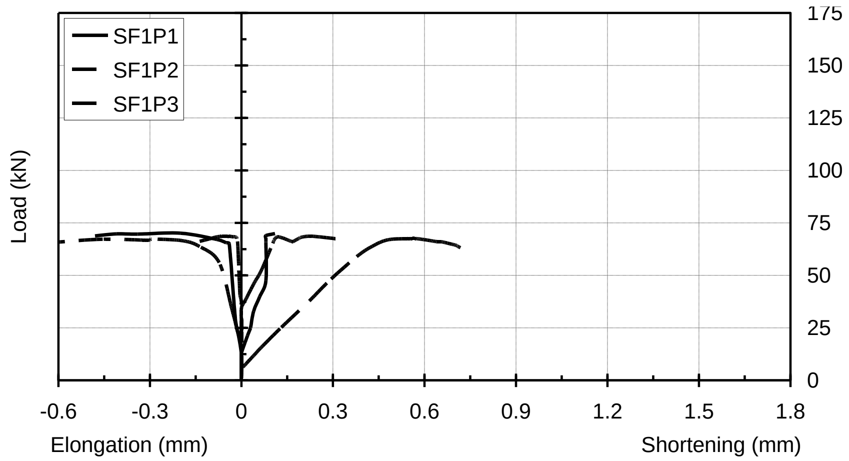


**Figure 6.7** Load vs. Elongation/Shortening Graph of SF1P Specimens

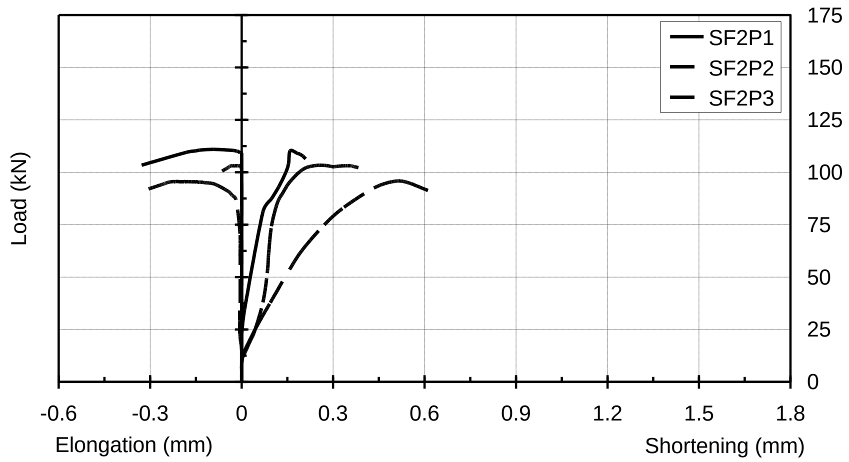


**Figure 6.8** Load vs. Elongation/Shortening Graph of SF2P Specimens

**2nd Series:**

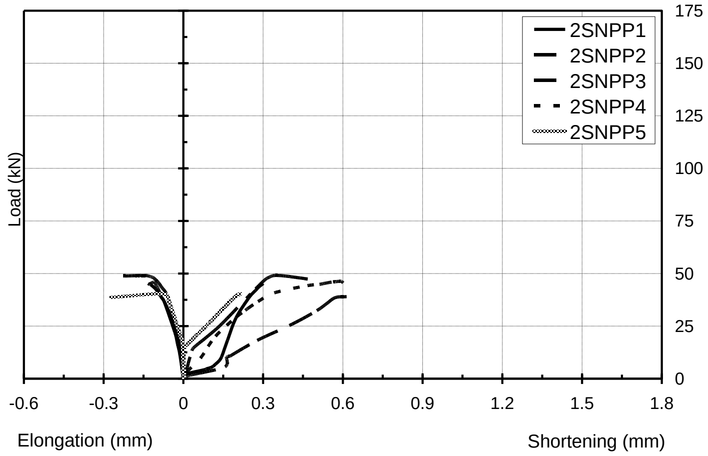


**Figure 6.9** Load vs. Elongation/Shortening Graph of 2SNPP Specimens

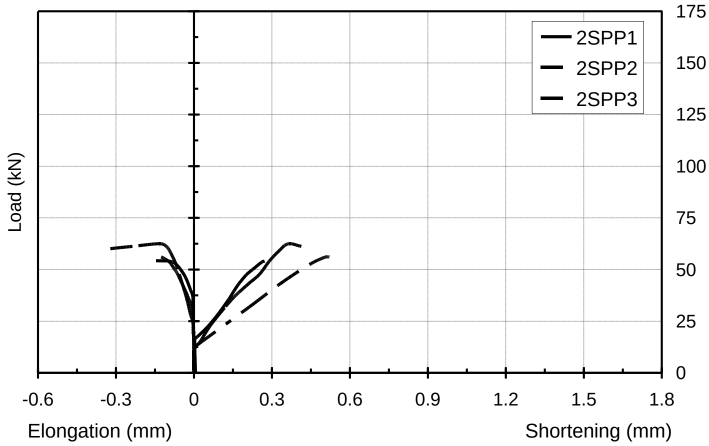


**Figure 6.10** Load vs. Elongation/Shortening Graph of 2SPP Specimens

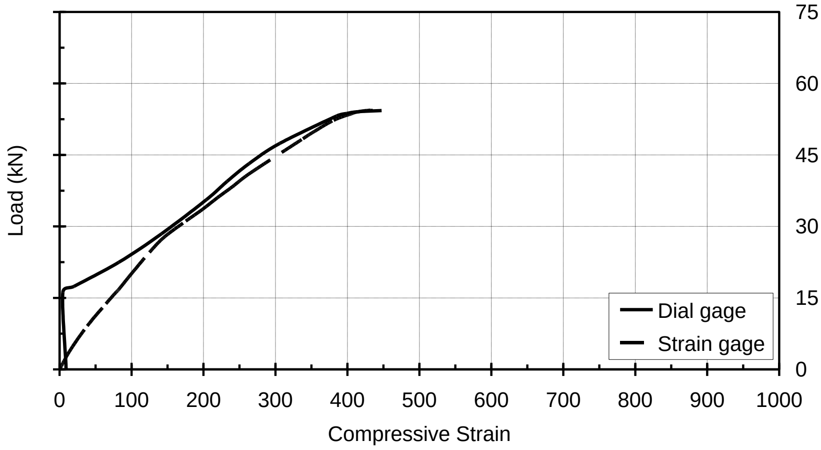


**Figure 6.11** Load vs. Compressive Strain Graph of 2SPP1 Specimen

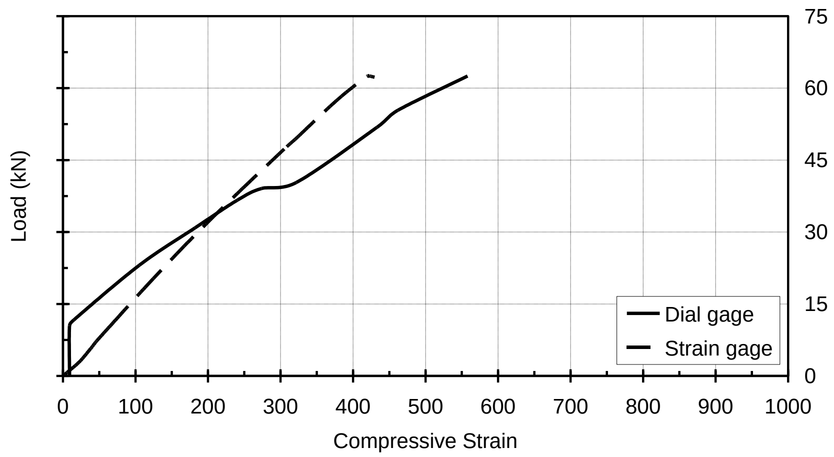


**Figure 6.12** Load vs. Compressive Strain Graph of 2SPP2 Specimen

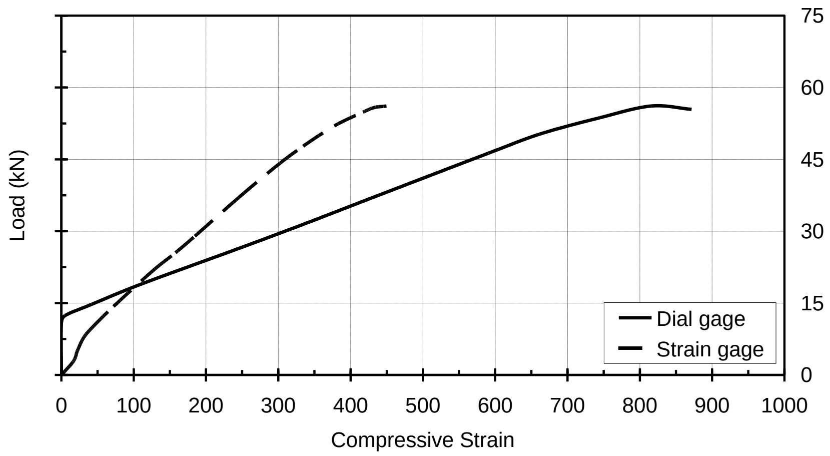


**Figure 6.13** Load vs. Compressive Strain Graph of 2SPP3 Specimen

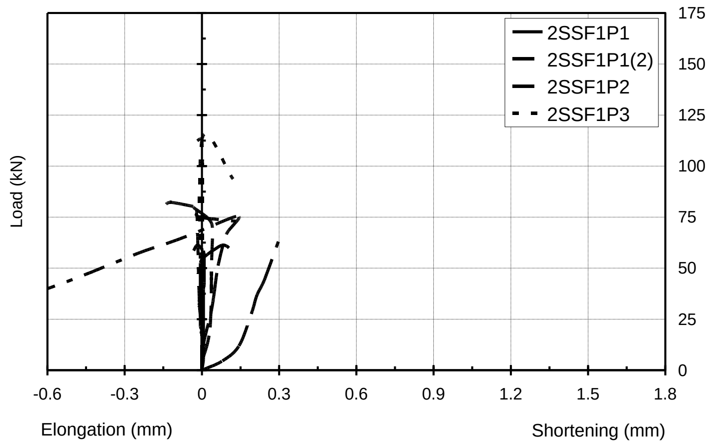


**Figure 6.14** Load vs. Elongation/Shortening Graph of 2SSF1P Specimens

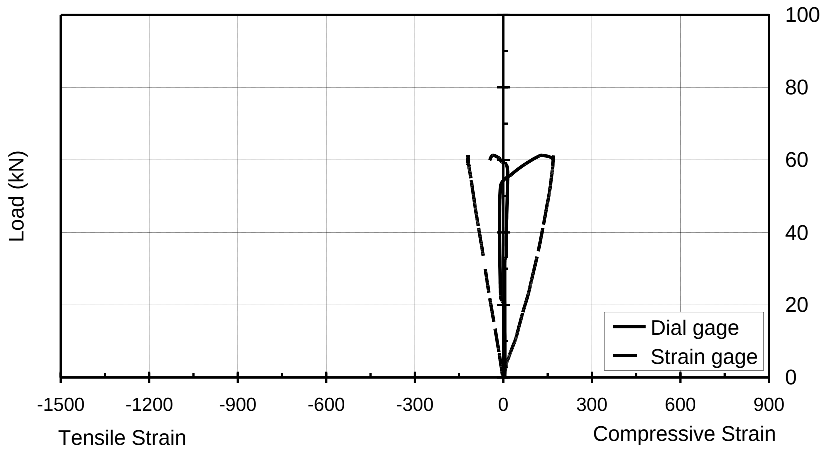


**Figure 6.15** Load vs. Tensile/Compressive Strain Graph of 2SSF1P1 Specimen

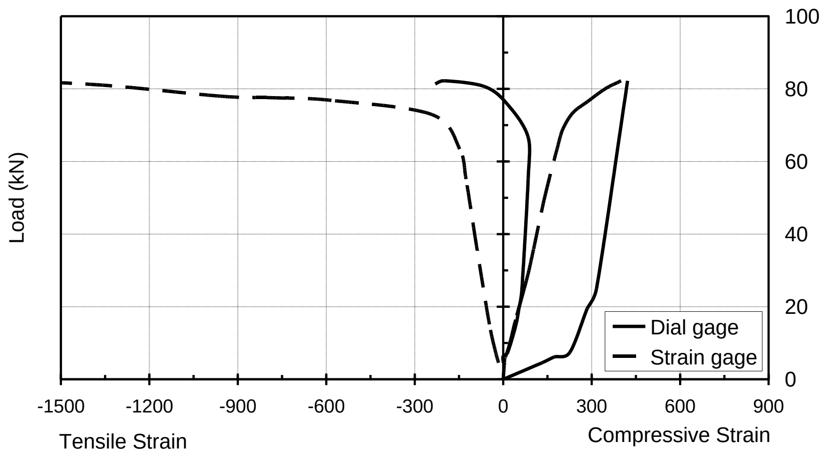


**Figure 6.16** Load vs. Tensile/Compressive Strain Graph of 2SSF1P1(2) Specimen

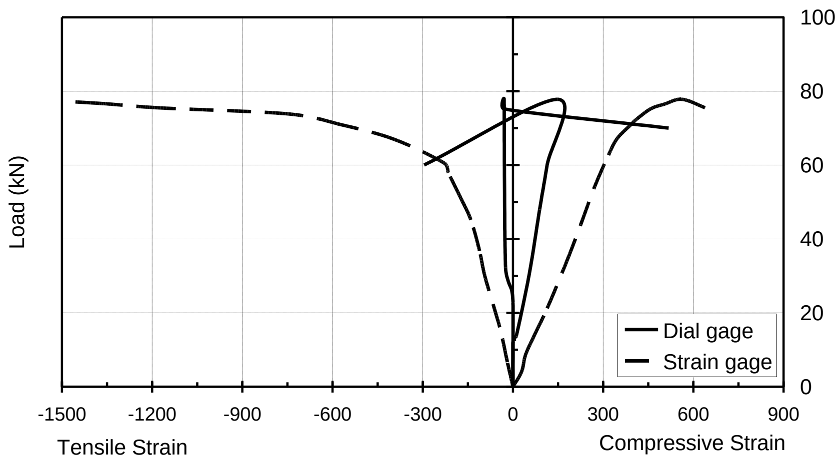


**Figure 6.17** Load vs. Tensile/Compressive Strain Graph of 2SSF1P2 Specimen

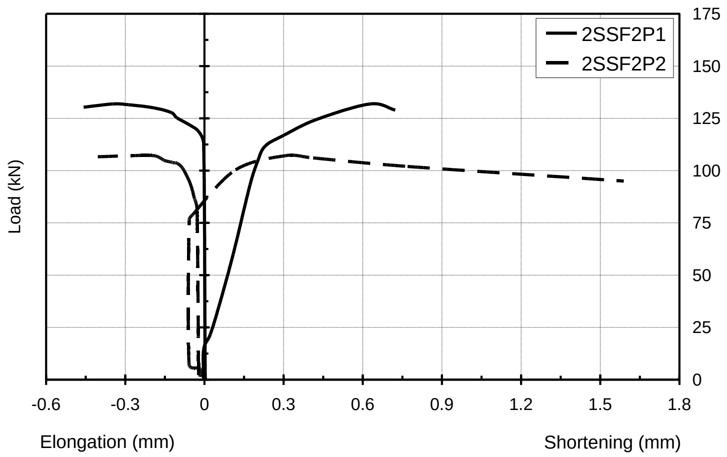


**Figure 6.18** Load vs. Elongation/Shortening Graph of 2SSF2P Specimens

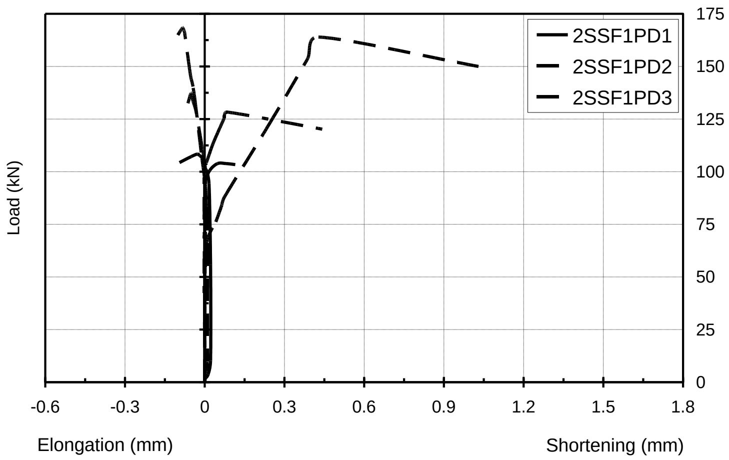


**Figure 6.19** Load vs. Elongation/Shortening Graph of 2SSF1PD Specimens

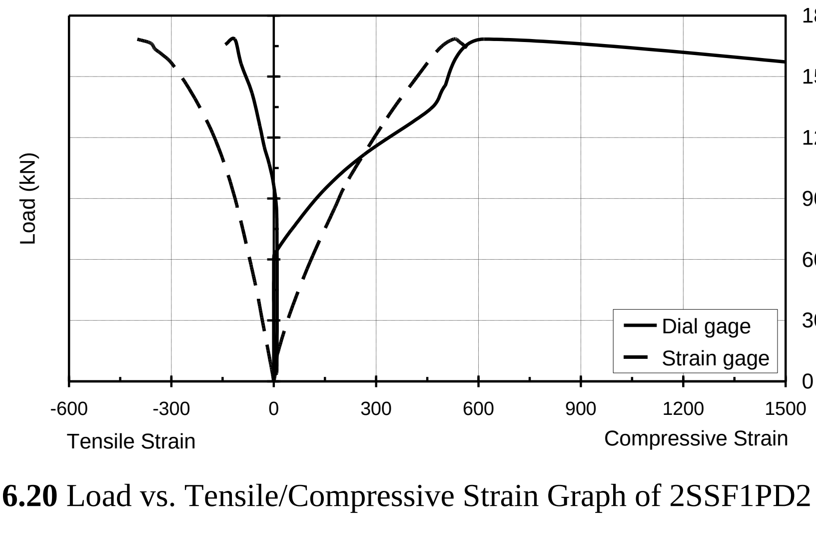


**Figure 6.20** Load vs. Tensile/Compressive Strain Graph of 2SSF1PD2 Specimen

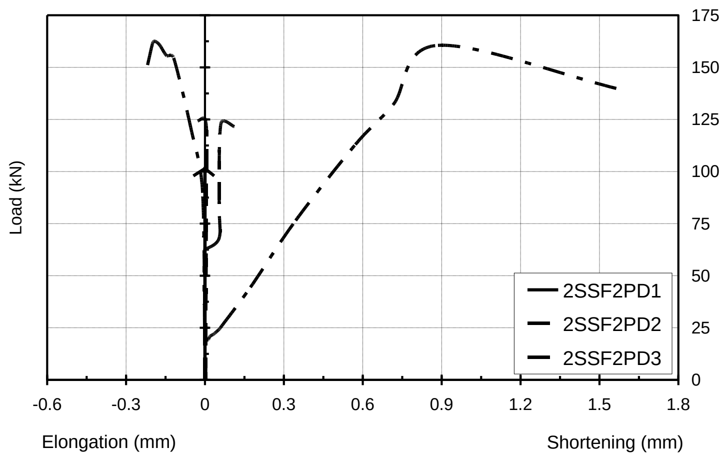


**Figure 6.21** Load vs. Elongation/Shortening Graph of 2SSF2PD Specimens

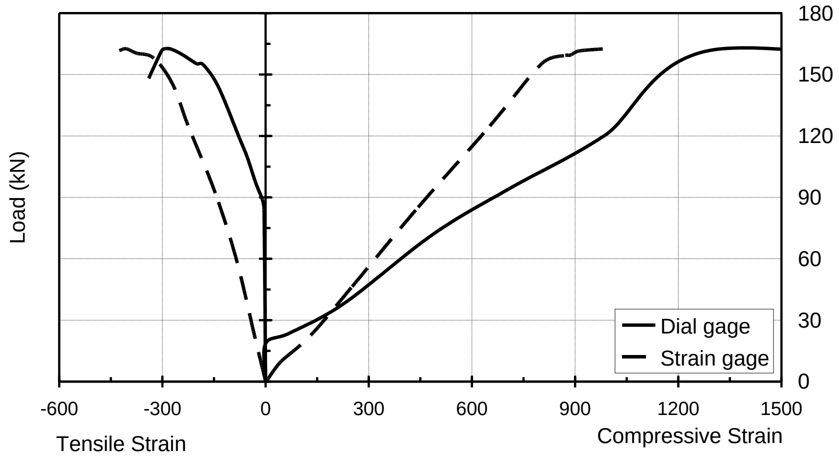


**Figure 6.22** Load vs. Tensile/Compressive Strain Graph of 2SSF2PD3 Specimen

**Table 6.11** Observed Damage of the First Series Panel Specimens

| Panel | Observed Damage |
|---|---|
| NPP-1 | * |
| NPP-2 | Diagonal zig-zag cracking in the loading direction along brick laying mortar. |
| NPP-3 | Diagonal cracking in the loading direction along brick laying mortar. |
| PP-1 | Diagonal cracking in the loading direction along brick laying mortar. |
| PP-2 | Diagonal cracking in the loading direction. One dial gage lifted up with plaster. |
| PP-3 | Diagonal cracking in the loading direction. One dial gage lifted up with plaster. |
| SF1P-1 | Diagonal cracking. |
| SF1P-2 | Diagonal cracking. |
| SF1P-3 | Arc-wise diagonal cracking in the loading direction. Crack parallel to side. |
| SF2P-1 | Two sides, perpendicular to the loading direction, lifted up. Diagonal cracking at the bottom of the panel. Crushing of the bricks and plaster near steel head. |
| SF2P-2 | Same behavior as SF2P-1.No crushing of the bricks or plaster at the cap region. |
| SF2P-3 | No cracking at the top. Crushing of the bricks and plaster at bottom cap region. |

* Healthy test data could not be taken due to a problem caused by the set-up.

**Table 6.12** Observed Damage of the Second Series Panel Specimens

| Panel | Observed Damage |
|---|---|
| 2SNPP-1 | Diagonal zig-zag cracking. |
| 2SNPP-2 | Diagonal zig-zag cracking along loading direction and crushing of brick corners along cracking path. Separation and falling of the bricks at caps. |
| 2SNPP-3 | Zig-zag cracking in the loading direction; but not perfectly diagonal. Cracking path is 3 bricks off from diagonal. |
| 2SNPP-4 | No diagonal cracking. Crushing of the bricks at the region of one cap. |
| 2SNPP-5 | Diagonal cracking along the bricks. |
| 2SPP-1 | Diagonal cracking. |
| 2SPP-2 | Arc-wise diagonal cracking in the loading direction. Crack parallel to side. |
| 2SPP-3 | Splitting due to diagonal cracking. Cracks at the sides joining orthogonally to the diagonal crack. |
| 2SSF1P-1, 2SSF1P-1(2) | First a diagonal crack occurred. Then, a crack at the cap region occurred. Plaster of one side, perpendicular to the loading direction, lifted up. |
| 2SSF1P-2 | Plaster of one side, perpendicular to the loading direction, lifted up and slid. |
| 2SSF1P-3 | Crushing of the bricks at one loading head and cracking of plaster at top. |
| 2SSF2P-1 | Crushing of the bricks at loading head. No cracking at plaster. The plaster separated from the brick layer completely and it slid by rotating around one cap. After plaster lift-up, diagonal cracking in the brick layer observed. |
| 2SSF2P-2 | There was crushing of the bricks at one of the caps' region. Also, there was a bending/buckling crack in the plaster which was parallel to one of the sides of the cap. After removing plaster, it was seen that there was crushing of the bricks at the top at one of the caps' region and there was diagonal cracking. |
| 2SSF2P-3 | ** |
| 2SSF1PD-1 | No cracking occurred at the top and bottom. Only, there was a slight crushing of the bricks at the region of one cap. |
| 2SSF1PD-2 | Clamps were fixed at two sides perpendicular to the loading direction, in order to prevent lifting up of SFRM. Crushing of the bricks was observed at one of the caps' region Plaster at the cap region lifted up, since it could not move at the other sides. |
| 2SSF1PD-3 | Clamps were used as in 2SSF1PD-2. Crushing was excessive. |
| 2SSF2PD-1 | Both plasters at the top and bottom separated from the brick layer, Plaster at top slid by rotating around one of the caps. Brick layer was completely divided into two parts due to diagonal cracking. |
| 2SSF2PD-2 | Clamps were used as in 2SSF1PD-2. Separation of the plaster at the bottom at one of the caps' region was identified. The brick layer was divided into two parts due to diagonal cracking. |
| 2SSF2PD-3 | Crushing of bricks at one of the caps' region was seen. Top plaster separated from brick layer. The specimen slid. |

* Test was repeated by placing the specimen in the set-up again because of a problem caused by the set-up during the test.

** Test could not be performed because specimen was broken during preparation to the test while placing in the set-up.

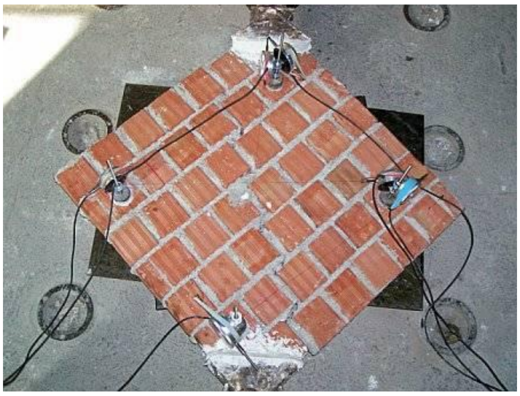

**Figure 6.23** View of NPP-2

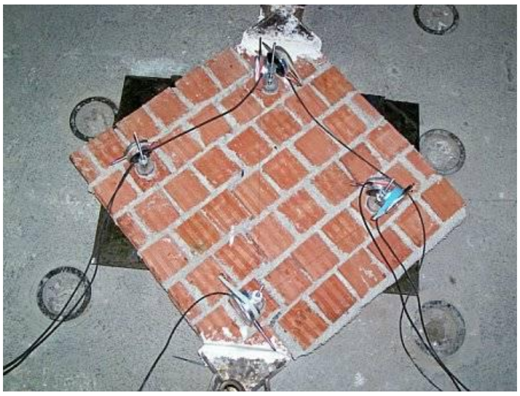

**Figure 6.24** View of NPP-3

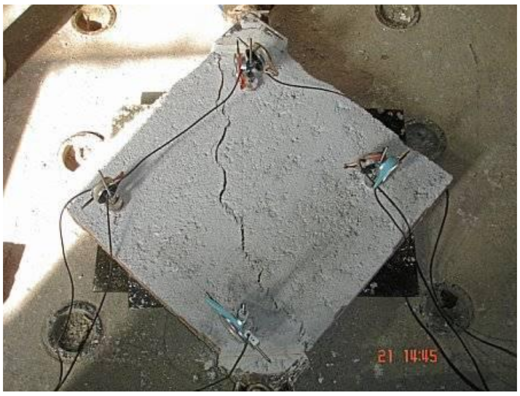



**Figure 6.25** View of PP-1

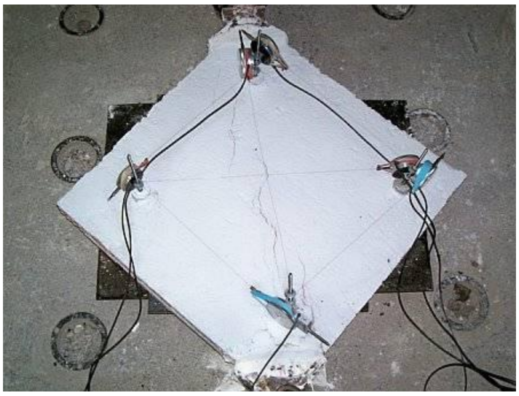

**Figure 6.26** View of PP-2

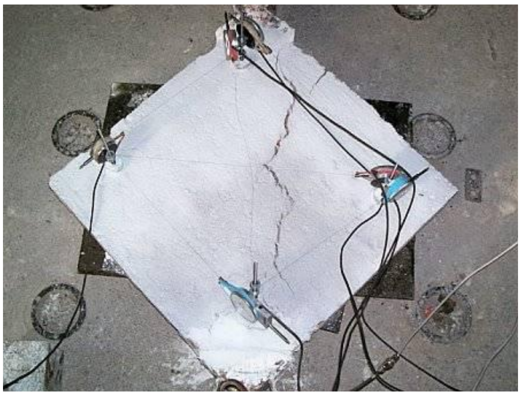

**Figure 6.27** View of PP-3

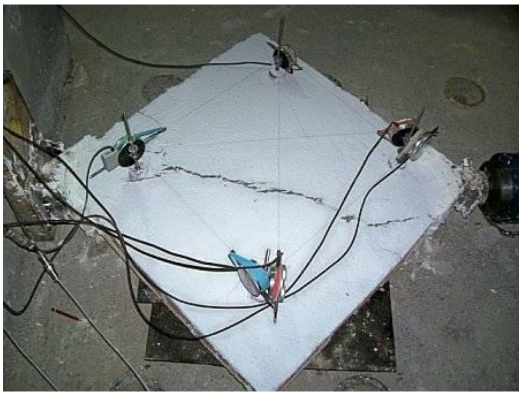

**Figure 6.28** View of SF1P-1

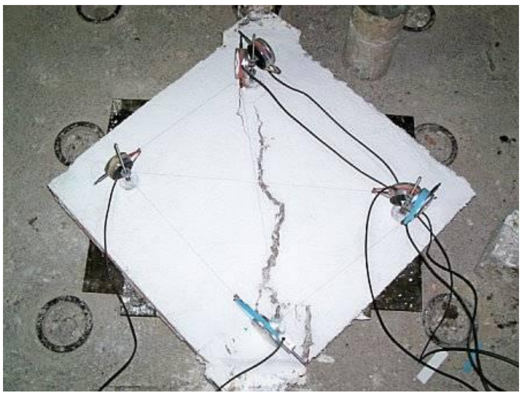

**Figure 6.29** View of SF1P-2

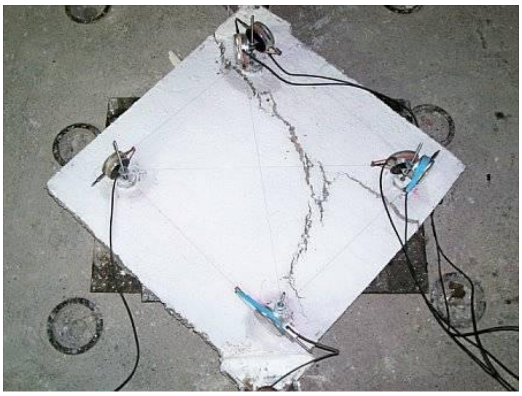

**Figure 6.30** View of SF1P-3


**Figure 6.31** Views of SF2P-1

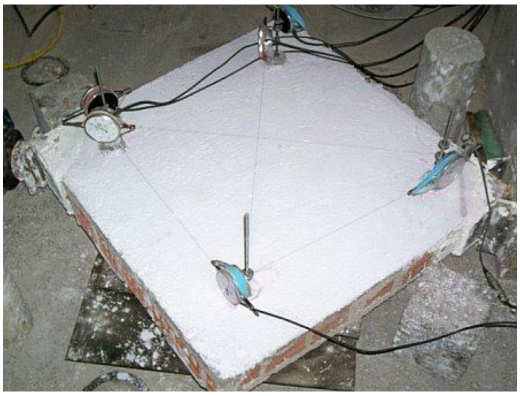


**Figure 6.32** Views of SF2P-2

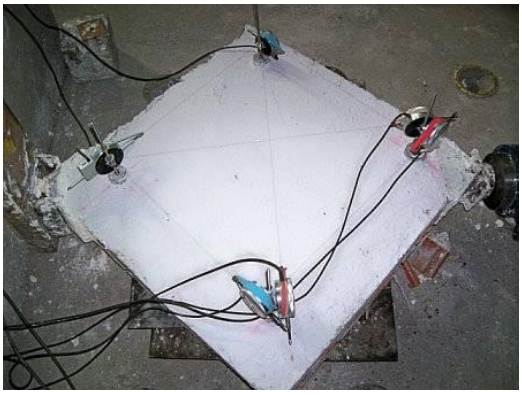


**Figure 6.33** Views of SF2P-3

**Figure 6.34** View of 2SNPP-1

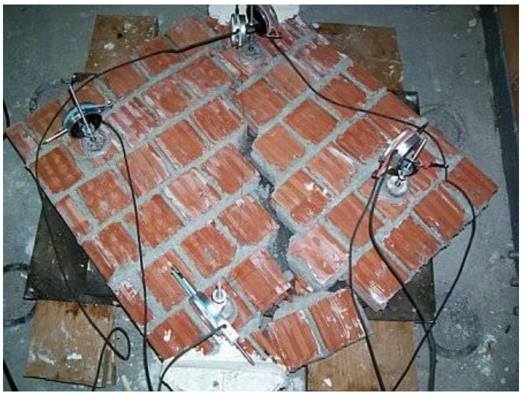

**Figure 6.35** View of 2SNPP-2

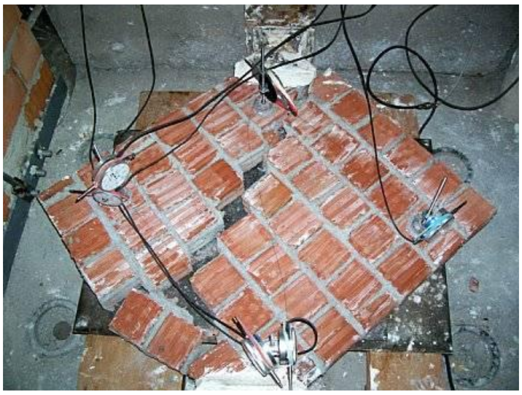

**Figure 6.36** View of 2SNPP-3

**Figure 6.37** View of 2SNPP-4

**Figure 6.38** View of 2SNPP-5

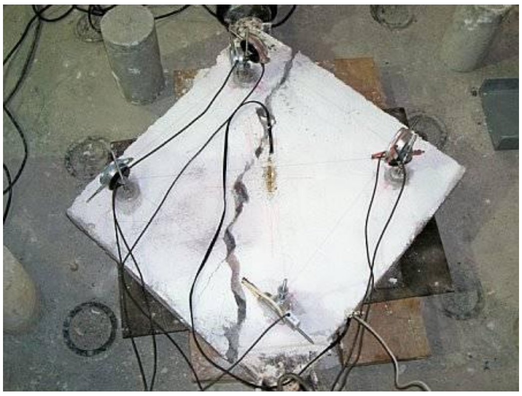

**Figure 6.39** View of 2SPP-1

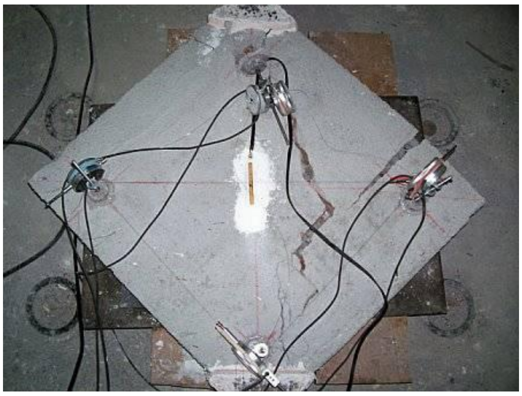

**Figure 6.40** View of 2SPP-2

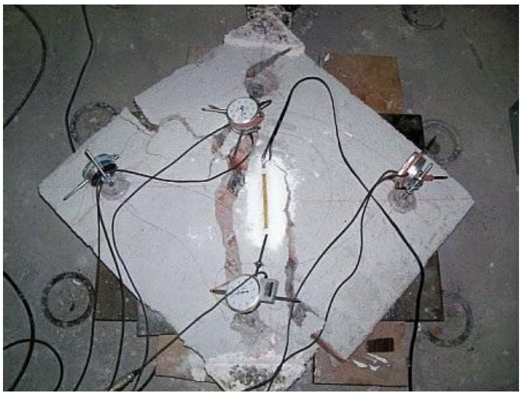

**Figure 6.41** View of 2SPP-3

**Figure 6.42** View of 2SSF1P-1, second test

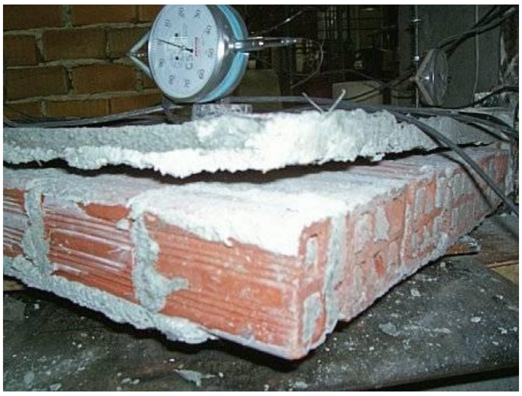

**Figure 6.43** View of 2SSF1P-2

**Figure 6.44** View of 2SSF1P-3

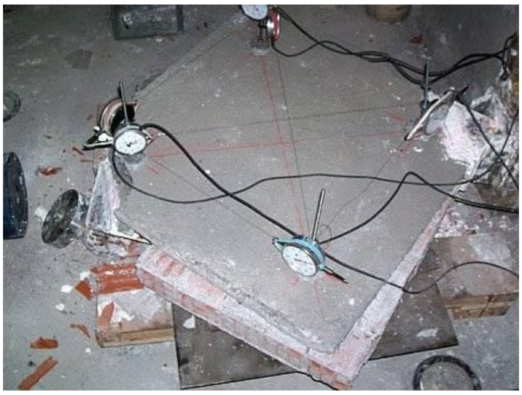

**Figure 6.45** View of 2SSF2P-1

**Figure 6.46** Views of 2SSF2P-2

**Figure 6.47** View of 2SSF1PD-1

**Figure 6.48** View of 2SSF1PD-2

**Figure 6.49** View of 2SSF1PD-3

**Figure 6.50** View of 2SSF2PD-1

**Figure 6.51** View of 2SSF2PD-2

**Figure 6.52** View of 2SSF2PD-3

### 6.2.4 Evaluation of the Test Results

In the scope of the panel tests, 1:3 scale, 30 infill panels with different properties were tested under diagonal compression. Due to non-homogeneous structure of the specimens, it is difficult to obtain any reliable modulus of elasticity and Poisson's ratio using the test data for any specimen.

**a) Failure Modes**

- ***First Series Panel Tests***

In the first series, 11 panel specimens were tested under diagonal compression. The mortar thickness was 10 mm in all specimens. In **Table 6.13**, results and comparisons for the first series panel tests are presented.

**Table 6.13** Summary of the Test Results for the First Series Panel Specimens

| **Panel** | **Average Load Carrying Capacity (kN)** | **Load Carrying Capacity Compared to that of** | |
|---|---|---|---|
| | | **NPP** | **PP** |
| NPP | 10.30 | ~ 1.0 times | ~ 0.32 times |
| PP | 31.83 | ~ 3.09 times | ~ 1.0 times |
| SF1P | 68.69 | ~ 6.67 times | ~ 2.16 times |
| SF2P | 103.04 | ~ 10.0 times | ~ 3.24 times |

In the first series panel tests, the highest average load carrying capacity was obtained in the 20 mm thickness of mortar with 2% volumetric ratio of steel fiber applied plastered wall specimen (on one side).

NPP specimens failed in a brittle manner. The failure was due to mortar between the hollow bricks and the path was consequently stepwise diagonally between the loading corners. PP specimens represent the current infill walls in most R/C framed structures in Turkey, and therefore, represent the main reference specimens of the research. The test data shows that plaster existence on infill surface increases the ultimate load capacity considerably (~3.09 times of NPP). Tensile stresses perpendicular to the diagonal crack caused the failure of PP specimens. SF1P specimens with 10 mm strengthening mortar reached ~2.16 times ultimate load capacity of the reference PP. SF2P specimens with 20 mm strengthening mortar resulted in ~3.24 times ultimate load capacity of the reference [46]. In **Figure 6.53**, one representative test data from each sub-group is presented.

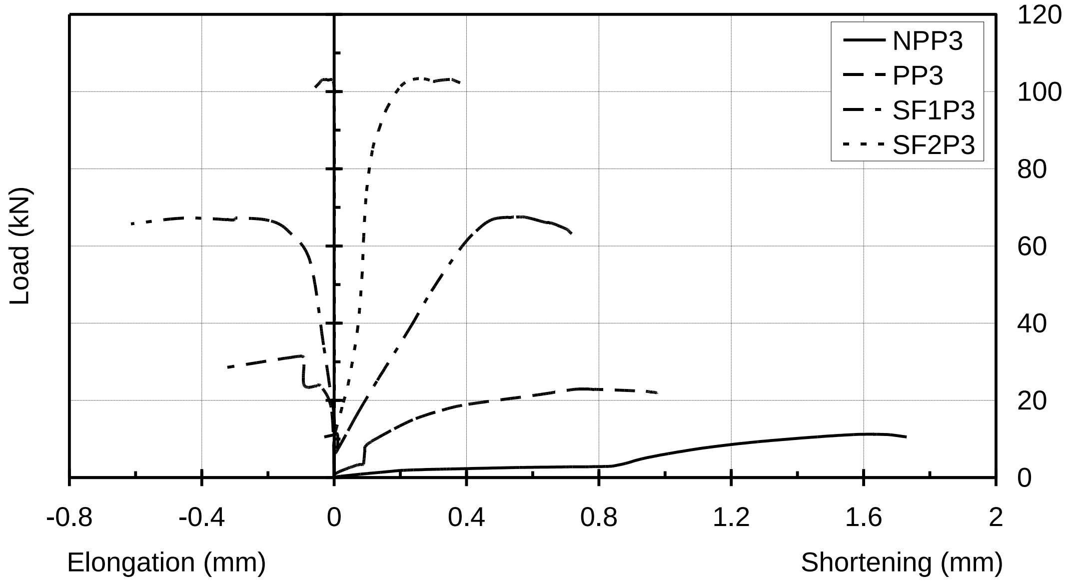


**Figure 6.53** Load vs. Elongation/Shortening Graph of First Series Specimens

- ***Second Series Panel Tests***

In this series, total of 5 2SNPP reference specimens were tested. In the 1st group tests due to high slender nature of the panel body, difficulty of placing non-plastered wall panels into the setup was experienced. In order to get reliable number of test data, 5 specimens were prepared and all of them were successfully tested.

In the 2SNPP-2 test, the cord of the dial gage in the tension direction was broken. In the 2SSF1P-1 test, strain gage in tension direction stopped strain reading near to the end of the test. For the 2SSF1P-3, 2SSF2P-2, 2SSF1PD-2, 2SSF1PD-3, and 2SSF2PD-2 tests, in order to prevent lifting up of the plaster, two small clamps were used at the two perpendicular ends to the loading direction. In general, because of grinding of the plaster at the cap regions, the plaster became thin at those regions. In **Table 6.14**, results and comparisons for the second series panel tests are presented.

**Table 6.14** Summary of the Test Results for the Second Series Panel Specimens

| Panel | Average Load Carrying Capacity (kN) | Load Carrying Capacity Compared to that of | |
|---|---|---|---|
| | | 2SNPP | 2SPP |
| 2SNPP | 44.11 | ~ 1.0 times | ~ 0.77 times |
| 2SPP | 57.64 | ~ 1.31 times | ~ 1.0 times |
| 2SSF1P | 85.33 | ~ 1.94 times | ~ 1.48 times |
| 2SSF2P | 119.55 | ~ 2.71 times | ~ 2.07 times |
| 2SSF1PD | 132.06 | ~ 2.99 times | ~ 2.29 times |
| 2SSF2PD | 128.53 | ~ 2.91 times | ~ 2.23 times |

In the second series panel tests, the highest average load carrying capacity was obtained in the 10 mm thickness of mortar with 2% volumetric ratio of steel fiber applied plastered wall specimen (on double sides).

The average maximum load reached to 44.11 kN with a stepwise failure mode, while it was 10.30 kN in the first series' NPP specimens. Approximately 3 times increase in brick laying mortar strength as compared to the first series resulted in roughly 4 times increase in diagonal shear capacity. 2SPP specimens failed at an average maximum load of 57.64 kN. In the first series the ratio between the non-plastered and plastered panels was 3 fold whereas in the second series the increase was just 30%. The reason for the limited increase in the second series can be attributed to the increase in brick laying mortar strength that governed the capacity and to the decrease in plaster thickness.

The maximum average diagonal compressive force of 2SSF1P specimens was measured as 85.33 kN resulting in an improvement of approximately 1.5 times that of the reference specimen. However, it should be noted that these panels behaved very stiff as compared to the first series' SF1P specimens. This can be attributed to higher mortar and plaster strengths. 2SSF2P specimens reached an average ultimate diagonal compressive force of 119.55 kN.

2SSF1PD specimens were strengthened by steel fiber reinforced mortar application on both sides. These panels behaved very stiff up to ultimate load of 132.06 kN in average. The average diagonal compressive force capacity of 2SSF2PD specimens was 128.53 kN. Besides, it should be noted that capacities of 2SSF1PD and 2SSF2PD specimens varied a lot in each sub-group. Application of reinforced mortar on both sides of the panel results in a considerable amount of increase in ultimate diagonal compression capacity with respect to the one side application. Double side application provided very stiff behavior but high variation in ultimate strength as well [46]. In **Figure 6.54**, one test data from each sub-group is presented.

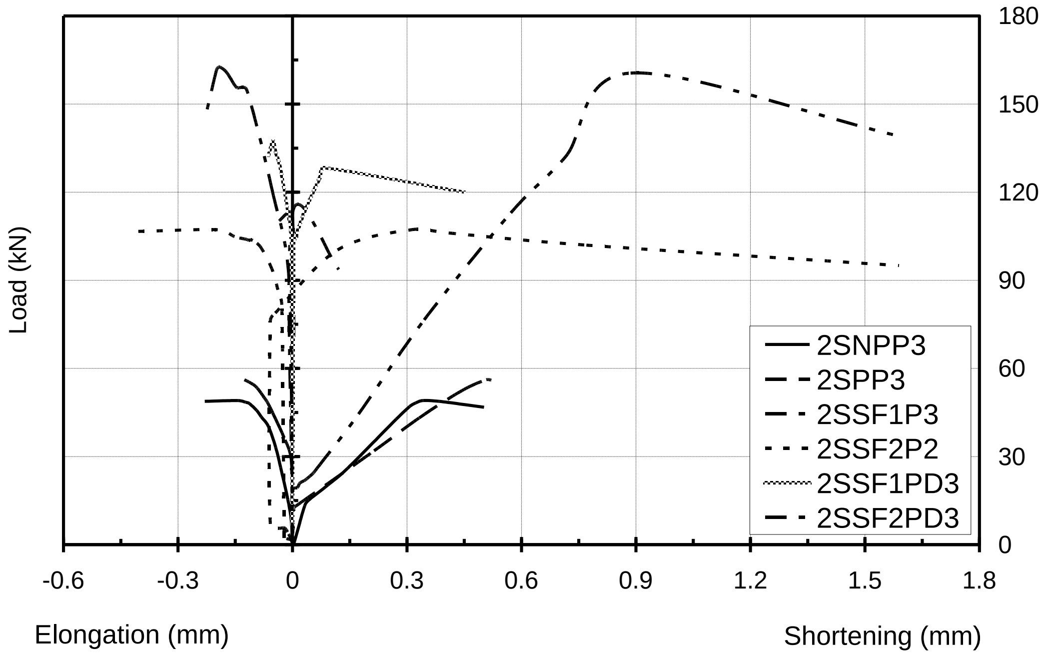


**Figure 6.54** Load vs. Elongation/Shortening Graph of Second Series Specimens

### b) Strength Characteristics

The samples were subjected to diagonal compression test. Panels were modeled in SAP2000 with finite element approach to understand better the stress distribution. Panels were fine meshed into 40×40 shell elements (total of 1600 elements). The panel was loaded diagonally as shown in **Figure 6.55**. The corresponding center point stresses are also shown in the same figure. The stresses are normalized for average stress $\bar{\tau} = 0.707 P_d / (bt)$. $P_d$ is the applied diagonal force. $b$ and $t$ are the width and thickness of the panel, respectively. To better simulate the real tests, panel was also modeled as shown in **Figure 6.56**. In this model, the load and support are distributed over an area that is equal to the steel head dimensions. On the same figure, the midpoint stress distribution and midpoint principal stresses are given as well. The Mohr's Circle is presented in **Figure 6.57** for the last model. There is not much difference for midpoint stresses between the two models. However, the internal stress distribution changes especially near by the loading corners. The principal stress distribution is shown by arrows for the second model in **Figure 6.58**.

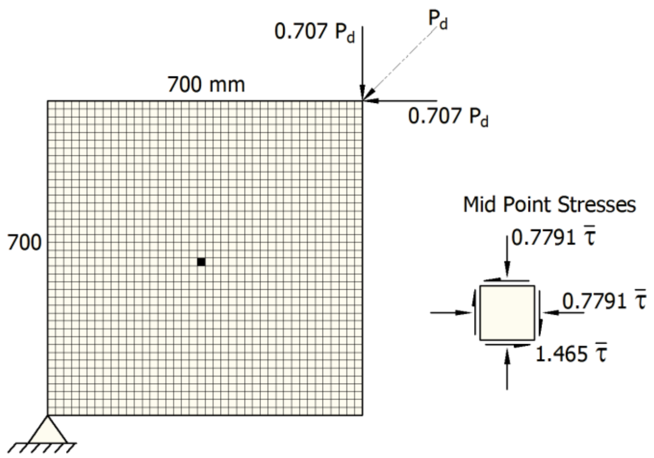


**Figure 6.55** Finite Element Model of Test Panel

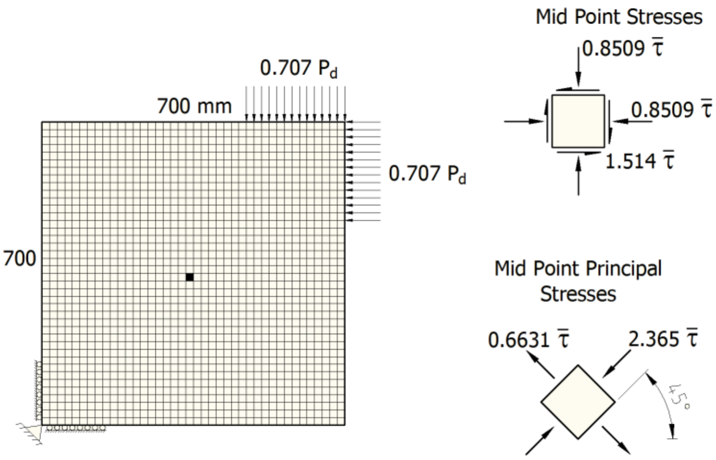


**Figure 6.56** Finite Element Model of Test Panel with different boundary conditions

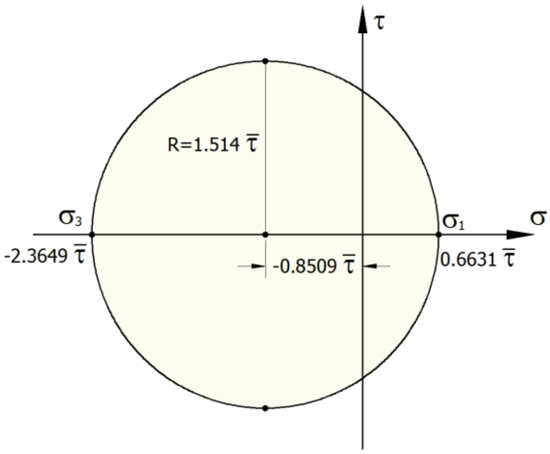


**Figure 6.57** Mohr Circle representation of midpoint stresses

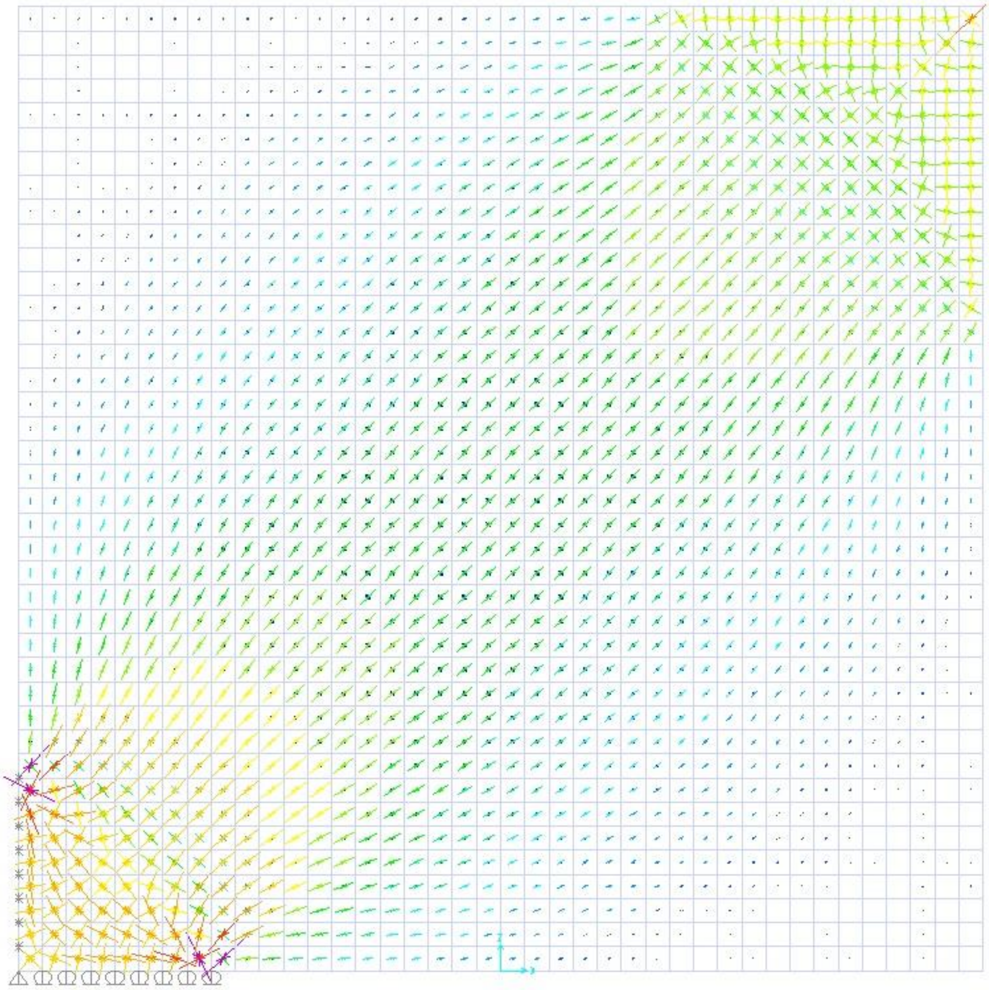

**Figure 6.58** Principal Stress Directions

The model assumes the masonry panel as isotropic, linearly elastic, and homogenous globally. Compressive stresses are shown as negative and tensile stresses as positive. Since failure is brittle and diagonal cracking initiates at or near the center, Mohr-Coulomb failure hypothesis will be used to calculate cracking strength [47, 48]. For the non-plastered plain specimens, failure occurred in the brick laying mortar in a zigzag manner pattern. Therefore, for the non-plastered tests, the mortar strength will be considered instead of brick strength during the calculation of capacity. Considering Mohr-Coulomb failure surface for the biaxial state of stress given in **Figure 6.59**, the tensile strength of mortar can be calculate as follows.

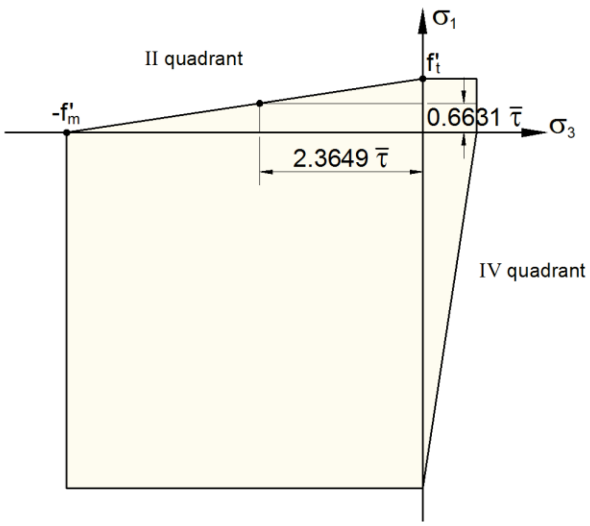


**Figure 6.59** Mohr-Coulomb Yield Surface

Equation of line in the second quadrant is $\sigma_1 = a\sigma_3 + b$. The unknown $a$ is the slope of the line and $b$ is the intersection point on $\sigma_1$ axis which is tensile strength of material, $f_t'$. Two point are known on this line. The first point is compressive strength of material, $f_m'$, and second point is the test results obtained from the diagonal compression test of panels.

$$@ \quad \sigma_1 = 0 \quad \rightarrow \quad \sigma_3 = f_m' \quad \Rightarrow \quad a = -\frac{b}{f_m'} \qquad \textbf{(6.1)}$$

$$@ \quad \sigma_1 = 0.6631\bar{\tau} \quad \rightarrow \quad \sigma_3 = -2.365\bar{\tau} \quad \Rightarrow \quad b = \frac{0.6631\bar{\tau}\, f_m'}{f_m' + 2.365\bar{\tau}} \qquad \textbf{(6.2)}$$

The average shear stress is defined as $\bar{\tau} = \dfrac{0.707\, P_d'}{b\,t}$.

$$b = f_t' = \frac{0.4688\ f_m'\, P_d'}{f_m'\, b\,t + 1.672\ P_d'} \qquad \textbf{(6.3)}$$

Knowing the compressive and tensile strength of mortar, the Coulomb-Mohr criteria yields in the second quadrant, **Equation 6.4**:

$$\frac{\sigma_1}{f_t'} - \frac{\sigma_3}{f_m'} = 1 \qquad \textbf{(6.4)}$$

The finite element analysis gave for the principal stress:

$\sigma_1 = 0.6631\bar{\tau}$ & $\sigma_3 = 2.365\bar{\tau}$

Substituting these values into the criteria and considering the average shear stress as cracking stress, **Equation 6.5**:

$$\tau_{cr} = \frac{f_t' \, f_m'}{0.6631 \; f_m' - 2.365 \; f_t'} \quad \textbf{(6.5)}$$

Two series of panel tests were conducted in this study. The brick laying mortar strengths were 3.5 MPa and 10 MPa, respectively. It is believed that these values cover typical mortar strength. Their corresponding tensile strength was calculated 0.1113 MPa and 0.5053 MPa, respectively. For the tensile strength of mortar, a line can be proposed considering that the line should intersect the origin, **Equation 6.6**:

$$f_t' = 0.05 \; f_m' \quad \textbf{(6.6)}$$

The proposed equation overestimates the tensile strength slightly. Therefore, the following equation is also proposed, **Equation 6.7**:

$$f_t' = 0.003 \, f_m'^{\,2} + 0.02 \, f_m' \quad \textbf{(6.7)}$$

For the tensile strength of plaster applied on the brick surface or of the strengthening mortar, the equations proposed above will not be used. Those equations are only valid for the mortar in between bricks. For the plaster, the regular equation for concrete will be used, **Equation 6.8**:

$$f_t' = 0.35\sqrt{f_{plaster}'} \quad \textbf{(6.8)}$$

For 2% steel fiber added mortar, twice the above value will be used, **Equation 6.9**:

$$f_t' = 0.70\sqrt{f_{plaster}'} \quad \textbf{(6.9)}$$

Once the tensile strength of materials is determined, the cracking shear strength of the materials is calculated and the force contribution is easily calculated from the average shear stress definition. **Table 6.15** shows the test results and theoretically calculated capacities. The plaster strength in the first series was not determined accidentally. Therefore, it is assumed for the sake of calculation as 8 MPa which fits test results.

**Table 6.15** Comparison of Calculated vs. Test Results

| | Panel | Test Load (kN) | Mortar Str. (MPa) | Plaster Str. (MPa) | Str. Mortar (MPa) | Brick Force (kN) | Plaster Force (kN) | Str. Mortar Force | Total | Ratio |
|---|---|---|---|---|---|---|---|---|---|---|
| 1st Series | NPP | 10.3 | 3.5 | - | - | 10.3 | - | - | 10.3 | 1.00 |
| | PP | 31.8 | 3.5 | 8.0 | - | 10.3 | 20.5 | - | 30.8 | 0.97 |
| | SF1P | 68.7 | 3.5 | 8.0 | 21.2 | 10.3 | 20.5 | 31.2 | 62.0 | 0.90 |
| | SF2P | 103.0 | 3.5 | 8.0 | 21.2 | 10.3 | 20.5 | 62.4 | 93.2 | 0.90 |
| 2nd Series | 2SNPP | 44.1 | 10.0 | 4.0 | - | 43.7 | - | - | 43.7 | 0.99 |
| | 2SPP | 57.6 | 10.0 | 4.0 | - | 43.7 | 7.7 | - | 51.4 | 0.89 |
| | 2SSF1P | 85.3 | 10.0 | 4.0 | 29.2 | 43.7 | 7.7 | 38.6 | 90.0 | 1.06 |
| | 2SSF2P | 119.6 | 10.0 | 4.0 | 29.2 | 43.7 | 7.7 | 77.3 | 128.7 | 1.08 |
| | 2SSF1PD | 132.1 | 10.0 | 4.0 | 29.2 | 43.7 | 7.7 | 77.3 | 128.7 | 0.97 |
| | 2SSF2PD | 128.5 | 10.0 | 4.0 | 29.2 | 43.7 | 7.7 | 154.5 | 205.9 | 1.60 |

### 6.2.5 Conclusions

The contribution of a new strengthening technique on shear behavior of individual hollow brick infill wall panels was experimentally investigated in this study. Some conclusions from the limited test results can be stated as:

- Applying steel fiber reinforced mortar onto the existing plaster layer increases the diagonal compressive capacity of hollow brick infill panels when compared to that of reference specimens.
- Double side, strengthened specimens behaved very stiff up to the ultimate stage. It can be concluded that, one sided – 20 mm thick steel fiber reinforced mortar application gives the optimum results by means of maximum diagonal compressive force and behavior.
- There is difference between the brick laying mortar and SFRM strengths of the first series and second series panel tests. This problem occurred, because the worker used different mixture proportions for each series. The effect of brick laying mortar strength on infill panel behavior is obvious for non-plastered infill panels. Approximately 3 times increase in mortar strength

results in approximately 4 times increase in diagonal compressive capacity.

- Strain gage applications to the panel specimens were found to be very effective in determining the strain better and reliable than obtaining it from displacement measurements.

The Mohr-Coulomb failure hypothesis was used to calculate cracking strength. For the non-plastered specimens, the mortar strength was considered instead of brick strength in the calculation of capacity. The tensile strength of mortar was calculated using the Mohr-Coulomb failure surface for the biaxial state of stress. A line was proposed for the tensile strength of mortar, **Equation 6.6**. Another equation was also proposed, **Equation 6.7**, since the proposed line equation overestimated the tensile strength slightly. For the plaster, the regular equation for concrete was used, **Equation 6.8**. For the steel fiber reinforced mortar, twice the value in **Equation 6.8** was utilized, **Equation 6.9**.

After determining the tensile strength of materials, the cracking shear strength of the materials was calculated and the force contribution was calculated from the average shear stress definition.

Assuming plaster strength of 8 MPa, the first series test results were estimated with approximately 10% error. For the second series, test results were predicted in 11% error range except the last test. Because of excessive thickness of strengthening mortar, either the strengthening mortar separated prematurely or brick crushed. Therefore, the theoretical expected load could not be achieved in these tests. Theoretically, there is no difference between 2SSF2P and 2SSF1PD. Both have total of 20 mm strengthening mortar. The former has 20 mm mortar at one side whereas the latter has 10 mm mortar on both sides. The test results between them shows 10% increase in capacity for the double sided one. This difference attributed to the symmetry of the second one and eccentric of the first one.

This preliminary study showed that, proposed technique increases the shear capacity of individual hollow brick infill walls. As a further information, in the second step of the main research, technique was applied to deficient R/C infilled frames considering a number of parameters such as; steel fiber reinforced mortar thickness, anchorage, etc. and several frames were tested under reversed cyclic loading. The average seismic performance improvement levels of frames by means of lateral load capacities are very similar to that of individual wall panels [46].

# CHAPTER 7

# ANALYTICAL STUDIES

## 7.1 GENERAL

The aim of this chapter is to model analytically the existing hollow brick infill walls strengthened by fiber reinforced mortar (FRM). Consequently, the contribution of strengthened infill walls to the system will be determined.

Truss models have been increasingly used for analysis purposes of infills. In the sixties, Smith [49-53] and Carter [53] modeled hollow brick infill walls as compression struts. In the studies performed in the Structural Mechanics Laboratory of the Middle East Technical University, Altın [2] and Sonuvar [9] modeled reinforced concrete infill walls as compression struts. Nevertheless, the modeling of the strengthening made using FRM is not like either the modeling of hollow brick infill walls, or the modeling of reinforced concrete infill walls. Moreover, anchorages of the frames cause additional difficulty to the modeling. If this problem is solved, then modeling strengthened hollow brick infill walls with equivalent truss bars will be a proper method to be used in the design step of the strengthening works [54].

In this chapter, hollow brick infill walls strengthened by FRM will be presented by equivalent diagonal struts.

## 7.2 MODELING THE STRENGTHENED HOLLOW BRICK INFILL WALL AS EQUIVALENT DIAGONAL STRUT

In this part of the study, the hollow brick infill walls strengthened by the application of FRM will be modeled as equivalent diagonal compression struts connected to the frame at the beam-column joints. It is intended to obtain a proper and reliable method to be used in the design works. The plastered hollow brick infill wall strengthened by FRM will be modeled as two separate compression struts. The first strut, which will be positioned diagonally and connected to the frame at the beam-column joints, will be used to model the plastered hollow brick infill wall. The second strut will be used to model the FRM [54].

The equivalent strut concept was first used by Smith [49-53] and Carter [53] in their studies. They intended to predict the lateral stiffness and strength of the infilled frames. A similar method was also recommended by FEMA 356 [55] for brick infills.

## 7.3 EQUIVALENT STRUT MODEL

When the load is applied to the frame, the infill wall is separated from the frame along a certain length of the beam or the column and the contact between the frame and the infill wall remains at the other two opposite corners. At this stage, a line drawn from one corner to the other, at which there is connection between the frame and the infill wall, shows the direction of compression. The infill transfers compression along this line. For this reason, the infill can be modeled as an equivalent virtual diagonal strut, **Figure 7.1**. The following equations are given by FEMA [55] to determine mechanical and geometrical properties of this virtual compression strut representing the infill, **Equations 7.1** and **7.2**

$$\lambda = \sqrt[4]{\frac{E_{infill} b_w \sin(2\beta_s)}{4EIh}} \quad \textbf{(7.1)}$$

where $E_{infill}$ is the modulus of elasticity of the infill, $E$ is the modulus of elasticity of the column, $b_w$ is the thickness of the infill, $\beta_s$ is the angle which has a tangent of infill height to length, $I$ is the moment of inertia of the column, and $h$ is the height of the infill.

The effective width of the equivalent compression strut is expressed by a parameter, $a_{infill}$ , **Equation 7.2**.

$$a_{infill} = 0.175(\lambda \cdot h_{col})^{-0.4} d \quad \textbf{(7.2)}$$

where $a_{infill}$ is the effective width of the equivalent compression strut, $h_{col}$ is the height of the column measured between the beam-column joints, and $d$ is the diagonal length of the infill wall.

The width of the equivalent strut should be the same as the width of the modeled infill wall. Modulus of elasticity of the frame concrete was calculated as in **Equation 7.3** [56].

$$E_c = 4750\sqrt{f_c} \quad \text{(MPa)} \quad \textbf{(7.3)}$$

As mentioned in Chapter 6, hollow brick infill walls, similar to the hollow brick infills of the frame specimens, were tested under compression applied along one of the diagonals. Average compressive strength and average modulus of elasticity in the diagonal direction were determined as $f_{c,infill}$ = 4.5 MPa and $E_{infill}$ = 7000 MPa.

The average compressive strength was determined from the applied maximum load and from average diagonal area which can be defined as panel thickness times the width of steel heads. From the displacement measurements in diagonal direction, the average strains were calculated. Knowing the stress and strains, the modulus of elasticity of panels were determined. The high modulus of elasticity value can be attributed to the hollow brick infill that has a length scale of 1/3. Although the exterior dimensions of the bricks are decreased according to the scale, it was not possible to decrease the thicknesses in the same scale. Therefore, void ratio decreased and accordingly average elastic modulus increased.

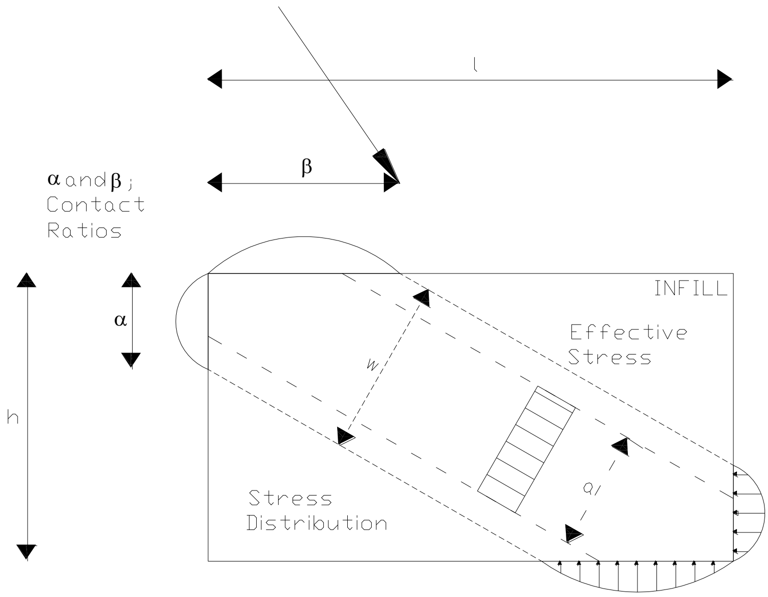


$$d = \sqrt{l^2 + h^2}$$

**Figure 7.1** Compression Region Forming in the Infill Wall under Lateral Load and Equivalent Virtual Diagonal Strut Representing the Infill Walls

Using the experimental results, the strength of the compression strut used in the modeling can be calculated using the equation below, **Equation 7.4**.

$$F_{c,infill} = f_{c,infill} \cdot a_{infill} \cdot b_w \qquad \textbf{(7.4)}$$

The width and modulus of elasticity of the equivalent strut should be the same as that of the infill wall it models. The rigidity of the equivalent compression strut can be calculated using FEMA [55] as in **Equation 7.5**.

$$k_{infill} = \frac{b_w \cdot a_{infill} \cdot E_{infill}}{d} \tag{7.5}$$

Using **Equations 7.4** and **7.5**, the strength and initial rigidity of the compression strut used to model the infill wall were calculated respectively as 62.50 kN and 69.44 kN/mm. Then, the load-deformation curve necessary for the computer program was prepared as in **Figure 7.2**.

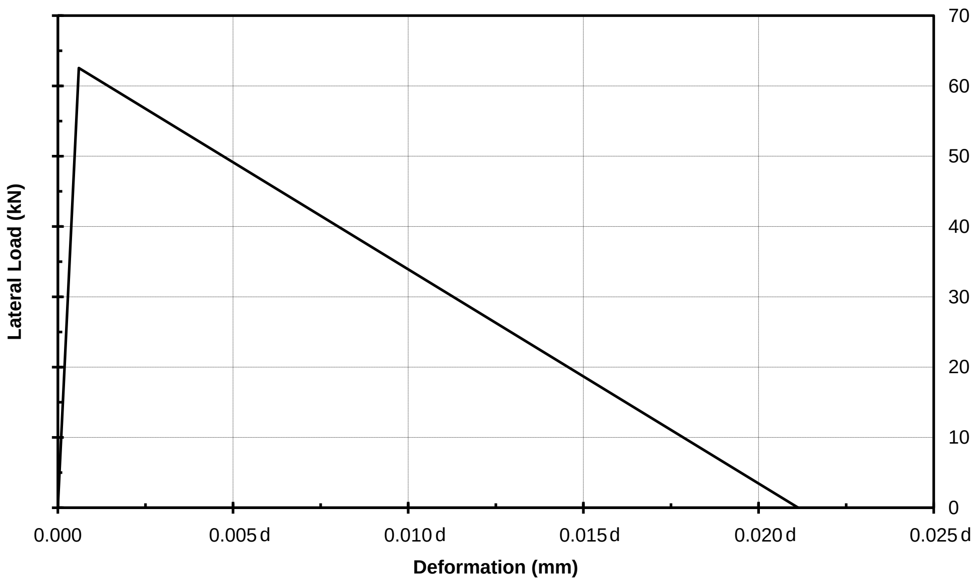


**Figure 7.2** Simplified Load-Deformation Curve of the Compression Strut Modeling the Plastered Hollow Brick Infill Wall

Up to this point, the modeling of the first equivalent compression strut is shown. The second compression strut will model the FRM. As the mortar can be accepted as a homogeneous and isotropic material, the geometrical properties of the panel modeling will be done by using a method proposed by Smith [49-53] and Carter [53].

Smith and Carter defined the relative stiffness of the infill to the column by a dimensionless parameter, $\lambda h$. $\lambda$ can be found using **Equation 7.1**. The length of the contact surface of the column and the infill can be found using ‘ free beam on an elastic foundation, subjected to a concentrated load’ analogy as in **Equation 7.6**.

$$\frac{\alpha}{h} = \frac{\pi}{2\lambda h} \qquad \ldots..(\alpha \leq h/2) \tag{7.6}$$

where $h$ is the height of the column between beam-column joints. Smith [49-53] and Carter [53] made some assumptions. First one is that the infill has no rotation. Second assumption is that there exists a triangular stress distribution along the contact length of the column and the infill. Third assumption is that the infill is not connected to the frame. The last assumption is that $\beta$ is equal to the half of the infill length.

Theoretical values of infill’s rigidity can be calculated from the assumption of stress distribution affecting on the infill’s sides. In **Table 7.1**, theoretically calculated $w_{panel}/d$ ratios for different panel proportions, $l/h$, and different contact ratios, $a/h$, are given. In this table, $d$ is the diagonal length of infill and $w_{panel}$ is the width of the compression strut. The values in **Table 7.1** are given for a homogeneous and isotropic material. Modulus of elasticity of the panels are calculated using **Equation 7.3**.

Push-over analysis was made in order to analytically proof the experimental results. Push-over analysis is a type of non-linear static analysis method which examines the performance of the structures under lateral loads [9]. In this method, first a load pattern is selected. Then, these loads are applied to the structure in small increments. The procedure is shown in **Figure 7.3**.

**Table 7.1** Theoretical Values of the ‘ $w_{panel}/d$ ’ Ratio

| Contact Ratios | | Panel Proportions $(l/h)$ | | | |
|---|---|---|---|---|---|
| $\alpha/h$ | $\beta/l$ | 1:1 | 1.5:1 | 2.0:1 | 2.5:1 |
| 1/8 | ½ | 0.24 | 0.22 | 0.18 | 0.16 |
| 1/4 | ½ | 0.30 | 0.27 | 0.23 | 0.18 |
| 3/8 | ½ | 0.35 | 0.32 | 0.26 | 0.22 |
| 1/2 | ½ | 0.38 | 0.38 | 0.30 | 0.25 |

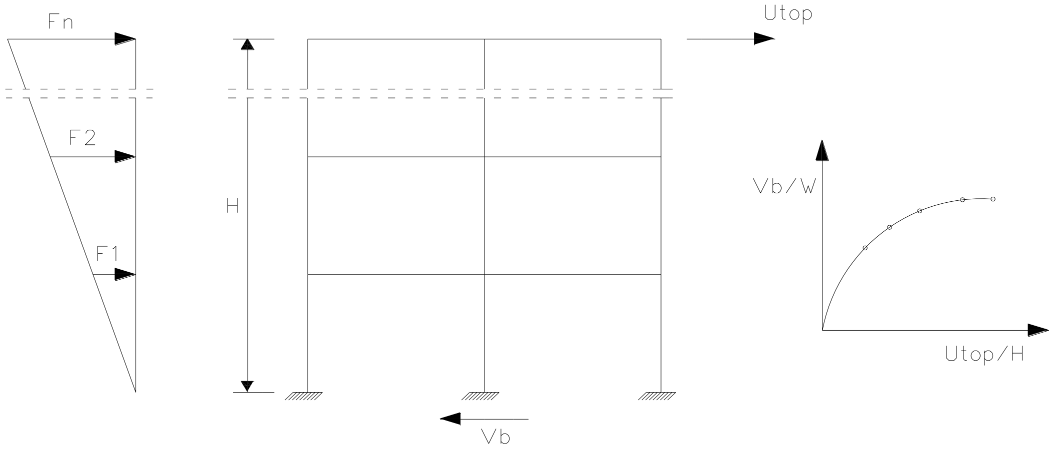


**Figure 7.3** Push-Over Analysis

Inelastic plane frame program DRAIN-2Dx [57] was used for the push-over analysis of the frames used in the experiments. In this program, analysis can be done either as load controlled or displacement controlled. Prakash, Powell, and Campbell [58] recommended displacement controlled type of push-over analysis, because in the force controlled loading some numerical problems may be seen due to reduction in the stiffness of the structure. In the displacement controlled loading, a selected lateral displacement pattern is applied to structure in increments.

The software accepts axial load-moment interaction curve as yield/rupture surface for frame specimens or moment capacity value as yield criteria independent from axial load. In this study, interaction curves for the columns and moment capacity values (elasto-plastic) for the beams are used in the program. For the beams and columns, type 02-plastic hinge beam-column element and for the struts, type 09-compression/tension link element was used.

The plastered hollow brick infill walls are defined in the program as no tension carrying elastic, brittle struts. For this reason, the equivalent axial rigidities and strengths of these struts, used for modeling the plastered hollow brick infill wall, should be calculated [48]. Specially produced, 1/3 scaled hollow bricks were used as infill material for all of the frames. The brick used in the study was previously shown in **Figure 3.17**.

The interaction diagrams for the columns of the test specimens defined for the program [59] are presented in **Figure 7.4**.

Load carrying capacity of the equivalent compression strut used to model the FRM can be calculated using **Equation 7.7**.

$$F_{c,FRM} = \lambda \cdot f_{c,FRM} \cdot b_{w,FRM} \cdot w_{FRM} \tag{7.7}$$

where $F_{c,FRM}$ is the lateral load carrying capacity of the equivalent compression strut, $\lambda$ is a constant dependent on the FRM strength, $f_{c,FRM}$ is the compressive strength of the FRM, $b_w$ is the thickness of the equivalent compression strut (mm), and $w_{FRM}$ is the width of the equivalent compression strut.

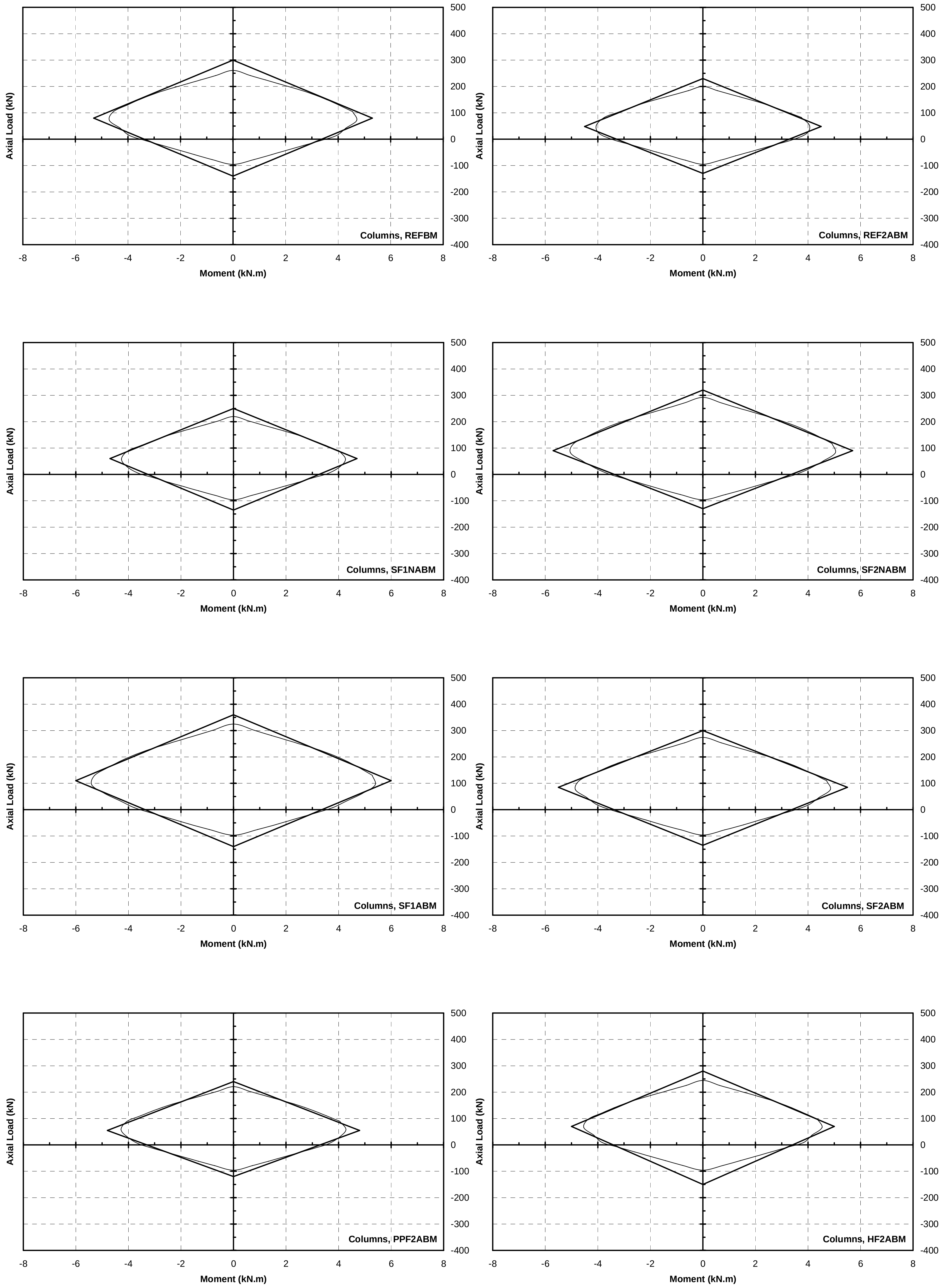


**Figure 7.4** Axial Load-Moment Interaction Curves for the Columns of the Specimens

Non-linear push-over analysis (displacement controlled) of the frame specimens were performed for different values of $\lambda$. The mean value and the standard deviation of the $\lambda$ values for which the analytical and experimental envelope curves best fit each other are calculated respectively as 0.3779 for anchored frames and 0.2209 for non-anchored frames.

Best-fit push-over curves of the specimens are given in **Figure 7.5**. The analytical curves in **Figure 7.5** were drawn by modeling the hollow brick infill walls strengthened by application of FRM as two equivalent diagonal compression struts.

Panel compressive strengths and $\lambda$ values of the frame specimens are shown in **Figure 7.6** and **Figure 7.7**. An approximate trend line for all of the points on the graph is drawn and the equation of the line is given in **Equation 7.8**. The trendlines are given in power forms in order to ease the simplification of the final equations.

$$\lambda = 4\left(f_{c,FRM}\right)^{-0.75} \quad \text{for anchored frames} \tag{7.8}$$

$$\lambda = 2\left(f_{c,FRM}\right)^{-0.75} \quad \text{for non-anchored frames}$$

Then, the lateral load carrying capacity of the panel compression strut can be calculated as in **Equation 7.9**.

$$F_{c,FRM} = 4 \cdot \left(f_{c,FRM}\right)^{0.25} \cdot b_{w,FRM} \cdot w_{FRM} \quad \text{for anchored frames} \tag{7.9}$$

$$F_{c,FRM} = 2 \cdot \left(f_{c,FRM}\right)^{0.25} \cdot b_{w,FRM} \cdot w_{FRM} \quad \text{for non-anchored frames}$$

The rigidity of the equivalent compression strut can be calculated using FEMA [55] as in **Equation 7.10**. Load-deformation curves of the compression strut modeling the FRM are presented in **Figures 7.8** and **7.9**.

$$k_{FRM} = \frac{b_{w,FRM} \cdot a_{FRM} \cdot E_{FRM}}{d} \tag{7.10}$$

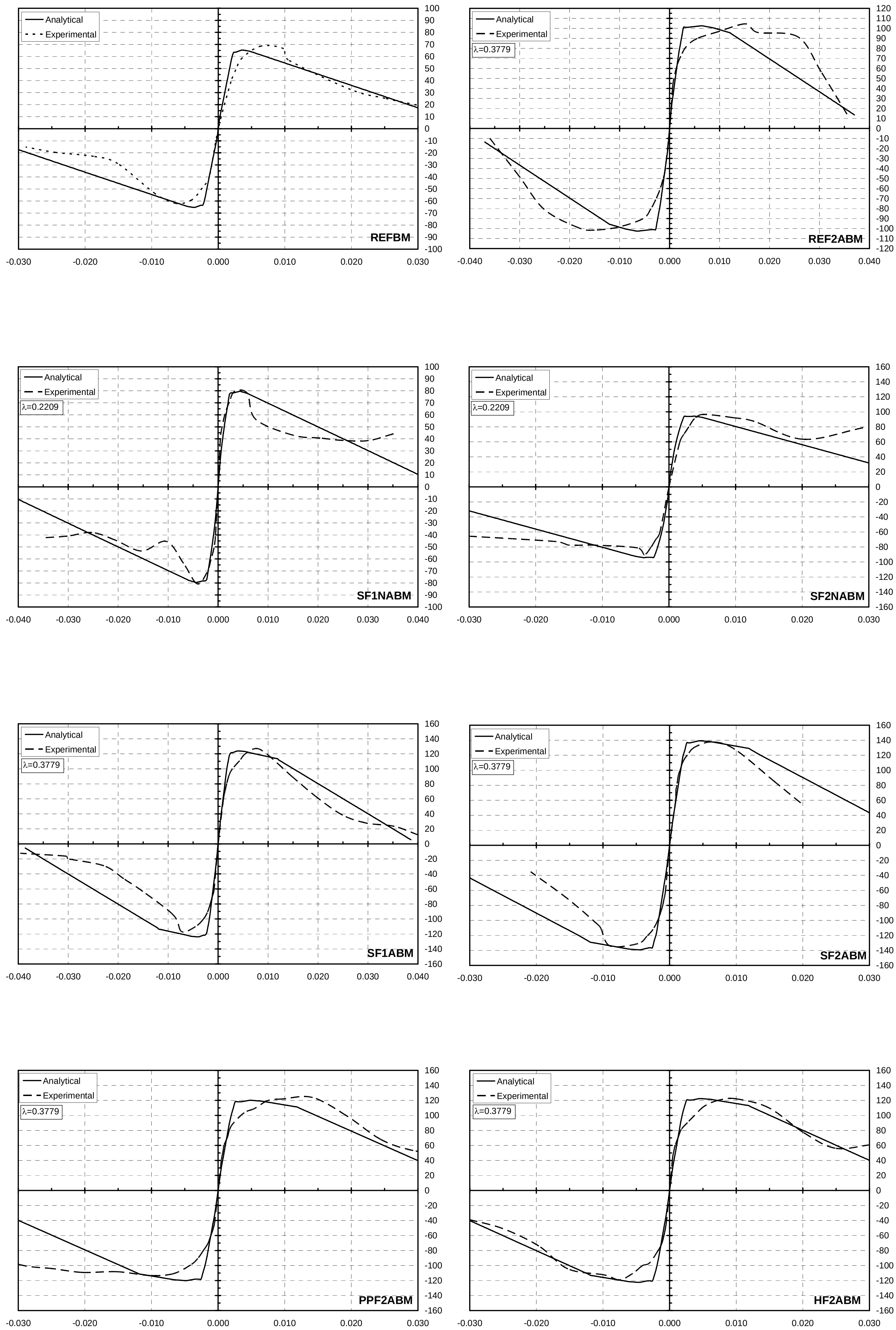


**Figure 7.5** Response Envelopes and Best-Fit Push-Over Curves of the Specimens

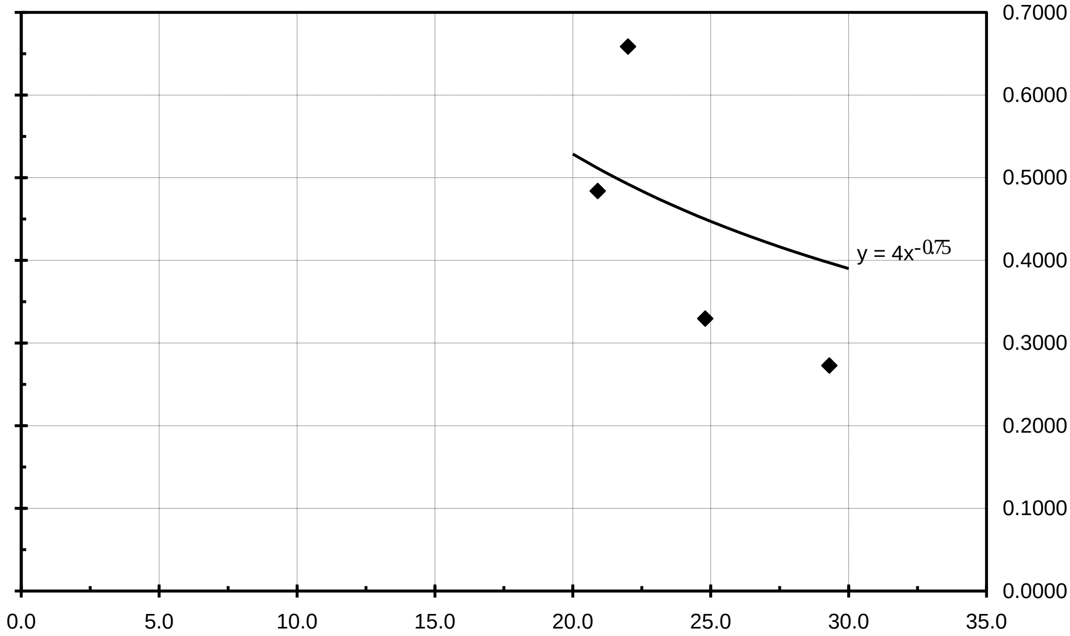


**Figure 7.6** Panel Compressive Strengths-$\lambda$ Values for Anchored Frames

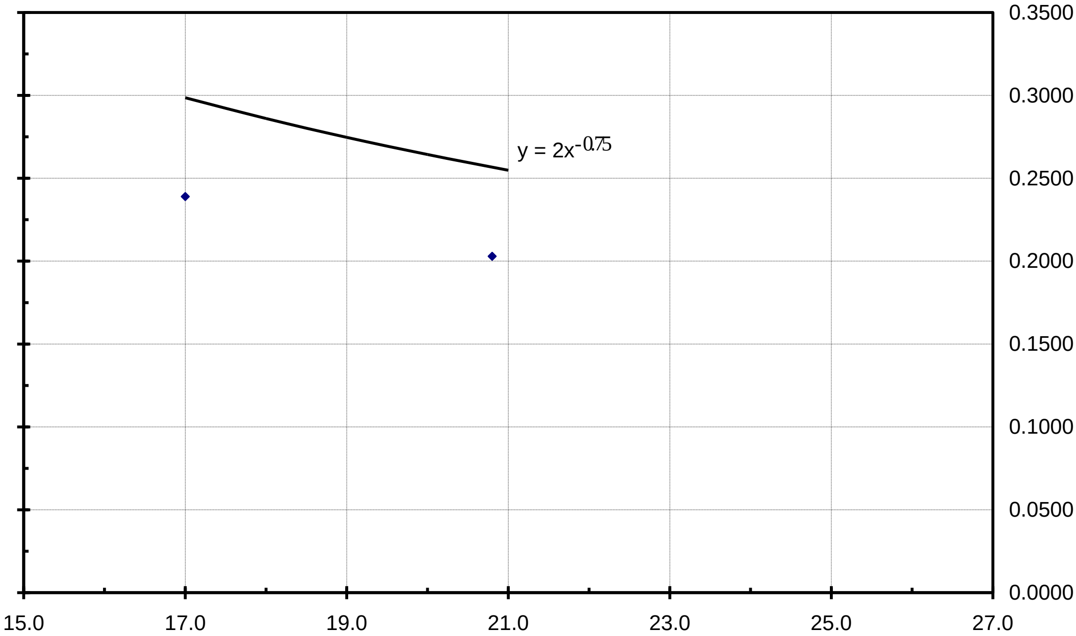


**Figure 7.7** Panel Compressive Strengths-$\lambda$ Values for Non-Anchored frames

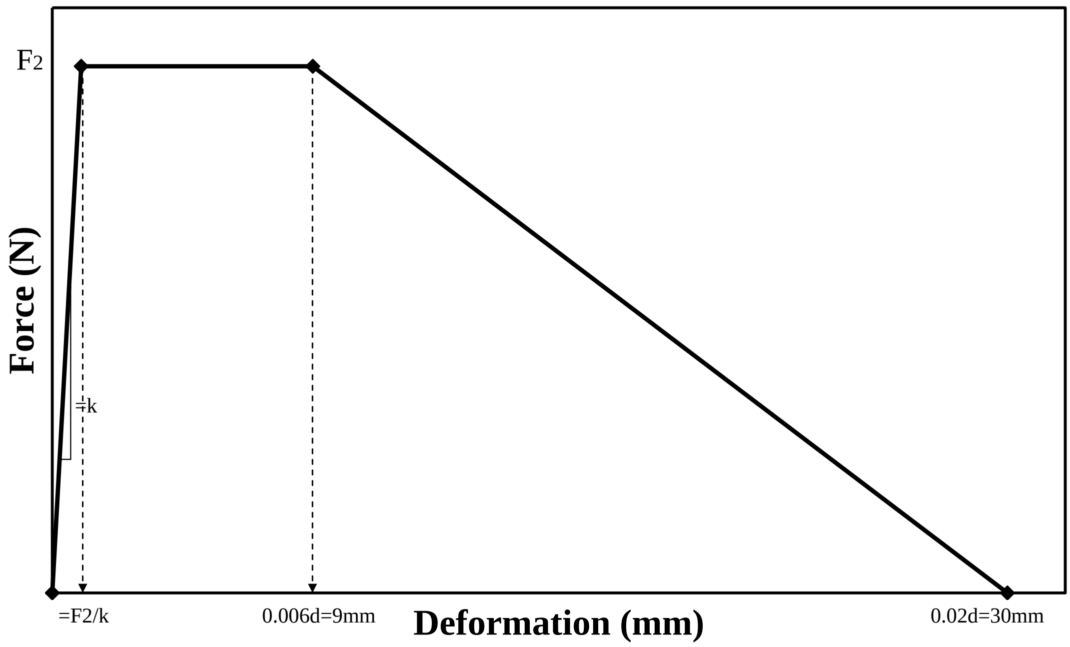


**Figure 7.8** Load-Deformation Curve of the Compression Strut Modeling the FRM of Anchored Specimens

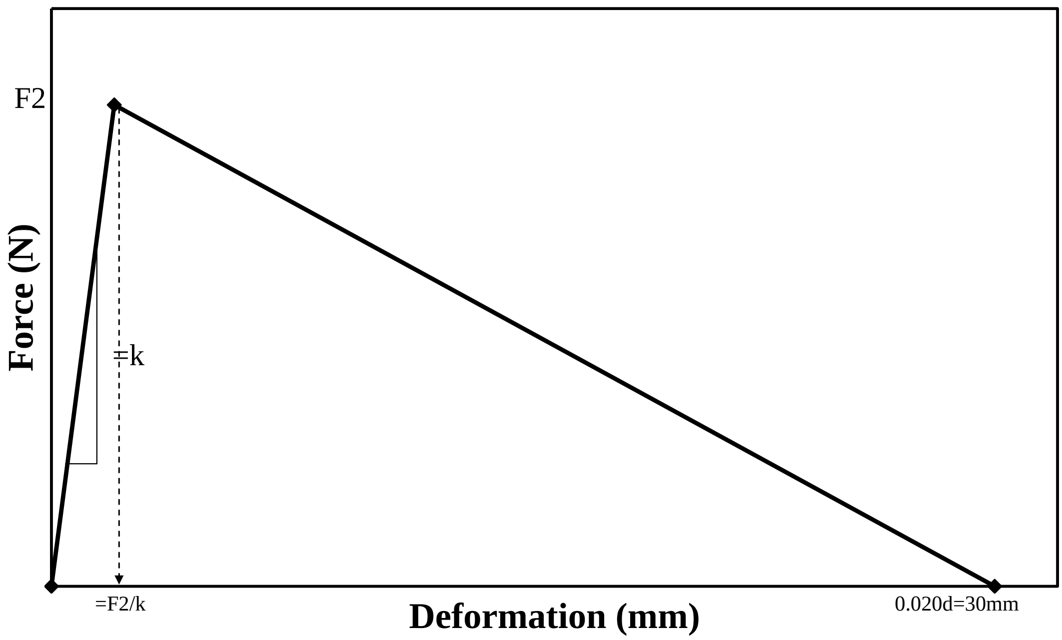


**Figure 7.9** Load-Deformation Curve of the Compression Strut Modeling the FRM of Non-Anchored Specimens

In the anchored frames, the stress distribution is much regular. For that reason, the model in **Figure 7.8** was used. Sound results were obtained using this model. In the non-anchored frames, the stress distribution is less and the model in **Figure 7.9** fits this behavior.

In summary, as two equivalent compression struts are used in the analytical modeling of the frame specimens the following equation can be written, **Equation 7.11**.

$$F_{strut} = F_{c,\inf ill} + F_{c,FRM} \qquad \textbf{(7.11)}$$

## 7.4 PUSH-OVER ANALYSIS OF THE FRAME SPECIMENS MODELED BY EQUIVALENT COMPRESSION STRUTS

An analytical model as shown in **Figure 7.10** is prepared for the frame specimens following the steps mentioned above. The hollow brick infill walls strengthened by the application of FRM are modeled with two different compression struts. One of the struts is used for the modeling of plastered hollow brick infill wall and the other is used for the modeling of the FRM layer.

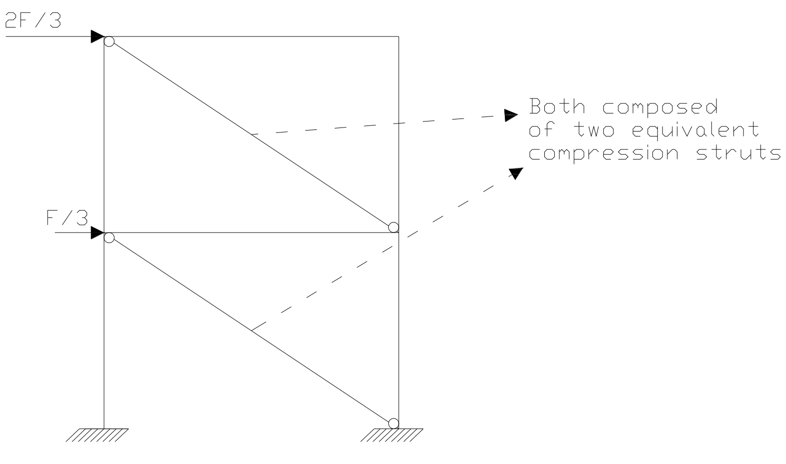


**Figure 7.10** Analytical Modeling of the Strengthened Frame Specimens

Comparison of response envelopes and load-deformation curves of equivalent strut model are presented in **Figure 7.11**. According to the results obtained from the push-over analysis of the frame specimens, the **Equation 7.11**, in which the lateral load carrying capacity of the equivalent compression strut is calculated, can be safely used. Adequate results were obtained by using **Equation 7.9**. This equation gives sound values for the lateral load carrying capacity of the panel compression strut modeling the FRM. It is necessary that the FRM layer be anchored properly to the frame according to the test results.

The equivalent strut method adequately simulates the behavior of the frame specimens. This method can be safely used for easy determination of the lateral load carrying capacity of the frames strengthened with FRM. A constant value of $\lambda$, 0.3779 for anchored frames and 0.2209 for non-anchored frames, is used. Moreover, equivalent strut method can be easily added to the existing frame model of the buildings. Considerable time and work might be saved by the usage of this method for quick determination of the ultimate load carrying capacities of the frames strengthened with FRM.

However, these observations are limited only to the tests performed in this study. Generalization of the conclusions should be made carefully for the equivalent strut method used in this study.

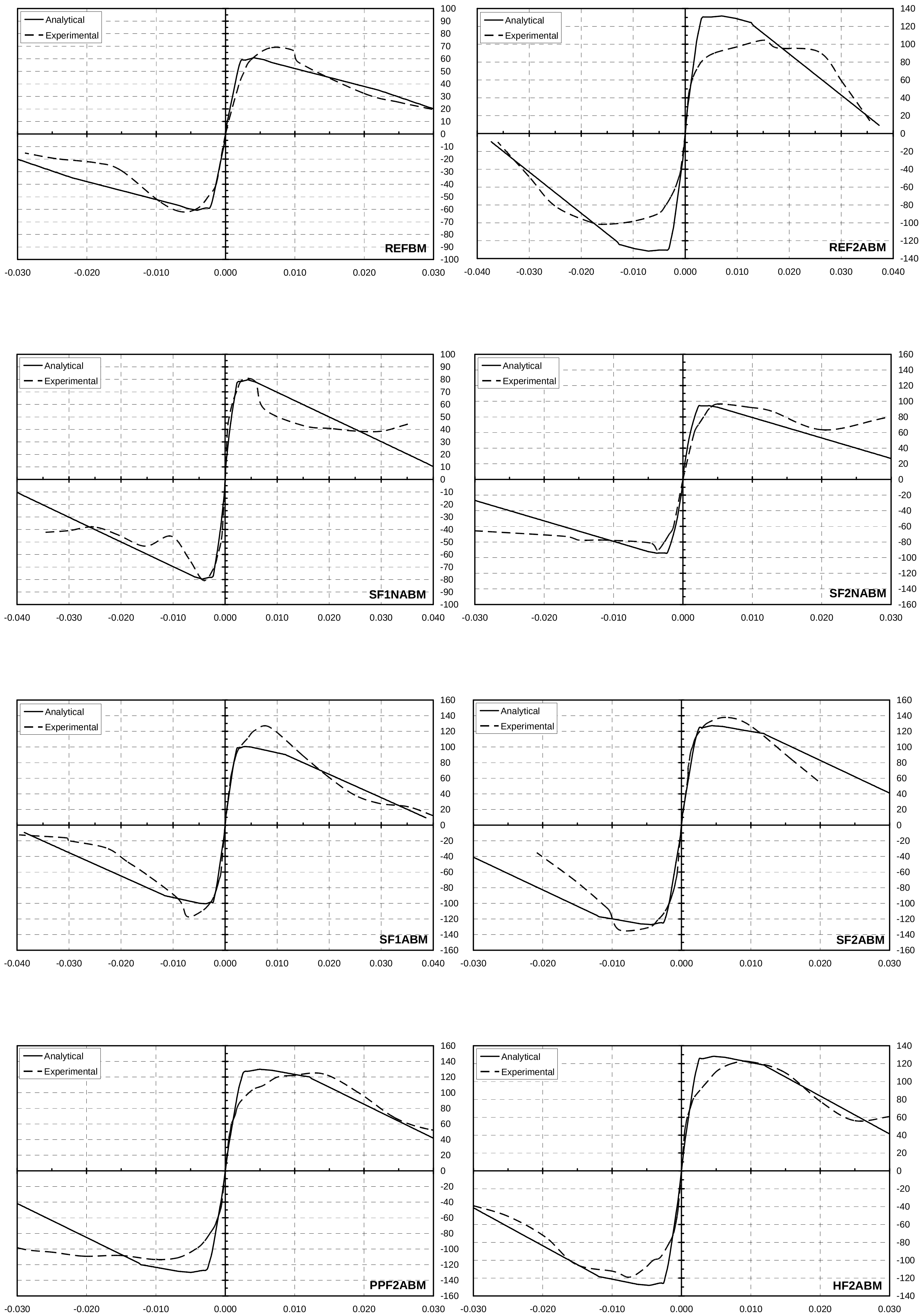


**Figure 7.11** Comparison of Response Envelopes and Load-Deformation Curves of Equivalent Strut Model

# CHAPTER 8

# CONCLUSIONS AND RECOMMENDATIONS

A series of experimental and analytical studies have been performed in the Structural Mechanics Laboratory of the Middle East Technical University with the aim of developing an economical, practical, and occupant-friendly strengthening technique. This study was also conducted within this scope as well. In the experimental study, steel fiber reinforced higher strength mortar was applied on the nonstructural walls. By this application, brick walls were converted to lateral load carrying members.

In the first part of the research, material tests were performed and physical properties of cement, aggregate, and mortar determined. Additionally, an optimum amount of steel fiber percentage for mortar was decided.

As the second component of the study, two series of panel tests were carried out. Different kind of configuration of brick walls were tested which constituted information for the modeling of walls in the frame.

In the last part of experimental study, 10 frames were tested with different steel fiber reinforced mortar configuration. Specimens were tested under reversed cyclic lateral loads simulating earthquake. The frames were 1/3 scale, 1 bay, and 2 story. The variables were mortar thickness, anchorage usage on surrounding frame, and different fiber types. 3 frame tests were prepared as reference.

After experimental studies, the test results were evaluated considering strength, stiffness, energy dissipation, and story drift characteristics. In the analytical works, infill walls strengthened by the application of steel fiber reinforced mortar (SFRM) were modeled by means of equivalent diagonal compression struts.

The conclusions drawn here should be used carefully with the limitations of the tests performed and not be generalized. The following conclusions are based on the results and analyses from the tests in this study:

From the material tests:

- Maximum of 2% volume content of steel fiber should be used in strengthening applications. Higher steel fiber content cause bonding problem of mortar on wall.

From the panel tests:

- Applying steel fiber reinforced mortar onto the plaster layer increases the diagonal compressive capacity of hollow brick infill panels when compared to that of reference specimens.
- In the first series of panel tests, the highest average load carrying capacity was obtained in panel specimens with strengthening mortar of 20 mm thickness and 2% volumetric ratio of steel fiber on one side.
- In the second series panel tests, the highest average load carrying capacity was obtained in the 10 mm thickness of mortar with 2% volumetric ratio of steel fiber applied wall specimen (on double sides).

- The difference between the first and second series panel specimens was the brick laying (bed) mortar strength caused by non-standardized practical preparation of mortar or briefly caused by workmanship. The effect of brick laying mortar strength on infill panel behavior is obvious primarily for non-plastered infill panels. Approximately 3 times increase in mortar strength results in approximately 4 times increase in diagonal compressive capacity of non-plastered panels.
- The maximum diagonal force of panel can be calculated with the equation given below:

$$P_d = \left( \frac{f_t' f_m'}{0.6631 f_m' - 2.365 f_t'} \right) \frac{b\,t}{0.707}$$

- For brick panels under diagonal loading, it is observed that failure occurs due to the mortar in between bricks. Therefore, the mortar compressive and tensile strengths should be used in the above equations instead of brick strength.
- The tensile strength of mortar can be approximately estimated as 5% of compressive strength, $f_t' = 0.05\, f_m'$.
- For the plaster applied on the panels, the tensile strength can be taken as $f_t' = 0.35\sqrt{f_{plaster}'}$ .
- For the strengthening mortar, the tensile strength is proposed as $f_t' = 0.70\sqrt{f_{plaster}'}$ .
- The first series test results were estimated with approximately 10% error with aforementioned tensile strengths. For the second series, test results were predicted in 11% error range except the last test.
- Theoretically, there is no difference between 2SSF2P specimen with 20 mm mortar at one-side, and 2SSF1PD specimens with 10 mm mortar on both sides. The double-sided specimen showed 10% higher capacity. This difference is attributed to the symmetry of the second one and eccentric of the first one.

- Strain gage applications to the panel specimens were found to be effective in determining the strain better and reliable than obtaining it from displacement measurements.

From frame tests:

- Strengthening by the application of steel fiber reinforced mortar, SFRM, on plastered infill walls of frames was found to be practical, occupant-friendly and economical technique for strengthening seismically vulnerable R/C structures.
- Compared to that of reference specimens, strengthened specimens performed better from strength and stiffness point of view.
- Application of strengthening mortar on brick masonry wall retards the early out of plane failure and converts the existing non-structural wall into load carrying wall.
- Strengthened specimens without anchorage to the surrounding frame, SF1NABM and SF2NABM, showed apparently less load carrying capacities among the strengthened specimens. The damage of these specimens localized near by the beam-column joints. Therefore, to get safe results and ensure load transfer between frame and strengthened wall, anchorage should be used along the surrounding frame of the wall.
- The proposed strengthening method was observed to be effective in that the strengthened frame specimens behaved as monolithic cantilevers rather than a frame. The frame behavior was seen in the reference specimens. In these specimens, the frame lost its lateral rigidity after the separation of the infill wall from the frame. The non-anchored strengthened specimens also did not behave as monolithic cantilevers; but showed classical frame behavior.
- When the effect of anchorage is considered, it can be concluded that using anchorages increases the lateral load carrying capacity approximately 45%.

- Considering the effect of thickness, it can be said that doubling the strengthening mortar thickness increases lateral strength approximately 12% only.
- When the effect of steel fibers in strengthening mortar is to be considered, two specimens, REF2ABM and SF2ABM, can be compared. Despite the disadvantage in mortar strength of the specimen SF2ABM, lateral strength was 34% higher than the REF2ABM.
- The interstory drifts should be limited to 1%. After this drift ratios, damage increases and strength decreases rapidly.
- The ratio of the cumulative dissipated energy of the strengthened specimens to that of the reference specimen varied in between 1.87 and 3.51 that indicates seismic improvement.
- When compared with the other occupant friendly strengthening techniques such as wire mesh reinforced mortar, FRP sheets, and RC panels applied on the brick walls, the steel fiber reinforced mortar offers similar enhancements in terms of strength and displacement.
- Strengthened frames can be modeled with two compression struts. Plastered hollow brick and strengthening layer should be modeled separately. The existing infill can be modeled according to the FEMA [55]. The FRM can acceptably be modeled with the identified method in this study.
- The experimental results were replicated reasonably well with the aforementioned modeling approach. The results are in-between 10% accuracy for strength and 15% for displacement calculations.

The following recommendations can be made for future research on this topic:

- Panel tests should be performed with frame resembling the real boundary conditions and preferably under cyclic loading.

- Strain gage should be applied to all of the panel specimens to get accurate strain values.
- The mortar and plaster mix proportions should be standardized in order to get similar strengths consistently.
- As in the panel tests, double side FRM application should be made also for the frame specimens.
- Multi-story multi-bay frames should be tested in order to obtain results that are more realistic.

# REFERENCES

[1] Pampanin, S., ‘Controversial Aspects in Seismic Assessment and Retrofit of Structures in Modern Times: Understanding and Implementing Lessons from Ancient Heritage’, Bulletin of the New Zealand Society for Earthquake Engineering, Vol. 39, Jun. 2006, pp. 120-133.

[2] Altın, S., ‘Strengthening of Reinforced Concrete Frames with Reinforced Concrete Infills’, Ph.D. Thesis, Middle East Technical University, Ankara, Turkey, 1990.

[3] Altın, S., Ersoy, U., Tankut, T., ‘Hysteretic Response of Reinforced-Concrete Infilled Frames’, Journal of Structural Engineering, ASCE, Vol. 118, Aug. 1992, pp. 2133-2150.

[4] Haider, S., ‘In-Plane Cyclic Response of Reinforced Concrete Frames with Unreinforced Masonry Infills’, M.Sc. Thesis, Rice University, Houston, Texas, U.S., 1995.

[5] Crisafulli, F.J., ‘Seismic Behavior of Reinforced Concrete Structures with Masonry Infills’, Ph.D. Thesis, University of Canterbury, Christchurch, New Zealand, 1997.

[6] Marjani, F., ‘Behavior of Brick Infilled Reinforced Concrete Frames under Reversed Cyclic Loading’, Ph.D. Thesis, Middle East Technical University, Ankara, Turkey, 1997.

[7] Dymiotis, C., Kappos, A.J., Chryssanthopoulos, M.K., ‘Seismic Reliability of Masonry-Infilled RC Frames’, Journal of Structural Engineering, ASCE, Vol. 127, Mar. 2001, pp. 296-305.

[8] Calvi, G.M., Bolognini, D., ‘Seismic Response of Reinforced Concrete Frames Infilled with Weakly Reinforced Masonry Panels’, Journal of Earthquake Engineering, Vol. 5, Apr. 2001, pp. 153-185.

[9] Sonuvar, M.O., ‘Hysteretic Response of Reinforced Concrete Frames Repaired by means of Reinforced Concrete Infills’, Ph.D. Thesis, Middle East Technical University, Ankara, Turkey, 2001.

[10] Canbay, E., ‘Contribution of RC Infills to the Seismic Behavior of Structural Systems’, Ph.D. Thesis, Middle East Technical University, Ankara, Turkey, 2001.

[11] Mertol, H.C., ‘Carbon Fiber Reinforced Masonry Infilled Reinforced Concrete Frame Behavior’, M.Sc. Thesis, Middle East Technical University, Ankara, Turkey, 2002.

[12] Keskin, R.S.O., ‘Behavior of Brick Infilled Reinforced Concrete Frames Strengthened by CFRP Reinforcement: Phase I’, M.Sc. Thesis, Middle East Technical University, Ankara, Turkey, 2002.

[13] Erduran, E. ‘Behavior of Brick Infilled Reinforced Concrete Frames Strengthened by CFRP Reinforcement: Phase II’, M.Sc. Thesis, Middle East Technical University, Ankara, Turkey, 2002.

[14] Shing, P.B., Mehrabi, A.B., ‘Behavior and Analysis of Masonry-Infilled Frames’, Progress in Structural Engineering and Materials, Vol. 4, Jul./Sept. 2002, pp. 320-331.

[15] Anıl, Ö., ‘Betonarme Çerçevelerin Boşluklu Betonarme Dolgu Duvarlar ile Güçlendirilmesi’, Ph.D. Thesis, Gazi University, Ankara, Turkey, 2002.

[16] Hanoğlu, K.B., ‘Fiber Reinforced Plastic Overlay Retrofit of Hollow Clay Tile Masonry Infilled Reinforced Concrete Frames’, Ph.D. Thesis, Boğaziçi University, İstanbul, Turkey, 2002.

[17] Colangelo, F., ‘Experimental Evaluation of Member-by-Member Models and Damage Indices for Infilled Frames’, Journal of Earthquake Engineering, Vol. 7, Jan. 2003, pp. 25-50.

[18] Duvarcı, M., ‘Seismic Strengthening of Reinforced Concrete Frames with Precast Concrete Panels’, M.Sc. Thesis, Middle East Technical University, Ankara, Turkey, 2003.

[19] Öktem, O., 'Betonarme Çerçeve Sistemlerin Lineer Olmayan Hesabı ve Dolgu Duvarların Modellenmesi', M.Sc. Thesis, İstanbul Technical University, İstanbul, Turkey, 2003.

[20] Erdem, İ., 'Strengthening of Existing Reinforced Concrete Frames', M.Sc. Thesis, Middle East Technical University, Ankara, Turkey, 2003.

[21] Erdem, İ., Akyüz, U., Ersoy, U., Özcebe, G., 'An Experimental Study on Two Different Strengthening Techniques for RC Frames', Engineering Structures, Vol. 28, Nov. 2006, pp. 1843-1851.

[22] Özcebe, G., Ersoy, U., Tankut, T., Erduran, E., Keskin, R.S.O., Mertol, H.C., 'Strengthening of Brick-Infilled RC Frames with CFRP', SERU-Structural Engineering Research Unit, TÜBİTAK, Middle East Technical University, Ankara, Turkey, 2003.

[23] Süsoy, M., 'Seismic Strengthening of Masonry Infilled Reinforced Concrete Frames with Precast Concrete Panels', M.Sc. Thesis, Middle East Technical University, Ankara, Turkey, 2004.

[24] Gün, B., 'Sünek Olmayan Betonarme Çerçevelerin Betonarme Dolgu Duvarla Kesme Dayanımının İyileştirilmesi', M.Sc. Thesis, Gazi University, Ankara, Turkey, 2005.

[25] Baran, M. 'Precast Concrete Panel Reinforced Infill Walls for Seismic Strengthening of Reinforced Concrete Framed Structures', Ph.D. Thesis, Middle East Technical University, Ankara, Turkey, 2005.

[26] Güney, M.E., 'A Numerical Procedure for the Nonlinear Analysis of Reinforced Concrete Frames with Infill Walls', M.Sc. Thesis, Middle East Technical University, Ankara, Turkey, 2005.

[27] Öztürk, M.S., 'Effects of Masonry Infill Walls on the Seismic Performance of Buildings', M.Sc. Thesis, Middle East Technical University, Ankara, Turkey, 2005.

[28] Malekkianie, B., 'Dolgu Duvarlı Betonarme Çerçevelerde Karbon Lifler Kullanılarak Güçlendirme', M.Sc. Thesis, İstanbul Technical University, İstanbul, Turkey, 2006.

[29] Dönmez, S., ‘Deprem Etkisinde Betonarme Binalarda Hasarın Oluşmasında Dolgu Duvarların Modellenmesi ve Taşıyıcı Sisteme Katkısı’, M.Sc. Thesis, İstanbul Technical University, İstanbul, Turkey, 2006.

[30] Kara, M.E., ‘Sünek Olmayan Betonarme Çerçevelerin Betonarme Parçasal Dolgu Duvarlarıyla Güçlendirilmesi’, Ph.D. Thesis, Gazi University, Ankara, Turkey, 2006.

[31] Akın, L.A., ‘Behavior of Reinforced Concrete Frames with Masonry Infills in Seismic Regions’, Ph.D. Thesis, Purdue University, West Lafayette, Indiana, U.S., 2006.

[32] Binici, B., Özcebe, G., ‘Analysis of Infilled Reinforced Concrete Frames Strengthened with FRPs’, Advances in Earthquake Engineering for Urban Risk Reduction, Wasti, S.T., Özcebe, G. (Editors), Springer, Netherlands, 2006.

[33] Shaingchin, S., Lukkunaprasit, P., Wood, S.L., ‘Influence of Diagonal Web Reinforcement on Cyclic Behavior of Structural Walls’, Engineering Structures, Vol. 29, Apr. 2007, pp. 498-510.

[34] El-Sokkary, H., ‘Analytical Study on Upgrading the Seismic Performance of Nominally Ductile RC Frame Structures Using Different Rehabilitation Techniques’, M.Sc. Thesis, Concordia University, Montreal, Quebec, Canada, 2007.

[35] Erduran, E., Yakut, A., ‘Component Damage Functions for Reinforced Concrete Frame Structures’, Engineering Structures, Vol. 29, Sept. 2007, pp. 2242-2253.

[36] Tucker, C.J., ‘Predicting the In-Plane Capacity of Masonry Infilled Frames’, Ph.D. Thesis, Tennessee Technological University, Crossville, Tennessee, U.S., 2007.

[37] Altın, S., Anıl, Ö., Kara, M.E., Kaya, M., ‘An Experimental Study on Strengthening of Masonry Infilled RC Frames Using Diagonal CFRP Strips’, Composites Part B: Engineering, Vol. 39, Jun. 2008, pp. 680-693.

[38] Puglisi, M., Uzcategui, M., Florez-Lopez, J., ‘Modeling of Masonry of Infilled Frames, Part I: The Plastic Concentrator’, Engineering Structures, Vol. 31, Jan. 2009, pp. 113-118.

[39] Puglisi, M., Uzcategui, M., Florez-Lopez, J., ‘Modeling of Masonry of Infilled Frames, Part II: Cracking and Damage’, Engineering Structures, Vol. 31, Jan. 2009, pp. 119-124.

[40] ‘Turkish Earthquake Code: Specifications for the Buildings to be Constructed in Disaster Areas’, Ministry of Public Works and Settlement, Ankara, Turkey, 1998.

[41] ‘2007 California Building Code, California Code of Regulations, Title 24, Part 2, Volume 2 of 2’, California Building Standards Commission, Sacramento, California, U.S., 2007.

[42] Sezen, H., Moehle, J.P., ‘Shear Strength Model for Lightly Reinforced Concrete Columns’, Journal of Structural Engineering’, ASCE, Vol. 130, Nov. 2004, pp. 1692-1703.

[43] Acun, B., Sucuoglu, H., ‘Strengthening Of Masonry Infill Walls In Reinforced Concrete Frames With Wire Mesh Reinforcement ", 8th U.S. National Conference on EQ. Eng., California, USA, p.No: 1852, 2006.

[44] Özcebe, G., Ersoy, U., Tankut, T., Erduran, E., Keskin, R.S.O., Mertol, H.C., ‘Strengthening of Brick-Infilled RC Frames with CFRP’, SERU - Structural Engineering Research Unit, TUBITAK - METU Report, 2003.

[45] Tankut, T., Ersoy, U., Ozcebe, G., Baran, M., Okuyucu, D., ‘In Service Seismic Strengthening of RC Framed Buildings’, Seismic Assessment and Rehabilitation of Existing Buildings, International Closing Workshop, NATO project Sfp 977231, Istanbul, Turkey, 2005.

[46] Okuyucu, D., Sevil, T., Canbay, E., ‘Shear Behavior of Hollow Brick Infill Wall Panels Strengthened by Precast Reinforced Concrete Panels and Steel Fiber Reinforced Plaster’, WCCE - ECCE - TCCE Joint Conference on Earthquake & Tsunami, Istanbul, Turkey, Jun. 2009.

[47] Yokel, F.Y, Fattal, S.G., 'Failure Hypothesis for Masonry Shear Walls', Journal of the Structural Division, ASCE, Vol. 102, Mar. 1976, pp. 515-532.

[48] Sucuoğlu, H., McNiven, H.D., 'Seismic Shear Capacity of Reinforced Masonry Piers', Journal of Structural Engineering, ASCE, Vol. 117, Jul. 1991, pp. 2166-2186.

[49] Smith, B., S., 'Lateral Stiffness of Infilled Frames', ASCE Journal of Structural Division, Vol. 88, ST. 6, December 1962, pp.183-199.

[50] Smith, B., S., 'Behaviour of Square Infilled Frames', ASCE Journal of Structural Division, Vol. 92, ST. 1, February 1966.

[51] Smith, B., S., 'Methods for Predicting the Lateral Stiffness and Strength of Multi-Storey Infilled Frames', Building Science, Vol. 2, 1967, pp. 247-257.

[52] Smith, B. S., 'Model Test Results of Vertical and Horizontal Loading of Infilled Specimens', ACI Journal, August 1968, pp. 618-624.

[53] Smith, B., S., Carter, C., 'A Method of Analysis for Infilled Frames', Proc. ICE, Vol. 44, September 1969, pp. 31-48.

[54] Baran, M., Canbay, E., Tankut, T., 'Konut Yapılarının Önüretimli Beton Panellerle Güçlendirilmesi: Kuramsal Çalışmalar', Teknik Dergi, TMMOB İnşaat Mühendisleri Odası, Vol. 21, Jan. 2010, pp. 4959-4978.

[55] Federal Emergency Management Agency (FEMA), NEHRP GUIDELINES FOR THE SEISMIC REHABILITATION OF BUILDINGS, FEMA 356, November 2000.

[56] ACI, American Concrete Institute, Committee 318, Building Code Requirements for Reinforced Concrete (ACI 318-95) and Commentary (ACI 318 R-95), Michigan, October 1995.

[57] Allahabadi, R., 'Drain 2Dx-Seismic Response and Damage Assessment for 2D Structures', Ph.D. Dissertation, University of California, Berkeley, California, 1981.

[58] Prakash, V., Powell, G. H., Campbell, S., ‘Drain-2DX Base Program Description and User Guide’, Version 1.10, Department of Civil Engineering, University of California, Berkeley, California, November 1993.

[59] Response 2000, Reinforced Concrete Sectional Analysis, Response-2k Version 1.0.5., Evan C. Bentz and Micheal P. Collins, 2000, Canada.

# APPENDIX A

## EVALUATION OF SHEAR DEFORMATIONS

In this appendix, the computation of shear displacement is presented. Shear deformations on the panels were measured by means of diagonally placed dial gages. Since two displacement readings were taken along the diagonals, it is possible to determine the deformed shape of the wall panel. Approximate deformed shape of the panel is presented in **Figure A.1**.

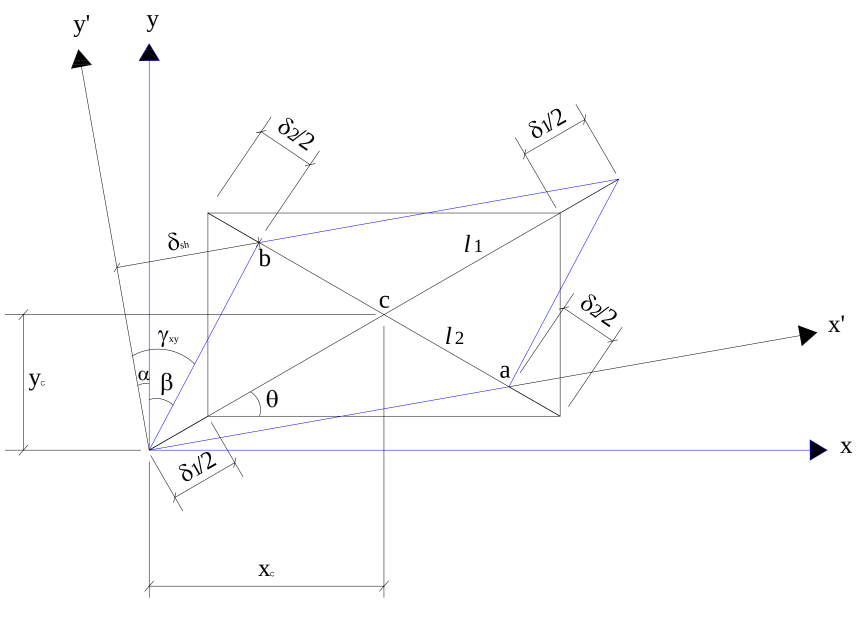


**Figure A.1** Rectangular Shape Distortion

According to the geometry shown in the previous page, shear deformations can be computed approximately as follows:

$$\theta = \arctan\left(h/w\right)$$

$h$ : height of the rectangle

$w$ : width of the rectangle

$$l_1^{'} = l_1 + \delta_1 = l_1(1+\varepsilon_1)$$

$$l_2^{'} = l_2 + \delta_2 = l_2(1+\varepsilon_2)$$

$l_1$ : length of diagonal 1

$l_2$ : length of diagonal 2

$l_1^{'}$ : length of diagonal 1 after deformation

$l_2^{'}$ : length of diagonal 2 after deformation

$\varepsilon_1$ : strain in diagonal 1 direction

$\varepsilon_2$ : strain in diagonal 2 direction

$\delta_1$ : total elongation in diagonal 1 direction

$\delta_2$ : total elongation in diagonal 2 direction

$$x_c = \tfrac{l_1^{'}}{2}\cos(\theta)$$

$$y_c = \tfrac{l_1^{'}}{2}\sin(\theta)$$

$$x_a = x_c + \frac{l_2^{'}}{2}\cos(\theta) = \left(\frac{l_1^{'} + l_2^{'}}{2}\right)\cos(\theta)$$

$$y_a = y_c - \frac{l_2^{'}}{2}\sin(\theta) = \left(\frac{l_1^{'} - l_2^{'}}{2}\right)\sin(\theta)$$

$$x_b = x_c - \frac{l_2^{'}}{2}\cos(\theta) = \left(\frac{l_1^{'} - l_2^{'}}{2}\right)\cos(\theta)$$

$$y_b = y_c + \frac{l_2^{'}}{2}\sin(\theta) = \left(\frac{l_1^{'} + l_2^{'}}{2}\right)\sin(\theta)$$

Shear deformation $\gamma_{xy}$ is defined as the sum of the angles $\alpha$ and $\beta$ shown in **Figure A.1**. Angles $\alpha$ and $\beta$ can be obtained easily from the following equations:

$$\alpha = \arctan\left(\frac{y_a}{x_a}\right) = \arctan\left(\frac{\left(\frac{l_1^{'} - l_2^{'}}{2}\right)\sin(\theta)}{\left(\frac{l_1^{'} + l_2^{'}}{2}\right)\cos(\theta)}\right) = \arctan\left(\frac{l_1^{'} - l_2^{'}}{l_1^{'} + l_2^{'}}\tan(\theta)\right)$$

$$= \arctan\left(\frac{l_1^{'} - l_2^{'}}{l_1^{'} + l_2^{'}}\left(h/w\right)\right) = \arctan\left(\frac{\varepsilon_1 - \varepsilon_2}{2 + \varepsilon_1 + \varepsilon_2}\left(h/w\right)\right)$$

$$\beta = \arctan\left(\frac{x_b}{y_b}\right) = \arctan\left(\frac{\left(\frac{l_1^{'} - l_2^{'}}{2}\right)\cos(\theta)}{\left(\frac{l_1^{'} + l_2^{'}}{2}\right)\sin(\theta)}\right) = \arctan\left(\frac{l_1^{'} - l_2^{'}}{l_1^{'} + l_2^{'}}\cot(\theta)\right)$$

$$= \arctan\left(\frac{l_1^{'} - l_2^{'}}{l_1^{'} + l_2^{'}}\left(w/h\right)\right) = \arctan\left(\frac{\varepsilon_1 - \varepsilon_2}{2 + \varepsilon_1 + \varepsilon_2}\left(w/h\right)\right)$$

$$\gamma_{xy} = \alpha + \beta$$

$\delta_{sh}$ shown in **Figure A.1** could easily be obtained from geometry. The shear-displacement values could than be computed using the following equation:

$$\delta_{sh} = \gamma_{xy} \cdot h$$

Shear-displacement value $\left(\delta_{sh}\right)$ measured for each panel was the inter-story shear-displacement for that story. Total shear-displacement curve can be calculated by summing the shear-displacements of each panel.

It must be realized that the sensitivity and placement of the instrumentation was not sufficient to obtain accurate values of the shear distortions at infill panel. It is difficult to get accurate measurements of shear deformations due to uncertainties introduced by panel cracking.

# VITA

Tuğçe Sevil was born on February 20, 1977 in İzmir, Turkey. She received her secondary and high school educations in Antalya. In 1994, she went to the Middle East Technical University (METU), Ankara to study Civil Engineering. She was awarded a B.Sc. degree in Civil Engineering in 1998. She worked as a research assistant in the Department of Civil Engineering of METU from September 1998 to December 2001. In 2001, she was awarded her M.Sc. degree in Structural Engineering from the Institute of Natural and Applied Sciences of METU. She worked as a project assistant of the Scientific and Technical Research Council of Turkey (TÜBİTAK) during her doctorate. In February 2010, she received her Ph.D. degree in Structural Engineering from METU.